

University of Alberta

Structure-based design of inhibitors for the human neuraminidase enzymes NEU2, NEU3, and
NEU4

by

Amgad Mohamed Roshdi Albohy

A thesis submitted to the Faculty of Graduate Studies and Research
in partial fulfillment of the requirements for the degree of

Doctor of Philosophy

Department of Chemistry

© Amgad Mohamed Roshdi Albohy
Spring 2014
Edmonton, Alberta

*To my parents who taught me to love science,
to Amira, my great wife who was always my support
and
to Omar and Habiba, my kids who gave me the passion.*

Abstract

Sialidases (neuraminidases) are a group of enzymes responsible for the hydrolysis of sialic acid from glycoconjugates. In humans, there are four different isoenzymes that play important roles in health and disease. The human neuraminidase enzymes (hNEU) were discovered somewhat recently, and there are few known inhibitors. In this thesis we present studies towards the development of inhibitors for the human sialidases, NEU2, NEU3 and NEU4. We used the reported crystal structure of NEU2, and homology models of NEU3 and NEU4, to understand the substrate recognition by these enzymes. Our models were tested using site directed mutagenesis. Molecular modeling was used to design selective, potent inhibitors. Most notably, we report the design and testing of a highly selective nanomolar inhibitor of NEU4. In addition, an STD NMR study of NEU3 with an analog of GM3 provides insight into substrate recognition by this important enzyme. These results provide a critical foundation for future development of inhibitors and tools for understanding the role of these enzymes in human health.

Acknowledgement

I want to take this chance to thank all the great people who participated to this work and make it possible that this thesis comes to the light. First and foremost, I want to thank my supervisor Dr. Christopher Cairo for his support and guidance. I think I was blessed to work under his supervision for my PhD where I learned lots of scientific stuff but more important I learned how to think and analyze.

I also want to thank Ruixiang Blake Zheng who taught me all the molecular biology techniques I have used. I believe I bothered him a lot with my questions but he was always very helpful. I also want to thank Drs. Michele R Richards and Hashem Taha for their great help, support and useful discussion using AMBER software. I want to thank Mark Miskolzie for his advice and support in the NMR experiments.

I also want to thank all the collaborators and colleagues who provided samples that were used for this work including Yao Zou and Dr. Yi Zhang for providing the inhibitors tested and Victoria Smutova and Dr. Alexey V. Pshezhetsky (University of Montreal) for providing NEU1 samples.

Finally, I want to thank my parents, my wife and kids for their support and patience waiting for me for more than five years to finish my job.

Table of content

1	Introduction	1
1.1	Sialic Acids	2
1.2	Human sialidases	3
1.3	Human versus viral sialidases	7
1.4	Physiological and pathological roles of human sialidases	10
1.4.1	NEU1	11
1.4.2	NEU2	13
1.4.3	NEU3	14
1.4.4	NEU4	15
1.5	Expression systems and purification methods used for the human sialidases	17
1.6	Inhibition of human sialidase enzymes	18
1.7	Project objectives	22
1.8	References	24
2	Insight into substrate recognition and catalysis by the human neuraminidase 3 (NEU3) through molecular modeling and site-directed mutagenesis	39
2.1	Introduction	40
2.2	Results	42
2.2.1	Homology modeling and molecular docking of NEU3	49
2.2.2	Site-directed mutagenesis of recombinant NEU3	51
2.2.3	Purification and characterization of NEU3 mutants	57
2.2.4	Effect of additives on NEU3 activity	61
2.2.5	NEU3 catalytic mechanism	63
2.3	Discussion	66
2.4	Conclusion	73
2.5	Methods	73
2.5.1	NEU3 expression in E. coli (pET28a vector)	73
2.5.2	Site-directed mutagenesis of Neu3 and purification of fusion proteins	74
2.5.3	Screening of mutant enzyme activity	80
2.5.4	Enzyme kinetics and inhibition by DANA	81
2.5.5	Homology modeling of NEU3	81
2.6	References	83

3 Inhibition of human neuraminidase 3 (NEU3) by C9-triazole derivatives of 2,3-didehydro-N-acetyl-neuraminic acid and the identification of selective nanomolar inhibitors of the human neuraminidase, NEU4	91
3.1 Introduction	92
3.2 Results and Discussion	97
3.2.1 C9 and N5 libraries test against NEU3	97
3.2.2 Testing of a focused library against the human sialidase isozymes (hNEU1-hNEU4)	106
3.3 Conclusions	116
3.4 Methods	117
3.4.1 Molecular docking of inhibitors to NEU3	117
3.4.1 Molecular docking of inhibitors to NEU4	118
3.4.2 NEU3 inhibition assays	121
3.4.3 NEU1, NEU2, NEU3, and NEU4 testing of the focused library	121
3.4.4 NEU4 inhibition of glycolipid cleavage	122
3.5 References	124
4 Identification of selective inhibitors for human neuraminidase isoenzymes using C4, C7-modified 2-deoxy-2,3- didehydro-N-acetylneuraminic acid (DANA) analogues'	135
4.1 Introduction	136
4.2 Results	139
4.2.1 Inhibitor Synthesis	139
4.2.2 Inhibition Assays	141
4.2.3 Molecular Modeling	147
4.2.4 Convergence and total energy of molecular dynamics simulations	152
4.3 Discussion	153
4.4 Conclusion	155
4.5 Methods	156
4.5.1 General Protocol for Inhibition Assays	156
4.5.2 K _i Determinations	157
4.5.3 Molecular Modeling	158
4.6 References	159
5 Mapping the substrate interactions of the human membrane-associated neuraminidase, NEU3, using STD NMR	170
5.1 Introduction	171

5.2 Results	175
5.2.1 1D ¹ H NMR assignment	175
5.2.2 Protein expression	181
5.2.3 STD NMR of NEU3(Y370F)–substrate complexes	181
5.2.4 STD NMR of NEU3(Y370F)– 5.2 complex	184
5.2.5 STD NMR of NEU3(Y370F)– 5.4 complex	189
5.2.6 MD simulations of NEU3–substrate interactions	192
5.3 Discussion	198
5.4 Conclusions	204
5.5 Methods	204
5.5.1 Synthetic ligands	204
5.5.2 Protein expression	204
5.5.3 NMR sample preparation	206
5.5.4 NMR experiments	207
5.5.5 Molecular dynamics	207
5.6 References	209
6 Future directions	217
6.1 Finding potent selective inhibitors for each of the four human sialidases	218
6.1.1 High throughput screening	219
6.1.2 Modeling as a source of new scaffolds	220
6.2 The use of new assays to test the specificity of the four sialidases	220
6.3 Follow up on the NEU4 selective nanomolar inhibitor	221
6.4 Improved homology models for NEU3 and NEU4	221
6.5 References	223
A Appendices	224
A.1 Supporting data for Chapter 1	225
A.2 Supporting data for Chapter 2	227
A.3 Supporting data for Chapter 3	235
A.4 Supporting data for Chapter 4	274

List of tables

Table 2.1: Predicted substrate interactions in NEU3	46
Table 2.2: Truncated mutant sequences	54
Table 2.3: Kinetics of 4MU-NA hydrolysis by MBP-NEU3	60
Table 2.4: Primers used for generation of NEU3 mutants	76
Table 3.1: Previously reported inhibitors of NEU3	96
Table 3.2: Inhibition of NEU3	100
Table 3.3: Inhibition of the focused library against neuraminidase enzymes.....	108
Table 4.1: Inhibition of Neuraminidase Isoenzymes	143
Table 4.2: Ki Determinations.....	147
Table 5.1: STD and MD results for NEU3–octyl-GM3	178
Table 5.2: STD and MD results for NEU3–4MU-NANA	180
Table 5.3: Facial recognition of lactoside residues by STD NMR and MD.....	201

List of figures

Figure 1.1: pH profiles of the four human sialidases.....	6
Figure 1.2: Active site topology of NEU enzymes.....	8
Figure 2.1: Alignment of NEU2 and NEU3 using ClustalW.....	43
Figure 2.2: NEU3 Homology model evaluation.....	44
Figure 2.3: Homology model of the NEU3 active site and molecular docking....	48
Figure 2.4: NEU3 construct sequences. The protein sequence for His-tagged NEU3 and MBP-NEU3 including the linker used.....	50
Figure 2.6: Activity of truncated NEU3.....	53
Figure 2.7: Relative activity of point mutations generated.....	56
Figure 2.8: pH activity profile of wild-type and purified NEU3.....	57
Figure 2.9: Purification of NEU3 mutants as MBP fusion proteins.....	58
Figure 2.10: Effects of additives on NEU3 enzymatic activity.....	62
Figure 2.11: Catalytic mechanism of NEU3 studied by ¹ H NMR spectroscopy.....	64
Figure 2.12: Catalytic mechanism of NEU3 by NMR.....	65
Figure 2.13: Putative glycolipid interactions.....	69
Figure 2.14: Proposed catalytic mechanism for NEU3.....	72
Figure 3.1: DANA analog synthetic targets.....	97
Figure 3.2: Molecular docking of DANA and 3.6a.....	104
Figure 3.3: Structures of the focused library.....	106
Figure 3.4: Potency and selectivity of compound 3.6f against hNEU.....	111
Figure 3.5: Molecular model of compound 3.6f in the active site of NEU4.....	113
Figure 3.6: Selectivity of compound 6f for NEU4 over NEU2.....	114

Figure 3.7: Compound 3.6f inhibits NEU4 cleavage of a glycolipid substrate, GM3.	116
Figure 3.8: Convergence and total energy during MD calculation.....	119
Figure 3.9: Quality of NEU4 homology model.	120
Figure 4.1: IC ₅₀ curves of 4.5c and 4.8b for the four human neuraminidase isoenzymes.....	146
Figure 4.2: Molecular models of the NEU2 and NEU3 active sites.....	148
Figure 4.3: Molecular interactions of 4.8b.....	150
Figure 5.1: Compounds used in this study: GM3 (5.1), octyl-GM3 (5.2), octyl-lactoside (5.3), and 4MU-NANA (5.4).	174
Figure 5.2: NMR assignment of octyl-GM3.....	176
Figure 5.3: STD NMR Controls.....	183
Figure 5.4: NMR studies of octyl-GM3 in complex with NEU3(Y370F).....	185
Figure 5.5: NMR studies of octyl-GM3 in complex NEU3(Y370F), expansion of the carbohydrate region (3.2- 4.2 ppm).	186
Figure 5.7: STD NMR studies of 4MU-NANA in the presence of NEU3(Y370F).....	190
Figure 5.8: STD epitope map of 4MU-NANA (top) and comparison of MD and STD NMR results (bottom).	191
Figure 5.9: Molecular model of 4MU-NANA in the NEU3 active site.....	193
Figure 5.10: Molecular model of octyl-GM3 in the NEU3 active site..	195
Figure 5.11: Observed conformations of octyl-GM3 aglycone by MD.....	196
Figure 5.12: Homology map of the NEU3 model.....	203

List of schemes

Scheme 1.1: Structures of Neu5Ac (1.1) and KDN (1.2).	2
Scheme 1.2: Structure of viral sialidase inhibitors.	7
Scheme 1.3: Early inhibitors of human sialidases	20
Scheme 1.4: Human sialidase inhibitors synthesized by Chen and coworkers. ...	21
Scheme 1.5: Cores used in the sialyldendrimers study.....	22
Scheme 3.1: Synthesis of C9-Azide derivatives.	98
Scheme 3.2: Synthesis of N5Ac-azido and -triazolyl derivatives.....	99
Scheme 4.1: Inhibitor targets	139
Scheme 4.2: Synthesis of C4- and C4,C7-substituted DANA derivatives	140
Scheme 4.3: Synthesis of C7-substituted DANA derivatives.....	141

List of Abbreviations

4MU-NANA	2'-(4-methylumbelliferyl)- α -D- <i>N</i> -acetylneuraminic acid
BSA	bovine serum albumin
CAZy	carbohydrate active enzymes database
CuAAC	Cu-catalyzed azide–alkyne cycloaddition
DANA	2-deoxy-2,3-didehydro- <i>N</i> -acetylneuraminic acid
EDTA	ethylenediaminetetraacetic acid
EGFR	epidermal growth factor receptor
Gal	galactose
GH	glycosyl hydrolase
Glc	glucose
GST	glutathione S-transferase
GT	glycosyl transferase
hNEU	human neuraminidase enzyme
HPLC	high performance liquid chromatography
HRMS	high resolution mass spectrometry
IPTG	Isopropyl β -D-1-thiogalactopyranoside
KDN	2-keto-3-deoxy-D-glycero-D-galactonononic acid
LB	lysogeny broth
MBP	maltose binding protein
MD	molecular dynamics
MOPS	morpholinopropane sulfonic acid
NANA	<i>N</i> -acetylneuraminic acid

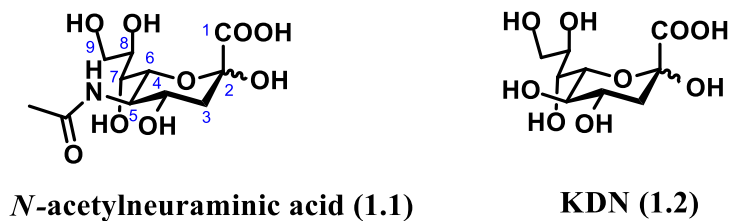
NEU	neuraminidase (Sialidase)
Neu5Ac	<i>N</i> -acetylneuraminic acid
NMR	nuclear magnetic resonance
OMIM	Online Mendelian Inheritance in Man
PCR	polymerase chain reaction
PDB	protein data bank
PPCA	protective protein/cathepsin A
RMS	root mean square
SAR	structure–activity relationship
SDM	site-directed mutagenesis
siRNA	small interfering RNA
ST	sialyl transferase
STD NMR	saturation transfer difference nuclear magnetic resonance
vcNEU	<i>Vibrio cholerae</i> sialidase
vNEU	viral sialidase

1 Introduction¹

¹ A portion of this chapter (Section 1.3) has been published: Albohy, A.; Mohan, S.; Zheng, R. X. B.; Pinto, B. M.; Cairo, C. W., Inhibitor selectivity of a new class of oseltamivir analogs against viral neuraminidase over human neuraminidase enzymes. *Bioorganic & Medicinal Chemistry* **2011**, *19* (9), 2817-2822.

1.1 Sialic Acids

Vertebrate glycoconjugates are composed mainly of hexoses or pentoses. One important exception is the sialic acids.¹ The sialic acids are not a single compound, but rather a family that constitute more than 50 members.² The common characteristic among sialic acids is that they are 9-carbon α -ketoacid sugars, also known as nonulosonic acids.³ The term, sialic acid is commonly used to refer to a specific compound, the most common sialic acid found in vertebrates which is 5-*N*-acetylneuraminic acid, [5-acetamido-2-keto-3,5-dideoxy-D-glycero-D-galactonononic acid] (**1.1**; Scheme 1.1) which is also abbreviated as Neu5Ac or NANA. Sialic acid was first reported by Blix and Klenk as a hydrolytic product of glycolipids or mucins which were later found to be the same material.⁴ In fact, the word sialic is derived from the Greek word sialos meaning saliva which was the source of mucins while the term ‘neuraminic acid’ is derived from neuro- which refers to the neurological source of the glycolipids.¹ Another commonly encountered sialic acid is KDN (**1.2**) [2-keto-3-deoxy-D-glycero-D-galactonononic acid].⁵ (Scheme 1.1)



Scheme 1.1: Structures of Neu5Ac (1.1) and KDN (1.2). Numbers shown on 1.1 will be used through the thesis.

Several characteristics make sialic acids unique structural components of glycoconjugates. Sialic acids are acidic sugars that will be negatively charged at physiological pH which makes them ideal for ionic interactions with other charged species such as amino acids. In addition, sialic acids are usually the terminal sugars in glycoconjugates which makes them accessible for intermolecular interactions.¹ The diversity of sialic acids is increased by several modifications which include acetylation, methylation, sulfonation and phosphorylation.⁶ The sialic acid linkage is another source of diversity. Four different sialyltransferase families have been reported in humans which includes ST3Gal, ST6Gal, ST6GalNAc, and ST8Sia. These four sialyltransferases form the different known sialic acids linkages.⁷ Sialic acids are also found in animals, fungi, protozoa, bacteria and viruses; but there is no evidence for sialic acids in plants.¹ Sialic acid metabolism varies between eukaryotes and bacteria,² but this subject is beyond the scope of this discussion.

1.2 Human sialidases

Sialidases, also known as neuraminidases (NEU), are a group of glycosidase enzymes that hydrolyze α -linked sialic acids.⁸ Sialidases have been found in mammals, bacteria, protozoa and viruses. They are classified into α -exosialidase (EC 3.2.1.18) or α -endosialidases (EC 3.2.1.129).⁹ Exosialidases can hydrolyze the glycosidic linked terminal sialic acids from glycoconjugates including oligosaccharides, glycoproteins, glycolipids, colominic acid and synthetic substrates. Endosialidases, on the other hand, can hydrolyze the internal glycosidic linkages in polysialyated compounds.⁹ In addition, β -sialidase activity

has been reported with some mutated enzymes such as the Y370G mutant of *Micromonospora viridifaciens* sialidase.¹⁰ Sialidases are classified according to their sequence similarities, a classification adopted by the carbohydrate active enzymes (CAZy) database.¹¹ In this classification the sialidases from influenza viruses are grouped in the Glycosyl Hydrolases family 34 (GH34). Most bacterial, human and protozoal sialidases are in GH33. Endosialidases are grouped in a separate family known as GH58.⁵

The first report of sialidase activity in humans was in a commercial preparations of bovine and human glycoproteins from Cohn Fraction VI.¹² The first mammalian sialidase to be expressed and purified was the mouse cytosolic sialidase in 1993.¹³ To date, four different sialidases are known in humans which are named as NEU1, NEU2, NEU3 and NEU4. This classification depends on their sequences and order of cloning and expression in humans. For example, NEU1 was first cloned by three different groups^{14,15,16} in 1996 and early 1997. This was followed by the cloning¹⁷ and expression¹⁸ of the human cytosolic NEU2 in 1999. NEU3 was cloned in 1999¹⁹ by Miyagi and then expressed the subsequent year by Monti and coworkers.²⁰ It was not until 2003 when NEU4 was found in mice,²¹ then in humans the following year.²²

Human sialidases differ in their sequences, expression, subcellular location and specificity. Although the four human sialidases have a conserved active site, the homology between them is not high. The most distinct is NEU1 which is only 28% homologous to NEU2 while the other three sialidase have a homology around 42-45 %.²³

Among the human sialidases, only NEU2 has been crystalized.^{24,25} Due to problems caused by aggregation and poor solubility of NEU3 and NEU4, as well as the need for a co-expression system for NEU1 (*vide infra*), attempts to crystalize other sialidases have failed so far. The lack of crystal structures limit the ability of researchers to study these enzymes and to design specific inhibitors, and thus experimental data on the structure of these enzymes can be critical. A solution for this limitation is to generate homology models for these enzymes using the NEU2 crystal structure as a template. A homology model was reported for NEU1, NEU3 and NEU4.²³ Unfortunately, the models generated were not made available. Also, the homology between NEU1 and NEU2 is only 28%, which is not enough to generate high quality models. In addition, these models were subjected only to minimization and 100 fs molecular dynamics with no evidence of convergence. We will discuss improved models of NEU3²⁶ and NEU4²⁷ which have been validated by more extensive modeling and site-directed mutagenesis by our group.

The human neuraminidase enzymes (hNEU) have tissue-specific expression. NEU1 is highly expressed in kidneys, pancreas, placenta, lungs, skeletal muscle, liver and brain. NEU2 is known to be expressed in muscle. NEU3 is mainly expressed in the adrenal gland, thymus, testis and heart. NEU4 has the highest expression in brain, skeletal muscle, heart, placenta, and liver.⁶ In general, NEU1 is the most highly expressed sialidase with 10-20 times higher expression than NEU3 and NEU4. NEU2 is the lowest-expressed sialidase based on real time PCR (RT-PCR) in human brain and lung.²⁸ In addition to variable tissue

expression, hNEU differ in their subcellular locations. For example, NEU1 and NEU3 are found at the plasma and lysosomal membranes; NEU2 is a cytosolic protein; and NEU4 is found associated with mitochondria.²⁹ Moreover, hNEU differ in their specificity and optimal pH. NEU3 has been found to have a preference for ganglioside substrates. NEU4 and NEU2 can hydrolyze oligosaccharides, glycolipids, and glycoproteins. NEU1 can hydrolyze glycoproteins and oligosaccharides.⁸ The optimal pH of the enzymes shows some significant differences. NEU2 is most active close to neutral pH (5.5-6.5), compared to the other three human sialidases which are most active close to pH 4.5 (Figure 1.1).³⁰

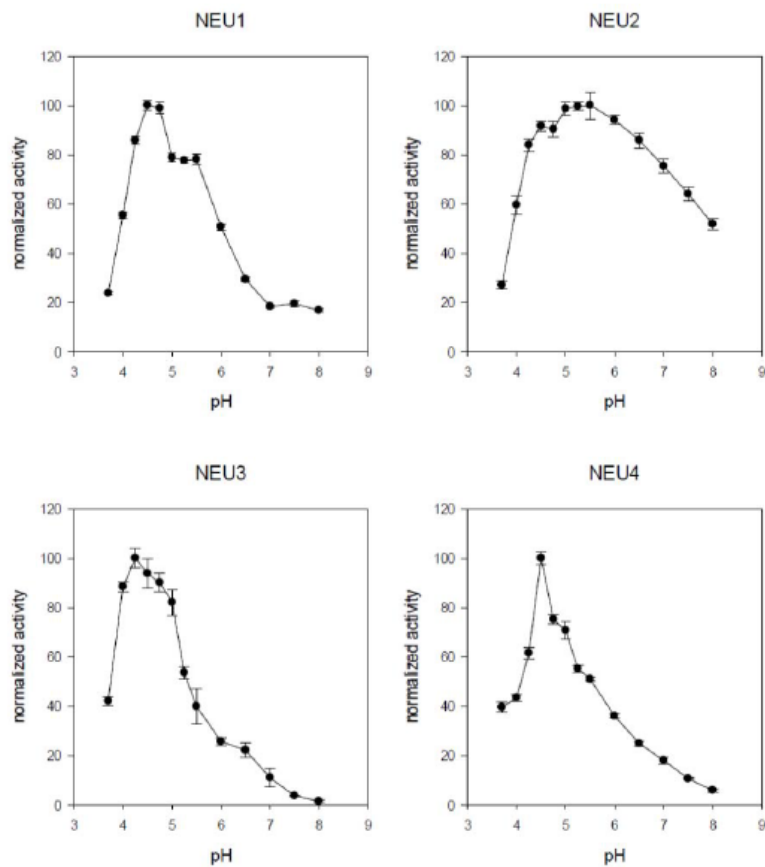


Figure 1.1: pH profiles of the four human sialidases.³⁰ Relative enzyme activity was determined by cleavage of 4MU-NANA substrate.

1.3 Human versus viral sialidases

The development of anti-viral drugs against influenza infection continues to be a major area of research in medicinal chemistry.³¹ The most successful small molecule anti-influenza strategies have targeted the viral neuraminidase enzymes (vNEU), members of glycosyl hydrolase family 34 which cleave terminal *N*-5-acetyl-neuraminic acid (Neu5Ac) residues from host glycoproteins (EC3.2.1.18).¹¹ The most successful vNEU inhibitors are proposed transition-state mimics based on 2-deoxy-2,3-didehydro-*N*-5-acetylneuraminic acid (**1.3**)

The nine influenza type A neuraminidase enzyme isoforms are classified into two groups. Interestingly, members of group-1 contain an additional pocket adjacent to the substrate binding site which is not found in group-2 enzymes, known as the 150-pocket (*Figure 1.2a*).³⁵

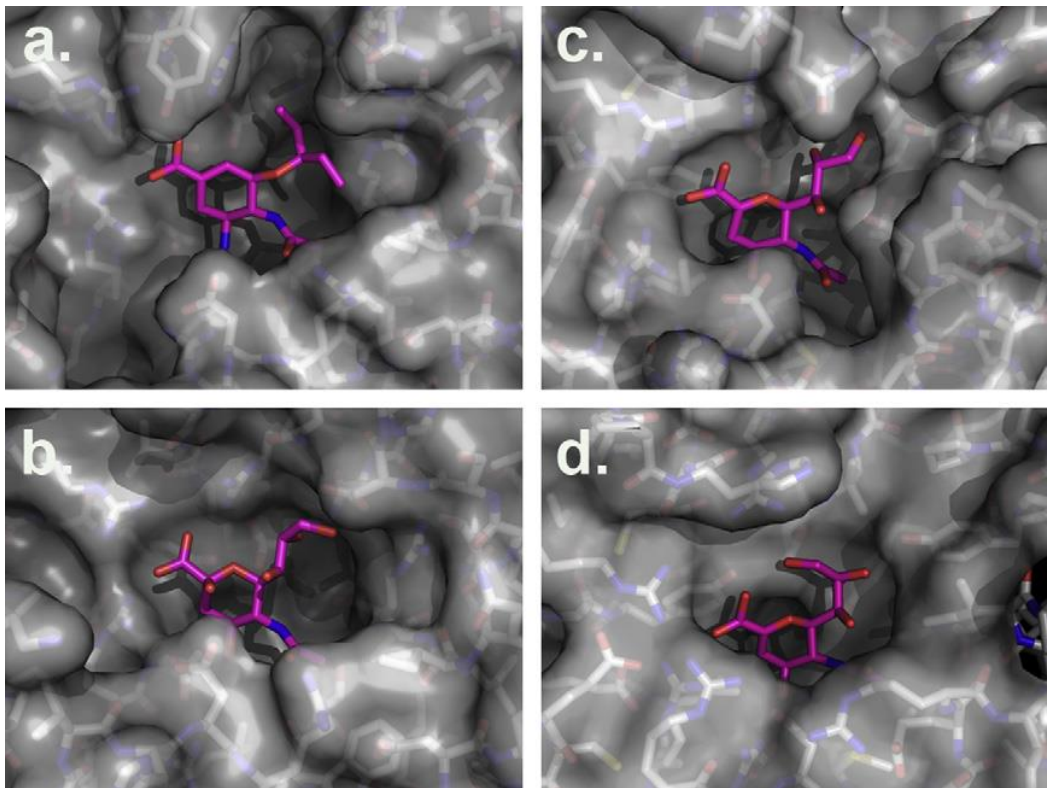


Figure 1.2: Active site topology of NEU enzymes: The active site topology of viral and mammalian neuraminidases show distinct differences. (a) The viral N8 isoform can adopt an open conformation which exposes the 150-pocket (in the lower left quadrant) adjacent to the C5 position. The enzyme is shown in complex with oseltamivir (PDB: 2HT7).³⁵ (b) The viral N2 enzyme is shown in complex with sialic acid (PDB: 2BAT).³⁶ Note that the 150-pocket is not present. (c) The mammalian NEU2 enzyme is shown in complex with DANA (PDB: 1VCU).²⁴ (d) A homology model of NEU3 is shown in complex with DANA.²⁶

This observation has led to the design of compounds which can take advantage of this feature to improve inhibitor affinity.^{37,38,39} Such strategies may help to avoid viral resistance by providing alternative lead compounds.⁴⁰ Structure-based drug design of inhibitors against hNEU has relied on the crystal structure of NEU2,^{41,42,43,25,44} which remains the only member of the family which has been crystallized.^{25,24} The high homology within the family has been used to construct models of the remaining three isoforms.^{23,26} A number of mutations in NEU1 lend support to the predictions of the homology model,^{45,46,47} and the NEU3 and NEU4 model has been tested directly using site-directed mutagenesis.^{48,26}

There have been few studies which have tested the activity of synthetic inhibitors against the hNEU, and fewer still to compare activity between the eukaryotic and viral enzymes. The activity of oseltamivir, zanamivir, and DANA against the hNEU isoforms has been previously examined.²⁸ Zanamivir was found to be a micromolar inhibitor of NEU2 and NEU3, and DANA showed micromolar activity against NEU2, NEU3 and NEU4. Importantly, oseltamivir was found to be inactive against all of the hNEU enzymes. This finding suggested that the C7–C9 binding pocket of the human enzymes are distinct from that of the viral enzymes. Synthetic derivatives of DANA which incorporate C9 modifications have been found to be active against NEU1⁴¹ and NEU3.⁴³

Inhibitors of vNEU have recently been designed to take advantage of the 150-pocket found in group-1 enzymes. Wen et al. designed inhibitors which included modifications of the C4 group of zanamivir with IC₅₀ values of ~2 μM.³⁸

Mohan et al. have reported a series of oseltamivir analogs which incorporated a 1,2-olefin and a series of *C3* substituents. When tested against vNEU, the best of the *C3* triazole-modified compounds showed slightly reduced potency (5, $K_i = 72$ nM) as compared to zanamivir ($K_i = 0.2$ nM). Critically, these results confirmed that one could access the 150-cavity through the replacement of the *C5*-amino group with functionalized triazole substituents on the oseltamivir-like template and still maintain high potency. These compounds provide, therefore, an essential new lead for vNEU inhibitor design. These compounds were tested against NEU3 and NEU4 and found not to interfere with these human sialidases.⁸²

1.4 Physiological and pathological roles of human sialidases

The presence of multiple neuraminidase isozymes could be used by cells to control a range of physiological processes. Sometimes these isozymes could play opposing roles through different pathways. For example, NEU1 and NEU3 were found to play opposing roles in $\beta 4$ integrin-mediated signaling in colon cancer cells. NEU1 was found to be important in the regulation of $\beta 4$ integrin-mediated signaling in HT-29 colon cancer cells, leading to suppression of metastasis.⁴⁹ On the other hand, NEU3 was found to regulate cell proliferation through $\beta 4$ integrin signaling on laminin-5 in DLD-1 colon cancer cells. This leads to acceleration in the malignancy of cancer cells.⁵⁰ These findings show that NEU1 and NEU3 act on the similar targets to give different effects.⁸ The presence of hNEU isoforms makes the identification of selective inhibitors critical for understanding their biological roles.

The NEU1 isoenzyme is the only hNEU for which genetic disorders have been reported. This may be a result of the overlapping roles played by different sialidase isoenzymes.⁶ A NEU2 nonsynonymous polymorphism (R41Q) found in the Asian population was found to increase NEU2 inhibition by oseltamivir, a viral sialidase inhibitor. Although still being debated, this nonsynonymous polymorphism has been proposed to result in neurological side effects seen in this specific population.⁵¹

A Neu3 knockout mouse was found to be healthy and showed normal ganglioside patterns, which the authors explained by possible redundancy with NEU4.⁵² The mouse was even less susceptible to drugs that induced colitis in the colon as compared to the wild type mice. On the other hand, a Neu4 knockout mouse was found to have an altered ganglioside profile in the brain with vacuolized cells in spleen and lungs.⁵³

1.4.1 NEU1

The human sialidase (NEU1) is currently proposed to have two main functions. NEU1 plays a role in the catabolism of sialylated glycoconjugates in the lysosome and it has also a role in the cellular immune response.⁴⁵ Inside the lysosome, NEU1 is found associated with β -galactosidase and protective protein/cathepsin A (PPCA) as a complex. Dissociation of this complex leads to loss of the sialidase activity.⁸ Two diseases are associated with NEU1 malfunction, named sialidosis (OMIM# 256550) and galactosialidosis (OMIM# 256540). Each disease is caused by different genetic defects. Sialidosis is an autosomal recessive disorder which is the result of frame shift insertions and

missense mutations in the sialidase gene, whereas galactosialidosis is caused by mutations in the gene coding for cathepsin A leading to a combined inactive NEU1 and β -galactosidase.⁴⁵ There are two types of sialidosis, the mild late onset type I and the severe early onset type II. Type I patients develop visual defects, myoclonus syndrome and seizures, while type II patients have added mental retardation and hepatosplenomegaly symptoms.⁴⁵

Recently, it was found that NEU1 in an active form is expressed in the human airway epithelia which can regulate epidermal growth factor receptor (EGFR) and mucin 1 (MUC1) dependent signaling and bacterial adhesion. This indicates that NEU1 catalytic activity might be another way of regulating the airway epithelial cells response to ligands, pathogens, and injury.⁵⁴ Furthermore, it was found that epithelial cells in the lung express NEU3 in addition to NEU1, and that NEU1 plays a role in the remodeling of epithelial tissue after injury by restraining cell migration.⁵⁵

NEU1 has also been proposed to play a role in asthma. Studies in the NEU1 deficient mouse strain (SM/J) suggested that there was an induction of the hyaluronic acid (HA) receptor binding to CD4⁺ T helper cells which was inhibited by sialidase inhibitors. This finding supported the proposal that T helper-mediated airway inflammation in asthmatic patients is dependent on NEU1.⁵⁶

Recently, NEU1, as well as NEU3, were found on the membrane of human erythrocytes. Interestingly, NEU1 was found separate from the usual complex with PPCA. The two enzymes are released by alkaline treatment giving

active sialidase enzymes. In addition, both enzymes are progressively lost with erythrocyte aging. It is not clear what function these sialidases have in erythrocytes, but the authors suggested that the continuous loss of enzyme activity during erythrocyte life could be a way to prevent erythrocyte sialic acid degradation to avoid early ageing of erythrocyte.⁵⁷

1.4.2 NEU2

Human cytosolic sialidase NEU2 was the first in the family to be crystalized.²⁴ Because of the low expression level mentioned earlier, it is unclear what role NEU2 plays in the human cells.⁸ Despite this fact, several physiological roles have been linked to NEU2. Unlike other sialidases, NEU2 is able to hydrolyze a wider variety of substrates near the neutral pH.⁸

Although NEU2 is highly expressed in skeletal muscle, it is unclear what role it may play in these cells. NEU2 is up-regulated during the differentiation of C2C12 myoblasts. When these cells were transfected with the Neu2 gene, over-expressing cells were able to spontaneously start differentiation under standard growth conditions.⁵⁸ This effect is regulated at least in part by the effect of insulin-like growth factor 1 signaling.⁵⁹ In addition, it was found that NEU2 was degraded in myotubes by lysosomal enzymes in the case of myoblast atrophy.⁶⁰

In addition, NEU2 transcription was found to be induced in PC12 cells on treatment with neuronal differentiation growth factors such as nerve growth factor and fibroblast factor 2. Since PC12 cells are a good model for neuronal differentiation, this suggests that NEU2 also plays a role in neuron development.⁶¹ Furthermore, myeloid leukemic K562 cells have suppressed levels of sialidase

NEU2. If Neu2 was transfected into K562 cells, a marked decrease in antiapoptotic factors such as Bcl-XL and Bcl-2 was observed. This effect could increase the susceptibility of cells to apoptosis and decrease proliferation rates.⁶² Also, transfection of B16 melanoma cells with Neu2 resulted in the suppression of pulmonary metastasis.⁶³

1.4.3 NEU3

NEU3 was first characterized and expressed in 1999 and characterized as a plasma membrane associated-sialidase specific for hydrolyzing gangliosides.¹⁹ Since then, this important enzyme has been linked to several physiological and pathological roles. NEU3 was found to be over-expressed in human colon cancer cells with significant elevation of sialidase activity. This change was associated with accumulation of lactosylceramide and protection against programmed cell death (apoptosis).⁶⁴ In terms of adhesion, NEU3 was found to control colon cell (DLD-1) adhesion through two different pathways depending on the extracellular matrix. NEU3 was found to increase adhesion to laminin but at the same time decrease adhesion to integrin leading to a differential control of cell proliferation.⁵⁰ In addition, NEU3 transgenic mice were found to be more susceptible to azoxymethane (dimethyldiazene-1-oxide) induced lesions,⁶⁵ while NEU3-lacking mice showed reduced susceptibility to colitis-associated colon carcinogenesis.⁵²

Similar results have been seen in other cancer types. For example, renal cell carcinoma, ACHN cells, showed NEU3 up-regulation compared to adjacent non-tumor tissue. This resulted in an increase of cell motility and reduction of

apoptosis through the interleukin-6 (IL-6) pathway.⁶⁶ NEU3 expression was also found to be higher in prostate cancer tissue and cell lines compared to normal prostate tissue. Silencing NEU3 with siRNA resulted in reduction of invasion and migration. NEU3 siRNA was successfully used as a gene therapy in mice to prevent metastasis. A reduction in bone metastasis in mice previously injected with prostate cancer cells (PC-3M) was seen after treating the mice with attenuated salmonella carrying NEU3 siRNA.⁶⁷ NEU3 was also found to control the progression of prostate cancer into the more resistant androgen independent forms through the androgen receptor signaling pathway.⁶⁸ In addition, over-expression of NEU3 in mice muscle tissue led to the development of diabetic symptoms associated with hyperinsulinemia and increased beta-cell mass. Compared with the wild type, insulin-receptor sensitivity was significantly reduced.⁶⁹ On the other hand, hepatic NEU3 over-expression improved glucose tolerance and insulin sensitivity in the insulin-resistant KKAY mice.⁷⁰ These results demonstrate that NEU3 plays complex and important roles in the control of blood sugar which may require further investigation.

1.4.4 NEU4

Human sialidase NEU4 was the last mammalian sialidase to be discovered in mouse²¹ and human.²² It was found that NEU4 can clear accumulated stored material from the lysosomes of cells with sialidosis and galactosialidosis. This suggests that NEU4 could be the basis for new therapies against these conditions.⁷¹ NEU4 knockout mice were found to be morphologically normal, but had marked lysosomal storage and vacuolization in spleen and lung cells. This

finding suggested a role for NEU4 in glycolipid catabolism.⁵³ On the other hand, mice deficient in both NEU4 and hexoaminidase A suffered epileptic seizures and neuronal degeneration with the accumulation of multiple layers of GM2 gangliosides. This suggests that NEU4 can reduce the severity of Tay-Sachs disease in the mouse model through metabolic bypass.⁷² There is some debate about the subcellular localization of NEU4. Seyrantepe suggested that NEU4 is a lysosomal lumen sialidase playing a role in the glycolipid catabolism.^{71,73} More recently, NEU4 was found to have two different forms, a short form and a long form (NEU4L) that has 12 extra amino acids at the *N*-terminus. This peptide is believed to be a mitochondrial targeting sequence. The short form of NEU4 lacking these peptides was found to localize in the endoplasmic reticulum.^{74,75} NEU4 also plays a role in the pathogenesis of colon cancer. It was found that down regulation of NEU4 in human colon cancer cells may contribute to their invasive properties.⁷⁶ In addition, NEU4 expression was decreased during retinoic acid-induced differentiation of Neuro2a cells. Suppression of neurite formation was also seen when NEU4 was over-expressed.⁷⁷

Thymoquinone was found to activate NEU4 in different cell types including fibroblasts, macrophages and dendritic cells. This activation is proposed to be through a membrane targeting of G alpha i subunit of the protein G coupled receptor and through matrix metalloproteinase-9 activation.⁷⁸ This activation was found to play a role in macrophages and pro-inflammatory cytokines activation *in-vivo*.⁷⁹

1.5 Expression systems and purification methods used for the human sialidases

NEU1 was first expressed in human skin fibroblasts WG544 transfected with the pCMV vector carrying the Neu1 gene.¹⁶ In some studies, NEU1 has been used as a cell homogenate without further purification. Part of the problem is that in order to have active NEU1, the enzyme must be in complex with other enzymes (*vide supra*).

Human NEU2 was first expressed by Monti and coworkers in COS-7 cells transfected with the pCDL-NEU2 expression vector. They reported that there was no evidence of peptide glycosylation. To get larger amounts of the enzyme, it was expressed in *E. coli* transfected with the gene carried in the pGEX-2T vector and then purified by a glutathione S-transferase (GST) affinity column. This was followed by release of the tag using thrombin cleavage to give a pure band at 43 kDa.¹⁸ This is the same procedure used for NEU2 crystalized by Chavas and coworkers, but with extra purification steps with anionic and cationic chromatography.²⁴ Earlier expression of mammalian cytosolic sialidases such as that of rats in *E. coli*¹³ and Chinese hamster from CHO cells⁸⁰ have also been reported. We have also reported the expression of NEU2 as a maltose binding protein (MBP) tagged protein in *E. coli* using the pMAL expression vector.³⁰

Human NEU3 was first expressed by Monti and coworkers in 2000. They used COS-7 cells transfected with the pCDL-NEU3 expression vector.²⁰ NEU3 carried in the pME18S vector was also expressed in COS-1 cells and purified over a HiTrap Ni²⁺ column.⁸¹ Four years later, expression and purification in *E. coli*

was reported by Ha et al. using the pRESTc-NEU3 vector and then purified on a Ni²⁺-NTA column.⁴⁸ This gave a pure protein band at about 48 kDa with better yields compared to expression in COS-7 or COS-1 cells. Our group also expressed NEU3 as an MBP-NEU3 tagged protein from *E. coli*.²⁶

NEU4 from rat brain was the first mammalian NEU4 to be isolated and expressed in COS-7 cells using the pcDNA3-NEU4 vector.²¹ This was followed by expression of human NEU4 in the same cell line.²² We reported the expression of NEU4 in *E. coli* as a GST-fusion protein.⁸²

It is important here to mention that several labs working in the area of human sialidase inhibitors are using cell homogenates instead of the purified proteins. For example, Magesh et al. were able to over-express the four human sialidases in HEK-293 cells, but chose to use cell homogenate for their assays.⁴¹ This raises the concern that inhibition studies may be confounded by the presence of multiple isoenzymes.

1.6 Inhibition of human sialidase enzymes

In contrast to the viral sialidases which have gained a great deal of research interest due to viral pathology, human sialidases have had a limited number of investigations into small molecule inhibitors. The ultimate goal of human sialidase inhibition would be to have a potent and selective inhibitor for each of the four sialidase enzymes. These inhibitors would be powerful tools for determining the contributions of each isoenzyme to human glycobiology. To date, the number of potent selective human sialidase inhibitors is very small. Research in the area of human sialidase inhibitors has been delayed due to the limitations

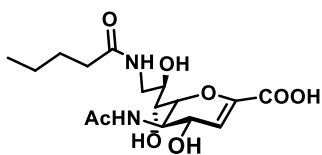
associated with inhibitor assays. Most prominent among these is the lack of robust expression systems for each of the four enzymes in purified form. Additionally, the chemical synthesis of new inhibitors can be challenging, and the lack of crystal structures for three out of the four human sialidases limits structure-based design approaches.

The first work in this area was started by testing the known viral inhibitors against human sialidases. Hata et al. tested zanamivir and oseltamivir carboxylate against a human sialidase enzymes purified by FLAG-affinity column.²⁸ They found that oseltamivir carboxylate was not able to inhibit any of the 4 enzymes even up to 1 mM concentrations. Zanamivir on the other hand was able to inhibit NEU2 and NEU3 with low micromolar inhibitory constant (K_i). Ha et al. also tested DANA which is a general sialidase inhibitor and found it to be a nonspecific micromolar inhibitor.²⁸

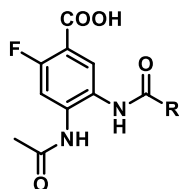
New inhibitors were first introduced as modifications of the DANA scaffold. A series of *C9* modified DANA amides were prepared by Kiso and coworkers and tested for their inhibition for the human sialidases. The best hit was the *n*-butyl derivative (**1.7**) (Scheme 1.3) which showed an IC_{50} of 10 μ M against NEU1 with no inhibition for the other three sialidases up to 1 mM. Interestingly, the compounds were tested at only four concentrations from 50 μ M to 1 mM and then IC_{50} curves were plotted. Another caveat regarding these results is that the enzymes used were not purified, but instead were cell homogenates that may have contained multiple isoenzymes.⁴¹

In 2009, Magesh and coworkers tried to develop the first non-sugar analogs of DANA based on a benzoic acid motif. They synthesized a series of 4-acetamido-5-acylamido-2-fluoro benzoic acids (**1.8**) and tested them against homogenates of HEK-293 cells transfected with different human sialidase genes. The prepared compounds were tested at 1 mM concentration and none of them showed any potent activity against the human sialidases.⁴²

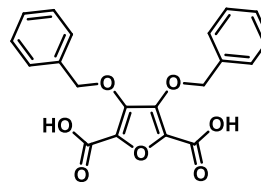
Virtual screening was also used as a method to generate new scaffolds for sialidase inhibitors. Starting from a database of 72,766 compounds and through an iterative selection approach a final compound was chosen and tested as an inhibitor for the human sialidases. The resulting molecule, 3,4-di(benzyloxy)furan-2,5-dicarboxylic acid (**1.9**), showed the best inhibition with NEU4 at an IC₅₀ of 670 μM.⁸³



n-butyl derivative at the C9 position of DANA (**1.7**)



4-acetamido-5-acylamido-2-fluoro benzoic acids (**1.8**)

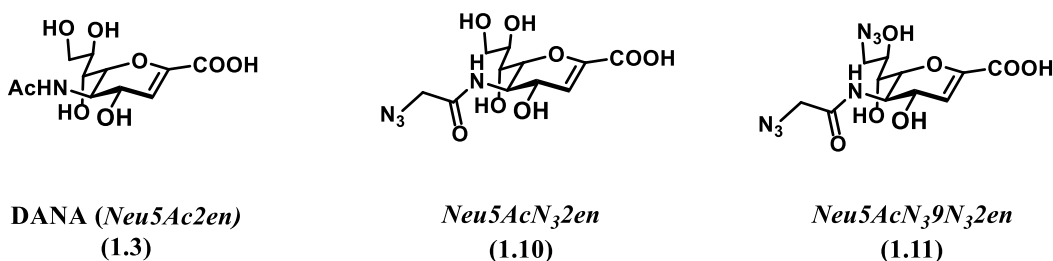


3,4-di(benzyloxy)furan-2,5-dicarboxylic acid (**1.9**)

Scheme 1.3: Early inhibitors of human sialidases.^{41, 42, 83}

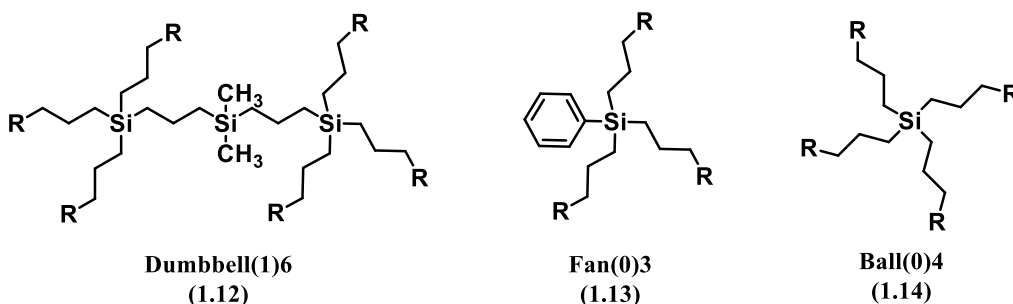
Chen and coworkers have also investigated derivatives of DANA that may act as inhibitors of NEU2. They synthesized several azido derivatives of DANA (Neu5Ac2en) (**1.10**) and then evaluated them against NEU2 and bacterial sialidases. In 2010, Chen and coworkers reported testing C5-modified DANA against NEU2 and bacterial sialidases. They found the N5-azidoacetyl derivative

(Neu5AcN₃2en) was selective for NEU2 over bacterial sialidases tested including *V. cholera* sialidase (V.C.) and *Salmonella typhimurium* sialidase (S.T.) using *p*-nitrophenyl-tagged $\alpha(2-3)$ - and $\alpha(2-6)$ -linked sialosides.⁸⁴ However, no selectivity among the human sialidase enzymes was tested. In 2012, Chen and coworkers also reported several other similar modifications at the C9- or both the C9- and N5- DANA derivatives. Addition of an azido group at both the N5 and C9 positions (Neu5AcN₃9N₃2en) (**1.11**) gave the best inhibitors with the highest potency against NEU2 and best selectivity over several other bacterial sialidases tested.⁸⁵ (See Scheme 1.4)



Scheme 1.4: Human sialidase inhibitors synthesized by Chen and coworkers.^{84,85}

Recently several synthetic sialyl dendrimers have been made and evaluated against recombinant NEU2 to test the effect of multivalency on inhibition.⁸⁶ Three carbosilane scaffolds (Scheme 1.5) have been tested including Dumbbell(1)6-S-Neu5Ac₆ (**1.12**), Fan(0) 3-S-Neu5Ac₃ (**1.13**) and Ball(0)4-S-NeuAc₄ (**1.14**). Among them, Dumbbell(1)6-SNeu5Ac₆ exhibited the most potent inhibitory activity with an IC₅₀ of 0.4-0.5 mM. These values are 6-7 times larger than the IC₅₀ of DANA under the same conditions (0.069 mM)⁸⁶



Scheme 1.5: Cores used in the sialyldendrimers study.⁸⁶

Later in this thesis (Chapters 3, and 4) we will present the development of several selective and potent inhibitors tested against the four human sialidase. These inhibitors could be used as tools to selectively inhibit one enzyme over the others which would allow for to the study of specific roles played by them. In addition, these inhibitors could be used as the basis for the design and development of important therapeutics in cancer progression and metastasis.

1.7 Project objectives

This thesis will first explore the active site topology of human sialidase enzymes (Chapter 2). These studies will develop a detailed understanding of substrate recognition of the enzymes, including experimental validation of these interactions using site-directed mutagenesis, STD NMR, and substrate kinetics (Chapter 2-5). We also present the design and preparation of highly potent and selective inhibitors for the human sialidase isoenzymes NEU2, NEU3, and NEU4 (Chapters 3 and 4). These studies represent significant strides towards specific inhibitors that can be used to investigate the different roles played by these enzymes. In addition, these tools could be used as probes to detect or label (with some modifications) different human sialidasases.

1.8 References

1. Angata, T.; Varki, A., Chemical diversity in the sialic acids and related alpha-keto acids: An evolutionary perspective. *Chemical Reviews* **2002**, *102* (2), 439-469.
2. Li, Y. H.; Chen, X., Sialic acid metabolism and sialyltransferases: natural functions and applications. *Applied Microbiology and Biotechnology* **2012**, *94* (4), 887-905.
3. Varki, A.; Cummings, R. D.; Esko, J. D.; Freeze, H. H.; Stanley, P.; Bertozzi, C. R.; Hart, G. W.; Etzler, M. E., *Essentials of glycobiology*. 2nd ed.; Cold Spring Harbor Laboratory Press: NY, 2009.
4. Blix, G., Sialic acid and neuraminic acid. *Acta Chemica Scandinavica* **1956**, *10* (1), 157-157.
5. Chen, X.; Varki, A., Advances in the biology and chemistry of sialic acids. *ACS Chemical Biology* **2010**, *5* (2), 163-176.
6. Pshezhetsky, A. V.; Ashmarina, L. I., Desialylation of surface receptors as a new dimension in cell signaling. *Biochemistry-Moscow* **2013**, *78* (7), 736-745.
7. Harduin-Lepers, A.; Mollicone, R.; Delannoy, P.; Oriol, R., The animal sialyltransferases and sialyltransferase-related genes: a phylogenetic approach. *Glycobiology* **2005**, *15* (8), 805-817.
8. Miyagi, T.; Yamaguchi, K., Mammalian sialidases: Physiological and pathological roles in cellular functions. *Glycobiology* **2012**, *22* (7), 880-896.
9. Schomburg, I.; Chang, A.; Placzek, S.; Sohngen, C.; Rother, M.; Lang, M.; Munaretto, C.; Ulas, S.; Stelzer, M.; Grote, A.; Scheer, M.; Schomburg, D.,

BRENDA in 2013: integrated reactions, kinetic data, enzyme function data, improved disease classification: new options and contents in BRENDA. *Nucleic Acids Research* **2013**, *41* (D1), D764-D772.

10. Watson, J. N.; Indurugalla, D.; Cheng, L. L.; Narine, A. A.; Bennet, A. J., The hydrolase and transferase activity of an inverting mutant sialidase using non-natural beta-sialoside substrates. *Biochemistry* **2006**, *45* (44), 13264-13275.

11. Cantarel, B. L.; Coutinho, P. M.; Rancurel, C.; Bernard, T.; Lombard, V.; Henrissat, B., The Carbohydrate-Active EnZymes database (CAZy): an expert resource for Glycogenomics. *Nucleic Acids Research* **2009**, *37*, D233-D238.

12. Warren, L.; Spearing, C. W., Mammalian sialidase (neuraminidase). *Biochemical and Biophysical Research Communications* **1960**, *3* (5), 489-492.

13. Miyagi, T.; Konno, K.; Emori, Y.; Kawasaki, H.; Suzuki, K.; Yasui, A.; Tsuiki, S., Molecular cloning and expression of cDNA-encoding rat skeletal-muscle cytosolic sialidase. *Journal of Biological Chemistry* **1993**, *268* (35), 26435-26440.

14. Bonten, E.; vanderSpoel, A.; Fornerod, M.; Grosveld, G.; dAzzo, A., Characterization of human lysosomal neuraminidase defines the molecular basis of the metabolic storage disorder sialidosis. *Genes & Development* **1996**, *10* (24), 3156-3169.

15. Milner, C. M.; Smith, S. V.; Carrillo, M. B.; Taylor, G. L.; Hollinshead, M.; Campbell, R. D., Identification of a sialidase encoded in the human major histocompatibility complex. *Journal of Biological Chemistry* **1997**, *272* (7), 4549-4558.

16. Pshezhetsky, A. V.; Richard, C.; Michaud, L.; Igdoura, S.; Wang, S. P.; Elsliger, M. A.; Qu, J. Y.; Leclerc, D.; Gravel, R.; Dallaire, L.; Potier, M., Cloning, expression and chromosomal mapping of human lysosomal sialidase and characterization of mutations in sialidosis. *Nature Genetics* **1997**, *15* (3), 316-320.
17. Monti, E.; Preti, A.; Rossi, E.; Ballabio, A.; Borsani, G., Cloning and characterization of NEU2, a human gene homologous to rodent soluble sialidases. *Genomics* **1999**, *57* (1), 137-143.
18. Monti, E.; Preti, A.; Nesti, C.; Ballabio, A.; Borsani, G., Expression of a novel human sialidase encoded by the NEU2 gene. *Glycobiology* **1999**, *9* (12), 1313-1321.
19. Miyagi, T.; Wada, T.; Iwamatsu, A.; Hata, K.; Yoshikawa, Y.; Tokuyama, S.; Sawada, M., Molecular cloning and characterization of a plasma membrane-associated sialidase specific for gangliosides. *Journal of Biological Chemistry* **1999**, *274* (8), 5004-5011.
20. Monti, E.; Bassi, M. T.; Papini, N.; Riboni, M.; Manzoni, M.; Venerando, B.; Croci, G.; Preti, A.; Ballabio, A.; Tettamanti, G.; Borsani, G., Identification and expression of NEU3, a novel human sialidase associated to the plasma membrane. *Biochemical Journal* **2000**, *349*, 343-351.
21. Comelli, E. M.; Amado, M.; Lustig, S. R.; Paulson, J. C., Identification and expression of Neu4, a novel murine sialidase. *Gene* **2003**, *321*, 155-161.
22. Monti, E.; Bassi, M. T.; Bresciani, R.; Civini, S.; Croci, G. L.; Papini, N.; Riboni, M.; Zanchetti, G.; Ballabio, A.; Preti, A.; Tettamanti, G.; Venerando, B.;

Borsani, G., Molecular cloning and characterization of NEU4, the fourth member of the human sialidase gene family. *Genomics* **2004**, 83 (3), 445-453.

23. Magesh, S.; Suzuki, T.; Miyagi, T.; Ishida, H.; Kiso, M., Homology modeling of human sialidase enzymes NEU1, NEU3 and NEU4 based on the crystal structure of NEU2: Hints for the design of selective NEU3 inhibitors. *Journal of Molecular Graphics & Modelling* **2006**, 25 (2), 196-207.

24. Chavas, L. M. G.; Tringali, C.; Fusi, P.; Venerando, B.; Tettamanti, G.; Kato, R.; Monti, E.; Wakatsuki, S., Crystal structure of the human cytosolic sialidase Neu2 - Evidence for the dynamic nature of substrate recognition. *Journal of Biological Chemistry* **2005**, 280 (1), 469-475.

25. Chavas, L. M. G.; Kato, R.; Suzuki, N.; von Itzstein, M.; Mann, M. C.; Thomson, R. J.; Dyason, J. C.; McKimm-Breschkin, J.; Fusi, P.; Tringali, C.; Venerando, B.; Tettamanti, G.; Monti, E.; Wakatsuki, S., Complexity in influenza virus targeted drug design: interaction with human sialidases. *Journal of Medicinal Chemistry* **2010**, 53 (7), 2998-3002.

26. Albohy, A.; Li, M. D.; Zheng, R. B.; Zou, C.; Cairo, C. W., Insight into substrate recognition and catalysis by the human neuraminidase 3 (NEU3) through molecular modeling and site-directed mutagenesis. *Glycobiology* **2010**, 20 (9), 1127-1138.

27. Albohy, A.; Zhang, Y.; Smutova, V.; Pshezhetsky, A. V.; Cairo, C. W., Identification of selective nanomolar inhibitors of the human neuraminidase, NEU4. *ACS Medicinal Chemistry Letters* **2013**, 4 (6), 532-537.

28. Hata, K.; Koseki, K.; Yamaguchi, K.; Moriya, S.; Suzuki, Y.; Yingsakmongkon, S.; Hirai, G.; Sodeoka, M.; von Itzstein, M.; Miyagi, T., Limited inhibitory effects of oseltamivir and zanamivir on human sialidases. *Antimicrobial Agents and Chemotherapy* **2008**, *52* (10), 3484-3491.
29. Monti, E.; Preti, A.; Venerando, B.; Borsani, G., Recent development in mammalian sialidase molecular biology. *Neurochemical Research* **2002**, *27* (7-8), 649-663.
30. Zhang, Y.; Albohy, A.; Zou, Y.; Smutova, V.; Pshezhetsky, A. V.; Cairo, C. W., Identification of selective inhibitors for human neuraminidase isoenzymes using C4,C7-modified 2-deoxy-2,3-didehydro-N-acetylneuraminic acid (DANA) analogues. *Journal of Medicinal Chemistry* **2013**, *56* (7), 2948-2958.
31. von Itzstein, M., The war against influenza: discovery and development of sialidase inhibitors. *Nature Reviews Drug Discovery* **2007**, *6* (12), 967-974.
32. Schauer, R., Origin and biological role of the great chemical diversity of natural sialic acids. *Trends in Glycoscience and Glycotechnology* **1997**, *9* (48), 315-330.
33. Altschul, S. F.; Madden, T. L.; Schaffer, A. A.; Zhang, J. H.; Zhang, Z.; Miller, W.; Lipman, D. J., Gapped BLAST and PSI-BLAST: a new generation of protein database search programs. *Nucleic Acids Research* **1997**, *25* (17), 3389-3402.
34. Buschiazzo, A.; Alzari, P. M., Structural insights into sialic acid enzymology. *Current Opinion in Chemical Biology* **2008**, *12* (5), 565-572.

35. Russell, R. J.; Haire, L. F.; Stevens, D. J.; Collins, P. J.; Lin, Y. P.; Blackburn, G. M.; Hay, A. J.; Gamblin, S. J.; Skehel, J. J., The structure of H5N1 avian influenza neuraminidase suggests new opportunities for drug design. *Nature* **2006**, *443* (7107), 45-49.
36. Varghese, J. N.; McKimmbreschkin, J. L.; Caldwell, J. B.; Kortt, A. A.; Colman, P. M., The structure of the complex between influenza-virus neuraminidase and sialic-acid, the viral receptor. *Proteins-Structure Function and Genetics* **1992**, *14* (3), 327-332.
37. Mohan, S.; McAtamney, S.; Haselhorst, T.; von Itzstein, M.; Pinto, B. M., Carbocycles Related to Oseltamivir as Influenza Virus Group-1-Specific Neuraminidase Inhibitors. Binding to N1 Enzymes in the Context of Virus-like Particles. *Journal of Medicinal Chemistry* **2010**, *53* (20), 7377-7391.
38. Wen, W.-H.; Wang, S.-Y.; Tsai, K.-C.; Cheng, Y.-S. E.; Yang, A.-S.; Fang, J.-M.; Wong, C.-H., Analogs of zanamivir with modified C4-substituents as the inhibitors against the group-1 neuraminidases of influenza viruses. *Bioorganic & Medicinal Chemistry* **2010**, *18* (11), 4074-4084.
39. Rudrawar, S.; Dyason, J. C.; Rameix-Welti, M.-A.; Rose, F. J.; Kerry, P. S.; Russell, R. J. M.; van der Werf, S.; Thomson, R. J.; Naffakh, N.; von Itzstein, M., Novel sialic acid derivatives lock open the 150-loop of an influenza A virus group-1 sialidase. *Nature Communications* **2010**, *1*.
40. Collins, P. J.; Haire, L. F.; Lin, Y. P.; Liu, J.; Russell, R. J.; Walker, P. A.; Skehel, J. J.; Martin, S. R.; Hay, A. J.; Gamblin, S. J., Crystal structures of

oseltamivir-resistant influenza virus neuraminidase mutants. *Nature* **2008**, 453 (7199), 1258-U61.

41. Magesh, S.; Moriya, S.; Suzuki, T.; Miyagi, T.; Ishida, H.; Kiso, M., Design, synthesis, and biological evaluation of human sialidase inhibitors. Part 1: Selective inhibitors of lysosomal sialidase (NEU1). *Bioorganic & Medicinal Chemistry Letters* **2008**, 18 (2), 532-537.

42. Magesh, S.; Savita, V.; Moriya, S.; Suzuki, T.; Miyagi, T.; Ishida, H.; Kiso, M., Human sialidase inhibitors: Design, synthesis, and biological evaluation of 4-acetamido-5-acylamido-2-fluoro benzoic acids. *Bioorganic & Medicinal Chemistry* **2009**, 17 (13), 4595-4603.

43. Zou, Y.; Albohy, A.; Sandbhor, M.; Cairo, C. W., Inhibition of human neuraminidase 3 (NEU3) by C9-triazole derivatives of 2,3-didehydro-N-acetylneuraminic acid. *Bioorganic & Medicinal Chemistry Letters* **2010**, 20 (24), 7529-7533.

44. Li, Y.; Cao, H.; Yu, H.; Chen, Y.; Lau, K.; Qu, J.; Thon, V.; Sugiarto, G.; Chen, X., Identifying selective inhibitors against the human cytosolic sialidase NEU2 by substrate specificity studies. *Molecular Biosystems* **2011**, 7 (4), 1060-1072.

45. Seyrantepe, V.; Poulpetova, H.; Froissart, R.; Zobot, M. T.; Marie, I.; Pshezhetsky, A. V., Molecular pathology of NEU1 gene in sialidosis. *Human Mutation* **2003**, 22 (5), 343-352.

46. Pattison, S.; Pankarican, M.; Rugar, C. A.; Graham, F. L.; Igdoura, S. A., Five novel mutations in the lysosomal sialidase gene (NEU1) in type II sialidosis

patients and assessment of their impact on enzyme activity and intracellular targeting using adenovirus-mediated expression. *Human Mutation* **2004**, *23* (1), 32-39.

47. Bonten, E. J.; Arts, W. F.; Beck, M.; Covanis, A.; Donati, M. A.; Parini, R.; Zammarchi, E.; d'Azzo, A., Novel mutations in lysosomal neuraminidase identify functional domains and determine clinical severity in sialidosis. *Human Molecular Genetics* **2000**, *9* (18), 2715-2725.

48. Ha, K. T.; Lee, Y. C.; Cho, S. H.; Kim, J. K.; Kim, C. H., Molecular characterization of membrane type and ganglioside-specific sialidase (Neu3) expressed in E-coli. *Molecules and Cells* **2004**, *17* (2), 267-273.

49. Uemura, T.; Shiozaki, K.; Yamaguchi, K.; Miyazaki, S.; Satomi, S.; Kato, K.; Sakuraba, H.; Miyagi, T., Contribution of sialidase NEU1 to suppression of metastasis of human colon cancer cells through desialylation of integrin beta 4. *Oncogene* **2009**, *28* (9), 1218-1229.

50. Kato, K.; Shiga, K.; Yamaguchi, K.; Hata, K.; Kobayashi, T.; Miyazaki, K.; Saijo, S.; Miyagi, T., Plasma-membrane-associated sialidase (NEU3) differentially regulates integrin-mediated cell proliferation through laminin- and fibronectin-derived signalling. *Biochemical Journal* **2006**, *394*, 647-656.

51. Li, C.-Y.; Yu, Q.; Ye, Z.-Q.; Sun, Y.; He, Q.; Li, X.-M.; Zhang, W.; Luo, J.; Gu, X.; Zheng, X.; Wei, L., A nonsynonymous SNP in human cytosolic sialidase in a small Asian population results in reduced enzyme activity: potential link with severe adverse reactions to oseltarnivir. *Cell Research* **2007**, *17* (4), 357-362.

52. Yamaguchi, K.; Shiozaki, K.; Moriya, S.; Koseki, K.; Wada, T.; Tateno, H.; Sato, I.; Asano, M.; Iwakura, Y.; Miyagi, T., Reduced susceptibility to colitis-associated colon carcinogenesis in mice lacking plasma membrane-associated sialidase. *Plos One* **2012**, *7* (7).
53. Seyrantepe, V.; Canuel, M.; Carpentier, S.; Landry, K.; Durand, S.; Liang, F.; Zeng, J. B.; Caqueret, A.; Gravel, R. A.; Marchesini, S.; Zwingmann, C.; Michaud, J.; Morales, C. R.; Levade, T.; Pshezhetsky, A. V., Mice deficient in Neu4 sialidase exhibit abnormal ganglioside catabolism and lysosomal storage. *Human Molecular Genetics* **2008**, *17* (11), 1556-1568.
54. Lillehoj, E. P.; Hyun, S. W.; Feng, C. G.; Zhang, L.; Liu, A. G.; Guang, W.; Nguyen, C.; Luzina, I. G.; Atamas, S. P.; Passaniti, A.; Twaddell, W. S.; Puche, A. C.; Wang, L. X.; Cross, A. S.; Goldblum, S. E., NEU1 Sialidase Expressed in Human Airway Epithelia Regulates Epidermal Growth Factor Receptor (EGFR) and MUC1 Protein Signaling. *Journal of Biological Chemistry* **2012**, *287* (11), 8214-8231.
55. Cross, A. S.; Hyun, S. W.; Miranda-Ribera, A.; Feng, C. G.; Liu, A. G.; Nguyen, C.; Zhang, L.; Luzina, I. G.; Atamas, S. P.; Twaddell, W. S.; Guang, W.; Lillehoj, E. P.; Puche, A. C.; Huang, W.; Wang, L. X.; Passaniti, A.; Goldblum, S. E., NEU1 and NEU3 Sialidase Activity Expressed in Human Lung Microvascular Endothelia NEU1 restrains endothelial cell migration, whereas NEU3 does not. *Journal of Biological Chemistry* **2012**, *287* (19), 15966-15980.
56. Katoh, S.; Maeda, S.; Fukuoka, H.; Wada, T.; Moriya, S.; Mori, A.; Yamaguchi, K.; Senda, S.; Miyagi, T., A crucial role of sialidase Neu1 in

hyaluronan receptor function of CD44 in T helper type 2-mediated airway inflammation of murine acute asthmatic model. *Clinical and Experimental Immunology* **2010**, *161* (2), 233-241.

57. D'Avila, F.; Tringali, C.; Papini, N.; Anastasia, L.; Croci, G.; Massaccesi, L.; Monti, E.; Tettamanti, G.; Venerando, B., Identification of lysosomal sialidase NEU1 and plasma membrane sialidase NEU3 in human erythrocytes. *Journal of Cellular Biochemistry* **2013**, *114* (1), 204-211.

58. Fanzani, A.; Giuliani, R.; Colombo, F.; Zizioli, D.; Presta, M.; Preti, A.; Marchesini, S., Overexpression of cytosolic sialidase Neu2 induces myoblast differentiation in C2C12 cells. *Febs Letters* **2003**, *547* (1-3), 183-188.

59. Fanzani, A.; Colombo, F.; Giuliani, R.; Preti, A.; Marchesini, S., Insulin-like growth factor 1 signaling regulates cytosolic sialidase Neu2 expression during myoblast differentiation and hypertrophy. *Febs Journal* **2006**, *273* (16), 3709-3721.

60. Rossi, S.; Stoppani, E.; Martinet, W.; Bonetto, A.; Costelli, P.; Giuliani, R.; Colombo, F.; Preti, A.; Marchesini, S.; Fanzani, A., The cytosolic sialidase Neu2 is degraded by autophagy during myoblast atrophy. *Biochimica Et Biophysica Acta-General Subjects* **2009**, *1790* (8), 817-828.

61. Fanzani, A.; Colombo, F.; Giuliani, R.; Preti, A.; Marchesini, S., Cytosolic sialidase Neu2 upregulation during PC12 cells differentiation. *Febs Letters* **2004**, *566* (1-3), 178-182.

62. Tringali, C.; Lupo, B.; Anastasia, L.; Papini, N.; Monti, E.; Bresciani, R.; Tettamanti, G.; Venerando, B., Expression of sialidase Neu2 in leukemic K562

cells induces apoptosis by impairing Bcr-Abl/Src kinases signaling. *Journal of Biological Chemistry* **2007**, 282 (19), 14364-14372.

63. Tokuyama, S.; Moriya, S.; Taniguchi, S.; Yasui, A.; Miyazaki, J.; Orikasa, S.; Miyagi, T., Suppression of pulmonary metastasis in murine B16 melanoma cells by transfection of a sialidase cDNA. *International Journal of Cancer* **1997**, 73 (3), 410-415.

64. Kakugawa, Y.; Wada, T.; Yamaguchi, K.; Yamanami, H.; Ouchi, K.; Sato, I.; Miyagi, T., Up-regulation of plasma membrane-associated ganglioside sialidase (Neu3) in human colon cancer and its involvement in apoptosis suppression. *Proceedings of the National Academy of Sciences of the United States of America* **2002**, 99 (16), 10718-10723.

65. Shiozaki, K.; Yamaguchi, K.; Sato, I.; Miyagi, T., Plasma membrane-associated sialidase (NEU3) promotes formation of colonic aberrant crypt foci in azoxymethane-treated transgenic mice. *Cancer Science* **2009**, 100 (4), 588-594.

66. Ueno, S.; Saito, S.; Wada, T.; Yamaguchi, K.; Satoh, M.; Arai, Y.; Miyagi, T., Plasma membrane-associated sialidase is up-regulated in renal cell carcinoma and promotes interleukin-6-induced apoptosis suppression and cell motility. *Journal of Biological Chemistry* **2006**, 281 (12), 7756-7764.

67. Li, X. J.; Zhang, L.; Shao, Y. T.; Liang, Z. W.; Shao, C.; Wang, B.; Guo, B. F.; Li, N.; Zhao, X. J.; Li, Y.; Xu, D. Q., Effects of a human plasma membrane-associated sialidase siRNA on prostate cancer invasion. *Biochemical and Biophysical Research Communications* **2011**, 416 (3-4), 270-276.

68. Kawamura, S.; Sato, I.; Wada, T.; Yamaguchi, K.; Li, Y.; Li, D.; Zhao, X.; Ueno, S.; Aoki, H.; Tochigi, T.; Kuwahara, M.; Kitamura, T.; Takahashi, K.; Moriya, S.; Miyagi, T., Plasma membrane-associated sialidase (NEU3) regulates progression of prostate cancer to androgen-independent growth through modulation of androgen receptor signaling. *Cell Death and Differentiation* **2012**, *19* (1), 170-179.
69. Sasaki, A.; Hata, K.; Suzuki, S.; Sawada, M.; Wada, T.; Yamaguchi, K.; Obinata, M.; Tateno, H.; Suzuki, H.; Miyagi, T., Overexpression of plasma membrane-associated sialidase attenuates insulin signaling in transgenic mice. *Journal of Biological Chemistry* **2003**, *278* (30), 27896-27902.
70. Yoshizumi, S.; Suzuki, S.; Hirai, M.; Hinokio, Y.; Yamada, T.; Yamada, T.; Tsunoda, U.; Aburatani, H.; Yamaguchi, K.; Miyagi, T.; Oka, Y., Increased hepatic expression of ganglioside-specific sialidase, NEU3, improves insulin sensitivity and glucose tolerance in mice. *Metabolism-Clinical and Experimental* **2007**, *56* (3), 420-429.
71. Seyrantepe, V.; Landry, K.; Trudel, S.; Hassan, J. A.; Morales, C. R.; Pshezhetsky, A. V., Neu4, a novel human lysosomal lumen sialidase, confers normal phenotype to sialidosis and galactosialidosis cells. *Journal of Biological Chemistry* **2004**, *279* (35), 37021-37029.
72. Seyrantepe, V.; Lema, P.; Caqueret, A.; Dridi, L.; Hadj, S. B.; Carpentier, S.; Boucher, F.; Levade, T.; Carmant, L.; Gravel, R. A.; Hamel, E.; Vachon, P.; Di Cristo, G.; Michaud, J. L.; Morales, C. R.; Pshezhetsky, A. V., Mice Doubly-

Deficient in Lysosomal Hexosaminidase A and Neuraminidase 4 Show Epileptic Crises and Rapid Neuronal Loss. *Plos Genetics* **2010**, *6* (9).

73. Seyrantepe, V.; Landry, K.; Canuel, M.; Zeng, J.; Gravel, R.; Morales, C.; Pshezhetsky, A., Lysosomal sialidase NEU4: potential novel role in glycolipid catabolism. *Journal of Inherited Metabolic Disease* **2005**, *28*, 178-178.

74. Yamaguchi, K.; Hata, K.; Koseki, K.; Shiozaki, K.; Akita, H.; Wada, T.; Moriya, S.; Miyagi, T., Evidence for mitochondrial localization of a novel human sialidase (NEU4). *Biochemical Journal* **2005**, *390*, 85-93.

75. Bigi, A.; Morosi, L.; Pozzi, C.; Forcella, M.; Tettamanti, G.; Venerando, B.; Monti, E.; Fusi, P., Human sialidase NEU4 long and short are extrinsic proteins bound to outer mitochondrial membrane and the endoplasmic reticulum, respectively. *Glycobiology* **2010**, *20* (2), 148-157.

76. Yamanami, H.; Shiozaki, K.; Wada, T.; Yamaguchi, K.; Uemura, T.; Kakugawa, Y.; Hujuya, T.; Miyagi, T., Down-regulation of sialidase NEU4 may contribute to invasive properties of human colon cancers. *Cancer Science* **2007**, *98* (3), 299-307.

77. Shiozaki, K.; Koseki, K.; Yamaguchi, K.; Shiozaki, M.; Narimatsu, H.; Miyagi, T., Developmental change of sialidase Neu4 expression in murine brain and its involvement in the regulation of neuronal cell differentiation. *Journal of Biological Chemistry* **2009**, *284* (32), 21157-21164.

78. Finlay, T. M.; Jayanth, P.; Amith, S. R.; Gilmour, A.; Guzzo, C.; Gee, K.; Beyaert, R.; Szewczuk, M. R., Thymoquinone from nutraceutical black cumin oil activates Neu4 sialidase in live macrophage, dendritic, and normal and type I

sialidosis human fibroblast cells via GPCR G alpha i proteins and matrix metalloproteinase-9. *Glycoconjugate Journal* **2010**, 27 (3), 329-348.

79. Finlay, T. M.; Abdulkhalek, S.; Gilmour, A.; Guzzo, C.; Jayanth, P.; Amith, S. R.; Gee, K.; Beyaert, R.; Szewczuk, M. R., Thymoquinone-induced Neu4 sialidase activates NF kappa B in macrophage cells and pro-inflammatory cytokines in vivo. *Glycoconjugate Journal* **2010**, 27 (6), 583-600.

80. Ferrari, J.; Harris, R.; Warner, T. G., Cloning and expression of a soluble sialidase from Chinese-hamster ovary cells - sequence alignment similarities to bacterial sialidases. *Glycobiology* **1994**, 4 (3), 367-373.

81. Wang, Y.; Yamaguchi, K.; Wada, T.; Hata, K.; Zhao, X. J.; Fujimoto, T.; Miyagi, T., A close association of the ganglioside-specific sialidase Neu3 with caveolin in membrane microdomains. *Journal of Biological Chemistry* **2002**, 277 (29), 26252-26259.

82. Albohy, A.; Mohan, S.; Zheng, R. X. B.; Pinto, B. M.; Cairo, C. W., Inhibitor selectivity of a new class of oseltamivir analogs against viral neuraminidase over human neuraminidase enzymes. *Bioorganic & Medicinal Chemistry* **2011**, 19 (9), 2817-2822.

83. Magesh, S.; Moriya, S.; Suzuki, T.; Miyagi, T.; Ishida, H.; Kiso, M., Use of structure-based virtual screening in the investigation of novel human sialidase inhibitors. *Medicinal Chemistry Research* **2010**, 19 (9), 1273-1286.

84. Li, Y. H.; Cao, H. Z.; Yu, H.; Chen, Y.; Lau, K.; Qu, J. Y.; Thon, V.; Sugiarto, G.; Chen, X., Identifying selective inhibitors against the human

cytosolic sialidase NEU2 by substrate specificity studies. *Molecular Biosystems* **2011**, 7 (4), 1060-1072.

85. Khedri, Z.; Li, Y. H.; Cao, H. Z.; Qu, J. Y.; Yu, H.; Muthana, M. M.; Chen, X., Synthesis of selective inhibitors against *V. cholerae* sialidase and human cytosolic sialidase NEU2. *Organic & Biomolecular Chemistry* **2012**, 10 (30), 6112-6120.

86. Rahman, M. M.; Kitao, S.; Tsuji, D.; Suzuki, K.; Sakamoto, J. I.; Matsuoka, K.; Matsuzawa, F.; Aikawa, S. I.; Itoh, K., Inhibitory effects and specificity of synthetic sialyldendrimers toward recombinant human cytosolic sialidase 2 (NEU2). *Glycobiology* **2013**, 23 (4), 495-504.

**2 Insight into substrate recognition and catalysis by the human
neuraminidase 3 (NEU3) through molecular modeling and site-
directed mutagenesis¹**

¹ A version of this chapter has been published: Albohy, A.; Li, M. D.; Zheng, R. B.; Zou, C.; Cairo, C. W., Insight into substrate recognition and catalysis by the human neuraminidase 3 (NEU3) through molecular modeling and site-directed mutagenesis. *Glycobiology* **2010**, *20* (9), 1127-1138.

2.1 Introduction

Several isoforms of mammalian neuraminidase (NEU) enzymes are known. All reported members are classified as family 33 glycoside hydrolases (GH33) with exo-glycosidase activity, within the CAZy database.¹ Of those isoforms, NEU3 is known as an ectoenzyme, a peripheral membrane-associated enzyme with activity at the outer leaflet.^{2,3,4} This glycosylhydrolase is selective for glycoproteins and glycolipids over soluble small molecules, suggesting that its native function is the processing of membrane-bound substrates.⁵ Cleavage of Neu5Ac α 2,3 and α 2,8 linkages has been reported using purified enzyme.⁶ Additionally, its enzymatic activity is modulated by signaling events such as protein kinase C stimulation in immune cells,⁷ and the protein is known to be recruited to raft domains through binding to caveolin.⁸ These findings suggest that NEU3 could directly mediate lipid raft structure through glycosidase activity.^{9, 10}

Glycolipids are an important component of membrane structure, and the specificity of NEU3 for these structures could place it in a central role for mediating membrane signaling.³ Key components of rafts in mammalian cells are the glycolipids GM1 and GM3; indeed, GM1 is used as a marker of raft structure.¹¹ Glycosphingolipids, such as GM3 and GD1a, contain terminal α 2,3-sialic acid residues and are known to be substrates for NEU3.^{6,12,13}

Mammalian NEU enzymes appear to play important roles in cell signaling and cancer.¹⁴ The substrate specificity and corresponding inhibitor strategies are well established for the viral NEU enzymes.¹⁵ Additionally, bacterial^{16,17} and trypanosomal¹⁸ enzymes have been well studied. The same is not true for the

mammalian NEU enzymes. While the first of these enzymes have been known for some time (NEU1 and NEU2)^{19,20}, NEU3²¹ and NEU4^{5, 22} have been identified more recently. Within the family, only NEU2 has been characterized by crystallography,²³ although homology models have been proposed for all members.²⁴ Little work has been done on inhibitor design for these enzymes. Some specific inhibitors have been reported for NEU1,²⁵ but prior to 2010 none had been reported for the other members of the family. Interestingly, recent results have suggested that known inhibitors of viral NEUs are poor inhibitors of this family of enzymes,²⁶ suggesting the possibility of designing specific substrates and inhibitors.

Often the enzymatic mechanism and structure of the binding site are critical data for the design of specific NEU inhibitors.²⁷ Only a few reports of the mechanism of the mammalian NEU enzymes are known²⁸. Previous work in bacterial and eukaryotic sialidases and trans-sialidases has found that a highly conserved tyrosine is the active site nucleophile,²⁹ which acts in concert with a glutamate residue acting as a general base.³⁰ Mutation of the nucleophilic tyrosine can alter the enzymatic mechanism.³¹ In the case of bacterial NEU, such as the *C. perfringens* sialidase, recent structural data have confirmed the role of the active site tyrosine residue which forms a covalent sialoside intermediate.³² Although alignments of NEU3 have been performed, the role of only a few individual amino acids in catalysis has been investigated. Wang et al.¹³ reported site-directed mutagenesis (SDM) studies of NEU3 and found support for the role of one member of the arginine triad (R25) common to all sialidases. Albouz-Abo et al.³³

have reported studies of NEU2, where they demonstrated the enzyme had a retaining mechanism and appeared to be Ca^{2+} dependent. No corresponding investigations of NEU3 have been reported.

To improve our understanding of the mammalian NEU family, we chose to investigate the catalytic mechanism of NEU3 and identify the key catalytic residues. Starting from a homology model of the protein, we identified potentially important catalytic residues within the sequence. By using site-directed mutagenesis (SDM), 14 single point mutants, two multi-site mutants and seven truncated mutants were screened and evaluated for their enzymatic activity. We then isolated and characterized the kinetics of eight mutants and the wild-type enzyme using a maltose-binding protein (MBP)-fusion protein strategy. We tested the effect of added metal ions, chelating agents, reducing agents and treatment with alkaline pH. No evidence for divalent cations in the enzymatic mechanism was found; however, the enzyme was inactivated by alkaline conditions. Finally, we confirmed that the enzyme is a retaining sialidase using ^1H nuclear magnetic resonance (NMR) spectroscopy.

2.2 Results

2.2.1 Homology modeling and molecular docking of NEU3

To date, no crystallography studies of NEU3 have been reported. However, homology models of the protein and other mammalian NEU have been described.²⁴ In order to identify potential catalytic residues, we followed a similar strategy. NEU2 and NEU3 have 38% identity after alignment using ClustalW (Figure 2.1).³⁴ Using the alignment, we generated a homology model of the

protein based on the crystal structure data for NEU2^{23, 35} using Modeller.³⁵ Our model was qualitatively similar to that reported by Magesh et al., and we set out to identify potentially important contacts for substrate and inhibitor structures in the binding site.

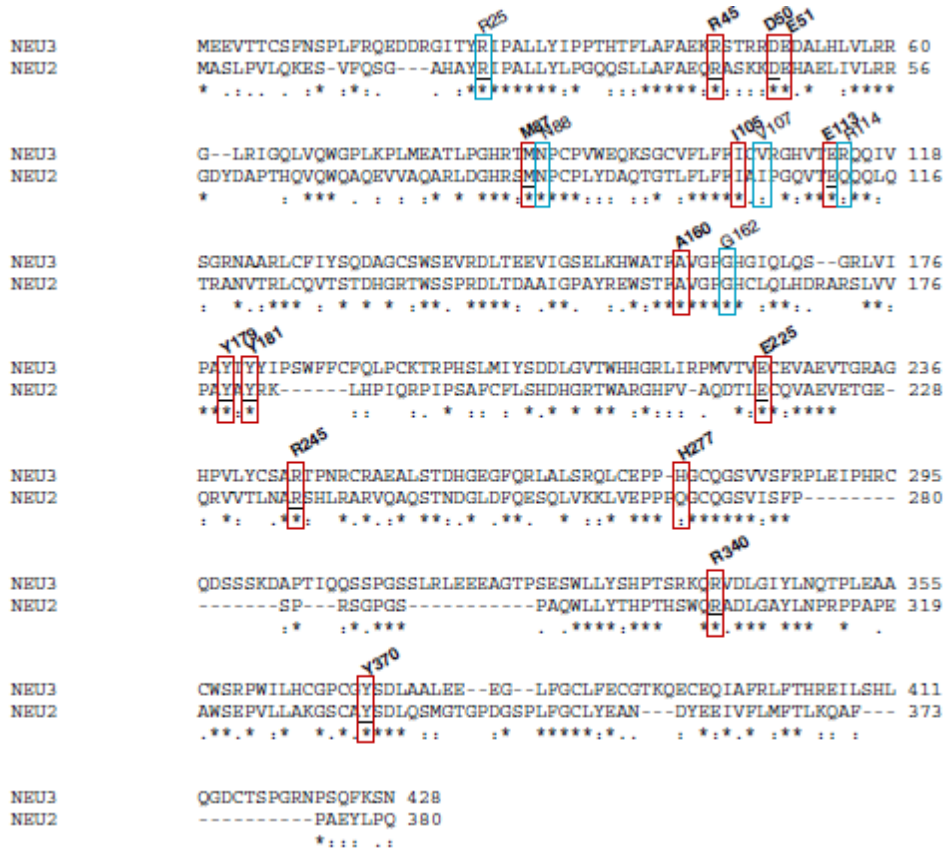


Figure 2.1: Alignment of NEU2 and NEU3 using ClustalW. The sequences of NEU2 (NEUR_2; Q9Y3R4) and NEU3 (NEUR_3; Q9UQ49) were aligned. The sequences show 38% identity, and individual sites are noted as being identical (*), conserved (:), or semi-conserved substitutions (.). NEU3 is shown on the top line of each row. NEU3 sites studied by mutagenesis are indicated by boxes, examples from previous studies (light)¹³ and this work (dark) are shown. Key NEU2 active site residues are underlined.²³

To assess the quality of the homology model, we determined the Z-score of the model relative to known crystal structures (Figure 2.2).

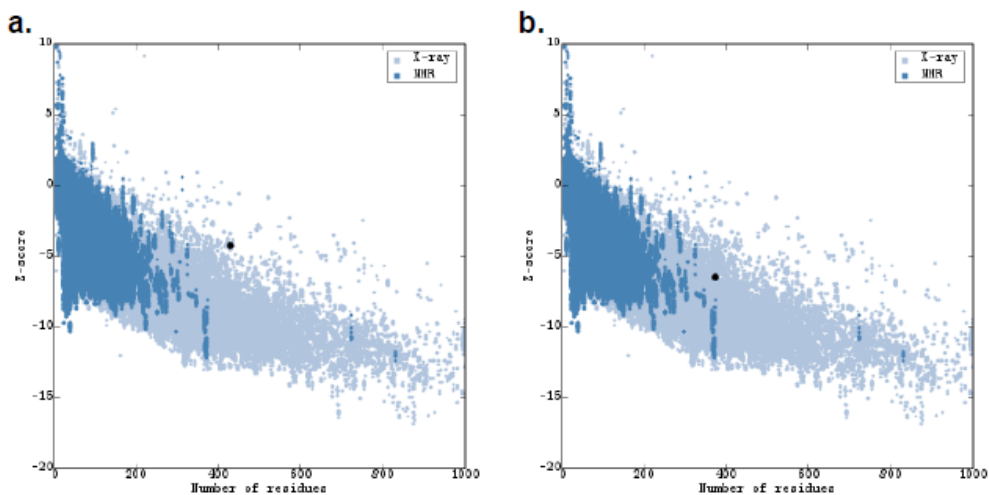


Figure 2.2: NEU3 Homology model evaluation. (a.) The NEU3 homology model used in this work is shown ($Z = -4.23$), (b.) in comparison to the NEU2 crystal structure that was used for generating the model ($Z = -6.44$) (PDB: 1VCU). The shaded areas represent values for protein structures found in the PDB determined by X ray diffraction (light blue) or NMR (dark blue). Plots shown were generated by ProSA-web.^{36,37} Additionally, examination of a Ramachandran plot gave more than 85% of the residues in most favoured regions, which was similar to the value found for the NEU2 crystal structure (81%)³⁸

Molecular docking calculations were performed for the binding of the transition state mimic 2-deoxy-2,3-dehydro-*N*-acetylneuraminic acid (DANA) to NEU3 using Autodock 4.^{39,40} Autodock has been used previously for docking of carbohydrate structures to lectin and glycosidase binding sites.^{41,42,39} We found

that Autodock was able to identify bound conformations of DANA in the active site consistent with the contacts seen in previous studies of NEU2 and molecular modeling.^{23, 24} The conformer selected from these calculations was from the lowest energy cluster (-7.07 kcal/mol) with a cluster root mean square (RMS) of 0.91. The second lowest energy cluster was missing interactions between the *C1* carboxylate and the arginine triad (-6.95 kcal/mol). We then generated a model of the glycosphingolipid, GM3, docked to the active site (Figure 2.3). The conformer of GM3 selected was from the lowest energy cluster (-3.96 kcal/mol) and had a cluster RMS of 0.50. Most of the variation seen in this cluster was within the lipid tail. Both structures found a similar orientation for the terminal sialic acid of GM3 and DANA and have similar molecular contacts to the enzyme, although DANA is more deeply buried in the active site. We tabulated the key contacts observed for sialic acid in both models (Table 2.1). Important residues include: D50, which sits over the *C2* position on the a-face of the ring; the arginine triad (R25, R245, R340), which coordinates the carboxylate; Y370, which is below the *C2* position on the b-face of the ring; and several hydrogen bond donors and acceptors (R45, E113, Y179, Y181), which coordinate the *O4* and glycerol sidechain hydroxy groups. We also noted the presence of a hydrophobic pocket which accommodates the *N5*-acetyl group (A160, M87, I105). The model of GM3 suggests that R48 could interact with the central galactose residue of GM3, and H277 and R114 may interact with the reducing-end glucose. We proceeded to validate the model using SDM and activity assays.

Table 2.1: Predicted substrate interactions in NEU3

Site	Relative Activity ^a	Source ^b	Putative Interaction ^c
WT	100 ± 2	Albohy et al. ⁴³	N/A
D50S	10.4 ± 0.3	Albohy et al. ⁴³	C2
Y370F	0.1 ± 0.1	Albohy et al. ⁴³	C2
Y370C	12.1	Wang et al. ¹³	C2
E225S	0.3 ± 0.1	Albohy et al. ⁴³	Y370F
R245A	-1.2 ± 0.1	Albohy et al. ⁴³	COO
R340A	1.3 ± 0.2	Albohy et al. ⁴³	COO
R25H	16.2	Wang et al. ¹³	COO
A160G	79 ± 4	Albohy et al. ⁴³	N5Ac
M87G	10.7 ± 0.2	Albohy et al. ⁴³	N5Ac
I105G	4.8 ± 0.1	Albohy et al. ⁴³	N5Ac
I105G + M87G	1.2 ± 0.1	Albohy et al. ⁴³	N5Ac
I105G + M87G + A160G	0.3 ± 0.1	Albohy et al. ⁴³	N5Ac
R45V	1.9 ± 0.1	Albohy et al. ⁴³	O4
E113A	8 ± 3	Albohy et al. ⁴³	O7-O8
Y179F	1.8 ± 0.5	Albohy et al. ⁴³	O8
Y181F	7 ± 2	Albohy et al. ⁴³	O8
G419STOP ^d	144 ± 9	Albohy et al. ⁴³	Truncation
L408STOP	1.1 ± 0.1	Albohy et al. ⁴³	Truncation
I407STOP	0.8 ± 1	Albohy et al. ⁴³	Truncation
T403STOP	-3 ± 2	Albohy et al. ⁴³	Truncation
N-10	80.3	Albohy et al. ⁴³	Truncation
N-20	-0.6 ± 0.3	Albohy et al. ⁴³	Truncation
N-50	-1.5 ± 0.2	Albohy et al. ⁴³	Truncation
H277F	124 ± 6	Albohy et al. ⁴³	
E51S ^d	119 ± 3	Albohy et al. ⁴³	
E51D	75.7	Wang et al. ¹³	
G162A	13.3	Wang et al. ¹³	
N88D	9.7	Wang et al. ¹³	
R114A	96.5	Wang et al. ¹³	
R114Q	71.6	Wang et al. ¹³	
V107M	9.0	Wang et al. ¹³	

^a Mutation experiments are tabulated as % of activity relative to wild-type enzyme, using 4MU-NA as a substrate at pH = 5.0. Data from Wang et al. were

reported at pH 4.6.¹³ ^b Source of activity data. ^c Assignment of interactions with the substrate was made from the homology model discussed above. ^d When observed at pH = 4.5, the activity of the E51S mutant was 96 ± 9% and of G419STOP was 95 ± 4%.

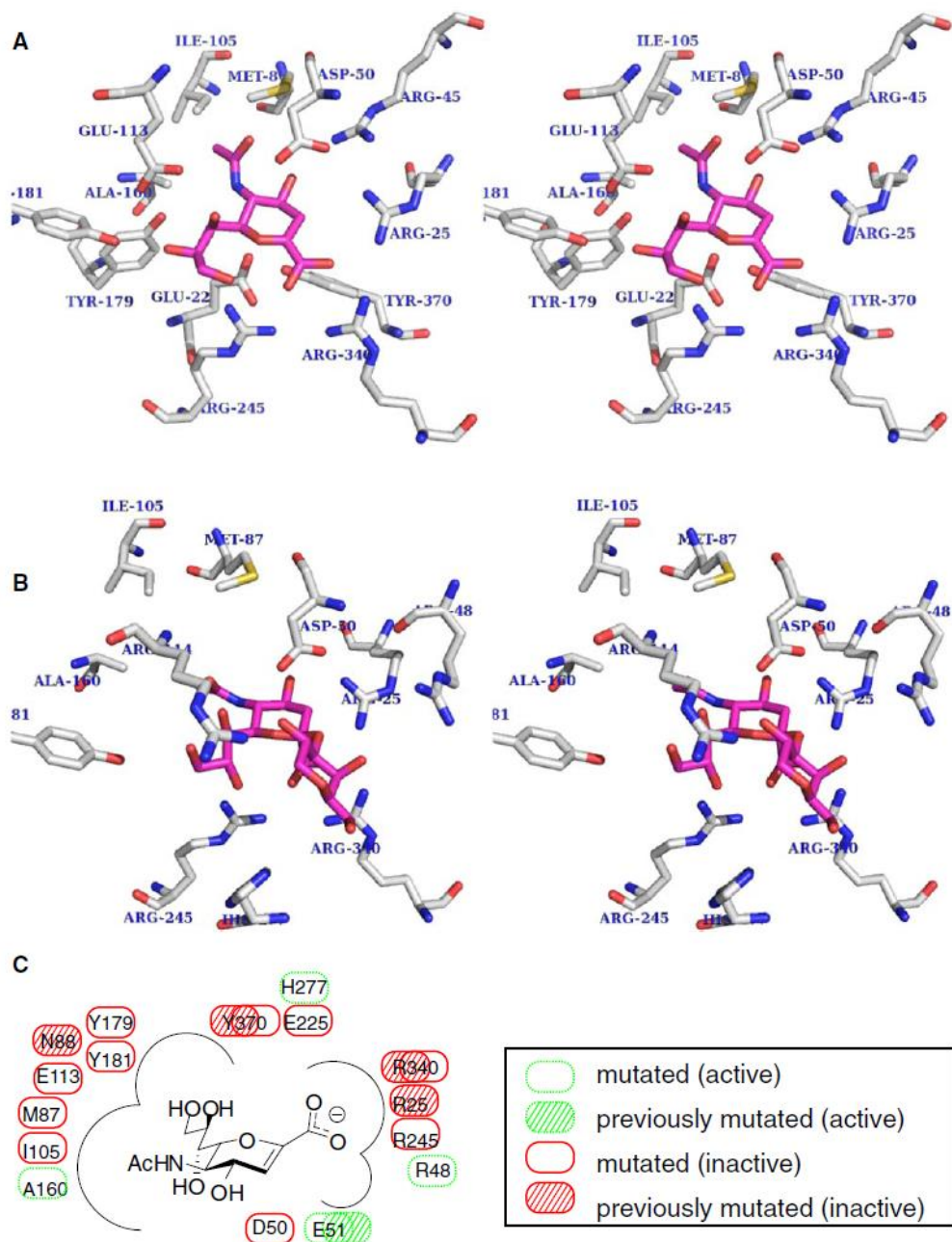


Figure 2.3: Homology model of the NEU3 active site and molecular docking. A homology model of NEU3 was constructed using Modeller 9v6.³⁵ Molecular docking with Autodock 4.0 was used to determine the binding mode of (A) DANA and (B) the glycolipid, GM3. Views of the active site are shown in stereo (crossed). Only the terminal Neu5Ac and Gal residues of GM3 are shown in (B)

for clarity. The binding site for sialic acid is similar to that of NEU2, with the O4 and N5 positions directed into the binding pocket, and the C2 and glycerol side-chain solvent exposed. Amino acid residues for site-directed mutagenesis were selected to test the model. (C) A schematic of the binding pocket is shown with previously tested mutations¹³ (hashed) and those tested in this study (open) shown. Mutations that significantly decreased activity (<10%) are shown in solid red, and those that did not eliminate activity are shown in dashed green.

2.2.2 Site-directed mutagenesis of recombinant NEU3

Expression of NEU3 has been reported in bacterial and mammalian cells.⁶
¹³ For our purposes, we required a system which could provide large quantities of protein for assay and could be easily manipulated. We found that mammalian expression systems had generally high sialidase background, complicating their use in the current study. Initial work with NEU3 in a pRSET vector gave poor yields in our hands.⁶ Therefore, we inserted the gene into pET28a vector with an N-terminal His-tag (see Figure 2.4) and expressed the protein in *E. coli* cells (see Materials and methods).

NEU3 (pET28a)

His-Tag

1 MGSSHHHHHHH SSGLVPRGSH MASMTGGQQM GRGS

NEU3

1 MEEVTTCSFN SPLFRQEDDR GITYRIPALL YIPPTHTFLA FAEKRSTRRD EDALHLVLR
61 GLRIGQLVQW GPLKPLMEAT LPGHRTMNPC PVWEQKSGCV FLFFICVRGH VTERQQIVSG
121 RNAARLCFIY SQDAGCSWSE VRDLTEEVIG SELKHWATFA VGPGHGIQLQ SGRLVIPAYT
181 YYIPSWFFCF QLPCCKTRPHS LMIYSDDLGV TWHHGRLIRP MVTVECEVAE VTGRAGHPVL
241 YCSARTPNRC RAEALSTDHG EGFQRLALSR QLCEPPHGCO GSVVSFRPLE IPHRCQDSSS
301 KDAPTIQQSS PGSSLRLEEE AGTPSESWLL YSHPTSRRQR VDLGIYLNQT PLEAACWSRP
361 WILHCGPCGY SDLAALIEEG LFGCLFECGT KQECEQIAFR LFTHREILSH LQGDCTSPGR
421 NPSQFKSN

NEU3-MBP fusion (pMAL-c2x)

MBP

1 MKIEEGKLVV WINGDKGYNG LAEVGKKFEK DTGIKVTVEH PDKLEEKFPQ VAATGDGPDI
61 IFWAHDRFVG YAQSGLLAEI TPDKAFQDKL YPFTWDVAVRY NGKLIAYPIA VEALSILYNK
121 DLLPNPPKTW EEIPALDKEL KAKGKSALMF NLQEPYFTWP LIAADGGYAF KYENGYDIK
181 DVGVDNAGAK AGLTFLVDLI KNKHMNADTD YSIAEAAFNK GETAMTINGP WAWSNIDTSK
241 VNYGVTVLPT FKGQPSKPFV GVLSAGINAA SPNKELAKEF LENYLLTDEG LEAVNKDKPL
301 GAVALKSYEE ELAKDPRIAA TMENAQKGEI MPNIPQMSAF WYAVRTAVIN AASGRQTVDE
361 ALKDAQTN

Linker

1 SSSNNNNNNN NNNLGIEGRI SEF

NEU3

1 MEEVTTCSFN SPLFRQEDDR GITYRIPALL YIPPTHTFLA FAEKRSTRRD EDALHLVLR
61 GLRIGQLVQW GPLKPLMEAT LPGHRTMNPC PVWEQKSGCV FLFFICVRGH VTERQQIVSG
121 RNAARLCFIY SQDAGCSWSE VRDLTEEVIG SELKHWATFA VGPGHGIQLQ SGRLVIPAYT
181 YYIPSWFFCF QLPCCKTRPHS LMIYSDDLGV TWHHGRLIRP MVTVECEVAE VTGRAGHPVL
241 YCSARTPNRC RAEALSTDHG EGFQRLALSR QLCEPPHGCO GSVVSFRPLE IPHRCQDSSS
301 KDAPTIQQSS PGSSLRLEEE AGTPSESWLL YSHPTSRRQR VDLGIYLNQT PLEAACWSRP
361 WILHCGPCGY SDLAALIEEG LFGCLFECGT KQECEQIAFR LFTHREILSH LQGDCTSPGR
421 NPSQFKSN

Figure 2.4: NEU3 construct sequences. The protein sequence for His-tagged NEU3 and MBP-NEU3 including the linker used.

We used the His-tag to confirm expression of the protein, and we observed intact NEU3 as well as proteolytic fragments of the protein (Figure 2.5). The intact protein was estimated to be close to 30% of the total His-tag protein found in lysate. However, the expressed protein was active, and mock-transfected cells showed no activity.

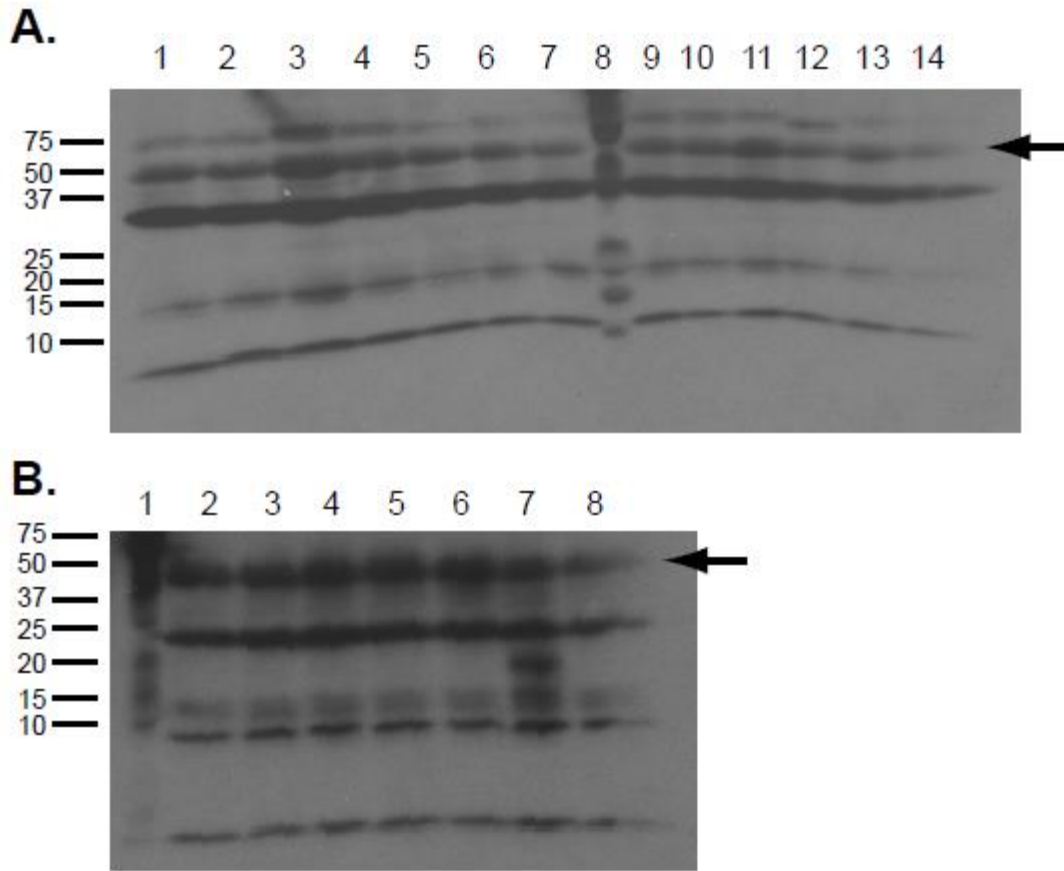


Figure 2.5: NEU3 content from unpurified lysate. Western blot of cell lysate for wild-type NEU3 (pET28a) and point mutants (visualized by direct detection with HisProbe-HRP, 1:5000, Thermo Scientific). The expected molecular weight of the protein is indicated with an arrow (49.1 kDa). The reactive band at the expected molecular weight was determined as $27 \pm 3\%$ of total intensity of individual lanes using densitometry. Lanes shown are: (A.) 1. I105G, 2. M87G, 3. Triple mutation (I105G, M87G, A160G), 4. D50S, 5. E225S, 6. Y370F, 7. wt, 8. MW markers (75, 50, 37, 25, 20, 15, and 10 kDa), 9. R340A, 10. H277F, 11. R45V, 12. L408STOP, 13. Y179F, 14. Y181F; (B.) 1. MW markers (75, 50, 37, 25, 20, 15, and 10 kDa),

2. *wt* 3. *A160G*, 4. *Double mutation (I105G, M87G)*, 5. *E51S*, 6. *G419STOP*, 7. *R245A*, 8. *E113A*.

Before conducting assays with these proteins, we sought to confirm that the proteolytic fragments would not complicate the assay data. We generated several truncated forms of the protein, with either *N*-terminal (-10, -20, -50) or *C*-terminal (-10, -21, -22, -26) truncations. In both cases, truncation of more than 10 residues from the protein abolished activity (see Figure 2.6 and Table 2.2). Since the major proteolyzed NEU3 band is more than 10 kDa lower in molecular weight than the intact protein, we conclude that these fragments are unlikely to contribute to observed activity. We proceeded to test the effects of point mutations on the activity of NEU3.

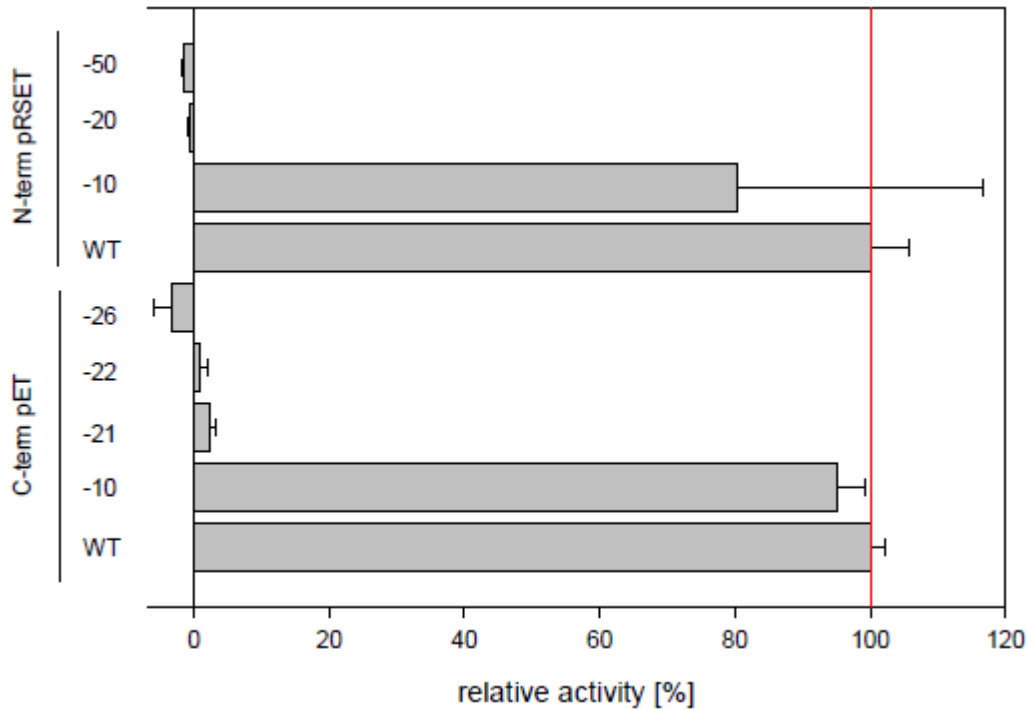


Figure 2.6: Activity of truncated NEU3. Truncated mutants were expressed in *E. coli* and assayed in bacterial lysate (N-terminal constructs were in pRSET vector; C-terminal mutants were in pET28a as described above). Mock cells showed no sialidase background activity. Assays were conducted in 0.1 M sodium acetate buffer pH 4.5, at a total protein concentration of 25 mg/mL as determined by A280. Lysate was incubated with 500 μ M 4MU-NA for 60 min at 37 °C, the reaction was stopped with 200 μ L of 0.2 M glycine/NaOH buffer pH 10.2 and activity was determined by fluorescence (365 nm excitation; 445 nm emission). Assays were performed in triplicate and error bars indicate the standard deviation of each point. Results are shown normalized to a wild-type control for each vector run in parallel.

Table 2.2: Truncated mutant sequences

<i>protein</i>	<i>NEU3 sequence</i>
wt	1-428
N-term -10	11-428
N-term -20	21-428
N-term -50	51-428
C-term -10	1-418
C-term -21	1-407
C-term -22	1-406
C-term -26	1-402

Truncated sequences used in Figure 2.6 were expressed in E. coli lysate and used without purification. N-terminal truncations were generated by deleting the corresponding nucleotide sequences in a pRSET vector. C-terminal truncations were generated by mutagenesis of the appropriate site to a stop codon in the pET28a vector. The expressed proteins correspond to the regions noted below from the sequence of NEU3 given in Table 2.2.

Based on the contacts observed in our model, we selected potentially important residues that could participate in catalysis or substrate recognition and generated mutants at these positions using the pET28a vector (Table 2.1). Previously reported SDM results relevant to the model are also included in Table I for comparison.¹³ Mutants were expressed and tested for enzymatic activity relative to the wild-type protein (Figure 2.7). We found that several mutations at positions predicted to interact at C2 (D50S, Y370F and E225S) and C1 (R245A and R340A) greatly reduced enzymatic activity. Interestingly, mutation of E225 to serine eliminated enzyme activity. Residue E225 is not predicted to interact directly with the substrate but likely interacts with Y370 to catalyze formation of the covalent sialoside intermediate.⁴⁴ We observed slightly increased activity after

mutation of H277 to phenylalanine and E51 to serine, consistent with our model, which places these residues distant from the binding site. Mutations targeted at the putative *N5* binding pocket showed mixed results, with minor (A160G) to substantial (M87G, I105G) reductions in enzymatic activity. We also tested combinations of these mutations as a double- (M87G + I105G) and triple-mutant (A160G + M87G + I105G), and both showed undetectable enzymatic activity. These results suggest that *N5* interactions are necessary for recognition of the substrate or that these residues play an essential structural role in ordering the binding site.⁴⁵ Mutations of sites predicted to interact with the *O4* (R45V) and glycerol side-chain (E113A, Y179F, and Y181F) all eliminated enzymatic activity, supporting the contribution of these groups to recognition of the sialic acid residue. Mutation data from these experiments were mapped to the active site model (Figure 2.3C). We also compared the activity of *C*-terminal truncations of the protein, with 10-residue truncation (G419STOP) leading to a slight increase in activity, and larger deletions (L408STOP) eliminating all activity. We proceeded to isolate and characterize several of these mutants to gain additional insight into their activity.

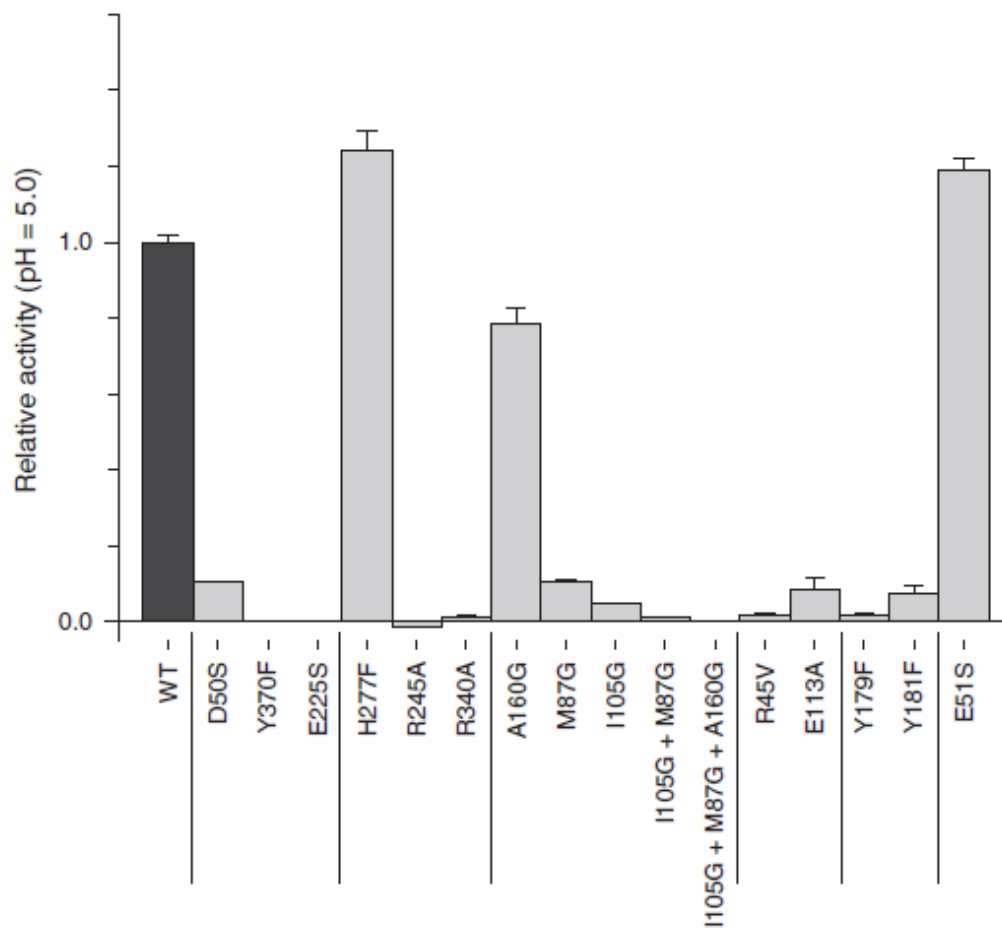


Figure 2.7: Relative activity of point mutations generated. *NEU3* proteins were expressed in *E. coli* (pET28a) and assayed in bacterial lysate (pH 5.0, 0.1 M sodium acetate). Mock cells showed no sialidase background activity. Assays were conducted at a total protein concentration of 25 mg/mL as determined by A280. Lysate was incubated with 2 μ L of 10 mM 4MU-NA for 60 min at 37°C, and activity was determined by fluorescence (365 nm excitation; 445 nm emission). Assays were performed in triplicate and error bars indicate the standard deviation of each point. Results are shown normalized to a wild-type control run in parallel.

2.2.3 Purification and characterization of NEU3 mutants

Initial attempts at purification of the protein using a Ni²⁺-NTA strategy were unsuccessful. This may have been due in part to the enzymes instability to alkaline pH (*vide infra*). We, therefore, used an alternative affinity tag, the MBP fused to the *N*-terminus of the sequence in place of the His-tag (Figure 2.4). Expression and purification of the MBP-NEU3 using an amylose column were successful, and the isolated protein was active. Attempts to remove MBP by cleavage of the linker with Factor Xa resulted in protein aggregation; therefore, all proteins were characterized as the MBP fusion. The pH profiles of the wild-type and fusion proteins were slightly different, with the fusion protein more closely matching previous reports (pH optimum 3.8–5) and the wild type protein showing a slight shift to a more alkaline range (pH optimum 5–6)^{2, 13} (see

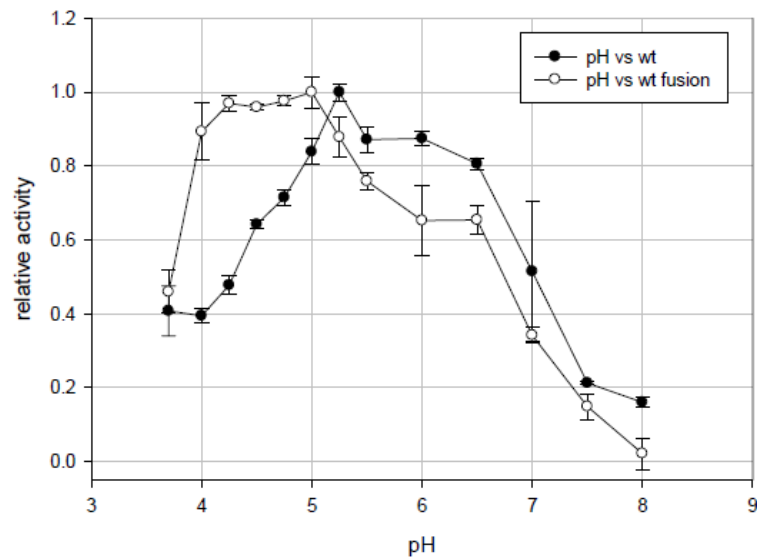


Figure 2.8).

Figure 2.8: pH activity profile of wild-type and purified NEU3. NEU3 was expressed in *E. coli* and used as unpurified NEU3 (*pET28a*) or as a purified

MBP-NEU3 fusion protein (pMAL-c2x). Unpurified samples were at a total protein concentration of 25 mg/mL and purified NEU3 samples were at a concentration of 0.1 mg/mL. The neuraminidase solution was incubated with 500 μ M 4MU-NA for 60 min at 37 °C, the reaction was stopped as above and activity was determined by fluorescence (365 nm excitation; 445 nm emission). Enzyme activity was measured at pH 3.7, 4.0, 4.25, 4.50, 4.75, 5.0, 5.5 (0.1 M sodium acetate buffer) and 5.25, 6.0, 6.5, 7.0, 7.5, 8.0 (0.1 M sodium phosphate buffer). Assays were performed in triplicate and error bars indicate the standard deviation of each point. Both curves are normalized to the maximum activity observed.

We expressed and purified eight mutants that were either active (A160G, E51S, H277F, R48N, R48S), weakly active (M87G) or inactive (D50S, Y370F) for further characterization (see Supporting information, Figure SI6).

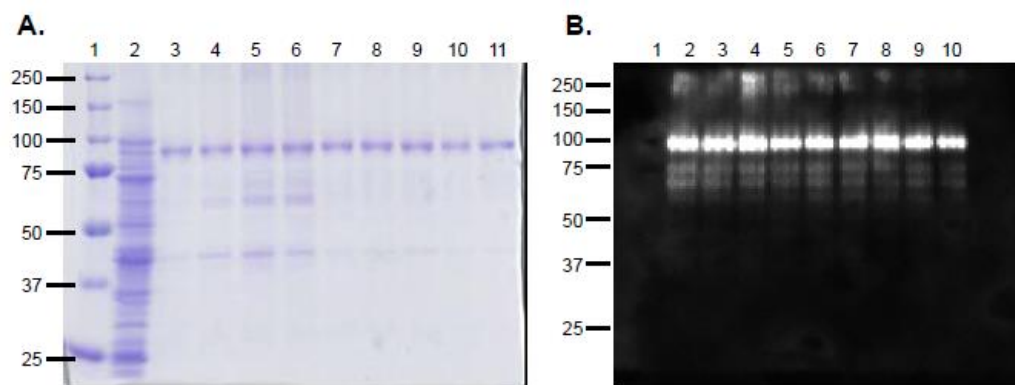


Figure 2.9: Purification of NEU3 mutants as MBP fusion proteins. Proteins were expressed in *E. coli* as MBP-fusion proteins (pMAL-c2x). After cell lysis,

proteins were purified over an amylose affinity column. The resulting proteins were used to determine kinetic parameters (see Table 2.3). The major band observed is consistent with the expected molecular weight of the MBP-NEU3 fusion proteins (92.3 kDa). **A.** Protein purity was assessed by SDS-PAGE (9 %) with coumassie staining. Lanes shown are: 1. MW markers (250, 150, 100, 75, 50, 37 and 25 kDa), 2. wt unpurified, 3. wt, 4. Y370F, 5. E51S, 6. D50S, 7. H277F, 8. M87G, 9. A160G, 10. R48S, 11. R48N. **B.** Purified proteins were also assessed by western blotting using an anti-MBP antibody (primary: anti-MBP, 1:20,000; secondary: goat-anti-mouse IgG-HRP, 1:100,000; New England Biolabs). Lanes shown are: 1. MW markers (250, 150, 100, 75, 50, 37, and 25 kDa), 2. wt, 3. Y370F, 4. E51S, 5. D50S, 6. H277F, 7. M87G, 8. A160G, 9. R48S, 10. R48N.

Typical yields of protein were 8 mg L⁻¹ of culture. We first examined the dependence of enzymatic activity on pH for each mutant. We observed that several mutants showed little deviation from the behavior of the wild type protein (pH optimum 4–5; E51S, H277, M87G), while others showed increased relative activity at alkaline pH (A160G, R48N, R48S). Inactive mutants (D50S, Y370F) did not show significant activity at any pH tested. Kinetic studies of the purified mutants and wild-type protein were also conducted (Table 2.3). The Michaelis constant (K_m) for these proteins indicated that mutation at E51 and R48 resulted in only slight changes in substrate affinity relative to wild type. Mutation at A160 and H277 led to an apparent decrease in K_m . In contrast, mutation at M87 caused a dramatic loss of affinity, suggesting that this site is important for substrate recognition. Mutation of M87 also resulted in a large drop in the rate of catalysis

by the enzyme (k_{cat}). These results may indicate that M87 is important for orienting the substrate in the active site. The corresponding Met residue has been observed to adopt several conformations in the active site of trans-sialidase enzymes.⁴⁵ Both E51S and R48S showed a large increase in k_{cat} (ca. 200% of wild type). Neither the D50S nor Y370F proteins retained enough activity to determine K_m or k_{cat} values.

Table 2.3: Kinetics of 4MU-NA hydrolysis by MBP-NEU3

Mutant	V_{max} [U s ⁻¹] ^a	K_m [μM] ^a	k_{cat} [h ⁻¹]	DANA IC ₅₀ [μM] ^a
WT	5.6 ± 0.1	45 ± 3	23 ± 1	43 ± 7
A160G	7.1 ± 0.3	21 ± 4	27 ± 4	300 ± 25
E51S	11.7 ± 0.4	38 ± 5	51 ± 1	29 ± 4
H277F	6.9 ± 0.2	18 ± 3	27 ± 1	31 ± 4
M87G	2.0 ± 0.2	140 ± 30	8 ± 1	> 500
R48N ^b	3.8 ± 0.1	33 ± 4	32 ± 1	63 ± 9
R48S	12.2 ± 0.5	32 ± 6	44 ± 2	53 ± 9
D50S	na	na	na	na
Y370F	na	na	na	na

^a Error calculated from nonlinear regression. ^b Concentration of enzyme

used for V_{max} determination was 0.83 μM for all mutants except R48N, which was run at 0.42 μM.

We also tested the effect of point mutations on competitive inhibition of NEU3 by DANA. For mutants with measurable activity, the IC₅₀ of DANA was determined (Table 2.3). Enzyme activity was measured by monitoring cleavage of the fluorogenic substrate, 4-methylumbelliferyl α-D-N-acetylneuraminic acid (4MU-NA). Cleavage of 4MU-NA by wild-type enzyme was inhibited by DANA at 43 ± 7 μM, similar to previous reports.²⁵ Slight increases to the inhibitory potency of DANA were seen in E51S (29 ± 4 μM) and H277F (31 ± 4 μM). Both R48 mutants showed moderate decreases for inhibition by DANA (R48N, 63 ± 9

μM ; R48S, $53 \pm 9 \mu\text{M}$), and the A160G and M87G mutants showed a major loss of potency for DANA ($>300 \mu\text{M}$). These results suggest that residues A160 and M87 are both critical for substrate recognition.

2.2.4 Effect of additives on NEU3 activity

Previous studies of mammalian NEU2 found that enzyme activity was dependent upon divalent metal ions, and large increases in relative activity were observed for Ca^{2+} , Mn^{2+} and Mg^{2+} ions.³³ We tested the effect of additives on the enzymatic activity of purified MBP-NEU3 for 4MU-NA (Figure 2.10). Relative to control samples, we observed only minor enhancement of NEU3 activity in the presence of Ca^{2+} (7 mM, $131 \pm 3\%$) and Mn^{2+} (7 mM, $136 \pm 4\%$). Treatment with ethylenediaminetetraacetic acid (EDTA) caused only a minor decrease in activity ($91 \pm 4\%$). Therefore, we concluded that NEU3 activity was not dependent on divalent metal ions. Despite the large number of cysteine residues in the sequence, treatment of the enzyme with DTT caused only a minor reduction in activity. Addition of surfactants (Triton X-100, $93 \pm 1\%$; and sodium cholate, $72 \pm 2\%$) resulted in a slight decrease in activity. We observed that copper salts were potent inhibitors of sialidase activity (Cu^{2+} 0.1 mM, $3 \pm 1\%$) and that the enzyme was unstable to brief treatment with alkaline pH (pH 11.5, 10 min, $10 \pm 5\%$). Both of these findings are consistent with observations made with NEU2.³³

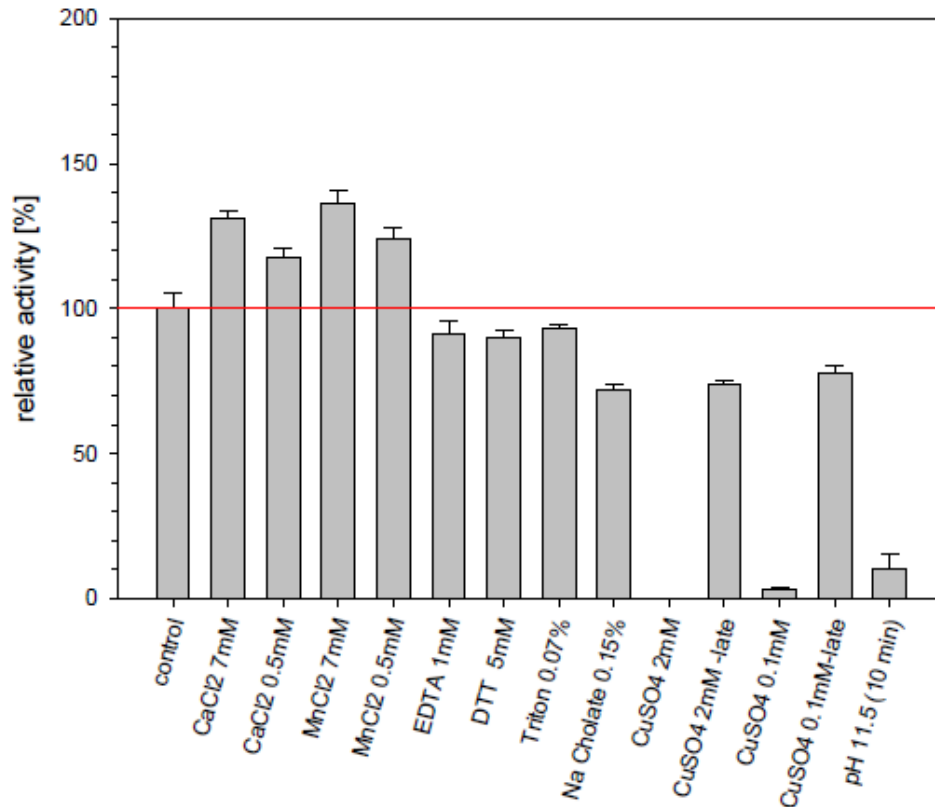


Figure 2.10: Effects of additives on NEU3 enzymatic activity. *NEU3* wild-type and mutant proteins were expressed in *E. coli* as the MBP-NEU3 fusion (pMAL-c2x) and purified as described. Assays were conducted in 0.1 M sodium acetate buffer pH = 5.0, at a protein concentration of 0.1 mg/mL as determined by A₂₈₀. Results are shown normalized to a wt control run in parallel. Additive solutions were: CaCl₂ (7 mM), CaCl₂ (0.5 mM), MnCl₂ (7 mM), MnCl₂ (0.5 mM), EDTA (1 mM), DTT (5 mM), triton X-100 (0.07 %), sodium cholate (0.15 %), CuSO₄ (2 mM), CuSO₄ (late addition, 2 mM), CuSO₄ (0.1 mM), CuSO₄ (late addition, 0.1 mM), pH 11.5 (10 min). Conditions noted as a late addition had additive treatment at the end of incubation period to test for any influence of the additive on the assay itself. The reaction was prepared by adding 4MU-NA (500 μM final

concentration), additive (to indicated final concentration) and purified enzyme (0.5 mg/mL final concentration) in a total volume of 0.04 mL. The mixture was incubated at 37 °C for 1 h, stopped and measured as described above. Each reaction was done three times along with a blank containing elution buffer instead of the enzyme. Error bars indicate the standard deviation of each point.

2.2.5 NEU3 catalytic mechanism

To obtain additional insight into the mechanism of NEU3 catalysis, we observed the enzymatic cleavage of 4MU-NA by ¹HNMR spectroscopy. The 4MU-NA substrate contains a sialic acid in an α 2,3 configuration. All known native sialidases are exclusively retaining enzymes.⁴⁶ Observation of 4MU-NA cleavage by a retaining sialidase should result in initial formation of free α -D-N-acetylneuraminic acid, though mutarotation to the β -anomer will occur subsequent to hydrolysis. A time-course of 4MU-NA hydrolysis by NEU3 is shown in Figure 2.11 and confirms that NEU3 was indeed a retaining sialidase. Additional experiments with MBP-NEU3 gave the same result (see Figure 2.12).

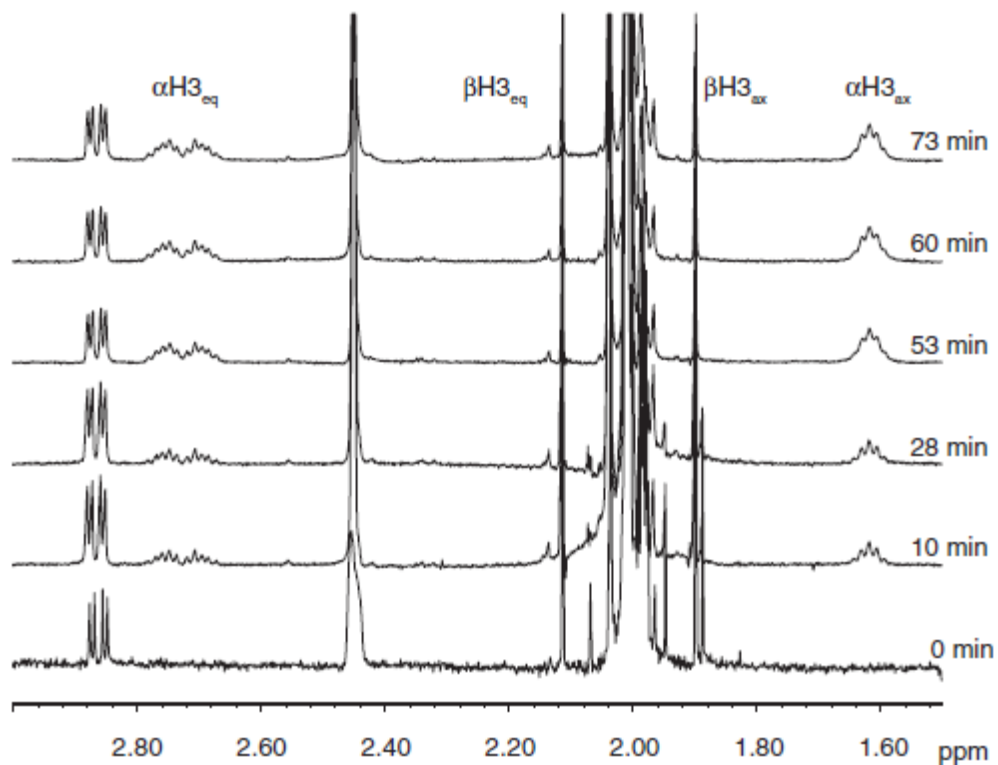


Figure 2.11: Catalytic mechanism of NEU3 studied by ^1H NMR spectroscopy.

The conversion of 4MU-NA to N-acetylneuraminic acid was observed by ^1H NMR spectroscopy (600 MHz). 4MU-NA was dissolved in D_2O (pH = 4.5, 0.1 M sodium acetate buffer; 2.9 ppm αH3_{eq}). NEU3 (pET28a, 3.8 mg/mL total protein concentration) was added to the NMR tube, and spectra were recorded at the indicated time points. During this period, only signals for the formation of α -D-N-acetylneuraminic acid (1.6 ppm αH3_{ax} , 2.7 ppm αH3_{eq}) were observed. Signals for the β -D-N-acetylneuraminic acid (1.9 ppm βH3_{ax} , 2.3 ppm βH3_{eq}) were not observed, indicating that the product was formed with retention of configuration.⁴⁶

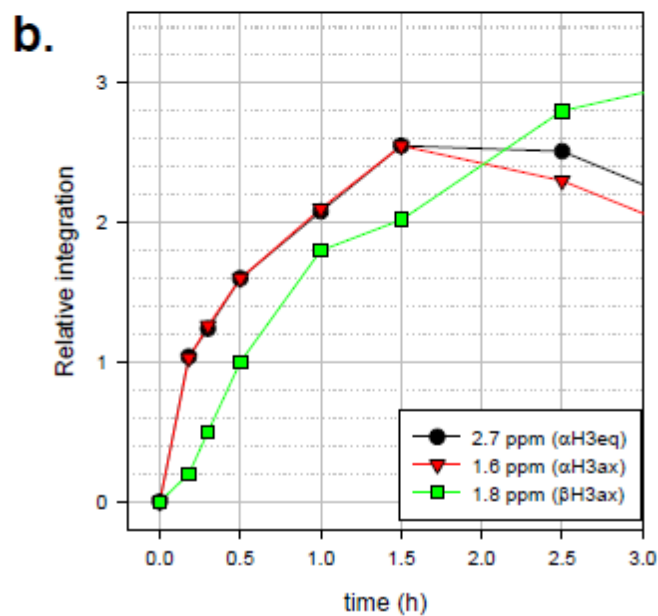
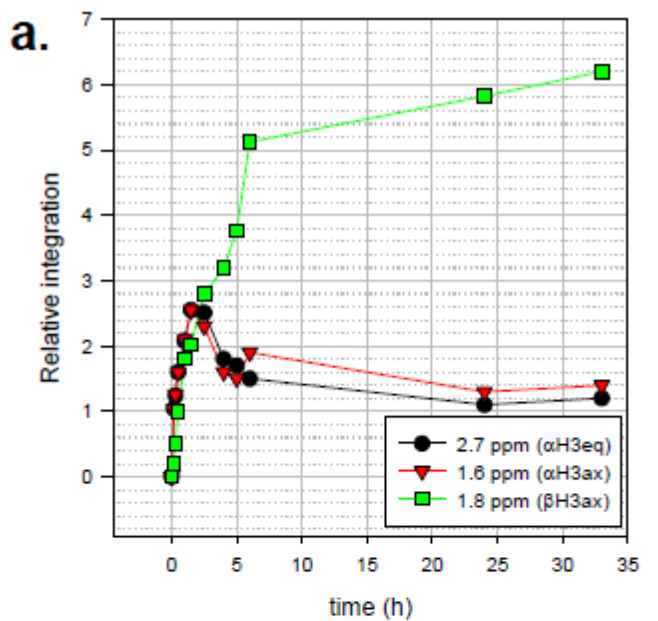


Figure 2.12: Catalytic mechanism of NEU3 by NMR. Purified MBP-NEU3 (100 μ L, 2.5 mg/mL) was mixed with 4MU-NA (4.7 mg) in D_2O with 40 mM sodium acetate buffer pH = 4.5 to a final volume of 0.7 mL. (a.) The reaction was

followed by ^1H NMR (600 MHz) at 27 °C for 35 h. Signals for α -D-N-acetylneuraminic acid (1.6 and 2.7 ppm), and β -D-N-acetylneuraminic acid (1.9 and 2.2 ppm), and 4MU-NA (2.85 ppm) were integrated and plotted as a percent of the total. (b.) An expansion plot shows the signals for α -D-N-acetylneuraminic acid precede those of the β -sialoside, consistent with a retaining sialidase mechanism.

2.3 Discussion

In this study, we provide a model of the substrate recognition and binding site topology of the human neuraminidase, NEU3. Structural studies of this membrane-associated enzyme have been hampered by its propensity for aggregation, and the model reported here adds critical new insight to the mode of substrate recognition and catalysis of NEU3. The model was validated by testing the activity of several enzyme mutants, which confirmed the identity of key catalytic residues and protein– ligand contacts. These experiments provide the most detailed model of the NEU3 active site to date and also identify residues of the enzyme which may be critical for recognition of glycolipid substrates. The binding mode of the small molecule inhibitor, DANA, and the glycolipid substrate, GM3, to NEU3 was predicted using molecular docking. We report the characterization of several important active site residues within the enzyme and collate these data with previously tested sites.¹³ Additionally, we have confirmed the structural predictions made by homology modeling of NEU3 to NEU2. Due to the low sialidase background found in *E. coli*, we were able to screen a large number of mutants in cell lysate and map out the topology of the binding site. Our

studies were enabled by the development of a robust purification strategy for recombinant protein using an MBP-fusion tag expressed in *E. coli* cells. Using purified protein, we were able to characterize the pH profile, kinetics and inhibition of NEU3. We confirmed that the enzyme is a retaining sialidase. Finally, we tested the role of metal ions, reducing agents, alkaline pH and surfactants on enzyme activity.

Our initial screening of NEU3 mutants confirms the predicted topology of the binding site found in the homology model shown in Figure 2.3. A similar model was first proposed by Magesh et al. ;²⁴ however, our results are the first to test several predictions which arise from the model. The role of E225 in catalysis had not been tested previously, and only the identity of R25 within the arginine triad (R25, R245 and R340) had been confirmed.¹³ Furthermore, we examined additional residues that likely contribute to substrate recognition through binding to sialic acid side chains. Mutation of residues predicted to form a hydrophobic binding pocket for the N5 acyl group (A160, M87, I105) and the glycerol side chain (R45, E113, Y179, and Y181) of sialic acid all lead to reduced activity in NEU3. It is interesting to note that Y179 and Y181 were previously proposed as part of a transmembrane domain (residues 174–194) within NEU3.⁴⁷ This model has been revised based on alignment to NEU2^{2, 13} and evidence that NEU3 is not a transmembrane protein but is instead a peripheral membrane-associated protein.⁴ Our data are consistent with this conclusion. Additional work will be needed to confirm the role of the putative N5 and glycerol-binding pockets. However, we note that the glycerol side-chain of Neu5Ac is much more solvent

accessible in the model than is observed in many bacterial sialidases, and even NEU2. In the NEU2 binding site, this pocket is obscured by the presence of a glutamine residue (Q270). The reason for this difference is not clear, although this feature may be one which can be exploited for the design of specific inhibitors.

Models of a small molecule inhibitor, DANA, and the glycolipid, GM3, docked to the active site of NEU3 provide valuable insight into the recognition of glycan substrates by the enzyme. In our model of GM3 substrate binding (Figure 2.3 B), we observed a possible contact between R48 and the central Gal residue of the ganglioside head group. It is interesting to note that the *O4* position of galactose is oriented towards R48, implying that attachment of a saccharide residue at this position could interfere with binding (See Figure 2.13). Examination of previous substrate specificity studies is consistent with this hypothesis. Several groups have shown that glycans that lack branching at the residue adjacent to Neu5Ac (whether α 2,3- or α 2,8-linked) are good substrates (sialyllactose, GM3, GD1a, GD1b, GD3 and GT1b), while glycans that have branching at the adjacent residue are poor substrates (GM1, GM2).^{2, 3, 6, 13, 48}

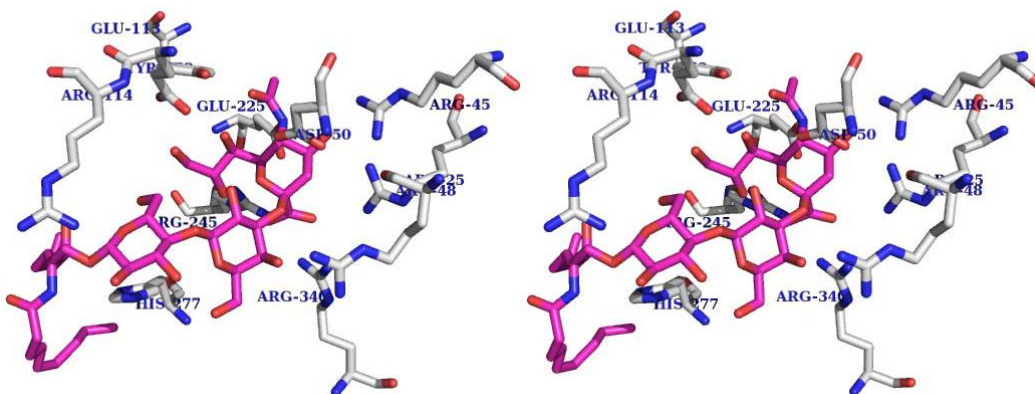


Figure 2.13: Putative glycolipid interactions. Additional residues that are predicted to interact with the glycan and lipid portions of GM3 are shown (also see Figure 2.3 B). H277 may interact with sphingosine and the reducing end carbohydrate residue (Glc). R48 is in position to interact with O4 of the galactose residue of GM3, and R114 may interact with the glucose residue of GM3. The structure is shown in stereo (crossed).

Glycolipids are the preferred substrate of NEU3; however, 4MU-NA is a moderate substrate for the enzyme, which allows for fluorescent assays to be carried out.² Using 4MU-NA, we were able to determine both the kinetic parameters of the active mutants, as well as the potency of a common sialidase inhibitor, DANA. Our measurement of the inhibition of 4MU-NA cleavage of NEU3 by DANA is in agreement with previous reports.²⁵ Mutation of D50 and Y370 eliminated measurable NEU3 activity, consistent with their role in catalysis. Modification of sites within the putative N5 pocket (A160, M87) reduced the potency of DANA significantly, with the M87G mutant exhibiting particularly low k_{cat} . Mutation of sites at the periphery of the binding site (E51, H277) had

only minor effects on inhibition by DANA, and E51S showed a large increase in rate of turnover. Alteration of R48 to serine, a site that we predict to interact with the glycan residue at the reducing end of the sialic acid, also leads to increased rate of turnover. The specificity of the active mutants for glycolipid substrates will be of interest in future work.

We first attempted to purify NEU3 using an *N*-terminal Histag. We found this strategy gave poor yields of protein, and we tried instead an *N*-terminal MBP-fusion protein. This strategy gave much better yields, and the enzyme gave a pH profile that was more consistent with previous reports. Although the MBP tag was linked to the protein with a Factor Xa cleavage site, we observed that attempts to isolate NEU3 after cleavage failed due to protein aggregation. Therefore, the more stable MBP-fusion protein was used for later experiments. These observations suggest that attempts at characterizing this enzyme by crystallography may be difficult. We examined the role of a number of conditions in the enzymatic activity of purified NEU3. We found little effect on catalysis from divalent metal ions (Ca^{2+} and Mn^{2+}) or EDTA, unlike the homolog NEU2.³³ Additionally, treatment with surfactants had only a small effect on enzymatic activity for 4MU-NA. This is in contrast to observations of NEU3 cleavage of glycolipid substrates, which found a large dependence upon surfactants. This discrepancy may indicate that the surfactant is critical for solubilizing the substrate, more than affecting enzyme structure. We also confirmed that the enzyme was unstable to alkaline pH, consistent with previous reports.⁴

All characterized native exo-sialidases are retaining enzymes, although mutagenesis can result in an inverting mechanism.⁴⁶ We confirmed that NEU3 is indeed a retaining sialidase using 1H NMR spectroscopy. The proposed mechanism of catalysis by exo-sialidases has undergone some revision²⁸ since the sequence of NEU3 was first analyzed using SDM.¹³ Our study was intended to identify the active site topology and catalytic residues of the enzyme. The expected catalytic motif includes an Asp on the b-face of the ring and a Tyr–Glu pair on the opposite face. We propose that, consistent with other GH33 family members, Tyr acts as the nucleophile after deprotonation by Glu, and the Asp residue serves as a general acid–base for the departing reducing-end glycan and an incoming water. The Tyr–Glu catalytic pair is a common feature of sialidase and trans-sialidase enzymes⁴⁴ and is most clearly supported by the observation of covalent sialyl-enzyme adducts.^{29, 45, 49} We propose that the identities of the catalytic residues in NEU3 are D50, Y370 and E225, which carry out hydrolysis of the substrate as shown in Figure 2.14.

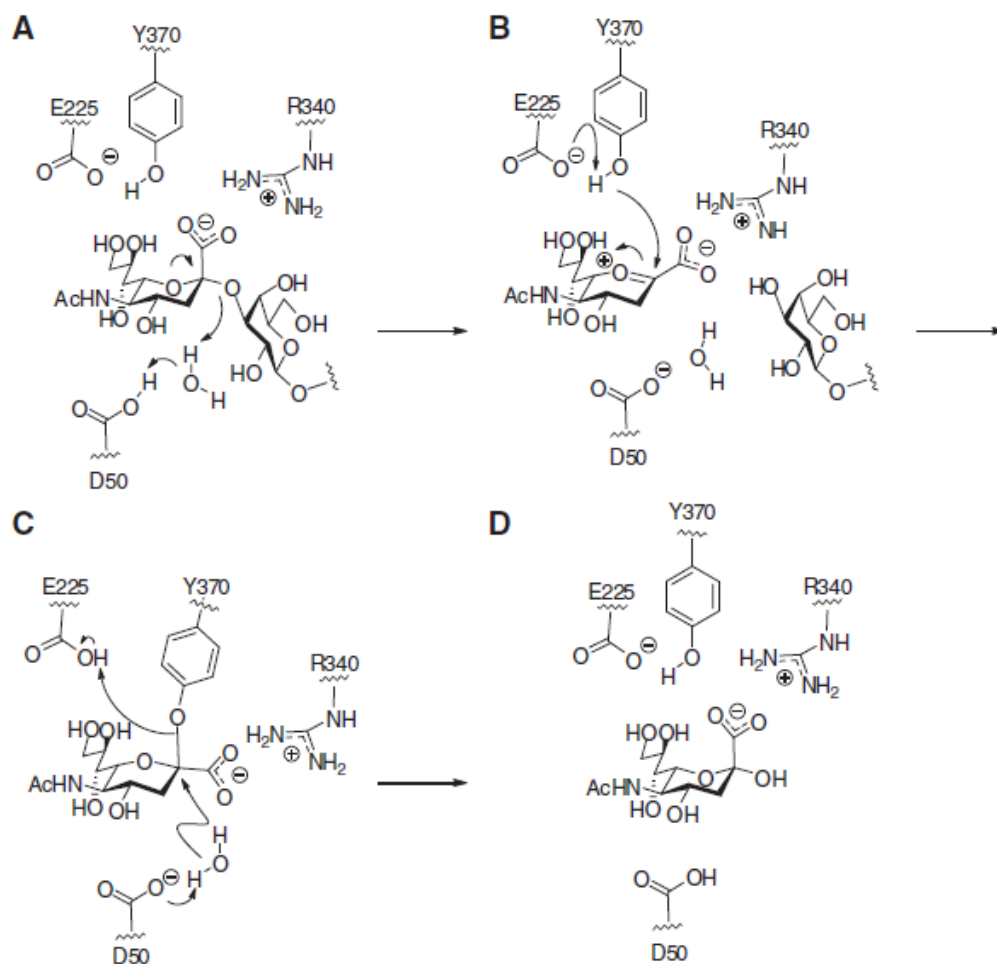


Figure 2.14: Proposed catalytic mechanism for NEU3. Based on the mutagenesis and NMR studies described, we propose the following enzymatic mechanism for NEU3 cleavage of sialosides. (A) In the first step, the reducing end of the saccharide dissociates via protonation by water or the D50 residue. (B) This results in the formation of an oxacarbenium intermediate which is attacked by the Y370 nucleophile, which requires the participation of the neighboring E225 residue. Steps A–B may occur concurrently or stepwise. (C) The enzymatic sialic acid adduct is hydrolyzed through catalysis by D50. (D) Finally, the free α -D-Neu5Ac is released from the active site.

2.4 Conclusion

In this chapter, we carried out a site-directed mutagenesis study for NEU3. The enzyme and mutants were expressed in *E.coli* and some of the mutants were purified as MBP-tagged proteins. We studied the relative efficiency of the mutants and wild type. In order to analyze the data we built a homology model for NEU3 based on the crystal structure of NEU2 which was used as a template. We tested the effects of additives on the catalytic effect of the enzyme wild type. We identified the catalytic residues of NEU3 and confirmed that it is a retaining exo-sialidase. These results help support the homology model of NEU3 by confirming sites which interact with substrates and contribute to enzyme specificity. These data will be essential in the design of experiments to observe NEU3 activity in the membrane.⁵⁰ Together, these studies provide critical insight into the active site topology of a human glycosidase enzyme involved in the pathology of cancer.¹⁴

2.5 Methods

2.5.1 NEU3 expression in *E. coli* (pET28a vector)

Sialidase expression vectors were generated by inserting human membrane-associated ganglioside sialidase 3 (NEU3) between the BamHI and XhoI sites of pET28a (Novagen, Gibbstown, NJ). The wild-type NEU3 was modified to have BglII and XhoI restriction sites by carrying out a polymerase chain reaction (PCR) using the Neu3 template, Pfu Ultra II fusion HS DNA polymerase (Stratagene, Santa Clara, CA), a forward primer for BglII (5'-GGG ATA T AGA TCT ATG GAA GTG ACA ACA TGC-3') and a reverse primer for XhoI (5'-ATT TAC TCG AGT TAA TTG CTT TTG AAT TGG CTT GGG TT-

3'). The reaction was cycled once at 95°C for 2 min followed by 30 cycles of 95°C for 20 s, 50°C for 20 s and 72°C for 25 s and 1 cycle of 72°C for 3 min. The modified Neu3 was then digested with BglIII and XhoI restriction enzymes and the pET28a vector digested with BamHI and XhoI. The digested Neu3 and pET28a were ligated together with T4 DNA ligase at a 3:1 insert to vector ratio. The resulting expression vector was transformed into electroporation competent XL1-Blue E. coli (Stratagene). Competent cells (50 µL) were mixed with plasmid DNA (3 µL, 10 ng/µL) and transferred to Gene Pulser cuvettes (BioRad, Hercules, CA). They were then electroporated (1.0 kV, 800 Ω), immediately mixed with 1 mL lysogeny broth (LB) media, grown with shaking at 37°C, 240 rpm, for 1 h and plated on LB agar with kanamycin (25 µg/mL). Clones were selected and grown in 25 µg/mL kanamycin LB medium, and the plasmids were isolated using the GeneJET Plasmid Miniprep Kit (Fermentas, Glen Burnie, MD). Clones were verified first by agarose gel electrophoresis, to check plasmid size, and then by gene sequencing with the BigDye Terminator Kit V.3.1 (Applied Biosystems, Carlsbad, CA).

2.5.2 Site-directed mutagenesis of Neu3 and purification of fusion proteins

Mutagenesis was carried out using the Quikchange II XL sitedirected mutagenesis kit (Stratagene) following the manufacturer's protocol. The following mutations were generated: R45V, D50S, E51S, M87G, I105G, E113A, A160G, Y179F, Y181F, E225S, R245A, H277F, R340A, Y370F, L408Stop, G419Stop, M87G-I105G double mutant and a M87G-I105GA160G triple mutant. The pET28a-Neu3

template described above was used as the dsDNA template for all mutations except the double and triple mutants, which used M87G and the M87G-I105G mutant plasmids, respectively, as templates. The oligonucleotide mutation primer designs are provided in Table 2.4.

Table 2.4: Primers used for generation of NEU3 mutants

Mutant		Sequences (5' -3')
D50S	native	g aag cgt tcc acg agg aga gat gag gat gct ctc
	forward	g aag cgt tcc acg agg aga tct gag gat gct ctc
	reverse	gag agc atc ctc aga tct cct cgt gga acg ctt c
E225S	native	att agg ccc atg gtt aca gta gaa tgt gaa gtg gca gag gtg
	forward	gg ccc atg gtt aca gta tca tgt gaa gtg gca gag g
	reverse	cac ctc tgc cac ttc aca tga tac tgt aac cat ggg c
Y370F	native	cac tgt ggg ccc tgt ggc tac tct gat ctg gct gct ctg g
	forward	ggg ccc tgt ggc ttc tct gat ctg gct gc
	reverse	gc agc cag atc aga gaa gcc aca ggg ccc
M87G	native	cta ccg ggg cat cgg acc atg aac ccc tgt cct gta tgg
	forward	ggg cat cgg acc ggg aac ccc tgt cct g
	reverse	c agg aca ggg gtt ccc ggt ceg atg ccc
I105G	native	tgt gtg ttc ctg ttc ttc atc tgt gtg cgg ggc cat gtc
	forward	gtg ttc ctg ttc ttc ggc tgt gtg cgg ggc
	reverse	gcc ceg cac aca gcc gaa gaa cag gaa cac
A160G	native	aag cac tgg gcc aca ttt gct gtg ggc cca ggt cat ggc atc
	forward	gcc aca ttt ggt gtg ggc cca ggt cat gg
	reverse	cc atg acc tgg gcc cac acc aaa tgt ggc
R245A	native	gtg cta tat tgc agt gcc cgg aca cca aac agg tgc cgg
	forward	cta tat tgc agt gcc gcg aca cca aac agg tgc c
	reverse	g gca cct gtt tgg tgt cgc ggc act gca ata tag
H277F	native	cag ctc tgt gag ccc cca cat ggt tgc caa ggg agt gtg g
	forward	ctc tgt gag ccc cca ttt ggt tgc caa ggg ag
	reverse	ct ccc ttg gca acc aaa tgg ggg ctc aca gag
R340A	native	cac cca acc agt agg aaa cag agg gtt gac cta ggt atc tat ctc
	forward	cac cca acc agt agg aaa cag gcc gtt gac cta ggt atc tat ctc
	reverse	gag ata gat acc tag gtc aac ggc ctg ttt cct act ggt tgg gtg
R45V	native	c ctg gcc ttt gca gag aag cgt tcc acg agg aga gat gag g
	forward	g gcc ttt gca gag aag gtt tcc acg agg aga gat g
	reverse	ctc atc tct cct cgt gga aac ctt ctc tgc aaa ggc
E113A	native	gtg cgg ggc cat gtc aca gag cgt caa cag att gtg tca ggc
	forward	gg ggc cat gtc aca gcg cgt caa cag att gtg
	reverse	cac aat ctg ttg acg cgc tgt gac atg gcc cc
Y179F	native	ggg aga ctg gtc atc cct gcg tat acc tac tac atc cct tcc
	forward	ctg gtc atc cct gcg ttt acc tac tac atc cc
	reverse	gg gat gta gta ggt aaa cgc agg gat gac cag
Y181F	native	g gtc atc cct gcg tat acc tac tac atc cct tcc tgg ttc
	forward	c atc cct gcg tat acc ttc tac atc cct tcc tgg
	reverse	cca gga agg gat gta gaa ggt ata cgc agg gat g
T403	native	cag att gcc ttc cgc ctg ttt aca cac cgg gag atc ctg

STOP	forward	g att gcc ttc cgc ctg ttt taa cac cgg gag atc c
	reverse	g gat ctc ccg gtg tta aaa cag gcg gaa ggc aat c
I407 STOP	native	ctg ttt aca cac cgg gag atc ctg agt cac ctg cag ggg
	forward	g ttt aca cac cgg gag taa ctg agt cac ctg cag ggg
	reverse	ccc ctg cag gtg act cag tta ctc ccg gtg tgt aaa c
L408 STOP	native	ca aca cac cgg gag atc ctg agt cac ctg cag ggg
	forward	ca aca cac cgg gag atc tag agt cac ctg cag ggg
	reverse	ccc ctg cag gtg act cta gat ctc ccg gtg tgt tg
G419 STOP	native	ggg gac tgc acc agc cct ggt agg aac cca agc caa ttc
	forward	g gac tgc acc agc cct tga agg aac cca agc c
	reverse	g gct tgg gtt cct tca agg gct ggt gca gtc c
E51 STOP	native	cgt tcc acg agg aga gat gag gat gct ctc cac ctg gtg
	forward	gt tcc acg agg aga gat tcc gat gct ctc cac ctg g
	reverse	c cag gtg gag agc atc gga atc tct cct cgt gga ac

Following mutagenesis, transformed clones were selected and grown in kanamycin LB medium. Plasmids were then isolated and confirmed as above. To express the mutant NEU3, plasmids were transformed into *E. coli* (DE3, Novagen) by adding 50 ng plasmid to 50 μ L competent cells and incubating on ice for 5 min followed by a 30 s, 42°C heat shock and returned to ice for 2 min. The transformation reactions were plated on LB agar plates with final concentrations of 35 μ g/mL chloramphenicol and 25 μ g/mL kanamycin. Clones were selected and grown in 35 μ g/mL chloramphenicol and 25 μ g/mL kanamycin LB medium for 7 h, after which 50% glycerol was added to a final concentration of 15%, and these stocks were stored at -80°C . Some cells were scraped from the frozen bacteria glycerol stock and transferred into 10 mL 1% glucose LB medium with chloramphenicol and kanamycin. The cultures were incubated on a shaker at 37°C at 225 rpm for 16 h. A culture of these cells (diluted to OD₆₀₀ of 0.3 in 10 mL) was collected by centrifugation at 16,000 \times g for 2 min and the supernatant decanted. These cells were then resuspended and grown at 37°C with shaking at

225 rpm in another 10 mL of 1% glucose LB media with antibiotics for >1 h until the OD₆₀₀ reached 0.5. Isopropyl β-D-1-thiogalactopyranoside (IPTG) was then added to a final concentration of 100 μM to induce transcription and incubated at 20°C with shaking at 225 rpm for 16 h. The culture was diluted to aliquots (OD₆₀₀ of 3.5 for 1 mL) and the cells collected by centrifugation at 16,000 × g for 2 min. The supernatants were decanted and the pellets stored in 1.5 mL microcentrifuge tubes at -80°C.

MBP-fusion proteins (MBP-NEU3) were generated from a pMAL-c2x/*Neu3* construct. The plasmid was cloned using pRSET/*Neu3* as a template. The *Neu3* gene was PCR-amplified using the forward primer OBZ51 (5'-AA TTC GAATTC ATG GAA GAA GTG ACA ACA TGC TCC-3') to introduce an *EcoRI* site at the 5' end and the reverse primer OBZ52 (5'- GG TTG AAG CTT TTA ATT GCT TTT GAA TTG GCT TGG-3') to introduce a *HindIII* site at the 3' end of the *Neu3* gene. The PCR product was purified from the reaction mixture using a QIAquick[®] PCR purification kit (Qiagen, Valencia, CA). The final DNA fragment resulting from the PCR reaction was digested with the restriction enzymes *EcoRI* and *HindIII*, isolated from a 1% agarose gel, and was then ligated into the pMAL-c2x vector which had been digested with *EcoRI* and *HindIII*. The resulting MBP-NEU3 plasmid was transformed into *E. coli* DH5α cells (Invitrogen, Carlsbad, CA). Selected transformants were screened for the presence of the recombinant plasmid by restriction mapping and DNA sequence analysis. The clone was termed pMBP-Neu3 and was subsequently transformed into a host

strain, competent *E. coli* TB1 cells (New England Biolabs, Ipswich, MA) for further expression.

Protein was isolated by culturing *E. coli* TB1 cells containing plasmid pMBP-Neu3 and its mutants in LB medium containing ampicillin (100 µg/mL) to OD₆₀₀ of 0.5 at 37°C. Production of the fusion protein was induced by adding IPTG to a final concentration of 0.3 mM at 20°C. Cells were harvested by centrifugation after 16 h of induction. The pellet was resuspended (50 mL/L of medium) in resuspension buffer (20 mM morpholinopropane sulfonic acid (MOPS), pH 7.2, 200 mM NaCl, 1 mM EDTA and 0.1% Triton X-100) supplemented with 1 complete protease inhibitor tablet (Roche). The lysate was passed through a cell disruptor once at 20,000 psi and then immediately pelleted by centrifugation at 105,000 × g for 60 min at 4°C. The supernatant was loaded onto an amylose column (New England Biolabs) equilibrated with 20 mM MOPS (200 mM NaCl, pH 7.2). MBP-fusion protein was eluted with running buffer containing 10% glycerol (v/v) and 10 mM maltose.

Proteins were detected by immunoblotting. For proteins expressed in pET28a, enzyme extract was separated using 10% sodium dodecyl sulfate–polyacrylamide gel electrophoresis. Proteins were transferred to nitrocellulose membrane using electroblotting (30 V, overnight). The membrane was blocked with 2.5% bovine serum albumin (BSA) in Trisbuffered saline Tween-20 buffer, and proteins were detected with anti-His-tag antibody (HisProbe-HRP, Thermo Scientific). Blots were visualized with an HRP chemiluminescent kit (Pierce). For MBP-NEU3 fusion proteins, blotting was performed with an anti-MBP antibody

(primary: anti-MBP, 1:20,000; secondary: goat-anti-mouse IgG-HRP, 1:100,000; New England Biolabs).

2.5.3 Screening of mutant enzyme activity

Stored pellets of cells (OD_{600} of 3.5) expressing NEU3 (pET28a) were lysed and the protein extracted by adding B-PER reagent (300 μ L) (Thermo Scientific, Waltham, MA). The samples were vortexed for 1 min and incubated on ice for 5 min. Total protein concentration in the lysate was determined using the A280 of serial dilutions. To determine NEU activity, 2'-(4-methylumbelliferyl)- α -D-N-acetylneuraminic acid (4MU-NA) was used as a fluorogenic substrate. For pH profiles, enzyme activity was measured at pH 3.7, 4.0, 4.25, 4.50, 4.75, 5.0, 5.5 (0.1 M sodium acetate), 5.25, 6.0, 6.5, 7.0, 7.5 and 8.0 (0.1 M sodium phosphate). All samples were run in triplicate, with negative controls containing buffer alone and 4MU-NA in buffer. Reaction mixtures of lysate (0.1 mg/ mL total protein, 200 μ L) and controls were briefly vortexed and incubated for 1 h at 37°C. To stop the reactions, 200 μ L 0.2 M glycine/NaOH pH 10.2 was added to each reaction. The mixtures were then centrifuged at 16,000 \times g for 10 min. Supernatant (200 μ L) was removed from each reaction to a 96- well plate. Fluorescence was then measured on a SpectraMax M2 microplate reader (Molecular Devices, Sunnyvale, CA) with excitation 365 nm and emission 445 nm. For comparison of activity between mutants, total protein concentration was adjusted to 25 mg/mL, and reactions were carried out at pH = 5.0 in 0.1 M sodium acetate buffer.

2.5.4 Enzyme kinetics and inhibition by DANA

Purified MBP-NEU3 fusion proteins were used to determine the kinetics of 4MU-NA cleavage. Reactions were prepared by mixing 4MU-NA (25, 50, 75, 100, 150, 200, 250, 300 μ M), purified fusion protein (0.04 mg/mL), and BSA (4 mg/mL) in sodium acetate buffer (0.1 M, pH = 5.0). The rate of product formation was observed in real-time by fluorescence (340 nm excitation and 455 nm emission) on a SpectraMax M2 microplate reader (Molecular Devices) for 90 min at 37°C. Kinetic parameters were determined by linear regression. For inhibitor studies, the kinetic assay described above was modified by adding 2 μ L of a serial dilution of DANA to 18 μ L of enzyme (0.1 mg/mL) to achieve final inhibitor concentrations of 5, 10, 20, 50, 100, 200, 500 and 1000 μ M. The mixture was incubated at 37°C for 30 min. After incubation, 2 μ L of 10 mM 4MU-NA and 18 μ L of 0.1 M acetate buffer (pH = 5.0) were added to the reaction tube and incubated for 1 h. The reactions were stopped and measured as described above. K_m and V_{max} were generated by non-linear regression of data using Michaelis–Menten equation:

$$v = \frac{V_{max} S}{K_m + S}$$

2.5.5 Homology modeling of NEU3

NEU2 and NEU3 sequences were obtained from the Uniprot database (accession NEU2: Q9Y3R4 and NEU3: Q9UQ49). The two sequences were aligned using ClustalW.³⁴ The NEU2 crystal structure was obtained from the

RCSB (PDB ID: 1VCU). Chain A, water and nonprotein residues were removed using pymol, and the homology model was generated using Modeller 9v6.³⁵ DANA and GM3 were docked in the active site using Autodock 4.0 with a grid box of $60 \times 40 \times 40 \text{ \AA}$.³⁹

2.6 References

1. Cantarel, B. L.; Coutinho, P. M.; Rancurel, C.; Bernard, T.; Lombard, V.; Henrissat, B., The Carbohydrate-Active EnZymes database (CAZy): an expert resource for Glycogenomics. *Nucleic Acids Research* **2009**, *37*, D233-D238.
2. Monti, E.; Bassi, M. T.; Papini, N.; Riboni, M.; Manzoni, M.; Venerando, B.; Croci, G.; Preti, A.; Ballabio, A.; Tettamanti, G.; Borsani, G., Identification and expression of NEU3, a novel human sialidase associated to the plasma membrane. *Biochemical Journal* **2000**, *349*, 343-351.
3. Kopitz, J.; Oehler, C.; Cantz, M., Desialylation of extracellular GD1a-neoganglioside suggests cell surface orientation of the plasma membrane-bound ganglioside sialidase activity in human neuroblastoma cells. *Febs Letters* **2001**, *491* (3), 233-236.
4. Zanchetti, G.; Colombi, P.; Manzoni, M.; Anastasia, L.; Caimi, L.; Borsani, G.; Venerando, B.; Tettamanti, G.; Preti, A.; Monti, E.; Bresciani, R., Sialidase NEU3 is a peripheral membrane protein localized on the cell surface and in endosomal structures. *Biochemical Journal* **2007**, *408*, 211-219.
5. Seyrantepe, V.; Landry, K.; Trudel, S.; Hassan, J. A.; Morales, C. R.; Pshezhetsky, A. V., Neu4, a novel human lysosomal lumen sialidase, confers normal phenotype to sialidosis and galactosialidosis cells. *Journal of Biological Chemistry* **2004**, *279* (35), 37021-37029.
6. Ha, K. T.; Lee, Y. C.; Cho, S. H.; Kim, J. K.; Kim, C. H., Molecular characterization of membrane type and ganglioside-specific sialidase (Neu3) expressed in E-coli. *Molecules and Cells* **2004**, *17* (2), 267-273.

7. Wang, P.; Zhang, J.; Bian, H.; Wu, P.; Kuvelkar, R.; Kung, T. T.; Crawley, Y.; Egan, R. W.; Billah, M. M., Induction of lysosomal and plasma membrane-bound sialidases in human T-cells via T-cell receptor. *Biochemical Journal* **2004**, *380*, 425-433.
8. Wang, Y.; Yamaguchi, K.; Wada, T.; Hata, K.; Zhao, X. J.; Fujimoto, T.; Miyagi, T., A close association of the ganglioside-specific sialidase Neu3 with caveolin in membrane microdomains. *Journal of Biological Chemistry* **2002**, *277* (29), 26252-26259.
9. Edidin, M., The state of lipid rafts: From model membranes to cells. *Annual Review of Biophysics and Biomolecular Structure* **2003**, *32*, 257-283.
10. Kalka, D.; von Reitzenstein, C.; Kopitz, J.; Cantz, M., The plasma membrane ganglioside sialidase cofractionates with markers of lipid rafts. *Biochemical and Biophysical Research Communications* **2001**, *283* (4), 989-993.
11. Yanagisawa, M.; Ariga, T.; Yu, R. K., Cholera toxin B subunit binding does not correlate with GM1 expression: a study using mouse embryonic neural precursor cells. *Glycobiology* **2006**, *16* (9), 19G-22G.
12. Li, S. C.; Li, Y. T.; Moriya, S.; Miyagi, T., Degradation of G(M1) and G(M2) by mammalian sialidases. *Biochemical Journal* **2001**, *360*, 233-237.
13. Wang, Y.; Yamaguchi, K.; Shimada, Y.; Zhao, X. J.; Miyagi, T., Site-directed mutagenesis of human membrane-associated ganglioside sialidase - Identification of amino-acid residues contributing to substrate specificity. *European Journal of Biochemistry* **2001**, *268* (8), 2201-2208.

14. Miyagi, T.; Wada, T.; Yamaguchi, K., Roles of plasma membrane-associated sialidase NEU3 in human cancers. *Biochimica Et Biophysica Acta-General Subjects* **2008**, *1780* (3), 532-537.
15. Zhang, J.; Yu, K. Q.; Zhu, W. L.; Jiang, H. L., Neuraminidase pharmacophore model derived from diverse classes of inhibitors. *Bioorganic & Medicinal Chemistry Letters* **2006**, *16* (11), 3009-3014.
16. Chien, C. H.; Shann, Y. J.; Sheu, S. Y., Site-directed mutations of the catalytic and conserved amino acids of the neuraminidase gene, nanH, of *Clostridium perfringens* ATCC 10543. *Enzyme and Microbial Technology* **1996**, *19* (4), 267-276.
17. Crennell, S.; Garman, E.; Laver, G.; Vimr, E.; Taylor, G., Crystal-structure of vibrio-cholerae neuraminidase reveals dual lectin-like domains in addition to the catalytic domain. *Structure* **1994**, *2* (6), 535-544.
18. Demir, O.; Roitberg, A. E., Modulation of catalytic function by differential plasticity of the active site: case study of *Trypanosoma cruzi* trans-sialidase and *Trypanosoma rangeli* sialidase. *Biochemistry* **2009**, *48* (15), 3398-3406.
19. Monti, E.; Preti, A.; Rossi, E.; Ballabio, A.; Borsani, G., Cloning and characterization of NEU2, a human gene homologous to rodent soluble sialidases. *Genomics* **1999**, *57* (1), 137-143.
20. Pshezhetsky, A. V.; Richard, C.; Michaud, L.; Igdoura, S.; Wang, S. P.; Elsliger, M. A.; Qu, J. Y.; Leclerc, D.; Gravel, R.; Dallaire, L.; Potier, M.,

Cloning, expression and chromosomal mapping of human lysosomal sialidase and characterization of mutations in sialidosis. *Nature Genetics* **1997**, *15* (3), 316-320.

21. Wada, T.; Yoshikawa, Y.; Tokuyama, S.; Kuwabara, M.; Akita, H.; Miyagi, T., Cloning, expression, and chromosomal mapping of a human ganglioside sialidase. *Biochemical and Biophysical Research Communications* **1999**, *261* (1), 21-27.

22. Monti, E.; Bassi, M. T.; Bresciani, R.; Civini, S.; Croci, G. L.; Papini, N.; Riboni, M.; Zanchetti, G.; Ballabio, A.; Preti, A.; Tettamanti, G.; Venerando, B.; Borsani, G., Molecular cloning and characterization of NEU4, the fourth member of the human sialidase gene family. *Genomics* **2004**, *83* (3), 445-453.

23. Chavas, L. M. G.; Tringali, C.; Fusi, P.; Venerando, B.; Tettamanti, G.; Kato, R.; Monti, E.; Wakatsuki, S., Crystal structure of the human cytosolic sialidase Neu2 - Evidence for the dynamic nature of substrate recognition. *Journal of Biological Chemistry* **2005**, *280* (1), 469-475.

24. Magesh, S.; Suzuki, T.; Miyagi, T.; Ishida, H.; Kiso, M., Homology modeling of human sialidase enzymes NEU1, NEU3 and NEU4 based on the crystal structure of NEU2: Hints for the design of selective NEU3 inhibitors. *Journal of Molecular Graphics & Modelling* **2006**, *25* (2), 196-207.

25. Magesh, S.; Moriya, S.; Suzuki, T.; Miyagi, T.; Ishida, H.; Kiso, M., Design, synthesis, and biological evaluation of human sialidase inhibitors. Part 1: Selective inhibitors of lysosomal sialidase (NEU1). *Bioorganic & Medicinal Chemistry Letters* **2008**, *18* (2), 532-537.

26. Hata, K.; Koseki, K.; Yamaguchi, K.; Moriya, S.; Suzuki, Y.; Yingsakmongkon, S.; Hirai, G.; Sodeoka, M.; von Itzstein, M.; Miyagi, T., Limited inhibitory effects of oseltamivir and zanamivir on human sialidases. *Antimicrobial Agents and Chemotherapy* **2008**, *52* (10), 3484-3491.
27. von Itzstein, M., The war against influenza: discovery and development of sialidase inhibitors. *Nature Reviews Drug Discovery* **2007**, *6* (12), 967-974.
28. Buschiazzo, A.; Alzari, P. M., Structural insights into sialic acid enzymology. *Current Opinion in Chemical Biology* **2008**, *12* (5), 565-572.
29. Watts, A. G.; Damager, I.; Amaya, M. L.; Buschiazzo, A.; Alzari, P.; Frasch, A. C.; Withers, S. G., Trypanosoma cruzi trans-sialidase operates through a covalent sialyl-enzyme intermediate: Tyrosine is the catalytic nucleophile. *Journal of the American Chemical Society* **2003**, *125* (25), 7532-7533.
30. Amaya, M. F.; Buschiazzo, A.; Nguyen, T.; Alzari, P. M., The high resolution structures of free and inhibitor-bound Trypanosoma rangeli sialidase and its comparison with T-cruzi trans-sialidase. *Journal of Molecular Biology* **2003**, *325* (4), 773-784.
31. Watson, J. N.; Newstead, S.; Narine, A. A.; Taylor, G.; Bennet, A. J., Two nucleophilic mutants of the Micromonospora viridifaciens sialidase operate with retention of configuration by two different mechanisms. *ChemBiochem* **2005**, *6* (11), 1999-2004.
32. Newstead, S.; Watson, J. N.; Knoll, T. L.; Bennet, A. J.; Taylor, G., Structure and mechanism of action of an inverting mutant sialidase. *Biochemistry* **2005**, *44* (25), 9117-9122.

33. Albouz-Abo, S.; Turton, R.; Wilson, J. C.; von Itzstein, M., An investigation of the activity of recombinant rat skeletal muscle cytosolic sialidase. *Febs Letters* **2005**, 579 (5), 1034-1038.
34. Thompson, J. D.; Higgins, D. G.; Gibson, T. J., CLUSTAL-W - improving the sensitivity of progressive multiple sequence alignment through sequence weighting, position-specific gap penalties and weight matrix choice. *Nucleic Acids Research* **1994**, 22 (22), 4673-4680.
35. Lambert, C.; Leonard, N.; De Bolle, X.; Depiereux, E., ESyPred3D: Prediction of proteins 3D structures. *Bioinformatics* **2002**, 18 (9), 1250-1256.
36. Sippl, M. J., Recognition of errors in 3-dimensional structures of proteins. *Proteins-Structure Function and Genetics* **1993**, 17 (4), 355-362.
37. Wiederstein, M.; Sippl, M. J., ProSA-web: interactive web service for the recognition of errors in three-dimensional structures of proteins. *Nucleic Acids Research* **2007**, 35, W407-W410.
38. Laskowski, R. A.; Macarthur, M. W.; Moss, D. S.; Thornton, J. M., PROCHECK - a program to check the stereochemical quality of protein structures. *Journal of Applied Crystallography* **1993**, 26, 283-291.
39. Goodsell, D. S.; Morris, G. M.; Olson, A. J., Automated docking of flexible ligands: Applications of AutoDock. *Journal of Molecular Recognition* **1996**, 9 (1), 1-5.
40. Morris, G. M.; Goodsell, D. S.; Huey, R.; Olson, A. J., Distributed automated docking of flexible ligands to proteins: Parallel applications of

AutoDock 2.4. *Journal of Computer-Aided Molecular Design* **1996**, *10* (4), 293-304.

41. Bernardi, A.; Potenza, D.; Capelli, A. M.; Garcia-Herrero, A.; Canada, F. J.; Jimenez-Barbero, J., Second-generation mimics of ganglioside GM1 oligosaccharide: A three-dimensional view of their interactions with bacterial enterotoxins by NMR and computational methods. *Chemistry-a European Journal* **2002**, *8* (20), 4598-4612.

42. Gestwicki, J. E.; Strong, L. E.; Borchardt, S. L.; Cairo, C. W.; Schnoes, A. M.; Kiessling, L. L., Designed potent multivalent chemoattractants for *Escherichia coli*. *Bioorganic & Medicinal Chemistry* **2001**, *9* (9), 2387-2393.

43. Albohy, A.; Li, M. D.; Zheng, R. B.; Zou, C.; Cairo, C. W., Insight into substrate recognition and catalysis by the human neuraminidase 3 (NEU3) through molecular modeling and site-directed mutagenesis. *Glycobiology* **2010**, *20* (9), 1127-1138.

44. Amaya, M. F.; Watts, A. G.; Damager, I.; Wehenkel, A.; Nguyen, T.; Buschiazzi, A.; Paris, G.; Frasch, A. C.; Withers, S. G.; Alzari, P. M., Structural insights into the catalytic mechanism of *Trypanosoma cruzi* trans-sialidase. *Structure* **2004**, *12* (5), 775-784.

45. Watts, A. G.; Oppezzo, P.; Withers, S. G.; Alzari, P. M.; Buschiazzi, A., Structural and kinetic analysis of two covalent sialosyl-enzyme intermediates on *Trypanosoma rangeli* sialidase. *Journal of Biological Chemistry* **2006**, *281* (7), 4149-4155.

46. Watson, J. N.; Dookhun, V.; Borgford, T. J.; Bennet, A. J., Mutagenesis of the conserved active-site tyrosine changes a retaining sialidase into an inverting sialidase. *Biochemistry* **2003**, *42* (43), 12682-12690.
47. Miyagi, T.; Wada, T.; Iwamatsu, A.; Hata, K.; Yoshikawa, Y.; Tokuyama, S.; Sawada, M., Molecular cloning and characterization of a plasma membrane-associated sialidase specific for gangliosides. *Journal of Biological Chemistry* **1999**, *274* (8), 5004-5011.
48. Papini, N.; Anastasia, L.; Tringali, C.; Croci, G.; Bresciani, R.; Yamaguchi, K.; Miyagi, T.; Preti, A.; Prinetti, A.; Prioni, S.; Sonnino, S.; Tettamanti, G.; Venerando, B.; Monti, E., The plasma membrane-associated sialidase MmNEU3 modifies the ganglioside pattern of adjacent cells supporting its involvement in cell-to-cell interactions. *Journal of Biological Chemistry* **2004**, *279* (17), 16989-16995.
49. Newstead, S. L.; Potter, J. A.; Wilson, J. C.; Xu, G.; Chien, C.-H.; Watts, A. G.; Withers, S. G.; Taylor, G. L., The structure of *Clostridium perfringens* NanI sialidase and its catalytic intermediates. *Journal of Biological Chemistry* **2008**, *283* (14), 9080-9088.
50. Cairo, C. W.; Key, J. A.; Sadek, C. M., Fluorescent small-molecule probes of biochemistry at the plasma membrane. *Current Opinion in Chemical Biology* **2010**, *14* (1), 57-63.

3 Inhibition of human neuraminidase 3 (NEU3) by C9-triazole derivatives of 2,3-didehydro-N-acetyl-neuraminic acid and the identification of selective nanomolar inhibitors of the human neuraminidase, NEU4^{1,2}

¹ Portions of this chapter have been published in: Albohy, A.; Zhang, Y.; Smutova, V.; Pshezhetsky, A. V.; Cairo, C. W., Identification of Selective Nanomolar Inhibitors of the Human Neuraminidase, NEU4. *ACS Med Chem Lett* **2013**, 4 (6), 532-537; Zou, Y.; Albohy, A.; Sandbhor, M.; Cairo, C. W., Inhibition of human neuraminidase 3 (NEU3) by C9-triazole derivatives of 2,3-didehydro-N-acetyl-neuraminic acid. *Bioorganic & Medicinal Chemistry Letters* **2010**, 20 (24), 7529-7533.

² Compounds used in these studies were synthesized and characterized by Yao Zou and Yi Zhang, University of Alberta. NEU1 was provided by Victoria Smutova and Alexey V. Pshezhetsky, University of Montreal.

3.1 Introduction

The mammalian sialidase enzymes are a family of glycosyl hydrolases which cleave the terminal sialic acid residue from glycoproteins and glycolipids.¹ Dysfunction of these enzymes can result in sialic acid storage disorders, such as type I and II sialidosis.^{2,3} Mammalian sialidase enzymes also play essential roles in cellular function, with reported effects on diverse processes including neurite outgrowth,⁴ immune cell activation,⁵ cellular communication,^{6, 7, 8} signaling,^{5, 9, 10,} adhesion,¹¹ as well as the apoptosis^{13,14} and metastasis of malignant cells.^{15,16} Selective, tight-binding inhibitors of sialidase isoforms could provide an essential tool for discerning the role of individual isozymes in cell biology. However, while nanomolar inhibitors are known for pathogenic neuraminidase enzymes, most notably the influenza viral neuraminidase, no inhibitors of similar potency are known for the human enzymes.¹⁷

Currently identified members of the sialidase enzyme family in humans consist of NEU1, NEU2, NEU3, and NEU4. All four enzymes are classified as exo-sialidases (EC 3.2.1.18) and members of glycoside hydrolase family 33 in the CAZy database.¹⁸ Among the mammalian enzymes, only the human NEU2 structure has been studied by crystallography, revealing that the enzyme adopts a six-bladed β -propeller fold.^{19,20} Homology models of all four human enzymes were first proposed by Magesh et al. in 2006; however, many of the specific features of the models remain to be experimentally tested.²¹ For example, the predicted catalytic residues have only been confirmed in NEU2¹⁹ and NEU3.²² There are few reports of inhibitors tested against the family of human NEU

enzymes. A panel of 9-amino-9-deoxy-2,3-didehydro-*N*-acetyl-neuraminic acid derivatives were tested against all four enzymes; the most potent of these inhibitors showed only low micromolar activity against NEU1.²³ A library of benzoic acid derivatives have also been tested against all four isozymes.²⁴ The viral neuraminidase inhibitors zanamivir and oseltamivir have limited potency against all of the human sialidases.²⁵ However, tight-binding (<1 μ M) and selective inhibitors for individual isozymes remain to be identified.

Our group is interested in the substrate recognition and catalysis of human NEU3, the plasma membrane-associated sialidase, which modifies glycolipid substrates.²² This enzyme is particularly challenging due to its hydrophobic character and propensity for aggregation. We tested the predictions of a NEU3 homology model using site-directed mutagenesis, and validated both the catalytic residues and several residues which are essential for substrate recognition (see Chapter 1). As part of that study, we performed molecular docking of a well-known sialidase inhibitor, 2,3-didehydro-*N*-acetyl-neuraminic acid (DANA). Our molecular docking studies of DANA in the NEU3 binding site revealed a relatively large hydrophobic pocket adjacent to the *C9* position of sialic acid. We hypothesized that this region of the binding site could be used to design improved inhibitors of NEU3 based on the DANA core structure.

Known substrates of NEU3 include α 2,3-linked sialosides (Table 3.1) found in glycolipid substrates, such as GM3.²⁶ Additionally, α 2,8-linked sialosides are known to be substrates for the enzyme, and there is evidence that the enzyme has a preference for this linkage.¹³ A common strategy for the design

of sialidase inhibitors relies on the use of DANA as a proposed transition state analog. The inhibition of NEU3 by DANA has been reported by several groups, and is usually found to be in the mid-micromolar range (Table 3.1).^{22,23,25} Interestingly, zanamivir, a potent viral NEU inhibitor has been reported to have low micromolar activity against NEU3, while oseltamivir is essentially inactive against the enzyme.²⁵ Magesh et al. found that NEU3 could tolerate a relatively bulky phenyl-amide group at the *C9* position of DANA, although these derivatives had relatively low potency (Table 3.1).²³ We considered that a potential strategy for rapidly exploring the structure activity relationships (SAR) of DANA analogs for NEU3 could revolve around a modular synthetic strategy which introduced modifications at the *C9*- and *N5Ac*-positions from a common intermediate. Li et al. first reported the use of click chemistry to generate viral NEU inhibitors from a *C4*-azido-derivative of DANA.²⁷ Lu and Gervay-Hague expanded on this strategy by generating *C4*- and *C7*-azido DANA analogs, which could be elaborated to triazoles and multivalent derivatives of zanamivir.²⁸ In a related strategy, non-hydrolyzable sialoside derivatives have been generated by incorporating an azide at *C2* of Neu5Ac.²⁹

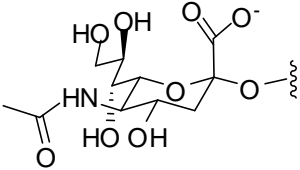
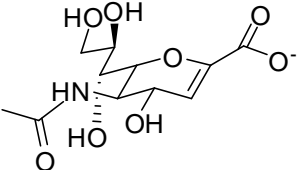
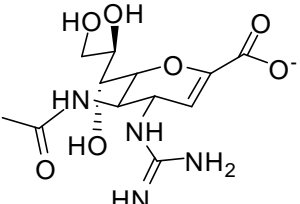
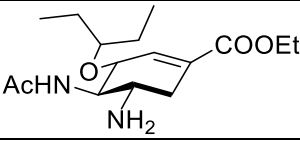
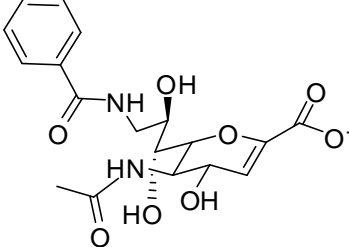
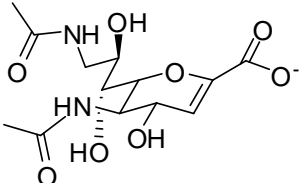
Furthermore, there are few reports of selective inhibitors against hNEU, and the most potent inhibitors currently known are of mid- to low-micromolar activity. Magesh et al. reported compounds selective for NEU1 ($IC_{50} \sim 10 \mu M$).²³ Inhibitors which target hNEU over bacterial NEU have been reported.^{30,31} Potent inhibitors of vNEU have only moderate activity against hNEU, with zanamivir being the most potent of these against NEU2 ($IC_{50} \sim 16 \mu M$).²⁵ We will discuss

studies from our group on the activity of oseltamivir derivatives that show mild selectivity for NEU3 over NEU4 (Chapter 1).³² Work to identify selective compounds using a series of C4, C7-modified DANA-analogs designed to target specific isoenzymes of hNEU will be discussed in Chapter 4. This study identified compounds with 12- to 40-fold selectivity against NEU2 and NEU3, respectively.³³ However, all these previous reports of inhibitors for hNEU have failed to identify compounds with sufficient potency or selectivity to be used *in vivo*.

In this chapter, we will first describe the generation of a small library of DANA analogs with modifications at the C9 and N5Ac as a means to explore the binding site topology of NEU3 and to identify new inhibitors of the enzyme. Part of this library was then tested against the whole human sialidase family (hNEU1-hNEU4) after development of these assays.

The identity and purity of the most potent compounds used in this study was confirmed by high resolution mass spectrometry, and HPLC was used to confirm that all samples were >95% purity. We then proceeded to test compounds for their ability to inhibit NEU1, NEU2, NEU3, and NEU4 enzymes.³⁴

Table 3.1: Previously reported inhibitors of NEU3

entry	compound	structure	NEU3 IC ₅₀	[μ M]
1	α -sialoside		na	
2	DANA		70 61 43	± 15 ^{25a} _{23b} ± 7 ^{35b}
3	zanamivir		7	± 3 ^{25a}
4	oseltavimivir		>10000	^{25a}
5	10b ^c		320	_{23b}
6	10a ^c		>1000	_{23b}

a Determined by inhibition of GM3 hydrolysis.

b Determined by inhibition of 4MU-NA hydrolysis.

c Nomenclature as used in Magesh *et al.*²³

3.2 Results and Discussion*

3.2.1 C9 and N5 libraries test against NEU3

The basis of our strategy relied on the generation of two derivatives, the 9-azido-9-deoxy (**3.6**) and N5-azidoacetyl- (**3.12**) DANA derivatives (Figure 3.1).

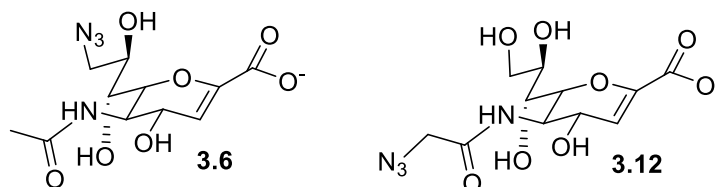


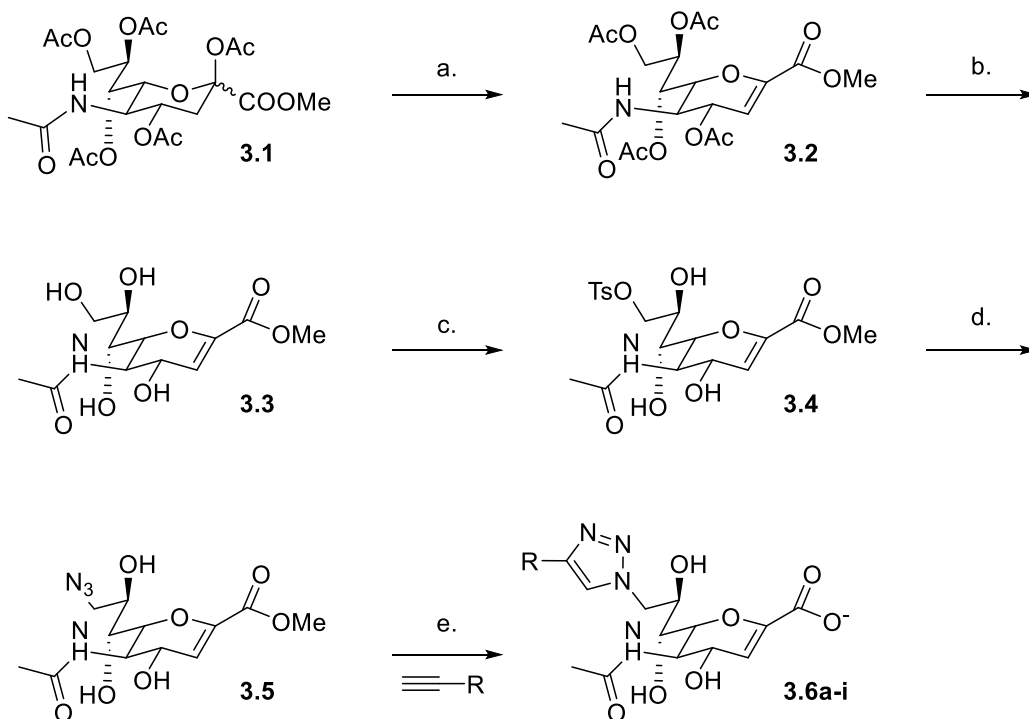
Figure 3.1: DANA analog synthetic targets.

We began our synthesis from N5-acetylneuraminic acid (Neu5Ac), which could be converted to the peracetylated methyl ester, **3.1**, following reported methods.^{36,37} We obtained moderate yields of the acetyl-protected 2,3-didehydro analog (**3.2**) using triphenylphosphine hydrobromide (Scheme 3.1).^{38,39} To prepare compound **3.6** and the related triazole derivatives, **3.2** was deacetylated⁴⁰ and the O9 position was selectively converted to a sulfonate ester, **3.4**.⁴¹ The sulfonate could then be displaced with sodium azide to give the methyl ester of **3.6**, compound **3.5**.⁴¹ Hydrolysis of **3.5** under basic conditions provided the target compound **3.6**. Alternatively, **3.5** could be used to generate triazole derivatives using the copper-catalyzed 1,3-dipolar Huisgen addition of an alkyne, also known as a Cu-catalyzed azide-alkyne cycloaddition (CuAAC).⁴² We generated a series

* Compounds used in these studies were synthesized and characterized by

Yao Zou and Yi Zhang, University of Alberta.

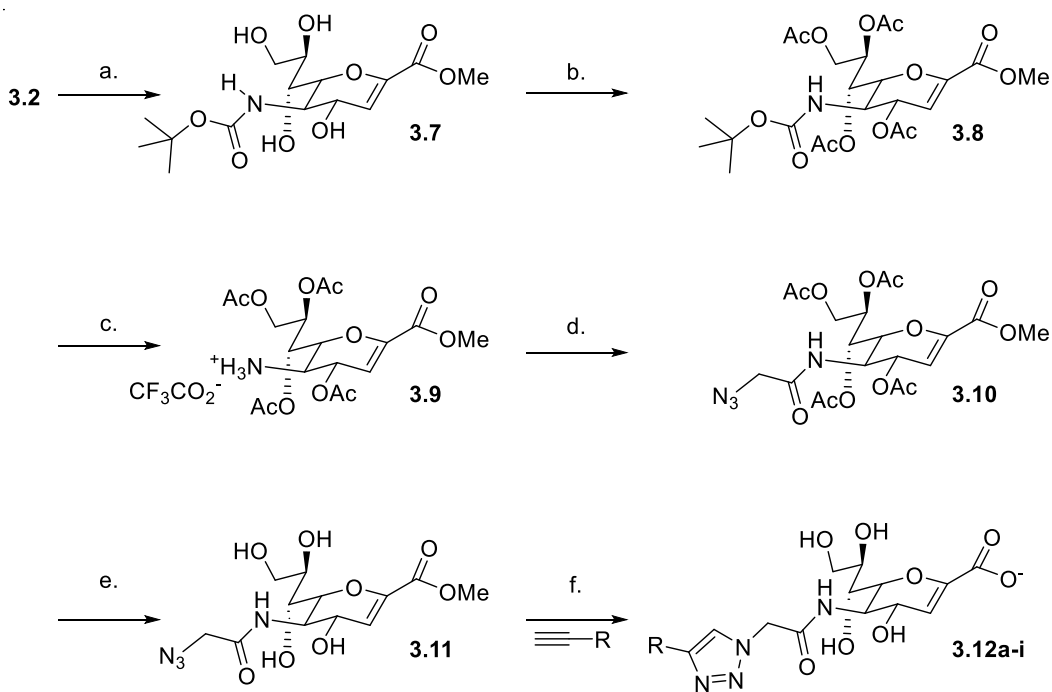
of nine triazole derivatives of **3.6** using standard conditions (compounds **3.6a-i**, Table 3.2).



Scheme 3.1: Synthesis of C9-Azide derivatives. Reagents and conditions: (a) PPh_3HBr , CH_3CN , $90\text{ }^\circ\text{C}$, 2 h (43%); (b) $NaOMe$, $MeOH$, $0\text{ }^\circ\text{C}$, 2 h (quant.); (c) $TsCl$, pyr , $0\text{ }^\circ\text{C}$, 48 h (47%); (d) NaN_3 , $acetone/H_2O$, 48 h , (74%); (e) sodium ascorbate, $CuSO_4$, $H_2O/tBuOH/DCM$ (1:2:1); then $NaOH$, Amberlite IR-120(H^+) (yields ranged from 23-81%).

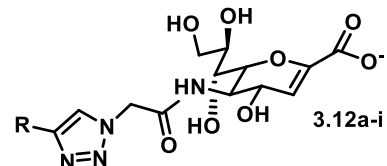
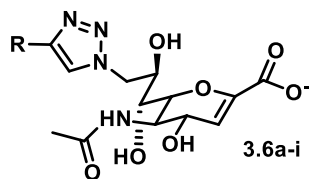
To prepare derivatives of compound **3.12**, we required selective deprotection of the *N5* side-chain. To achieve this, we first protected *N5* with di-tert-butylidicarbonate (Boc_2O), followed by deacetylation to generate **3.7** (Scheme 3.2).⁴³ Subsequent *O*-acetylation provided compound **3.8**, which could be selectively deprotected to reveal the free amine at *N5* (**3.9**). With the free

amine in hand, we could introduce a modified *N*-acyl group that contained an azide handle. We employed an activated ester of azidoacetic acid,^{44,45} which gave the azide **3.10** in excellent yield. Removal of the *O*-acetyl protecting groups provided the methyl ester **3.11**, which could be hydrolyzed to the target compound **3.12**. As before, we generated a series of triazole derivatives of **3.12** from **3.11** by CuAAC, followed by hydrolysis of the methylester (compounds **3.12a-i**, Table 3.2).

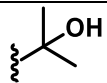
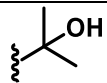


Scheme 3.2: Synthesis of N5Ac-azido and -triazolyl derivatives. Reagents and conditions: (a) Boc_2O , *N,N*-dimethylaminopyridine, THF, 2 h (quant.); then NaOMe, MeOH (92%); (b) Ac_2O , pyridine, 12 h, 0 °C (96%); (c) TFA, CH_2Cl_2 , 1.5 h; (d) *N*-hydroxysuccinimidyl-2-azidoacetate, triethylamine, 3 h, 0°C (99% over two steps); (e) NaOMe, MeOH, 1 h, (52%); (f) sodium ascorbate, CuSO_4 , $\text{H}_2\text{O}/t\text{BuOH}/\text{DCM}$ (1:2:1); then NaOH, Amberlite IR-120(H^+) (yields ranged from 31–96%).

Table 3.2: Inhibition of NEU3



<i>compound</i>	<i>R</i>	IC_{50}	μM^a	<i>compound</i>	<i>R</i>	IC_{50}	μM
DANA	na	48	± 5	DANA	na	48	± 4
3.6	na	70	± 20	3.12	na	21	± 8
3.6a		20	± 10	3.12a		> 500	
3.6b		23	± 4	3.12b		> 500	
3.6c		300	± 200	3.12c		> 500	
3.6d		130	± 20	3.12d		> 500	
3.6e		45	± 3	3.12e		> 500	
3.6f		300	± 400	3.12f		> 500	
3.6g		400	± 600	3.12g		> 500	

3.6h		500	± 200	3.12h		> 500	
3.6i		300	± 500	3.12i		> 500	

^a *Inhibitors which did not show significant change (>50% decrease from control) were fit using the maximum inhibition value for DANA.*

We described a bacterial expression system for NEU3 which could be exploited to test the potency of inhibitors (Chapter 2).²² Although there are previous reports of bacterial expression of this enzyme,⁴⁶ we found that expression of the protein as an *N*-terminal fusion with the maltose binding protein (MBP) helped to stabilize the protein and prevent aggregation. Additionally, producing the protein in bacterial cells avoided background signal due to contaminating activity of other sialidase isoforms present in mammalian cells. Using purified MBP-NEU3, we tested the inhibitory potency of the *C9* (compounds **3.6** and **3.6a–i**) and *N5Ac* (compounds **3.12** and **3.12a–i**) derivatives against NEU3 using a fluorescence assay based on the hydrolysis of 4-methylumbelliferyl α -D-*N*-acetylneuraminic acid (4MU-NA) (Table **3.2**).

As expected, we observed that DANA was a good inhibitor of NEU3, with an IC_{50} of approximately 40 μ M.^{22,23, 24} We found that modification of DANA at the *C9* position by a triazole with a hydrophobic group which lacked a hydrogen bond donor lead to improved activity. The most potent compounds were the phenyl **3.6a** ($20 \pm 10 \mu$ M), hexyl **3.6b** ($23 \pm 4 \mu$ M), and phenoxyethyl **3.6e** ($45 \pm 3 \mu$ M) derivatives. Importantly, the data suggest that the triazole portion of the inhibitor is partly responsible for the increased activity, as the azide derivative **3.6** has slightly reduced potency when compared to DANA ($70 \pm 20 \mu$ M). Bulky triazole substituents, such as **3.6d**, had reduced potency ($130 \pm 20 \mu$ M). More polar groups, including ethoxy **3.6c**, hydroxymethyl **3.6f**, hydroxyethyl **3.6g**, and hydroxypropyl **3.6h** all showed significantly reduced activity as compared to the parent DANA, or the azide **3.6**. Assays of compound **3.12** found a slightly

improved potency over DANA ($21 \pm 8 \mu\text{M}$), suggesting that the azide may provide some beneficial interactions. However, our data imply that the N5Ac pocket is relatively small, as all triazole derivatives of compound **3.12** tested (**3.12a–i**) had potencies that were significantly reduced when compared to DANA ($>500 \mu\text{M}$).

In order to understand the interactions responsible for the differences in potency among both series of compounds, we conducted molecular docking experiments using a previously reported homology model of NEU3.²² After docking, structures were subjected to molecular dynamics and minimized. Examination of the structures of DANA and compound **6a** in the NEU3 active site suggest that a hydrophobic pocket adjacent to the glycerol-binding pocket (C7–C9) could contribute to the activity of compounds related to **3.6a** (Figure 3.2). The hydrophobic pocket is made up of residues V222, V224, P247, and H277. We observed two changes to the active site residues upon binding of **3.6a**, D50 became reoriented to interact with HO7, and an apparent edge–face interaction developed between the phenyl ring and H277 (Figure 3.2).⁴⁷ The model of DANA binding is consistent with the limitations we observed for the N5Ac pocket, which would be predicted to be unable to accommodate the bulky triazole groups found in compounds **3.12a–i**. Additionally, the N5Ac pocket is relatively hydrophobic, although a carboxylate group from N88 is positioned close enough to contact C4 H-bond donors.

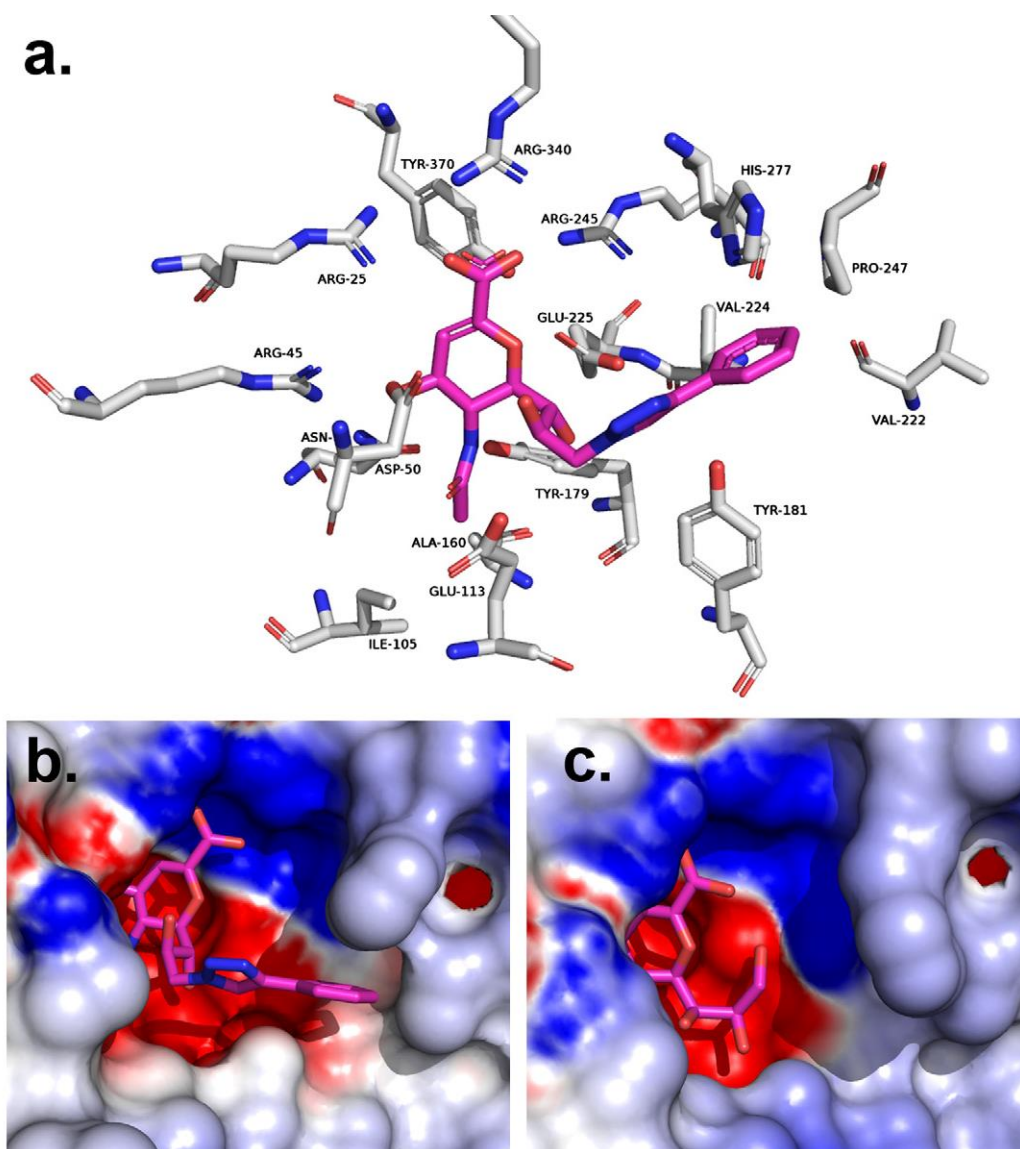


Figure 3.2: Molecular docking of DANA and 3.6a. Inhibitors were docked and subjected to molecular dynamics using a homology model of NEU3 to determine the binding mode of the triazole derivative **3.6a**.²² (a) The binding site of NEU3 has a large hydrophobic pocket adjacent to the C9 position including V222, V224, P247 and H277 which can accommodate hydrophobic groups, (b) an electrostatic potential map is shown for the docked structure of **3.6a**, and (c) DANA. Several residues have reoriented to accommodate **3.6a**, notably H277 is rotated to engage

in an edge-face interaction with the phenyl ring of 3.6a,⁴⁷ and D50 has become more solvent exposed.

These results supported our previous study of the active site topology of NEU3 using small molecule inhibitors based on DANA.²² The compounds tested here suggest that the *N5Ac* pocket of NEU3 is sterically limited, and cannot accommodate large groups such as the triazole derivatives tested here (**3.12a-i**). Importantly, we observed that modifications of the *C9* position are well tolerated, and may have some specific requirements for potent inhibitors of the enzyme. Although previous studies have identified a tolerance for bulky groups at *C9* (Table 3.1),²³ we observed that the addition of a triazole linker significantly improved activity (compounds **3.6a**, **3.6b** and **3.6e**). Based on our model of the active site, we propose that groups which bind in the *C9* pocket should contain H-bond acceptors, to interact with Y181, and also hydrophobic side-chains, to interact with V222 and V224 (Figure 3.2). Additional H-bond acceptors distal from *C9* may take advantage of contacts with K195 or H277. Our results suggest that potent inhibitors of NEU3 may be developed by incorporation of a modified *C9* side-chain of DANA analogs. Importantly, we identified compounds in this study with equivalent potency (**3.6a**) to the best reported inhibitors of the enzyme (zanamivir).²⁵ This feature of NEU3 recognition may indicate that the enzyme can tolerate unusual sialic acid modifications found at *C9*.⁴⁸

3.2.2 Testing of a focused library against the human sialidase isozymes (hNEU1-hNEU4)

Among the two libraries tested above against NEU3, we selected 11 compounds to test against a battery of all for human sialidase isoenzymes. The selected compounds are shown in the following Figure .

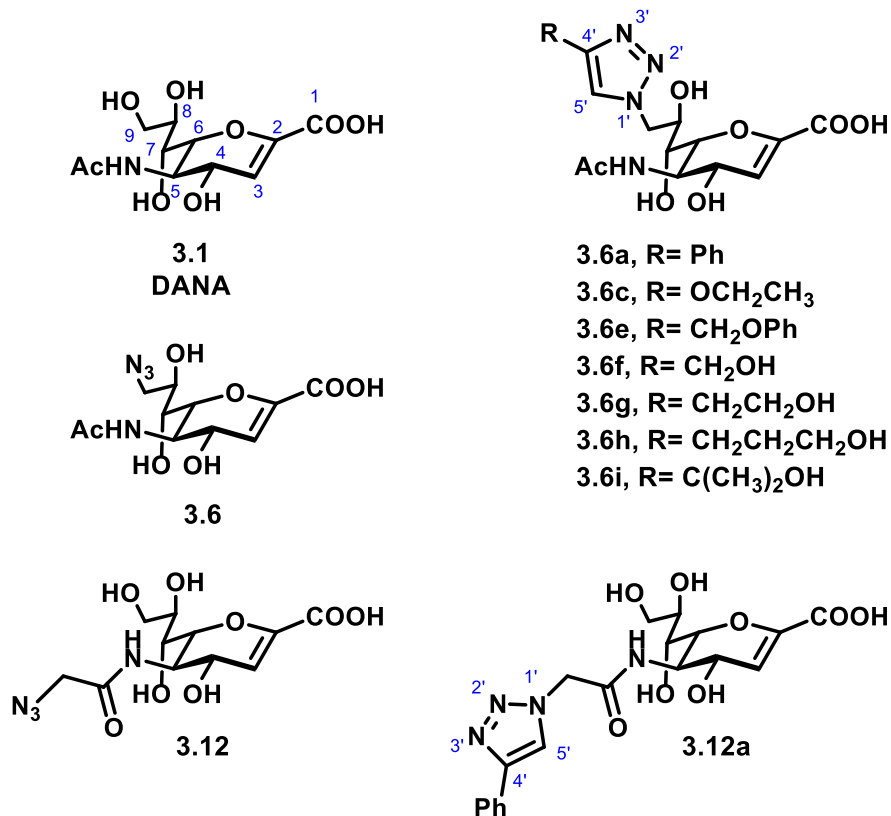


Figure 3.3: Structures of the focused library

The results of enzyme inhibition assays are summarized in Table 3.3. We confirmed that the parent compound, DANA, had broad activity against all four isoenzymes (7–90 μ M inhibition).^{23, 25, 33} Modification of DANA to the C9-azido derivative (**3.6**) resulted in decreased activity against all isoenzymes tested, with the greatest loss in potency observed against NEU1. The C4'-phenyl-C9-triazole

derivative of DANA (**3.6a**) had similar potency for NEU3 ($19.7 \pm 2.3 \mu\text{M}$) and NEU4 ($2.3 \pm 0.2 \mu\text{M}$) but little activity against NEU1 and NEU2 ($>200 \mu\text{M}$). The addition of a hydrogen bond donor and acceptor in the *C9*-triazole moiety (**3.6c**) resulted in moderate selectivity for NEU4 ($3.6 \pm 0.3 \mu\text{M}$) over other isoenzymes (25-fold selectivity). The *C4'*-methylphenoxy-*C9*-triazole analog of DANA (**3.6e**) was over 200-fold selective for NEU3 ($5.5 \pm 0.6 \mu\text{M}$) and NEU4 ($1.7 \pm 0.2 \mu\text{M}$) isoenzymes. In stark contrast, truncation of the *C4'*-side chain to a hydroxymethyl group (**3.6f**) provided the most potent compound in our study. Compound **3.6f** was found to have nanomolar potency for NEU4 ($0.16 \pm 0.01 \mu\text{M}$) yet maintained only micromolar activity against other isoenzymes (500-fold). A similar, though not as drastic, trend was observed for the *C4'*-hydroxyethyl derivative **3.6g** (NEU4, $0.81 \pm 0.04 \mu\text{M}$). Further extension of the *C4'* side chain to the hydroxypropyl derivative, **3.6h**, decreased potency for NEU4 ($2.1 \pm 0.1 \mu\text{M}$), whereas activity against NEU3 remained only moderate ($39 \pm 1 \mu\text{M}$). The branched *C4'*- side chain of compound **3.6i** provided a minor improvement in selectivity for NEU4; however, potency against the enzyme dropped by approximately 2-fold relative to that of compound **3.6h** ($4.0 \pm 0.3 \mu\text{M}$).

Table 3.3: Inhibition of the focused library against neuraminidase enzymes.

Compound	Relative activity ^b		IC ₅₀ (μM) ^a							
			NEU1		NEU2		NEU3		NEU4	
	Target	Selectivity	IC ₅₀	±	IC ₅₀	±	IC ₅₀	±	IC ₅₀	±
DANA (3.1)	n/a	n/a	76	6	90	10	6.3	0.5	13	1
3.6	NEU3	3	620	10	240	20	19.7	2.3	60	20
3.6a	NEU3,4	72	200	30	250	70	4.6	0.2	2.3	0.2
3.6c	NEU4	25	170	20	130	20	90	10	3.6	0.3
3.6e	NEU3,4	220	>1000	-	800	70	5.5	0.6	1.7	0.2
3.6f	NEU4	500	>1000	-	>1000	-	80	10	0.16	0.01
3.6g	NEU4	47	>1000	-	>1000	-	38	2	0.81	0.04
3.6h	NEU4	19	660	20	>1000	-	39	1	2.1	0.1
3.6i	NEU4	45	>1000	-	>1000	-	180	40	4.0	0.3
3.12	NEU3,4	6	29.0	0.5	37	5	4.7	0.3	4.5	0.1
3.12a	NEU2	28	>1000	-	9	1	>1000	-	250	40

^a Coloring of potency values is by relative ranking within each isoenzyme. Darker shades of red indicate higher potency compounds with activity below 500 μM, or which are ranked 1–7 among compounds tested. Darker shades of blue indicate weaker potency, with activities typically above 500 μM or which are ranked 8–11 among compounds tested. ^b Relative activity was determined by dividing the potency of the compound for its next weakest

target by that of its primary target. For cases where multiple isoenzymes are listed as the target, the average of these was used.

The *N*5-azidoacetate derivative of DANA (**3.12**) had previously been reported to have improved activity against NEU3³⁴ and NEU2.³¹ In this study we tested the compound against all four hNEU isoenzymes and found that it was most potent against NEU3 ($4.7 \pm 0.3 \mu\text{M}$) and NEU4 ($4.5 \pm 0.1 \mu\text{M}$) and had approximately 6-fold lower activity against NEU1 ($29 \pm 0.5 \mu\text{M}$) and NEU2 ($37 \pm 5 \mu\text{M}$). Testing of a DANA analog which included a triazole group at the *N*5-position (**3.12a**) revealed that only the NEU2 isoenzyme could tolerate this bulky side chain ($9 \pm 1 \mu\text{M}$). Importantly, compound **3.12a** was approximately 30-fold selective for NEU2 over the other isoenzymes and was the most potent compound for NEU2 among those tested here. The remarkable potency of compound **3.6f** against NEU4 led us to examine its activity in more detail. An overlay of the inhibition curves for compound **3.6f** against hNEU showed a clear separation between its activity for NEU4 and all other isoenzymes, establishing that the selectivity of the inhibitor was at least 500-fold over its next most active target (NEU3; Figure 3.3).

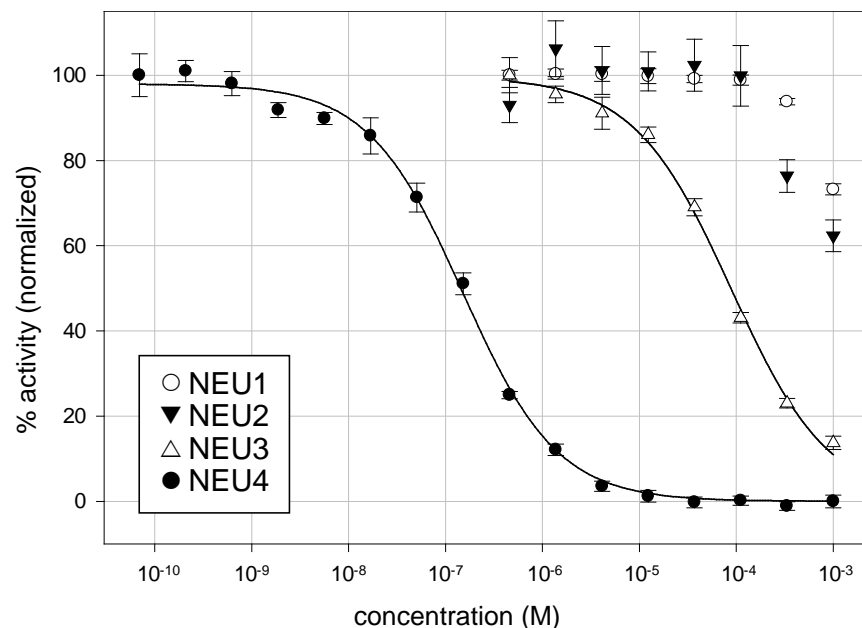


Figure 3.3: Potency and selectivity of compound 3.6f against hNEU. The potency of compound **3.6f** was determined using the 4-MU-NANA assay. IC_{50} curves of the compound with NEU1, NEU2, NEU3, and NEU4 are overlaid. The IC_{50} against NEU4 was 160 ± 10 nM, with a selectivity of at least 500-fold over the other three isoenzymes.

We then determined the inhibition constant (K_i) for compounds **3.6f** and **3.6g** against NEU4. These experiments found that compounds **3.6f** and **3.6g** had K_i values against NEU4 of 30 ± 19 nM and 60 ± 16 nM, respectively, making them the most potent and selective inhibitors reported for any hNEU enzyme. In order to understand the observed selectivity of these compounds in more detail, we developed a molecular model of the interaction of compound **3.6f** with its target, NEU4. No crystal structure data has been reported for NEU4 to date, so we used homology modeling with NEU2 as a template (see Methods section).¹⁹ After

docking of compound **3.6f** to the active site of the NEU4 homology model and subsequent molecular dynamics, we obtained a binding model (Figure 3.4) which maintained most of the expected contacts with the key features of the DANA core. Interestingly, we observed that the 4' - hydroxymethyl group of compound **3.6f** was able to engage in H- bond contacts with the carbonyl groups of S243 and W274 and the side chain of R242 (Figure 3.4b). Thus, our model suggests that the precise placement of the 4' -hydroxymethyl group is responsible for the remarkable activity of this compound against NEU4. This conclusion is also consistent with the activity of compounds **3.6g** and **3.6h**, which both show successive drops in potency with the homologation of methylene groups at 4' position. Our model of NEU4 also suggests that the lack of specificity for other isoenzymes, such as NEU2, is the result of differences in the glycerol side chain binding pocket.

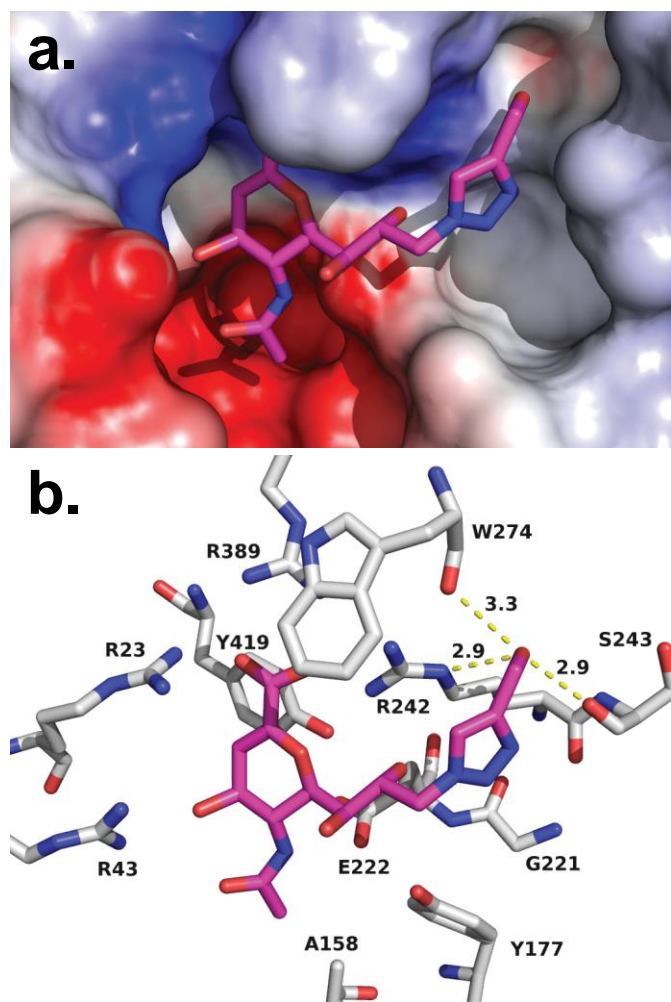


Figure 3.4: Molecular model of compound 3.6f in the active site of NEU4. Using our homology model of NEU4, compound **3.6f** was docked to the active site and then subjected to molecular dynamics (10 ns). (a) An electrostatic surface representation of the active site is shown with compound **3.6f** bound. (b) The general binding mode observed for DANA derivatives observed for NEU2 was preserved in our model, including contacts with the arginine triad (R23, R389, and R242). H-bond contacts are maintained between O4 and R43, as well as the glycerol side chain O8 with R242. The C4' -CH₂OH has multiple H-bond

contacts which include the backbone carbonyls of S243 (2.9 Å) and W274 (3.3 Å) and the N ϵ of R242 (2.9 Å).

An alignment of the NEU4 model to NEU2 finds a large conformational change between a loop of the enzyme that forms half of the binding pocket (see Figure 3.5). We attribute the difference in activity of compound **3.6f** to this conformational change.

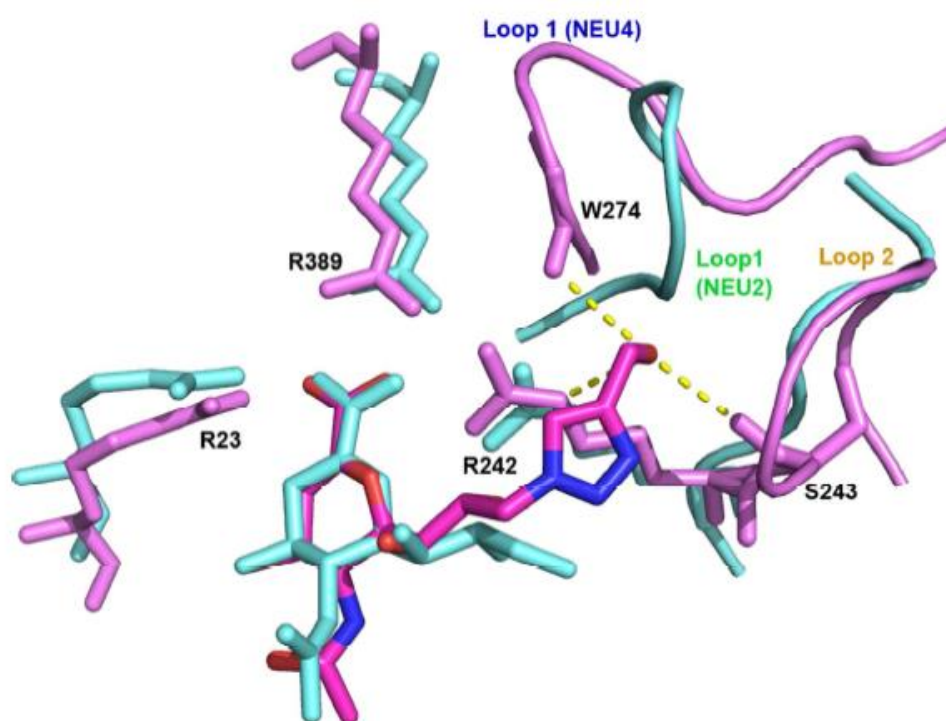


Figure 3.5: Selectivity of compound **6f for NEU4 over NEU2.** An overlay of our NEU4 homology model with a reported co-crystal of NEU2 illustrates one potential source of selectivity between these two isoenzymes. The proposed contacts between the C4'-sidechain and NEU4 are between R242, S243, and W274. Although the first two of these residues have identity in the NEU2 structure, the third is found on a loop (Loop 1, NEU4 R242-R248), which adopts

a radically different orientation in the NEU2 structure. Loop 1 of the NEU2 structure obscures the pocket occupied by the C4'-sidechain in the NEU4 model.

Our results suggested that **3.6f** was a potent competitive inhibitor of NEU4; however, the above assays exploit the fluorogenic substrate, 4MU-NANA, which is not a native substrate of the enzyme. To confirm that this class of inhibitors could, indeed, inhibit the cleavage of native NEU4 substrates, we adapted a reported assay which detects the generation of free sialic acid.⁴⁹ We tested our most potent NEU4 inhibitor, compound **3.6f**, for its ability to inhibit enzyme cleavage of GM3, a known glycolipid substrate of NEU4 (Figure 3.6).⁵⁰ We found that the IC₅₀ of **3.6f** with GM3 as a substrate was in the high nanomolar range (740 ± 70 nM) and was 350-fold more potent than DANA. These data confirm that compound **3.6f** is a potent inhibitor of NEU4 cleavage of native glycolipid substrates.

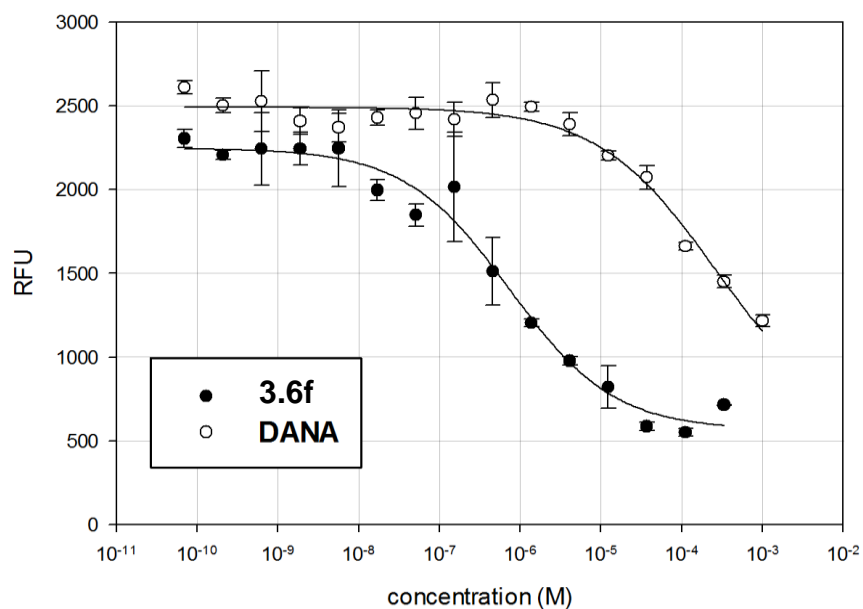


Figure 3.6: *Compound 3.6f inhibits NEU4 cleavage of a glycolipid substrate, GM3. An IC₅₀ curve demonstrating the inhibition of glycolipid hydrolysis catalyzed by NEU4 with compound 3.6f.⁴⁹ The determined IC₅₀ for 3.6f was 0.74 ± 0.07 μM, and that for DANA was 260 ± 40 μM, demonstrating an approximately 350-fold difference in activity. Assays were performed with four replicates for each point; error bars indicate the standard deviation.*

3.3 Conclusions

In this Chapter, we tested our hypothesis regarding the presence of a hydrophobic pocket at the C9 position in NEU3 that could tolerate modification at this position. We found that compounds with large hydrophobic groups at the C9 showed IC₅₀ values comparable to DANA, while hydrophilic substituents were not that potent against NEU3. We also tested similar modifications at the N5 position and we found that such modifications abolished the inhibitory effect

against NEU3. Furthermore, we tested a focused library against the four human sialidase hNEU. Our most potent compounds, **3.6f** and **3.6g**, are active against NEU4 with nanomolar K_i values. Several of the compounds are also specific against NEU4, with selectivities that ranged from 50-fold (**3.6g** and **3.6i**) to 500-fold (**3.6f**). These inhibitors were also demonstrated to act as nanomolar inhibitors of NEU4 processing of the ganglioside substrate, GM3. We also observed that DANA analogs containing a bulky *N5* group resulted in selective inhibition of NEU2 (28-fold, **3.12**). These results provide evidence that minor modifications of the DANA scaffold can generate potent and selective inhibitors of hNEU. Additionally, the range of activity and selectivity found among the panel of C9-modified compounds (**3.6a-3.6f**) supports our hypothesis that the binding sites for the glycerol side chain of Neu5Ac are diverse among hNEU.^{32,34} NEU4 was identified following the sequencing of the human genome, almost two decades later than other hNEU, but multiple studies have already implicated it in vital functions, such as processing of brain gangliosides,⁵¹ neuronal development,⁵² and cancer.⁵³ The development of specific and potent small molecule inhibitors of this enzyme will therefore provide a vital tool for future studies of pathways controlled by NEU4 and reveal new avenues of therapeutic intervention.

3.4 Methods

3.4.1 Molecular docking of inhibitors to NEU3

Compound **3.6a**, or DANA, was docked to the active site of a NEU3 homology model²² using Autodock 4.0 with a grid box of 60 x 40 x 40 Å.⁵⁴ A

representative structure of each inhibitor was obtained from the lowest energy cluster (-6.68 kcal mol⁻¹ ; cluster RMS 1.83). Clusters of higher energy (> 1 kcal mol⁻¹) were missing key interactions between the inhibitor and the arginine triad and the catalytic residues. The docked structures were minimized, and used for molecular dynamics simulations. The dynamics of compound 6a in the active site of NEU3 was calculated using MacroModel (10 ns, 300 K, implicit water solvation,⁵⁵ OPLS2005 force field).^{56,57} The simulation was carried out with residues found within 7 Å of the substrate free to move. The final structure was minimized without constraints to convergence. The electrostatic potential map was generated with the DelPhi software package.⁵⁸

3.4.1 Molecular docking of inhibitors to NEU4

Modelling of compound **3.6f** in the active site of NEU4 was done as described below. The NEU2 structure reported by Chavas et al. was used to develop a homology model of NEU4 (PDB ID: 1VCU).¹⁹ NEU4 and NEU2 sequences (accession numbers: Q8WWR8 and Q9Y3R4, respectively) were aligned using ClustalW227 and found to have 43% homology. Although the extended sequence of NEU4L (residues 287–374) did not align with any parts of NEU2, the full sequence was used to generate a preliminary homology model of NEU4 using SWISS-MODEL.⁵⁹ The sequence between residues 287 and 374 remained as an unorganized loop in the initial model. The model was first minimized and then DANA was docked to the active site, providing the initial structure for molecular dynamics calculations using MacroModel 9.9. The protein–ligand complex was equilibrated for 100 ps at 300 °K, followed by 10 ns

of dynamics at constant temperature with 1.5 fs time steps (see **Figure 3.7** and **Figure 3.8**). The force field used was AMBER*, with aqueous solvent modeled using GB/SA continuum solvation.⁶⁰ The final model of the complex was obtained after unconstrained minimization to convergence. After removing DANA from the active site, compound **3.6f** was docked using Autodock 4.2 with a 60³ Å grid centered on the active site (0.375 Å resolution.)^{54,61} The 200 lowest energy ligand poses were evaluated by cluster analysis, and the lowest energy conformer which maintained key contacts to the active site was selected. The resulting complex was again subjected to molecular dynamics following the same protocol described above to obtain a final model of the interaction of compound **3.6f** with NEU4. Final structures were visualized in PyMOL,⁶² and protein surfaces were calculated using DelPhi.⁵⁸

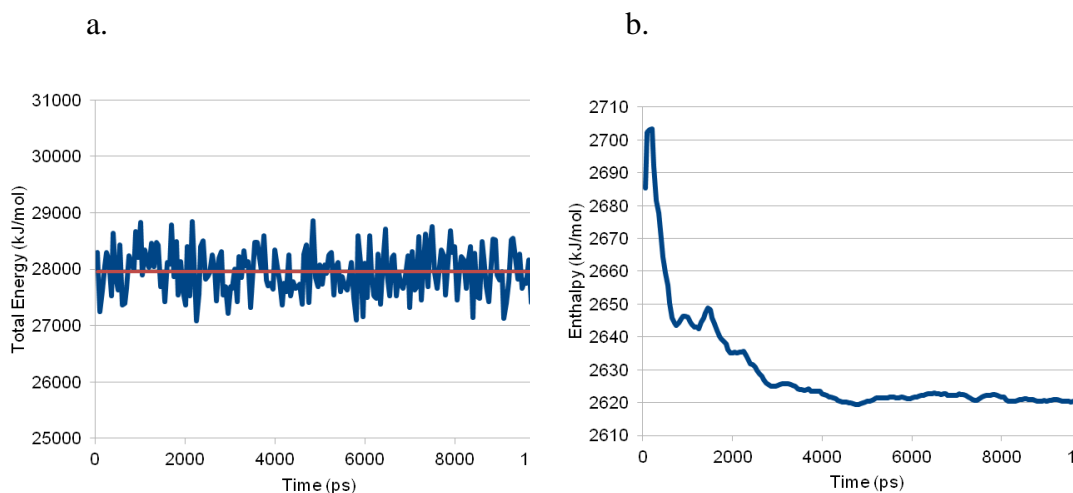


Figure 3.7: Convergence and total energy during MD calculation. The total energy of the system was conserved during the calculation, indicating the stability of the system (panel a). Molecular dynamics calculations were run to convergence, as illustrated below (panel b).

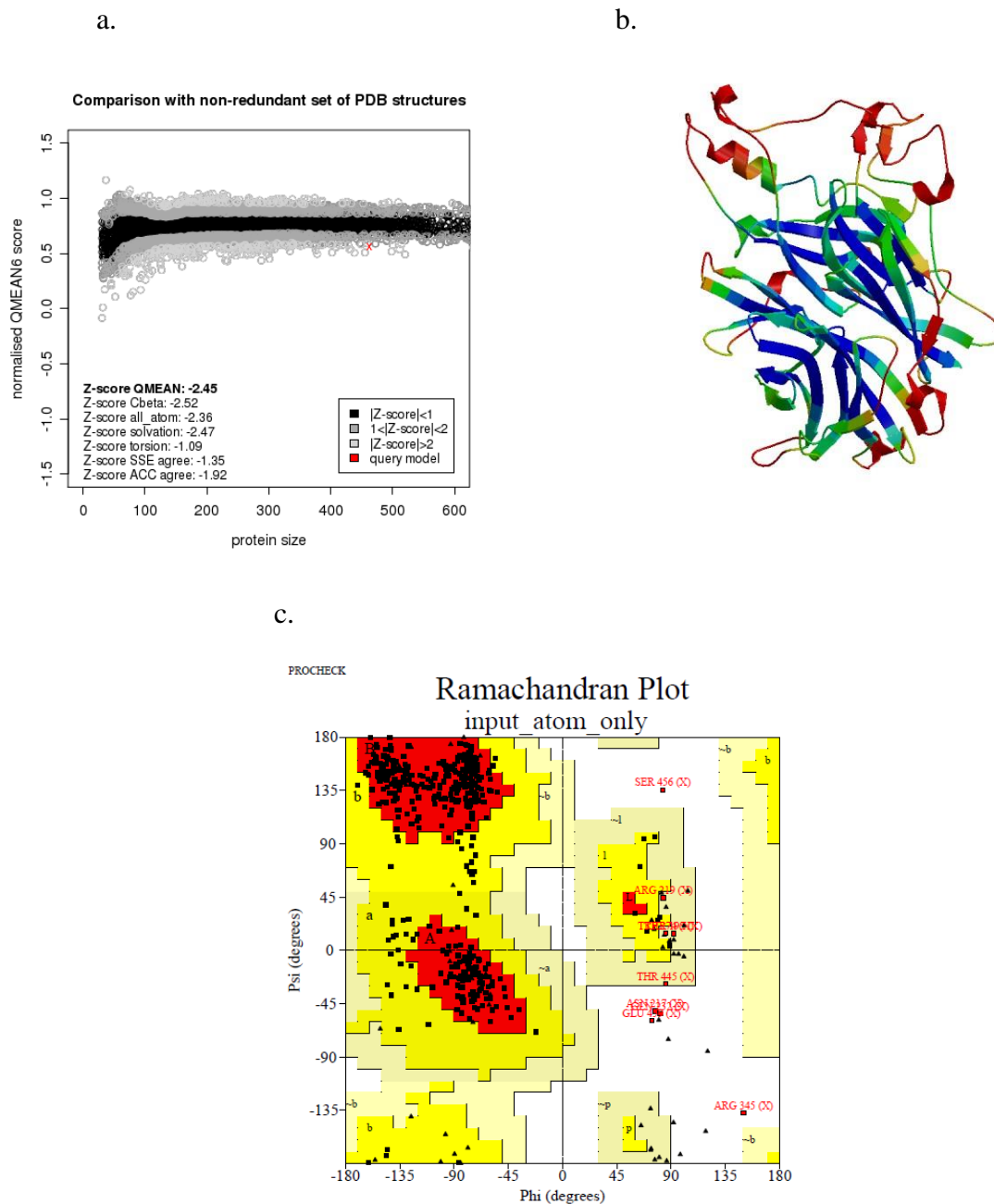


Figure 3.8: Quality of NEU4 homology model. The NEU4L sequence has an extended sequence (residues 287-374) that could not be aligned to the NEU2 template. This region formed a disorganized loop in the final model. Evaluation of the model using Swiss-model assessment tools shows that the quality of the model as whole is moderate with a Z-score of -2.451, which is close to extreme values

which are found in protein data bank (panel a). In terms of local score, most of the unreliable amino acids (shown in red) are part of the unaligned region, and the C-terminus of the protein (panel b). The Ramachandran plot shows that 97.4% of the amino acids are found in favoured or allowed conformational regions, while 1.1% is in the generously allowed region, and 1.4% (5 amino acids) are in the disallowed region (panel c).⁶³

3.4.2 NEU3 inhibition assays

NEU3 was expressed in *E. coli* as an MBP-NEU3 fusion (pMAL-c2x) and purified as described previously.²² Assays were conducted in 0.1 M sodium acetate buffer pH 5.0, at a protein concentration of 0.1 mg mL⁻¹ as determined by A₂₈₀. The neuraminidase solution was incubated with serial concentrations of 2-deoxy-2,3-didehydro-*N*-acetylneuraminic acid (DANA) (5, 10, 20, 50, 100, 200, 500 and 1000 μM) for 30 min at 37 °C. Fluorogenic substrate (4MU-NA, 500 μM final concentration) was added and incubated for 1 h. The reaction was quenched and activity was determined by fluorescence (365 nm excitation; 445 nm emission). Assays were performed with five replicates for each point, error bars indicate the standard deviation. Reported IC₅₀ values were determined by non-linear regression. For curves which showed less than 50% decrease in signal, fits were conducted using the maximum inhibition of DANA (compounds **12a-i**).

3.4.3 NEU1, NEU2, NEU3, and NEU4 testing of the focused library

For testing of the focused library against multiple enzymes, minor modifications of the protocol above were used. NEU3 and NEU2 were expressed

in *E. coli* as N-terminal MBP fusion proteins and purified as described previously.²² NEU4 was expressed as a GST fusion protein and purified as described.³² NEU1 was purified as previously described.⁶⁴ Assays were conducted in 0.1 M sodium acetate buffer at the enzyme optimum pH (4.5 for NEU1, NEU3, and NEU4; 5.5 for NEU2), using a similar amount of enzymatic activity for all four proteins, as determined by assay with 4MU-NANA. Inhibitors were subjected to 3- fold serial dilutions starting from a final concentration of 1 mM. Dilutions were performed in reaction buffer (20 μ L). The mixture was then incubated for 15 min at 37 °C. Fluorogenic substrate (4MU- NANA, 50 μ M final concentration) was added to the reaction buffer (20 μ L) and incubated at 37 °C for 30 min. The reaction was quenched with 200 μ L of 0.2 M sodium glycinate buffer pH = 10.7, and enzyme activity was determined by measuring fluorescence (λ_{ex} = 365 nm excitation; λ_{em} = 445 nm) in a 384 well plate using a plate reader (Molecular Devices, Sunnyvale, CA). Assays were performed with four replicates for each point; error bars indicate the standard deviation. Reported IC₅₀ values were determined by nonlinear regression using SigmaPlot 12. For curves which showed less than a 50% decrease in signal, fits were conducted using the maximum inhibition values found for DANA.

3.4.4 NEU4 inhibition of glycolipid cleavage

To test the potency of inhibitors against a glycolipid substrate, we adapted a known assay for the detection of free sialic acid.⁴⁹ The assay was conducted in 0.1 M sodium acetate buffer (pH 4.5) with NEU4. The reaction mixture was incubated for 30 min at 37 °C. Substrate (GM3, 500 μ M final concentration) was

added to the reaction mixture and incubated at 37 °C for 1 h. The reaction was quenched with 200 µL of 0.2 M sodium borate buffer (pH 9.5). A fluorogenic product was developed by the addition of malononitrile (40 µL of 0.8% solution) and heating at 80 °C for 20 min. Enzyme activity was determined by measuring fluorescence ($\lambda_{\text{ex}} = 357 \text{ nm}$ excitation; $\lambda_{\text{em}} = 443 \text{ nm}$) in a 384 well plate. Reported IC₅₀ values were determined by nonlinear regression.

For K_i Determinations, solutions of 4MU-NANA in sodium acetate buffer (0.1 M) at the optimum pH of the target enzyme were prepared with concentrations of 20, 40, 60, 80, and 100 µM. Each substrate solution (25 µL) was mixed with an equal volume of a solution containing serial concentrations of the inhibitor and the target enzyme. The inhibitor concentrations were selected as a range which included the determined IC₅₀ value. The reaction mixture (50 µL) was transferred to a 384-well plate. The rate of the product formation at 37 °C was followed by measuring the fluorescence ($\lambda_{\text{ex}} = 365 \text{ nm}$ excitation; $\lambda_{\text{em}} = 445 \text{ nm}$) every 30 s for 60 min using a plate reader (Molecular Devices, Sunnyvale, CA). Pseudo-first-order rates were determined using the initial linear part of the resulting curves. The double reciprocal plot (1/rate versus 1/[S]) for each inhibitor concentration was used to determine a slope according to the following equation

$$\frac{1}{v} = \frac{K_m}{V_{max}} \left(1 + \frac{[I]}{K_i} \right) \frac{1}{[S]} + \frac{1}{V_{max}}$$

and a plot of the slopes versus inhibitor concentration was fit to determine K_i.

3.5 References

1. Monti, E.; Preti, A.; Venerando, B.; Borsani, G., Recent development in mammalian sialidase molecular biology. *Neurochemical Research* **2002**, *27* (7-8), 649-663.
2. Caciotti, A.; Di Rocco, M.; Filocamo, M.; Grossi, S.; Traverso, F.; d'Azzo, A.; Cavicchi, C.; Messeri, A.; Guerrini, R.; Zammarchi, E.; Donati, M. A.; Morrone, A., Type II sialidosis: review of the clinical spectrum and identification of a new splicing defect with chitotriosidase assessment in two patients. *Journal of Neurology* **2009**, *256* (11), 1911-1915.
3. Seyrantepe, V.; Poulpetova, H.; Froissart, R.; Zobot, M. T.; Marie, I.; Pshezhetsky, A. V., Molecular pathology of NEU1 gene in sialidosis. *Human Mutation* **2003**, *22* (5), 343-352.
4. Valaperta, R.; Valsecchi, M.; Rocchetta, F.; Aureli, M.; Prioni, S.; Prinetti, A.; Chigorno, V.; Sonnino, S., Induction of axonal differentiation by silencing plasma membrane-associated sialidase Neu3 in neuroblastoma cells. *Journal of Neurochemistry* **2007**, *100* (3), 708-719.
5. Chen, X. P.; Enioutina, E. Y.; Daynes, R. A., The control of IL-4 gene expression in activated murine T lymphocytes - A novel role for neu-1 sialidase. *Journal of Immunology* **1997**, *158* (7), 3070-3080.
6. Papini, N.; Anastasia, L.; Tringali, C.; Croci, G.; Bresciani, R.; Yamaguchi, K.; Miyagi, T.; Preti, A.; Prinetti, A.; Prioni, S.; Sonnino, S.; Tettamanti, G.; Venerando, B.; Monti, E., The plasma membrane-associated

sialidase MmNEU3 modifies the ganglioside pattern of adjacent cells supporting its involvement in cell-to-cell interactions. *Journal of Biological Chemistry* **2004**, 279 (17), 16989-16995.

7. Ueno, S.; Saito, S.; Wada, T.; Yamaguchi, K.; Satoh, M.; Arai, Y.; Miyagi, T., Plasma membrane-associated sialidase is up-regulated in renal cell carcinoma and promotes interleukin-6-induced apoptosis suppression and cell motility. *Journal of Biological Chemistry* **2006**, 281 (12), 7756-7764.

8. Anastasia, L.; Papini, N.; Colazzo, F.; Palazzolo, G.; Tringali, C.; Dileo, L.; Piccoli, M.; Conforti, E.; Sitzia, C.; Monti, E.; Sampaolesi, M.; Tettamanti, G.; Venerando, B., NEU3 sialidase strictly modulates GM3 levels in skeletal myoblasts C2C12 thus favoring their differentiation and protecting them from apoptosis. *Journal of Biological Chemistry* **2008**, 283 (52), 36265-36271.

9. Sasaki, A.; Hata, K.; Suzuki, S.; Sawada, M.; Wada, T.; Yamaguchi, K.; Obinata, M.; Tateno, H.; Suzuki, H.; Miyagi, T., Overexpression of plasma membrane-associated sialidase attenuates insulin signaling in transgenic mice. *Journal of Biological Chemistry* **2003**, 278 (30), 27896-27902.

10. Carubelli, I.; Venerando, B.; Stamatou, N. M., Sialidases Neu1 and Neu3 on the surface of human monocyte-derived dendritic cells may influence cell activity by desialylating GM3 ganglioside. *Glycobiology* **2006**, 16 (11), 1159-1159.

11. Gadhoun, S. Z.; Sackstein, R., CD15 expression in human myeloid cell differentiation is regulated by sialidase activity. *Nature Chemical Biology* **2008**, 4 (12), 751-757.

12. Kato, K.; Shiga, K.; Yamaguchi, K.; Hata, K.; Kobayashi, T.; Miyazaki, K.; Saijo, S.; Miyagi, T., Plasma-membrane-associated sialidase (NEU3) differentially regulates integrin-mediated cell proliferation through laminin- and fibronectin-derived signalling. *Biochemical Journal* **2006**, *394*, 647-656.
13. Azuma, Y.; Sato, H.; Higai, K.; Matsumoto, K., Enhanced expression of membrane-associated sialidase Neu3 decreases GD3 and increases GM3 on the surface of Jurkat cells during etoposide-induced apoptosis. *Biological & Pharmaceutical Bulletin* **2007**, *30* (9), 1680-1684.
14. Kakugawa, Y.; Wada, T.; Yamaguchi, K.; Yamanami, H.; Ouchi, K.; Sato, I.; Miyagi, T., Up-regulation of plasma membrane-associated ganglioside sialidase (Neu3) in human colon cancer and its involvement in apoptosis suppression. *Proceedings of the National Academy of Sciences of the United States of America* **2002**, *99* (16), 10718-10723.
15. Uemura, T.; Shiozaki, K.; Yamaguchi, K.; Miyazaki, S.; Satomi, S.; Kato, K.; Sakuraba, H.; Miyagi, T., Contribution of sialidase NEU1 to suppression of metastasis of human colon cancer cells through desialylation of integrin beta 4. *Oncogene* **2009**, *28* (9), 1218-1229.
16. Miyagi, T.; Wada, T.; Yamaguchi, K.; Hata, K., Sialidase and malignancy: A minireview. *Glycoconjugate Journal* **2003**, *20* (3), 189-198.
17. Dyason, J. C.; von Itzstein, M., Anti-influenza virus drug design: Sialidase inhibitors. *Australian Journal of Chemistry* **2001**, *54* (11), 663-670.

18. Cantarel, B. L.; Coutinho, P. M.; Rancurel, C.; Bernard, T.; Lombard, V.; Henrissat, B., The Carbohydrate-Active EnZymes database (CAZy): an expert resource for Glycogenomics. *Nucleic Acids Research* **2009**, *37*, D233-D238.
19. Chavas, L. M. G.; Tringali, C.; Fusi, P.; Venerando, B.; Tettamanti, G.; Kato, R.; Monti, E.; Wakatsuki, S., Crystal structure of the human cytosolic sialidase Neu2 - Evidence for the dynamic nature of substrate recognition. *Journal of Biological Chemistry* **2005**, *280* (1), 469-475.
20. Chavas, L. M. G.; Kato, R.; Suzuki, N.; von Itzstein, M.; Mann, M. C.; Thomson, R. J.; Dyason, J. C.; McKimm-Breschkin, J.; Fusi, P.; Tringali, C.; Venerando, B.; Tettamanti, G.; Monti, E.; Wakatsuki, S., Complexity in influenza virus targeted drug design: interaction with human sialidases. *Journal of Medicinal Chemistry* **2010**, *53* (7), 2998-3002.
21. Magesh, S.; Suzuki, T.; Miyagi, T.; Ishida, H.; Kiso, M., Homology modeling of human sialidase enzymes NEU1, NEU3 and NEU4 based on the crystal structure of NEU2: Hints for the design of selective NEU3 inhibitors. *Journal of Molecular Graphics & Modelling* **2006**, *25* (2), 196-207.
22. Albohy, A.; Li, M. D.; Zheng, R. B.; Zou, C.; Cairo, C. W., Insight into substrate recognition and catalysis by the human neuraminidase 3 (NEU3) through molecular modeling and site-directed mutagenesis. *Glycobiology* **2010**, *20* (9), 1127-1138.
23. Magesh, S.; Moriya, S.; Suzuki, T.; Miyagi, T.; Ishida, H.; Kiso, M., Design, synthesis, and biological evaluation of human sialidase inhibitors. Part 1:

Selective inhibitors of lysosomal sialidase (NEU1). *Bioorganic & Medicinal Chemistry Letters* **2008**, *18* (2), 532-537.

24. Magesh, S.; Savita, V.; Moriya, S.; Suzuki, T.; Miyagi, T.; Ishida, H.; Kiso, M., Human sialidase inhibitors: Design, synthesis, and biological evaluation of 4-acetamido-5-acylamido-2-fluoro benzoic acids. *Bioorganic & Medicinal Chemistry* **2009**, *17* (13), 4595-4603.

25. Hata, K.; Koseki, K.; Yamaguchi, K.; Moriya, S.; Suzuki, Y.; Yingsakmongkon, S.; Hirai, G.; Sodeoka, M.; Von Itzstein, M.; Miyagi, T., Limited inhibitory effects of oseltamivir and zanamivir on human sialidases. *Antimicrobial Agents and Chemotherapy* **2008**, *52* (10), 3484-3491.

26. Valaperta, R.; Chigorno, V.; Basso, L.; Prinetti, A.; Bresciani, R.; Preti, A.; Miyagi, T.; Sonnino, S., Plasma membrane production of ceramide from ganglioside GM3 in human fibroblasts. *Faseb Journal* **2006**, *20* (8), 1227-+.

27. Li, J.; Zheng, M.; Tang, W.; He, P.-L.; Zhu, W.; Li, T.; Zuo, J.-P.; Liu, H.; Jiang, H., Syntheses of triazole-modified zanamivir analogues via click chemistry and anti-AIV activities. *Bioorganic & Medicinal Chemistry Letters* **2006**, *16* (19), 5009-5013.

28. Lu, Y.; Gervay-Hague, J., Synthesis of C-4 and C-7 triazole analogs of zanamivir as multivalent sialic acid containing scaffolds. *Carbohydrate Research* **2007**, *342* (12-13), 1636-1650.

29. Weiwer, M.; Chen, C.-C.; Kemp, M. M.; Linhardt, R. J., Synthesis and biological evaluation of non-hydrolyzable 1,2,3-triazole-linked sialic acid

derivatives as neuraminidase inhibitors. *European Journal of Organic Chemistry* **2009**, (16), 2611-2620.

30. Khedri, Z.; Li, Y.; Cao, H.; Qu, J.; Yu, H.; Muthana, M. M.; Chen, X., Synthesis of selective inhibitors against V. cholerae sialidase and human cytosolic sialidase NEU2. *Organic & Biomolecular Chemistry* **2012**, *10* (30), 6112-6120.

31. Li, Y.; Cao, H.; Yu, H.; Chen, Y.; Lau, K.; Qu, J.; Thon, V.; Sugiarto, G.; Chen, X., Identifying selective inhibitors against the human cytosolic sialidase NEU2 by substrate specificity studies. *Molecular Biosystems* **2011**, *7* (4), 1060-1072.

32. Albohy, A.; Mohan, S.; Zheng, R. B.; Pinto, B. M.; Cairo, C. W., Inhibitor selectivity of a new class of oseltamivir analogs against viral neuraminidase over human neuraminidase enzymes. *Bioorganic & Medicinal Chemistry* **2011**, *19* (9), 2817-2822.

33. Zhang, Y.; Albohy, A.; Zou, Y.; Smutova, V.; Pshezhetsky, A. V.; Cairo, C. W., Identification of selective inhibitors for human neuraminidase isoenzymes using C4,C7-modified 2-deoxy-2,3-didehydro-N-acetylneuraminic acid (DANA) analogues. *Journal of Medicinal Chemistry* **2013**, *56* (7), 2948-2958.

34. Zou, Y.; Albohy, A.; Sandbhor, M.; Cairo, C. W., Inhibition of human neuraminidase 3 (NEU3) by C9-triazole derivatives of 2,3-didehydro-N-acetylneuraminic acid. *Bioorganic & Medicinal Chemistry Letters* **2010**, *20* (24), 7529-7533.

35. Albohy, A.; Li, M. D.; Zheng, R. B.; Zou, C.; Cairo, C. W., Insight into recognition and catalysis of the mammalian neuraminidase 3 (NEU3) through molecular modeling and site directed mutagenesis. *Glycobiology* **2010**, *in press*.
36. Marra, A.; Sinay, P., Acetylation of N-acetylneuraminic acid and its methyl-ester. *Carbohydrate Research* **1989**, *190* (2), 317-322.
37. Martin, R.; Witte, K. L.; Wong, C. H., The synthesis and enzymatic incorporation of sialic acid derivatives for use as tools to study the structure, activity, and inhibition of glycoproteins and other glycoconjugates. *Bioorganic & Medicinal Chemistry* **1998**, *6* (8), 1283-1292.
38. Bolitt, V.; Mioskowski, C.; Lee, S. G.; Falck, J. R., Direct preparation of 2-deoxy-D-glucopyranosides from glucals without ferrier rearrangement. *Journal of Organic Chemistry* **1990**, *55* (23), 5812-5813.
39. Burkart, M. D.; Vincent, S. P.; Wong, C. H., An efficient synthesis of CMP-3-fluoroneuraminic acid. *Chemical Communications* **1999**, (16), 1525-1526.
40. Bhaskar, V.; Duggan, P. J.; Humphrey, D. G.; Krippner, G. Y.; McCarl, V.; Offermann, D. A., Phenylboronic acid as a labile protective agent: the selective derivatisation of 1,2,3-triols. *Journal of the Chemical Society-Perkin Transactions 1* **2001**, (9), 1098-1102.
41. Han, S.; Collins, B. E.; Bengtson, P.; Paulson, J. C., Homomultimeric complexes of CD22 in B cells revealed by protein-glycan cross-linking. *Nature Chemical Biology* **2005**, *1* (2), 93-97.

42. Meldal, M.; Tornøe, C. W., Cu-catalyzed azide-alkyne cycloaddition. *Chemical Reviews* **2008**, *108* (8), 2952-3015.
43. Johansson, S.; Nilsson, E.; Qian, W.; Guilligay, D.; Crepin, T.; Cusack, S.; Arnberg, N.; Elofsson, M., Design, synthesis, and evaluation of N-acyl modified sialic acids as inhibitors of adenoviruses causing epidemic keratoconjunctivitis. *Journal of Medicinal Chemistry* **2009**, *52* (12), 3666-3678.
44. Yu, H.; Huang, S.; Chokhawala, H.; Sun, M.; Zheng, H.; Chen, X., Highly efficient chemoenzymatic synthesis of naturally occurring and non-natural alpha-2,6-linked sialosides: A *P. damsela* alpha-2,6-sialyltransferase with extremely flexible donor-substrate specificity. *Angewandte Chemie-International Edition* **2006**, *45* (24), 3938-3944.
45. Loka, R. S.; Sadek, C. M.; Romaniuk, N. A.; Cairo, C. W., Conjugation of Synthetic N-Acetyl-Lactosamine to Azide-Containing Proteins Using the Staudinger Ligation. *Bioconjugate Chemistry* **2010**, *21* (10), 1842-1849.
46. Ha, K. T.; Lee, Y. C.; Cho, S. H.; Kim, J. K.; Kim, C. H., Molecular characterization of membrane type and ganglioside-specific sialidase (Neu3) expressed in E-coli. *Molecules and Cells* **2004**, *17* (2), 267-273.
47. Bissantz, C.; Kuhn, B.; Stahl, M., A medicinal chemist's guide to molecular interactions. *Journal of Medicinal Chemistry* **2010**, *53* (14), 5061-5084.
48. Varki, N. M.; Varki, A., Diversity in cell surface sialic acid presentations: implications for biology and disease. *Laboratory Investigation* **2007**, *87* (9), 851-857.

49. Markely, L. R. A.; Ong, B. T.; Hoi, K. M.; Teo, G.; Lu, M. Y.; Wang, D. I. C., A high-throughput method for quantification of glycoprotein sialylation. *Analytical Biochemistry* **2010**, *407* (1), 128-133.
50. Seyrantepe, V.; Canuel, M.; Carpentier, S.; Landry, K.; Durand, S.; Liang, F.; Zeng, J.; Caqueret, A.; Gravel, R. A.; Marchesini, S.; Zwingmann, C.; Michaud, J.; Morales, C. R.; Levade, T.; Pshezhetsky, A. V., Mice deficient in Neu4 sialidase exhibit abnormal ganglioside catabolism and lysosomal storage. *Human Molecular Genetics* **2008**, *17* (11), 1556-1568.
51. Seyrantepe, V.; Iannello, A.; Liang, F.; Kanshin, E.; Jayanth, P.; Samarani, S.; Szewczuk, M. R.; Ahmad, A.; Pshezhetsky, A. V., Regulation of phagocytosis in macrophages by neuraminidase 1. *Journal of Biological Chemistry* **2010**, *285* (1), 206-215.
52. Takahashi, K.; Mitoma, J.; Hosono, M.; Shiozaki, K.; Sato, C.; Yamaguchi, K.; Kitajima, K.; Higashi, H.; Nitta, K.; Shima, H.; Miyagi, T., Sialidase NEU4 hydrolyzes polysialic acids of neural cell adhesion molecules and negatively regulates neurite formation by hippocampal neurons. *Journal of Biological Chemistry* **2012**, *287* (18), 14816-14826.
53. Shiozaki, K.; Yamaguchi, K.; Takahashi, K.; Moriya, S.; Miyagi, T., Regulation of sialyl lewis antigen expression in colon cancer cells by sialidase NEU4. *Journal of Biological Chemistry* **2011**, *286* (24), 21052-21061.
54. Goodsell, D. S.; Morris, G. M.; Olson, A. J., Automated docking of flexible ligands: Applications of AutoDock. *Journal of Molecular Recognition* **1996**, *9* (1), 1-5.

55. Roux, B.; Simonson, T., Implicit solvent models. *Biophysical Chemistry* **1999**, 78 (1-2), 1-20.
56. Jorgensen, W. L.; Tiradorives, J., The OPLS potential functions for proteins - energy minimizations for crystals of cyclic-peptides and crambin. *Journal of the American Chemical Society* **1988**, 110 (6), 1657-1666.
57. Stortz, C. A.; Johnson, G. P.; French, A. D.; Csonka, G. I., Comparison of different force fields for the study of disaccharides. *Carbohydrate Research* **2009**, 344 (16), 2217-2228.
58. Gilson, M. K.; Sharp, K. A.; Honig, B. H., Calculating the electrostatic potential of molecules in solution - method and error assessment. *Journal of Computational Chemistry* **1988**, 9 (4), 327-335.
59. Arnold, K.; Bordoli, L.; Kopp, J.; Schwede, T., The SWISS-MODEL workspace: a web-based environment for protein structure homology modelling. *Bioinformatics* **2006**, 22 (2), 195-201.
60. Still, W. C.; Tempczyk, A.; Hawley, R. C.; Hendrickson, T., Semianalytical treatment of solvation for molecular mechanics and dynamics. *Journal of the American Chemical Society* **1990**, 112 (16), 6127-6129.
61. Morris, G. M.; Goodsell, D. S.; Halliday, R. S.; Huey, R.; Hart, W. E.; Belew, R. K.; Olson, A. J., Automated docking using a Lamarckian genetic algorithm and an empirical binding free energy function. *Journal of Computational Chemistry* **1998**, 19 (14), 1639-1662.
62. The PyMOL Molecular Graphics System, V. S., LLC: <http://www.pymol.org/> (November 15, 2012).

63. Benkert, P.; Schwede, T.; Tosatto, S. C. E., QMEANclust: estimation of protein model quality by combining a composite scoring function with structural density information. *Bmc Structural Biology* **2009**, *9*.
64. Pshezhetsky, A. V.; Potier, M., Association of N-acetylgalactosamine-6-sulfate sulfatase with the multienzyme lysosomal complex of beta-galactosidase, cathepsin A, and neuraminidase - Possible implication for intralysosomal catabolism of keratan sulfate. *Journal of Biological Chemistry* **1996**, *271* (45), 28359-28365.

4 Identification of selective inhibitors for human neuraminidase isoenzymes using C4, C7-modified 2-deoxy-2,3-didehydro-N-acetylneuraminic acid (DANA) analogues^{1,2}

¹ A portion of this chapter has been published in: Zhang, Y.; Albohy, A.; Zou, Y.; Smutova, V.; Pshezhetsky, A. V.; Cairo, C. W., Identification of Selective Inhibitors for Human Neuraminidase Isoenzymes Using C4,C7-Modified 2-Deoxy-2,3-didehydro-N-acetylneuraminic Acid (DANA) Analogues. *J Med Chem* **2013**, *56* (7), 2948-2958.

² Compounds were synthesized and characterized by Yi Zhang, University of Alberta and NEU1 was provided by Victoria Smutova and Alexey V. Pshezhetsky, University of Montreal.

4.1 Introduction

The glycosylation of proteins can alter cell signaling, protein– ligand and protein–protein interactions, and protein stability.^{1,2,3} Most of glycan biosynthesis occurs in the endoplasmic reticulum and Golgi compartments of the cell.¹ However, enzymatic modification of glycan structures also occurs after glycoprotein biosynthesis, a process known as glycan remodeling. The effects of this process can be seen in measures of the relative half-life of glycan structures versus the protein backbone.^{4,5} Glycan remodeling is gaining recognition as an important regulatory function within mammalian cells.⁶ While glycan remodeling is implicated in cell signaling,⁷ there remains a lack of chemical tools to probe the specific enzymes that participate in these processes. Two likely instigators of this process are glycosyl hydrolase (GH) and glycosyl transferase (GT) enzyme classes, which degrade and synthesize the glycosidic linkage, respectively. Thus, strategies for chemical inhibition of mammalian GH and GT are of interest for exploring cell signaling pathways.⁸ The challenge, however, is to design potent inhibitors with selectivity for specific isoenzymes within each class in order to avoid potentially toxic effects.

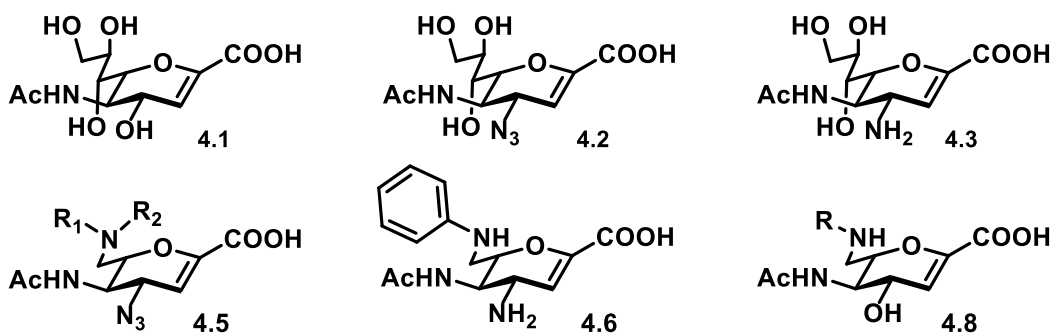
Membrane-associated GH regulate signaling pathways through cleavage of glycolipids and glycoproteins. A number of membrane-associated glycosidases are known in mammalian cells including β -galactosidase,⁹ β -glucosidase,¹⁰ α - and β -mannosidase,¹¹ α -fucosidase,¹² and four isoenzymes of neuraminidase (also known as sialidase).¹³ Among these enzymes, the neuraminidase enzymes (NEU1, NEU2, NEU3, and NEU4) have been shown to participate in a variety of

signaling pathways and pathologies including inflammation,^{14,15} adhesion,^{7,16} tumorigenesis,¹⁷ and cancer metastasis.^{18,19} Notably, sialic acid content in cells and serum is altered in autoimmune diseases; for example, multiple sclerosis patients have decreased levels of sialic acid on their cell membranes²⁰ and increased free sialic acid in serum.²¹ These and other examples support the hypothesis that hNEUs are important regulators in health and disease, and are therefore potential therapeutic targets. Yet there are few examples of specific inhibitors for this family of enzymes.

The design of specific chemical inhibitors for hNEU must take into account the similarities between isoenzymes. The four hNEU enzymes are classified as family 33 GH²² and exosialidases (EC 3.2.1.18).²³ They vary in their subcellular location and substrate specificity. NEU1 is localized at the lysosomal and plasma membranes.^{24,25} NEU2 is a soluble protein found in the cytosol.^{26,27,28} NEU3 is a membrane associated protein localized in the caveolae microdomains of plasma membranes,²⁹ as well as endosomal and lysosomal membranes.³⁰ The NEU4 gene can be differentially spliced, resulting in the appearance of two NEU4 isoforms that differ in the first 12 *N*-terminal amino acids.^{31,32} The short isoform of NEU4 is found predominantly on the ER membranes,^{31,32} whereas the long form is targeted to both mitochondria^{31,32} and lysosomes.³³ Genetic defects in NEU1 result in autosomal pediatric sialidosis disease associated with lysosomal storage of sialylated glycopeptides and oligosaccharides.³⁴ NEU3 is selective for glycolipids over glycoproteins³³ and has been reported to be modulated by signaling events such as protein kinase C activation in immune cells.³⁵

Only a few investigations have explored the substrate specificity of hNEU beyond native glycolipids,^{36,37} providing limited data for the design of synthetic substrates or inhibitors. Inhibitor selectivity for human NEU2 over bacterial enzymes has been investigated and seems to suggest that these two enzymes have significantly different preferences.^{37,38} Magesh et al. have reported compounds that selectively target NEU1 with micromolar activity.³⁹ However, inhibitors that target NEU2, NEU3, and NEU4 enzymes remain to be identified.

Following on our work to develop selective inhibitors of hNEU (Chapter 3), we set out to generate a small panel of 2-deoxy-2,3- didehydro-*N*-acetylneuraminic acid (DANA) analogues that contained modified *C7* side chains. Previous reports have suggested that a basic functional group at the *C4* position may increase inhibitory activity.⁴⁰ Therefore, *C4*-modified compounds were included in our scheme to probe the combination of these two strategies (Scheme 4.1). Upon testing of these DANA derivatives against the four human neuraminidase isoenzymes, as well as a bacterial isoenzyme (*Vibrio cholera* neuraminidase, *vc*NEU), we confirmed that NEU2 and NEU3 tolerate large hydrophobic groups at the *C7* position. Importantly, we found that modification of the DANA scaffold at the *C7* side chain can impart selectivity for inhibitors among members of the hNEU family. We identified a NEU3 inhibitor with nearly 40-fold selectivity over other isoenzymes (**4.5c**) and a NEU2 inhibitor with 12-fold selectivity (**4.8b**). We propose that these results can be used to accelerate the identification of more potent and isoenzyme-selective hNEU inhibitors.



Scheme 4.1: Inhibitor targets

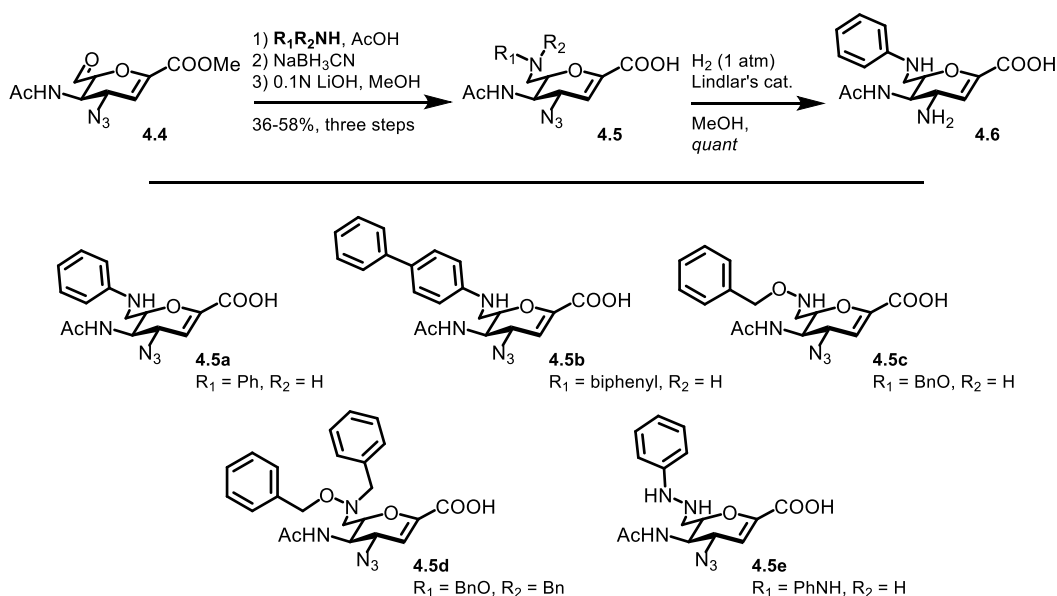
4.2 Results*

4.2.1 Inhibitor Synthesis.

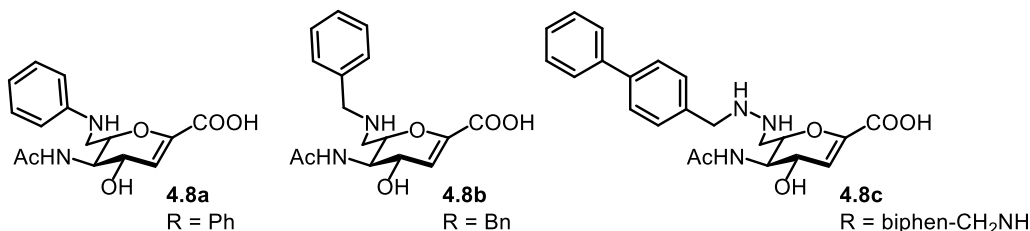
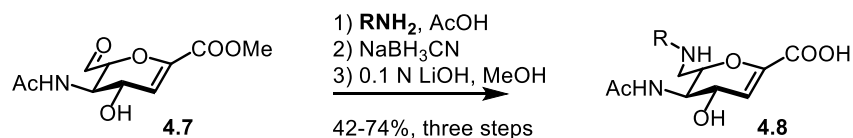
We set out to synthesize DANA (**4.1**) analogues containing *C4* and *C7* modifications individually or in combination (Scheme 4.1). To introduce an azide at *C4*, we employed established methods via nucleophilic opening of an oxazoline intermediate, producing compound **4.2** after deprotection.^{41,42} Subsequent reduction of the azide to an amine provided compound **4.3**. Modification at *C7* was accomplished via oxidative cleavage at *C7–C8* using sodium periodate⁴³ The resulting aldehyde could then be used for a variety of coupling chemistries including reductive amination and oxime or hydrazone formation. DANA analogues containing a *C4*-azide were generated by coupling to **4.4** (Scheme 4.2),^{44,45,46} while analogues with the *C4*-hydroxyl were generated by coupling to **4.7** (Scheme 4.3).⁴³ Reductive coupling of aldehyde **4.4** was

* Compounds were synthesized and characterized by Yi Zhang, University of Alberta

performed with several nucleophiles, including aromatic amines (**4.5a**, **4.5b**), phenylhydrazine (**4.5e**), and benzylic hydroxylamines (**4.5c**, **4.5d**). Reduction of the C4-azide of compound **4.5a** with Lindlar's catalyst afforded the corresponding amine **4.6**. Although we expected that the oxime linkage initially formed in the coupling of **4.5c** would be stable, we chose to reduce the oxime to avoid the formation of diastereomers.⁴⁷ Coupling of compound **4.7** followed an identical protocol to compound **4.4** using aniline (**4.8a**), benzylamine (**4.8b**), and biphenylmethylhydrazine (**4.8c**) nucleophiles.



Scheme 4.2: Synthesis of C4- and C4,C7-substituted DANA derivatives



Scheme 4.3: Synthesis of C7-substituted DANA derivatives

4.2.2 Inhibition Assays.

To determine the potency of DANA analogues against separate isoenzymes of hNEU, enzyme samples were produced either by recombinant expression or by purification from human cells. NEU1 was purified as a protein complex with β -galactosidase and cathepsin A, following previous protocols.⁴⁸ Human NEU2,⁴⁹ NEU3,⁵⁰ and NEU4⁵¹ were expressed as fusion proteins following previous reports. With all four human isoenzymes in hand, we first compared the pH profiles of each enzyme using a fluorogenic substrate, 2'-(4-methylumbelliferyl)- α -D-N-acetylneuraminic acid (4MU-NANA). All four enzymes had optimal enzymatic activity in acidic environments. NEU1, NEU3, and NEU4 showed narrow activity ranges between pH 4 and pH 5. In contrast, NEU2 gave a wide range of activity between pH 5 and pH 6. We then tested the potency of DANA against each enzyme using the 4MU-NANA substrate. We

found that DANA was indeed a general and nonselective inhibitor with low micromolar (6–90 μM) activity against hNEU (Table **4.1**). For comparison, we tested the activity of DANA against a bacterial enzyme, vcNEU. DANA was at least 4-fold more potent against all members of the hNEU family, relative to vcNEU. The inhibition constants (K_i) of DANA against three of the human isoenzymes were determined for comparison (NEU2, $5 \pm 2 \mu\text{M}$; NEU3, $2.2 \pm 0.5 \mu\text{M}$; NEU4, $1.0 \pm 0.6 \mu\text{M}$).

Table 4.1: Inhibition of Neuraminidase Isoenzymes

Compound	Relative activity ^b		IC ₅₀ (μM) ^a									
			NEU1		NEU2		NEU3		NEU4		V.c. sialidase	
	Target	Selectivity	IC ₅₀	±	IC ₅₀	±	IC ₅₀	±	IC ₅₀	±	IC ₅₀	±
DANA (4.1)	hNEU	4	80	10	90	10	6.3	0.5	13	1	170	30
4.2	NEU2,3	7	360	50	59	13	54	5	1000	60	540	60
4.3	NEU2	4	> 1000	-	44	3	180	20	720	70	> 1000	-
4.5a	NEU2	2	> 1000	-	131	31	440	300	300	20	> 1000	-
4.5b	NEU2, 3	3	> 1000	-	74	4	50	30	210	10	> 1000	-
4.5c	NEU3	38	> 1000	-	920	200	24	2	> 1000	-	550	70
4.5d	NEU3	7	> 1000	-	173	50	24	11	350	180	> 1000	-
4.5e	NEU2,3	33	> 1000	-	40	7	20	8	> 1000	-	> 1000	-
4.6	NEU3	1.5	> 1000	-	800	30	540	30	>1000	-	> 1000	-
4.8a	NEU2	4	> 1000	-	100	13	370	80	> 1000	-	> 1000	-
4.8b	NEU2	12	> 1000	-	86	17	> 1000	-	> 1000	-	470	80
4.8c	NEU2,3	3	> 1000	-	67	18	70	20	200	20	> 1000	-

^a Coloring of potency values is by relative ranking within each isoenzyme. Darker shades of red indicate higher potency compounds with activity below 500 μM or that are ranked in 1–7 among compounds tested. Darker shades of blue indicate weaker potency, with activities typically above 500 μM or that are ranked 8–12 among compounds tested.

^b Relative activity was determined by dividing the potency of the compound for its next weakest target by that of its primary target. For cases where multiple isoenzymes are listed as the target, the average of these was used.

Testing of the remaining compounds revealed that in comparison to DANA (**4.1**), modification of the *C4* substituent from a hydroxyl to a bulkier azide (**4.2**) reduced potency against NEU1 and NEU4. This effect was most pronounced in the case of NEU1 for the *C4*-amino derivative **4.3**. Interestingly, NEU2 was the most tolerant of *C4* modifications; compound **4.3** was 2- fold more potent than **4.1** against NEU2 and showed 4-fold selectivity over other isoenzymes. These results suggested that modifications to the *C4* position could be used to gain inhibitor selectivity for NEU2 and NEU3 over other isoenzymes.

The activity of compounds with *C4*, *C7*-modifications confirmed that these changes could impart NEU2 and NEU3 selectivity to DANA analogues. Comparison of the activity of compounds where the glycerol side chain of DANA was replaced with a phenylamine (**4.5a**, **4.6**, and **4.8a**) illustrated that the *C4*-azido, -amino, and -hydroxy groups cannot always compensate for significant modifications at the *C7* position. All three compounds had significantly reduced potency in comparison to DANA. Taken together with the results above for compounds **4.1–4.3**, we concluded that the *C7*-aniline was not able to gain significant contacts in the binding pocket, thus masking any apparent gains from modification at *C4*. Extension of the *C7* group to a phenylhydrazide (**4.5e**) resulted in a remarkable gain in potency for NEU2 and NEU3. Presumably, the addition of a H-bond acceptor/donor site was partly responsible for the observed 33-fold selectivity for NEU2 and NEU3 over other isoenzymes. Modification of the *C7*-site to a hydroxyamino group ablated one H-bond donor site from the side chain (**4.5c**). We observed that **4.5c** was remarkably selective for the NEU3

isoenzyme ($24 \pm 2 \mu\text{M}$, 38-fold selective) over all other enzymes tested. To the best of our knowledge, this compound is the first confirmed NEU3-specific inhibitor reported.

Examination of the potency data for **4.8b** and **4.5c** reveal a dramatic switch in selectivity from NEU2 to NEU3 (Table **4.1**). Compounds **4.8b** and **4.5c** differ in the *C4* substituent and the composition of the *C7* moiety. Although the addition of a *C4*- amino group improved potency for compound **4.3** against NEU2, compound **4.5c** had negligible activity against the enzyme. In contrast, the *C4*-hydroxy-*C7*-benzylamino analogue (**4.8b**) was 12-fold selective for NEU2. The apparent switch of selectivity between NEU2 and NEU3 is, therefore, not strictly tied to either the *C4* or *C7* substituents. Chavas et al. have previously observed that, at least in NEU2, the recognition of substrate is dynamic and requires significant rearrangement of the active site.⁵² Even so, we were surprised to find that additional steric bulk in the form of an N-benzyl group on **4.5d** did not disrupt NEU3 activity. Instead, this modification reduced NEU3 selectivity (7-fold selective) while improving activity against NEU2.

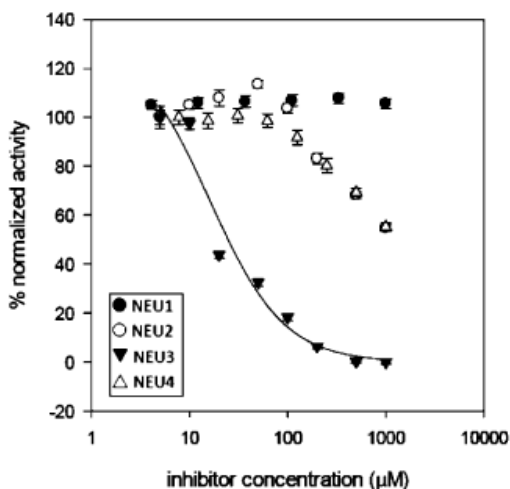
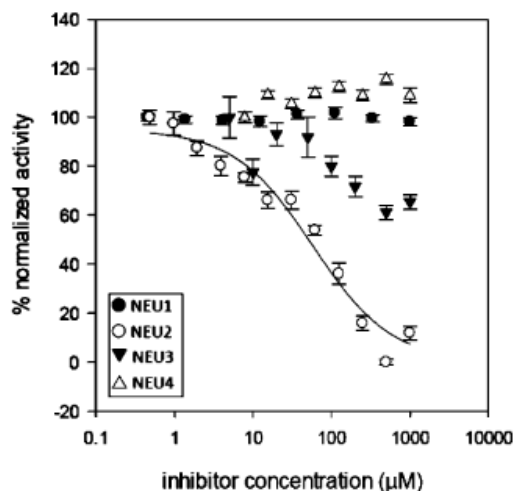
4.5c**4.8b**

Figure 4.1: IC_{50} curves of **4.5c** and **4.8b** for the four human neuraminidase isoenzymes. The experiments were performed as described in the Experimental Section. **4.5c** was 38 times more selective for NEU3, and **4.8b** was 12 times more selective for NEU2 over the other hNEU.

Next we examined the effect of a large aromatic group at the *C7* position. In our previous studies of NEU3, we observed that large hydrophobic groups could be tolerated at the *C9* position of DANA.⁵³ We wanted to determine if the loss of the glycerol side chain could be compensated by incorporation of a hydrazide group. The *C4*-azido-*C7*-biphenylamino analogue **4.5b** targeted both NEU2 and NEU3 with mid-micromolar activity. The mild selectivity of **4.5b** was similar to that of the *C4*-hydroxy-*C7*-biphenylmethylamino analogue **4.8c**. Both **4.5b** and **4.8c** had approximately 3-fold selectivity for NEU2 and NEU3, with only moderate activity for NEU4. Finally, we determined the K_i values for the two most potent compounds identified (with $IC_{50} < 25 \mu M$) against their target

enzyme, NEU3. We found that **4.5c** had a K_i of $8 \pm 1 \mu\text{M}$ against NEU3 and that **4.5e** had similar activity at $11 \pm 3 \mu\text{M}$ (Table 4.2).

Table 4.2: K_i Determinations

compound	enzyme	K_i (μM)
DANA (4.1)	NEU2	5 ± 2
DANA (4.1)	NEU3	2.2 ± 0.5
DANA (4.1)	NEU4	1.0 ± 0.6
4.5c	NEU3	8 ± 1
4.5e	NEU3	11 ± 3

4.2.3 Molecular Modeling.

We used molecular modeling to gain insight into the selectivity switch of **4.5c** and **4.8b** between the NEU3 and NEU2 active sites. We used the structural data reported by Chavas et al. to model ligand interactions with NEU2 (PDB code 1VCU).⁵² As no X-ray structure is currently available for NEU3, we employed a homology model of the enzyme that was previously developed in our group.⁵⁰ To provide a model of protein–ligand interactions, we performed molecular docking using Autodock 4.2,^{54,55} followed by an unrestrained 10 ns molecular dynamics simulation. We evaluated the binding of **4.5c** with NEU3 and of **4.8b** with NEU2 using this strategy.

The binding model of **4.5c** supported our hypothesis that the NEU3 active site can accommodate large hydrophobic groups (Figure 4.2). The model maintained key contacts between the *C1*-carboxylate and the arginine triad, as

well as those of the *N5*-Ac pocket. The *C4*-azido group was well accommodated by the *O4* pocket (I26, D50, M87, and N88). The *C7* side chain of **4.5c** contains a four-atom linker to the phenyl group and contains two H-bond acceptors and one H-bond donor. The distance between the pyranoside ring and the phenyl group would not allow for interactions with H277 (the groups are $\sim 5\text{--}6$ Å apart). However, the phenyl group could gain hydrophobic interactions with several residues of the active site (V224, V222, P247, P198). An inspection of the NEU2 active site revealed that the side chain of **4.5c**, were it in the same conformation as predicted for NEU3, would result in a steric clash with Q270.

We propose that this difference between the active site topology results in the selectivity observed for inhibitors with larger *C7* groups. Additionally, the model predicts that a shorter *C7* group would be better accommodated in the NEU2 active site.

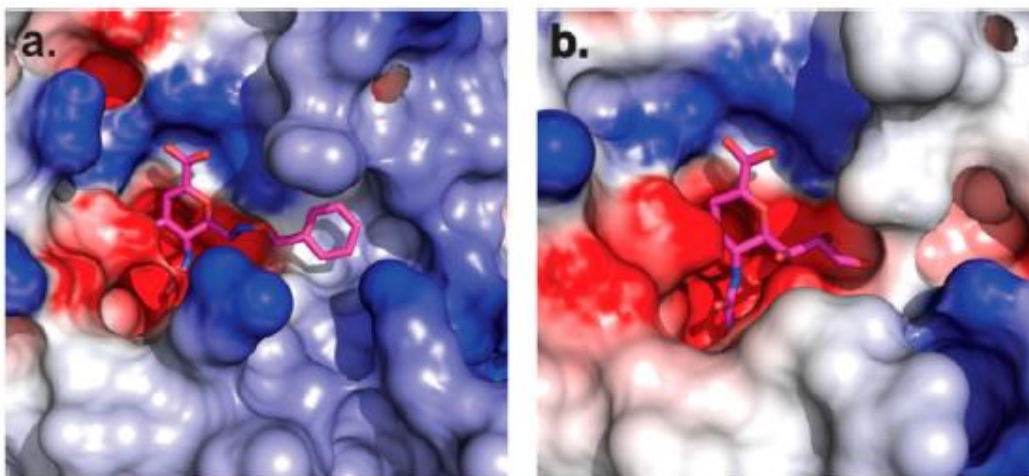


Figure 4.2: Molecular models of the NEU2 and NEU3 active sites. (a) A model of the protein–ligand complex was generated using docking and molecular dynamics (see Experimental Section). The large hydrophobic pocket of NEU3

accommodates the C7 side chain of compound 4.5c. (b) The active site topology of NEU2 (PDB code 1VCU)⁵² is shown for comparison and reveals a smaller pocket for the glycerol side chain of DANA (C7– C9). Electrostatic potential surfaces were generated with DelPhi⁵⁶ and visualized using PyMOL.⁵⁷

We next examined the selective binding of **4.8b** to the NEU2 active site (Figure 4.3). The model of **4.8b** maintained the same contacts to the active site for the *C1*-carboxylate, *O4*, and *N5Ac* groups as observed with DANA and NEU2. The *C7* side chain was the only point of departure from DANA. In this case the *C7* side chain contained a phenyl group; however, the linker between the pyranoside ring and the arene has been truncated to three atoms and contains only one H-bond donor and acceptor. In this binding mode, the linker could gain a H-bond contact with Y181 (3.4 Å) and hydrophobic interaction with L217 and Q270(Cβ). Thus, the relatively small *C7* side chain, with its shorter linker, packs into the restricted space available in the NEU2 pocket and gains contacts that improve its activity for the enzyme. In contrast, the NEU3 pocket is too large for effective packing of the **4.8b** side chain, resulting in a loss of one H-bond contact and leaving the phenyl ring more solvent exposed. The *C7* side chain of **4.8b** positions the phenyl group near relatively polar residues (H277, Y181, and R245), where it is unable to contact the hydrophobic groups that benefit **4.5c** binding in the NEU3 pocket.

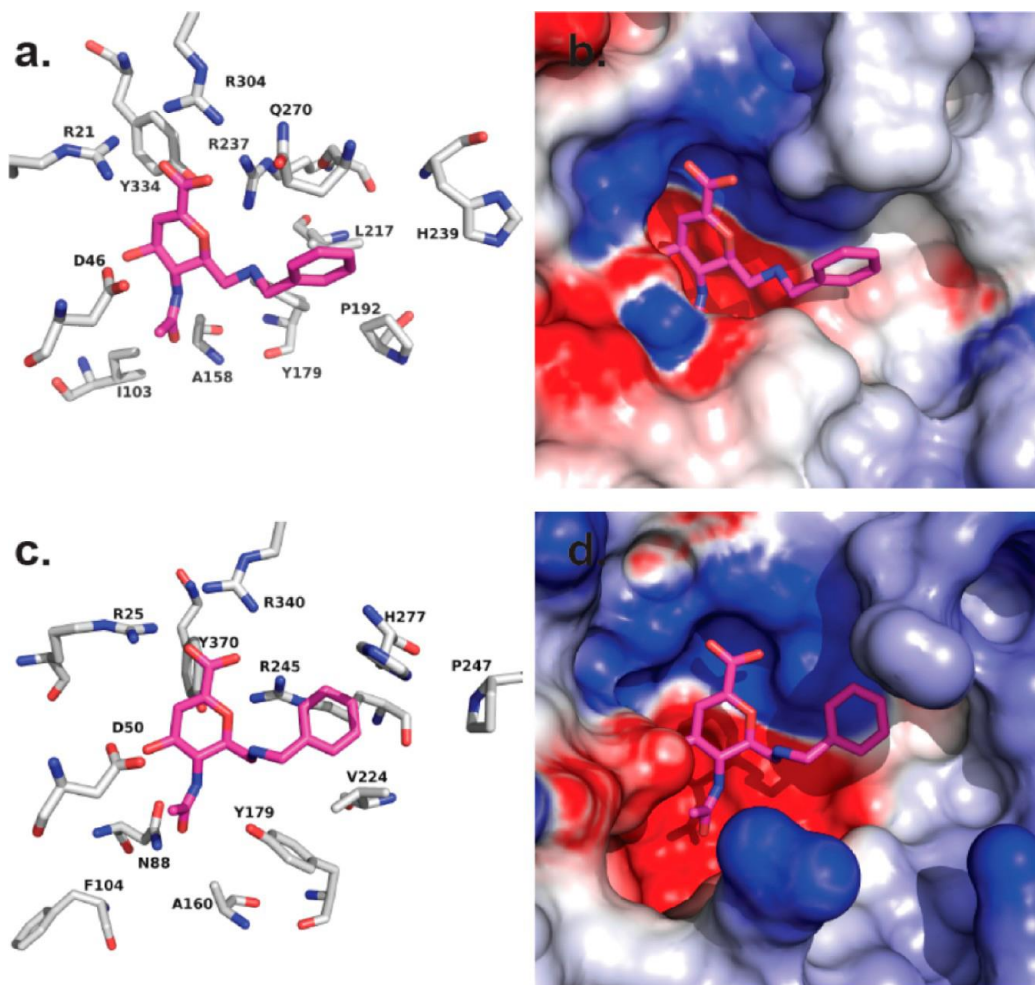


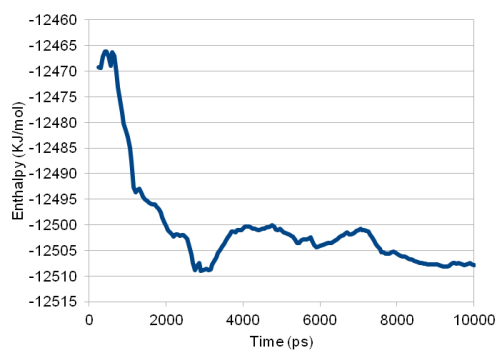
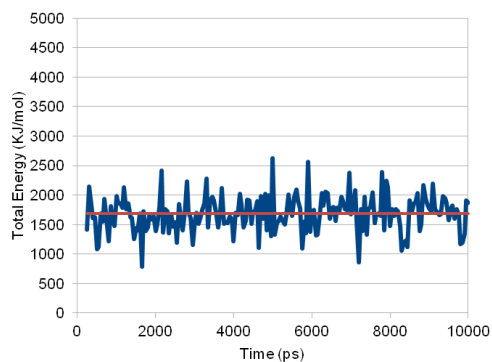
Figure 4.3: Molecular interactions of 4.8b. (a) A molecular model of compound 4.8b bound to NEU2 postulates a binding mode with the phenyl group interacting with the hydrophobic portion of Q270 and interacting with L217 and P192. (b) The electrostatic potential surface of NEU2 shows that the region interacting with the phenyl ring is relatively nonpolar. (c) A molecular model of 8b in the active site of NEU3 shows that while the C7 side chain can be accommodated sterically, the linker positions the phenyl ring in a region of the binding pocket where it cannot gain any significant contacts. (d) An electrostatic potential surface of

NEU3 reveals that the phenyl ring of 8b is positioned in a relatively polar region of the binding pocket.

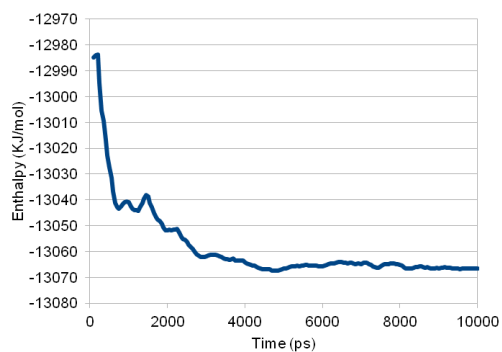
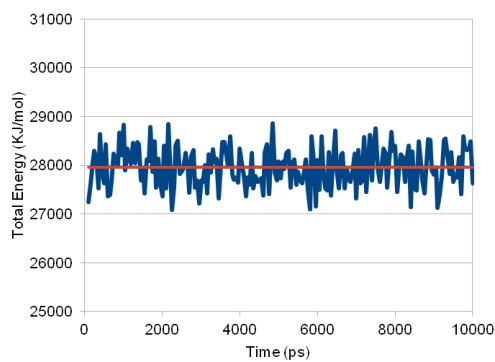
4.2.4 Convergence and total energy of molecular dynamics simulations

The total energy of the system was conserved during the calculation, indicating the stability of the system. The MD simulation was run to convergence over 10 ns as illustrated in the plots below for the complexes of (a.) compound **4.8b** and NEU2, (b.) compound **4.8b** with NEU3, and (c.) compound **4.5c** with NEU3.

a. Compound **4.8b** with NEU2



b. Compound **4.8b** with NEU3



a. Compound **4.5c** with NEU3

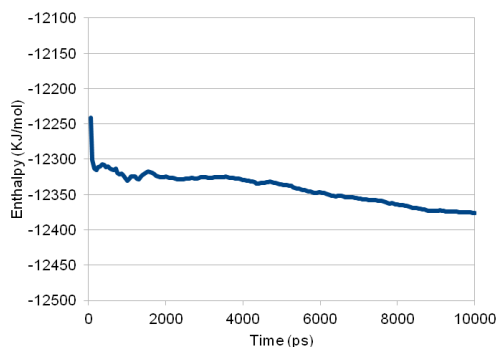
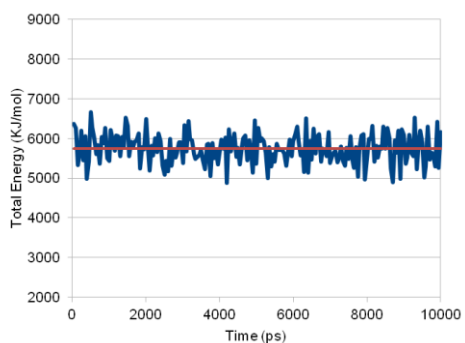


Figure 4.4: Convergence of molecular dynamics.

4.3 Discussion

In this study we have found that modification of the DANA inhibitor scaffold at the *C4* and *C7* positions resulted in compounds with improved specificity against the hNEU isoenzymes NEU2 and NEU3. Importantly, we identified lead compounds with 38-fold (**4.5c**) and 12-fold (**4.8b**) selectivity for these two isoenzymes, respectively. These are the first reported compounds that have been confirmed to be selective for NEU2 and NEU3 over other hNEUs. While our data confirmed that DANA (**4.1**) was a nonselective inhibitor of hNEU, we also identified compounds that could target a subset of hNEU isoenzymes. For example, compounds **4.2**, **4.5b**, **4.5e**, and **4.8c** inhibit NEU2 and NEU3 with comparable potency. These compounds provide an important starting point for the future design of more potent and selective compounds targeting individual human neuraminidases.

There are very few reports of isoenzyme-selective hNEU inhibitors, and yet selective small molecule inhibitors are needed to expand our understanding of this important family of enzymes. Despite the fact that nanomolar inhibitors of viral sialidases are known,⁵⁸ the most potent inhibitors reported for hNEU have inhibitory constants in the low micromolar range.^{39,53} Interestingly, nanomolar inhibitors of influenza viral sialidase are significantly less active against hNEU.^{51,59} Zanamivir (a *C4*-guanidino-modified DANA analogue) is reported to be the most potent of the viral inhibitors against hNEU, with moderate selectivity for NEU2.⁵⁹ We observed that a *C4*-azido analogue of DANA (**4.2**) had similar selectivity for both NEU2 and NEU3 isoenzymes. Few other reports have tested

inhibitors designed to target individual hNEUs among the four isoenzymes. Several compounds selective for NEU1 have been identified.³⁹ Our group has previously identified oseltamivir analogues that were weakly selective for NEU3 over NEU4.⁵¹ Although other studies have examined the activity of inhibitors against hNEU individually, without data on their activity against other isoenzymes it is difficult to judge their utility *in vivo* where they will compete against the full battery of hNEUs.^{38,53,60}

Known inhibitors of hNEU have primarily been based upon the 2-deoxy-2,3-didehydro-*N*-acetylneuraminic acid (**4.1**) core. The sequence homology of hNEU enzymes suggests that many recognition elements of the active site are preserved across the family.⁶¹ Although X-ray structural data are only available for NEU2, DANA analogues with fewer H-bond donor groups in place of the glycerol side chain are known to disrupt the H-bond network of the active site and reduce potency against NEU2.^{52,60} The recognition of the glycerol side chain of sialic acid by hNEUs involves contacts from multiple tyrosine residues.^{50,52,61} This arrangement is in contrast to the viral enzyme and could potentially be exploited to improve inhibitor selectivity.⁵¹ Modifications at the *C9* position have yielded NEU1 selective inhibitors.³⁹ We⁵³ and others^{37,38} have explored *C9*- and *N5*-Ac-modified analogues of DANA and their inhibitory potency against NEU3 and NEU2 isoenzymes, respectively. Modification of DANA by inclusion of a *C4*-guanidino group improved potency against NEU2⁶⁰ and NEU3.⁵⁹

Although the best compounds identified here have relatively low potency ($K_i \approx 8\text{--}11 \mu\text{M}$) for *in vivo* studies, they represent the first panel of compounds to

selectively target NEU2 and NEU3. The most interesting trends observed are the apparent selectivity switch observed between NEU2 and NEU3. The activity of several compounds suggests similarities between substrate recognition by these two isoenzymes. Compounds **4.2**, **4.5b**, **4.5e**, and **4.8c** show little distinction between NEU2 and NEU3. In contrast, **4.5c** and **4.8b** selectively target NEU3 and NEU2, respectively, with only minor structural differences between the compounds. Molecular modeling suggested that the differences between the recognition of these two active sites can be attributed to the topology of the glycerol side chain binding pocket. The NEU3 binding pocket is more accommodating to larger groups and contains several polar contacts that are distal to the position of the C9-hydroxyl of the native substrate. In the case of NEU2, the binding pocket relies on hydrophobic packing with smaller side chains. The NEU2 Q270 residue may act as a gatekeeper that prevents the binding of larger groups in this pocket.

4.4 Conclusion

On the basis of our results, we conclude that derivatives of the DANA scaffold can act as isoenzyme-selective hNEU inhibitors. Furthermore, the binding pocket for the glycerol side chain (C7–C9 of the sialic acid substrate) is a site of diverse enzyme–substrate interactions that can be exploited to improve the potency and selectivity of inhibitors. The human neuraminidase enzymes are of growing biological interest, and new tools are required to understand their roles in glycobiology. Previously, genetic approaches, such as gene targeting in mice or siRNA, have been used to study the biological roles of human neuraminidase

enzymes. However, small molecule inhibitors have inherent advantages because of their rapid onset and reversibility of their effects. Herein, we have described a panel of DANA analogues that achieve selective inhibition of one or multiple hNEU isoenzymes at low micromolar potency. These findings should guide future design of inhibitors with improved potency and selectivity for this family of enzymes. Future work will focus on the development of analogues with improved potency and selectivity, as well as compounds that can selectively target NEU4, the only remaining isoenzyme with no reported selective inhibitors.

4.5 Methods

4.5.1 General Protocol for Inhibition Assays.

NEU3 and NEU2 were expressed in *E. coli* as *N*-terminal MBP fusion proteins and purified as described previously.⁵⁰ NEU4 was expressed as a GST fusion protein and purified as described.⁵¹ NEU1 was purified as previously described.⁴⁸ Assays were conducted in 0.1 M sodium acetate buffer at the enzyme optimum pH (pH 4.5 for NEU1, NEU3, and NEU4; pH 5.5 for NEU2), using a similar amount of enzymatic activity for all four proteins, as determined by assay with 4MU-NANA. Inhibitors were subjected to 3-fold serial dilutions starting from a final concentration of 1 mM. Dilutions were performed in reaction buffer (20 μ L). The mixture was then incubated for 15 min at 37 °C. Fluorogenic substrate (4MU-NANA, 50 μ M final concentration) was added to the reaction buffer (20 μ L) and incubated at 37 °C for 30 min. The reaction was quenched with 200 μ L of 0.2 M sodium glycinate buffer, pH 10.7, and enzyme activity was

determined by measuring fluorescence ($\lambda_{\text{ex}} = 365$ nm excitation; $\lambda_{\text{em}} = 445$ nm emission) in a 384-well plate using a plate reader (Molecular Devices, Sunnyvale CA). Assays were performed with four replicates for each point. Error bars indicate the standard deviation. Reported IC_{50} values were determined by nonlinear regression using SigmaPlot 12. For curves that showed less than a 50% decrease in signal, fits were conducted using the maximum inhibition values found for DANA.

4.5.2 K_i Determinations.

Solutions of 4MU-NANA in sodium acetate buffer (0.1 M) at the optimum pH of the target enzyme were prepared with concentrations of 20, 40, 60, 80, and 100 μM . Each substrate solution (25 μL) was mixed with an equal volume of a solution containing serial concentrations of the inhibitor and the target enzyme. The inhibitor concentrations were selected as a range that included the determined IC_{50} value. The reaction mixture (50 μL) was transferred to a 384-well plate. The rate of the product formation at 37 $^{\circ}\text{C}$ was followed by measuring the fluorescence ($\lambda_{\text{ex}} = 365$ nm excitation; $\lambda_{\text{em}} = 445$ nm emission) every 30 s for 60 min using a plate reader (Molecular Devices, Sunnyvale CA). Pseudo-first-order rates were determined using the initial linear part of the resulting curves. The double reciprocal plot (1/rate versus 1/[S]) for each inhibitor concentration was used to determine a slope according to the following equation

$$\frac{1}{v} = \frac{K_m}{V_{max}} \left(1 + \frac{[I]}{K_i} \right) \frac{1}{[S]} + \frac{1}{V_{max}}$$

and a plot of the slopes versus inhibitor concentration was fit to determine K_i .

4.5.3 Molecular Modeling.

The homology model of NEU3 was the same as reported previously.⁵⁰ Molecular docking to the protein models was performed using Autodock 4.2 using a 60^3 Å grid centered on the active site with 0.375 Å resolution.^{54,55} The 200 lowest energy ligand poses were evaluated by cluster analysis, and the lowest energy conformer that maintained key contacts to the active site was selected as the starting point for further analysis by molecular dynamics calculations. Molecular dynamics were performed using MacroModel 9.9 from an initial protein–ligand complex obtained from docking. The complex was first equilibrated for 100 ps at 300 K, followed by 10 ns dynamics at 300 K with 1.5 fs time steps. The force field used was AMBER* with a GB/SA continuum solvation model.⁶¹ All simulations were observed to converge (See Figure 4.4). The converged structure was then subjected to unconstrained minimization, providing the final model of the protein–ligand complex. Models were visualized in PyMOL,⁵⁷ and protein surfaces were calculated using DelPhi.⁵⁶

4.6 References

1. Varki, A.; Etzler, M. E.; Cummings, R. D.; Esko, J. D., Discovery and classification of glycan-binding proteins. In *Essentials of Glycobiology*, 2nd ed.; Varki, A.; Cummings, R. D.; Esko, J. D.; Freeze, H. H.; Stanley, P.; Bertozzi, C. R.; Hart, G. W.; Etzler, M. E., Eds. Cold Spring Harbor (NY), 2009.
2. Dwek, R. A., Glycobiology: Toward understanding the function of sugars. *Chemical Reviews* **1996**, *96* (2), 683-720.
3. Culyba, E. K.; Price, J. L.; Hanson, S. R.; Dhar, A.; Wong, C.-H.; Gruebele, M.; Powers, E. T.; Kelly, J. W., Protein native-state stabilization by placing aromatic side chains in N-glycosylated reverse turns. *Science* **2011**, *331* (6017), 571-575.
4. Tauber, R.; Park, C. S.; Becker, A.; Geyer, R.; Reutter, W., Rapid intramolecular turnover of N-linked glycans in plasma-membrane glycoproteins - extension of intramolecular turnover to the core sugars in plasma-membrane glycoproteins of hepatoma. *European Journal of Biochemistry* **1989**, *186* (1-2), 55-62.
5. Tauber, R.; Park, C. S.; Reutter, W., Intramolecular heterogeneity of degradation in plasma-membrane glycoproteins - evidence for a general characteristic. *Proceedings of the National Academy of Sciences of the United States of America-Biological Sciences* **1983**, *80* (13), 4026-4029.
6. Parker, R. B.; Kohler, J. J., Regulation of intracellular signaling by extracellular glycan remodeling. *Acs Chemical Biology* **2010**, *5* (1), 35-46.

7. Pshezhetsky, A. V.; Hinek, A., Where catabolism meets signalling: neuraminidase 1 as a modulator of cell receptors. *Glycoconjugate Journal* **2011**, 28 (7), 441-452.
8. Gloster, T. M.; Vocadlo, D. J., Developing inhibitors of glycan processing enzymes as tools for enabling glycobiology. *Nature Chemical Biology* **2012**, 8 (8), 683-694.
9. Goi, G.; Bairati, C.; Massaccesi, L.; Lovagnini, A.; Lombardo, A.; Tettamanti, G., Membrane anchoring and surface distribution of glycohydrolases of human erythrocyte membranes. *Febs Letters* **2000**, 473 (1), 89-94.
10. Aureli, M.; Masilamani, A. P.; Illuzzi, G.; Loberto, N.; Scandroglio, F.; Prinetti, A.; Chigorno, V.; Sonnino, S., Activity of plasma membrane beta-galactosidase and beta-glucosidase. *Febs Letters* **2009**, 583 (15), 2469-2473.
11. Porwoll, S.; Loch, N.; Kannicht, C.; Nuck, R.; Grunow, D.; Reutter, W.; Tauber, R., Cell surface glycoproteins undergo postbiosynthetic modification of their N-glycans by stepwise demannosylation. *Journal of Biological Chemistry* **1998**, 273 (2), 1075-1085.
12. Cordero, O. J.; Merino, A.; de la Cadena, M. P.; Bugia, B.; Nogueira, M.; Vinuela, J. E.; Martinez-Zorzano, V. S.; de Carlos, A.; Rodriguez-Berrocal, F. J., Cell surface human alpha-L-fucosidase. *European Journal of Biochemistry* **2001**, 268 (11), 3321-3331.
13. Monti, E.; Bonten, E.; D'Azzo, A.; Bresciani, R.; Venerando, B.; Borsani, G.; Schauer, R.; Tettamanti, G., Sialidases in vertebrates: A family of enzymes

tailored for several cell functions. In *Advances in Carbohydrate Chemistry and Biochemistry*, Vol 64, Horton, D., Ed. 2010; Vol. 64, pp 403-479.

14. Feng, C.; Zhang, L.; Almulki, L.; Faez, S.; Whitford, M.; Hafezi-Moghadam, A.; Cross, A. S., Endogenous PMN sialidase activity exposes activation epitope on CD11b/CD18 which enhances its binding interaction with ICAM-1. *Journal of Leukocyte Biology* **2011**, *90* (2), 313-321.

15. Stamatos, N. M.; Carubelli, I.; van de Vlekkert, D.; Bonten, E. J.; Papini, N.; Feng, C.; Venerando, B.; d'Azzo, A.; Cross, A. S.; Wang, L.-X.; Gornat, P. J., LPS-induced cytokine production in human dendritic cells is regulated by sialidase activity. *Journal of Leukocyte Biology* **2010**, *88* (6), 1227-1239.

16. Nan, X.; Carubelli, I.; Stamatos, N. M., Sialidase expression in activated human T lymphocytes influences production of IFN-gamma. *Journal of Leukocyte Biology* **2007**, *81* (1), 284-296.

17. Yamaguchi, K.; Shiozaki, K.; Moriya, S.; Koseki, K.; Wada, T.; Tateno, H.; Sato, I.; Asano, M.; Iwakura, Y.; Miyagi, T., Reduced susceptibility to colitis-associated colon carcinogenesis in mice lacking plasma membrane-associated sialidase. *Plos One* **2012**, *7* (7).

18. Miyagi, T., Mammalian sialidases and their functions. *Trends. Glycosci. Glycotechnol.* **2010**, *22*, 162-172.

19. Miyagi, T.; Yamaguchi, K., Mammalian sialidases: Physiological and pathological roles in cellular functions. *Glycobiology* **2012**, *22* (7), 880-896.

20. Cherayil, G. D., Sialic-acid and fatty-acid concentrations in lymphocytes, red-blood-cells and plasma from patients with multiple-sclerosis. *Journal of the Neurological Sciences* **1984**, *63* (1), 1-10.
21. Stelmasiak, Z.; Solski, J.; Jakubowska, B., Sialic acids in serum and erythrocyte membranes in patients with MS. *Neuropsychiatrie* **1996**, *10* (4), 205-208.
22. Cantarel, B. L.; Coutinho, P. M.; Rancurel, C.; Bernard, T.; Lombard, V.; Henrissat, B., The Carbohydrate-Active EnZymes database (CAZy): an expert resource for Glycogenomics. *Nucleic Acids Research* **2009**, *37*, D233-D238.
23. Monti, E.; Preti, A.; Venerando, B.; Borsani, G., Recent development in mammalian sialidase molecular biology. *Neurochemical Research* **2002**, *27* (7-8), 649-663.
24. Lukong, K. E.; Seyrantepe, V.; Landry, K.; Trudel, S.; Ahmad, A.; Gahl, W. A.; Lefrancois, S.; Morales, C. R.; Pshezhetsky, A. V., Intracellular distribution of lysosomal sialidase is controlled by the internalization signal in its cytoplasmic tail. *Journal of Biological Chemistry* **2001**, *276* (49), 46172-46181.
25. Vinogradova, M. V.; Michaud, L.; Mezentsev, A. V.; Lukong, K. E.; El-Alfy, M.; Morales, C. R.; Potier, M.; Pshezhetsky, A. V., Molecular mechanism of lysosomal sialidase deficiency in galactosialidosis involves its rapid degradation. *Biochemical Journal* **1998**, *330*, 641-650.
26. Monti, E.; Preti, A.; Rossi, E.; Ballabio, A.; Borsani, G., Cloning and characterization of NEU2, a human gene homologous to rodent soluble sialidases. *Genomics* **1999**, *57* (1), 137-143.

27. Miyagi, T.; Tsuiki, S., Purification and characterization of cytosolic sialidase from rat-liver. *Journal of Biological Chemistry* **1985**, *260* (11), 6710-6716.
28. Tringali, C.; Papini, N.; Fusi, P.; Croci, G.; Borsani, G.; Preti, A.; Tortora, P.; Tettamanti, G.; Venerando, B.; Monti, E., Properties of recombinant human cytosolic sialidase HsNEU2 - The enzyme hydrolyzes monomerically dispersed GM1 ganglioside molecules. *Journal of Biological Chemistry* **2004**, *279* (5), 3169-3179.
29. Wang, Y.; Yamaguchi, K.; Wada, T.; Hata, K.; Zhao, X. J.; Fujimoto, T.; Miyagi, T., A close association of the ganglioside-specific sialidase Neu3 with caveolin in membrane microdomains. *Journal of Biological Chemistry* **2002**, *277* (29), 26252-26259.
30. Zanchetti, G.; Colombi, P.; Manzoni, M.; Anastasia, L.; Caimi, L.; Borsani, G.; Venerando, B.; Tettamanti, G.; Preti, A.; Monti, E.; Bresciani, R., Sialidase NEU3 is a peripheral membrane protein localized on the cell surface and in endosomal structures. *Biochemical Journal* **2007**, *408*, 211-219.
31. Yamaguchi, K.; Hata, K.; Koseki, K.; Shiozaki, K.; Akita, H.; Wada, T.; Moriya, S.; Miyagi, T., Evidence for mitochondrial localization of a novel human sialidase (NEU4). *Biochemical Journal* **2005**, *390*, 85-93.
32. Monti, E.; Bassi, M. T.; Bresciani, R.; Civini, S.; Croci, G. L.; Papini, N.; Riboni, M.; Zanchetti, G.; Ballabio, A.; Preti, A.; Tettamanti, G.; Venerando, B.; Borsani, G., Molecular cloning and characterization of NEU4, the fourth member of the human sialidase gene family. *Genomics* **2004**, *83* (3), 445-453.

33. Seyrantepe, V.; Landry, K.; Trudel, S.; Hassan, J. A.; Morales, C. R.; Pshezhetsky, A. V., Neu4, a novel human lysosomal lumen sialidase, confers normal phenotype to sialidosis and galactosialidosis cells. *Journal of Biological Chemistry* **2004**, *279* (35), 37021-37029.
34. Seyrantepe, V.; Poulpetova, H.; Froissart, R.; Zabet, M. T.; Marie, I.; Pshezhetsky, A. V., Molecular pathology of NEU1 gene in sialidosis. *Human Mutation* **2003**, *22* (5), 343-352.
35. Wang, P.; Zhang, J.; Bian, H.; Wu, P.; Kuvelkar, R.; Kung, T. T.; Crawley, Y.; Egan, R. W.; Billah, M. M., Induction of lysosomal and plasma membrane-bound sialidases in human T-cells via T-cell receptor. *Biochemical Journal* **2004**, *380*, 425-433.
36. Sandbhor, M. S.; Soya, N.; Albohy, A.; Zheng, R. B.; Cartmell, J.; Bundle, D. R.; Klassen, J. S.; Cairo, C. W., Substrate recognition of the membrane-associated sialidase neu3 requires a hydrophobic aglycone. *Biochemistry* **2011**, *50* (32), 6753-6762.
37. Li, Y.; Cao, H.; Yu, H.; Chen, Y.; Lau, K.; Qu, J.; Thon, V.; Sugiarto, G.; Chen, X., Identifying selective inhibitors against the human cytosolic sialidase NEU2 by substrate specificity studies. *Molecular Biosystems* **2011**, *7* (4), 1060-1072.
38. Khedri, Z.; Li, Y.; Cao, H.; Qu, J.; Yu, H.; Muthana, M. M.; Chen, X., Synthesis of selective inhibitors against V. cholerae sialidase and human cytosolic sialidase NEU2. *Organic & Biomolecular Chemistry* **2012**, *10* (30), 6112-6120.

39. Magesh, S.; Moriya, S.; Suzuki, T.; Miyagi, T.; Ishida, H.; Kiso, M., Design, synthesis, and biological evaluation of human sialidase inhibitors. Part 1: Selective inhibitors of lysosomal sialidase (NEU1). *Bioorganic & Medicinal Chemistry Letters* **2008**, *18* (2), 532-537.
40. Li, J.; Zheng, M.; Tang, W.; He, P.-L.; Zhu, W.; Li, T.; Zuo, J.-P.; Liu, H.; Jiang, H., Syntheses of triazole-modified zanamivir analogues via click chemistry and anti-AIV activities. *Bioorganic & Medicinal Chemistry Letters* **2006**, *16* (19), 5009-5013.
41. Vonitzstein, M.; Wu, W. Y.; Jin, B., The synthesis of 2,3-didehydro-2,4-dideoxy-4-guanidinyl-N-acetylneuraminic acid - a potent influenza-virus sialidase inhibitor. *Carbohydrate Research* **1994**, *259* (2), 301-305.
42. Lu, Y.; Gervay-Hague, J., Synthesis of C-4 and C-7 triazole analogs of zanamivir as multivalent sialic acid containing scaffolds. *Carbohydrate Research* **2007**, *342* (12-13), 1636-1650.
43. Meindl, P.; Tuppy, H., 2-Deoxy-2,3-dehydrosialic acids .3. Inhibition of *Vibrio-cholerae* neuraminidase by oxidation products of 2-deoxy-2,3-dehydro-N-acetyl-neuraminic acid. *Monatshefte Fur Chemie* **1970**, *101* (3), 639-&.
44. Smith, P. W.; Sollis, S. L.; Howes, P. D.; Cherry, P. C.; Copley, K. N.; Taylor, H.; Whittington, A. R.; Scicinski, J.; Bethell, R. C.; Taylor, N.; Skarzynski, T.; Cleasby, A.; Singh, O.; Wonacott, A.; Varghese, J.; Colman, P., Novel inhibitors of influenza sialidases related to GG167 - Structure-activity, crystallographic and molecular dynamic studies with 4H-pyran-2-carboxylic acid

6-carboxamides. *Bioorganic & Medicinal Chemistry Letters* **1996**, *6* (24), 2931-2936.

45. Smith, P. W.; Sollis, S. L.; Howes, P. D.; Cherry, P. C.; Starkey, I. D.; Cobley, K. N.; Weston, H.; Scicinski, J.; Merritt, A.; Whittington, A.; Wyatt, P.; Taylor, N.; Green, D.; Bethell, R.; Madar, S.; Fenton, R. J.; Morley, P. J.; Pateman, T.; Beresford, A., Dihydropyranocarboxamides related to zanamivir: A new series of inhibitors of influenza virus sialidases. 1. Discovery, synthesis, biological activity, and structure-activity relationships of 4-guanidino- and 4-amino-4H-pyran-6-carboxamides. *Journal of Medicinal Chemistry* **1998**, *41* (6), 787-797.

46. Sollis, S. L.; Smith, P. W.; Howes, P. D.; Cherry, P. C.; Bethell, R. C., Novel inhibitors of influenza sialidase related to GG167 - Synthesis of 4-amino and guanidino-4H-pyran-2-carboxylic acid-6-propylamides; Selective inhibitors of influenza A virus sialidase. *Bioorganic & Medicinal Chemistry Letters* **1996**, *6* (15), 1805-1808.

47. Politzer, P.; Murray, J. S., Some intrinsic features of hydroxylamines, oximes and hydroxamic acids: Integration of theory and experiment. In *The Chemistry of Hydroxylamines, Oximes and Hydroxamic Acid*, John Wiley & Sons, Ltd.: Chichester, U.K., 2008; pp 1-27.

48. Pshezhetsky, A. V.; Potier, M., Association of N-acetylgalactosamine-6-sulfate sulfatase with the multienzyme lysosomal complex of beta-galactosidase, cathepsin A, and neuraminidase - Possible implication for intralysosomal

catabolism of keratan sulfate. *Journal of Biological Chemistry* **1996**, 271 (45), 28359-28365.

49. Watson, D. C.; Leclerc, S.; Wakarchuk, W. W.; Young, N. M., Enzymatic synthesis and properties of glycoconjugates with legionaminic acid as a replacement for neuraminic acid. *Glycobiology* **2011**, 21 (1), 99-108.

50. Albohy, A.; Li, M. D.; Zheng, R. B.; Zou, C.; Cairo, C. W., Insight into substrate recognition and catalysis by the human neuraminidase 3 (NEU3) through molecular modeling and site-directed mutagenesis. *Glycobiology* **2010**, 20 (9), 1127-1138.

51. Albohy, A.; Mohan, S.; Zheng, R. B.; Pinto, B. M.; Cairo, C. W., Inhibitor selectivity of a new class of oseltamivir analogs against viral neuraminidase over human neuraminidase enzymes. *Bioorganic & Medicinal Chemistry* **2011**, 19 (9), 2817-2822.

52. Chavas, L. M. G.; Tringali, C.; Fusi, P.; Venerando, B.; Tettamanti, G.; Kato, R.; Monti, E.; Wakatsuki, S., Crystal structure of the human cytosolic sialidase Neu2 - Evidence for the dynamic nature of substrate recognition. *Journal of Biological Chemistry* **2005**, 280 (1), 469-475.

53. Zou, Y.; Albohy, A.; Sandbhor, M.; Cairo, C. W., Inhibition of human neuraminidase 3 (NEU3) by C9-triazole derivatives of 2,3-didehydro-N-acetyl-neuraminic acid. *Bioorganic & Medicinal Chemistry Letters* **2010**, 20 (24), 7529-7533.

54. Goodsell, D. S.; Morris, G. M.; Olson, A. J., Automated docking of flexible ligands: Applications of AutoDock. *Journal of Molecular Recognition* **1996**, *9* (1), 1-5.
55. Morris, G. M.; Goodsell, D. S.; Halliday, R. S.; Huey, R.; Hart, W. E.; Belew, R. K.; Olson, A. J., Automated docking using a Lamarckian genetic algorithm and an empirical binding free energy function. *Journal of Computational Chemistry* **1998**, *19* (14), 1639-1662.
56. Gilson, M. K.; Sharp, K. A.; Honig, B. H., Calculating the electrostatic potential of molecules in solution - method and error assessment. *Journal of Computational Chemistry* **1988**, *9* (4), 327-335.
57. The PyMOL Molecular Graphics System, v. S., LLC: New York; <http://www.pymol.org/> (accessed November 15, 2012).
58. von Itzstein, M., The war against influenza: discovery and development of sialidase inhibitors. *Nature Reviews Drug Discovery* **2007**, *6* (12), 967-974.
59. Hata, K.; Koseki, K.; Yamaguchi, K.; Moriya, S.; Suzuki, Y.; Yingsakmongkon, S.; Hirai, G.; Sodeoka, M.; von Itzstein, M.; Miyagi, T., Limited inhibitory effects of oseltamivir and zanamivir on human sialidases. *Antimicrobial Agents and Chemotherapy* **2008**, *52* (10), 3484-3491.
60. Chavas, L. M. G.; Kato, R.; Suzuki, N.; von Itzstein, M.; Mann, M. C.; Thomson, R. J.; Dyason, J. C.; McKimm-Breschkin, J.; Fusi, P.; Tringali, C.; Venerando, B.; Tettamanti, G.; Monti, E.; Wakatsuki, S., Complexity in influenza virus targeted drug design: Interaction with human sialidases. *Journal of Medicinal Chemistry* **2010**, *53* (7), 2998-3002.

61. Magesh, S.; Suzuki, T.; Miyagi, T.; Ishida, H.; Kiso, M., Homology modeling of human sialidase enzymes NEU1, NEU3 and NEU4 based on the crystal structure of NEU2: Hints for the design of selective NEU3 inhibitors. *Journal of Molecular Graphics & Modelling* **2006**, 25 (2), 196-207.

5 Mapping the substrate interactions of the human membrane-associated neuraminidase, NEU3, using STD NMR¹

¹ A version of this chapter has been submitted for publication: Albohy, A.; Richards, M. R.; Cairo, C. W., Mapping substrate interactions of the human membrane-associated neuraminidase, NEU3, using STD NMR, **2014**.

5.1 Introduction

The human membrane-associated neuraminidase, NEU3, is one of four neuraminidase isoenzymes identified in humans.¹ Previous work has provided evidence for NEU3 localization to the plasma membrane, endosome, and the nuclear envelope.^{2, 3} As its membrane localization may suggest, NEU3 has been associated with roles including control of apoptosis, cell signaling and regulation of cell-cell interactions.^{4, 5} Additionally, NEU3 is proposed to play important roles in the development of human cancer.⁶⁻⁸ NEU3 is a glycosyl hydrolase enzyme (GH; EC 3.2.1.18) and has an apparent preference for glycolipid substrates over glycoproteins.⁹⁻¹¹ The enzyme is likely involved in the regulation of glycolipid composition of the membrane through consumption of specific ganglioside substrates.¹² Despite the importance of NEU3 in disease, there is limited information on the specificity and recognition of the enzyme substrate.

NEU3 substrate specificity has primarily been tested against naturally occurring gangliosides. The enzyme has been reported to cleave GM3, GD1a, GD1b, and GT1b.¹⁰ Studies of membrane bound neuraminidase isolated from human brain tissue found activity for an $\alpha(2 \rightarrow 3)$ neuraminidase able to cleave GM3 (**5.1**), GM4, GD1a; as well as an $\alpha(2 \rightarrow 8)$ activity able to cleave GD3, GD2, GD1b, GT1b, and GQ1b.¹³ Relative to GM3, GD3 and GM4 were less active substrates (c.a. ~70%); while GD1a, GD1b and GD2 were significantly less active (c.a. ~50%).¹³ Notably, several studies have found that glycolipids with sialic acid at an internal branch point are poor substrates. The most common examples of this group are GM1 and GM2, which both contain an $\alpha(2 \rightarrow 3)$ Neu5Ac at an internal galactose residue with a $\beta(1 \rightarrow 4)$ GlcNAc linkage.^{10, 13}

Interestingly, lyso-gangliosides have been found to be cleaved by membrane neuraminidase, while *O*-acetylation at *C9* of the sialic acid was found to inhibit activity.¹³

Recombinantly expressed NEU3 has been used to test enzyme specificity showing similar results with commonly occurring gangliosides.¹¹ Investigations of NEU3 with synthetic GM3 analogs have found that the enzyme does not tolerate modifications to the *N5* sidechain, while the *C9* site can be modified with preservation of some activity.¹⁴ Importantly, this study found that the hydrophobic aglycone of the ganglioside substrate was critical for activity, yet could be substituted by a simple octyl chain. Additionally, a specific recognition site for the hydrophobic aglycone was proposed based on these findings. Although a range of substrate activity has been demonstrated for NEU3, there are still limited data on the structure of the active site or its recognition of specific substrates.

Although NEU2 has been studied by crystallography, there are currently no experimentally determined structures of the membrane-associated NEU3 reported. Homology models of NEU3 have been developed.^{15, 16} The model of NEU3 we previously reported has been tested extensively by site-directed mutagenesis and substrate studies.^{14, 16} We have used the homology model of NEU3 in the rational design of inhibitors for human neuraminidases.^{17, 18} Although the homology model of NEU3 has been a useful tool for inhibitor studies, we recognized that the model is likely incomplete. For example, a significant portion of our homology model does not overlap with the template NEU2 structure used to develop it, suggesting some portions of the protein may adopt a different fold than seen in NEU2.¹⁶ As a result, we set out to obtain more detailed structural information regarding substrate interactions with the NEU3 active site

and to identify portions of our model that require refinement. We turned to saturation transfer difference (STD) NMR as a method that provides details of substrate interactions with the enzyme.

Mayer and Meyer introduced STD NMR as a method to map the interaction of substrate epitopes in close contact with a protein binding site.^{19, 20} STD NMR has also been used to study the binding conformation of ligands in their active sites.^{21, 22} Carbohydrate-lectin interactions are often studied by this method due to their moderate binding affinity and substrate size.^{23, 24} von Itzstein and coworkers have used STD NMR to study the binding of free sialic acid and some of its derivatives to the *Vibrio cholerae* neuraminidase, revealing that the enzyme has a preference for the α -anomer.²⁵ Thus, we expected that STD NMR could provide crucial new insight into the active site of NEU3 and its interaction with the enzyme's most active ligand, GM3. To investigate the molecular features of the NEU3-GM3 enzyme-substrate complex, we needed to tailor the features of both the enzyme and its ligand. First, the native enzyme would rapidly hydrolyze the glycosidic linkage of the GM3 trisaccharide, making it difficult to study the intact complex. To deal with this issue, we used a catalytically inactive form of the enzyme, NEU3(Y370F), which we have previously characterized.¹⁶ The native glycosphingolipid substrate, GM3, is also known to have a high propensity for micelle formation,^{26, 27} which could interfere with the use of STD NMR. To avoid this problem, we chose to use a glycolipid analog of GM3 with an octyl chain as the aglycone, a substrate that has been previously shown to have comparable activity to GM3.¹⁴ Using STD NMR and molecular dynamics (MD), we report here the epitope mapping of the GM3-octyl derivative (Neu5Ac- α 2,3-Gal- β 1,4-Glc- β -octyl; **5.2**) and 2'-(4-

methylumbelliferyl)- α -D-*N*-acetylneuraminic acid (4MU-NANA; **5.4**) with the active site of NEU3 (Figure 5.1). We compare the experimentally obtained epitope maps to the predictions of the homology model using MD simulations of the complexes.

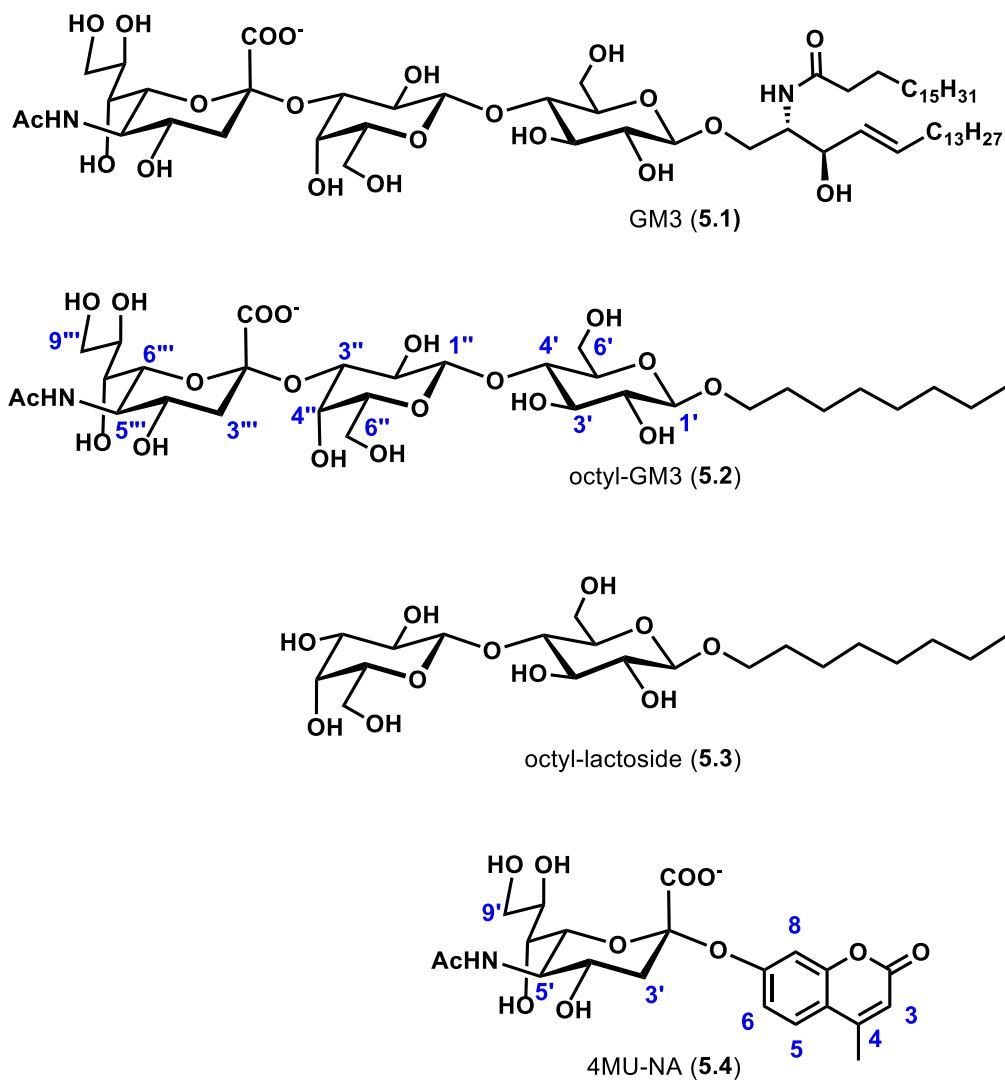


Figure 5.1: Compounds used in this study: GM3 (5.1), octyl-GM3 (5.2), octyl-lactoside (5.3), and 4MU-NANA (5.4).

5.2 Results

5.2.1 1D ¹H NMR assignment

To conduct STD NMR experiments, we first needed to determine a complete assignment for all the proton signals in the substrates to be used. Standard 1D and 2D experiments (1D ¹H NMR, 1D ¹³C, COSY, HMQC, HMBC and CSSF-TOCSY) were used to make assignments for ¹H signals of 2'-(4-methylumbelliferyl)- α -D-N-acetylneuraminic acid (4MU-NANA, **5.4**), octyl-lactoside (**5.3**), and the octyl-GM3 substrate (**5.2**). For example, CSSF-TOCSY experiments^{28, 29} were used to assign some overlapping signals in **5.2**. In these experiments (Figure **5.2**) each spin system was excited individually. This includes the octyl, glucose, galactose and sialic acid spin systems.

For **5.2**: ¹H NMR (700 MHz, D₂O) δ 4.52 (d, $J = 7.8$ Hz, 1H, H1''), 4.47 (d, $J = 8.1$ Hz, 1H, H1'), 4.11 (dd, $J = 8.4, 3.1$ Hz, 1H, H3''), 3.98 (d, $J = 11.7$ Hz, 1H, H6'a), 3.96 (d, $J = 1.7$ Hz, 1H, H4''), 3.93-3.88 (m, 1H, OCH), 3.87 (d, $J = 11.2$ Hz, 1H, H8'''), 3.83 (d, $J = 10.3$ Hz, 1H, H9''a), 3.81 (m, 1H, H6'b), 3.77 (m, 1H, H6'a), 3.74-3.70 (m, 2H, H6''', H7'''), 3.70-3.65 (m, 4H, H4''', H6'b, H5'', O-CH), 3.65-3.62 (m, 3H, H3', H5''' and H9''b), 3.61-3.55 (m, 3H, H4', H5' and H2''), 3.30 (t, $J = 7.8$ Hz, 1H, H2'), 2.76 (dd, $J = 12.4, 4.2$ Hz, 1H, H3'''eq), 2.03 (s, 3H, CH₃C=O), 1.80 (t, $J = 12.0$ Hz, 1H, H3'''ax), 1.62 (m, 2H, CH₂), 1.38-1.33 (m, 2H, CH₂), 1.33-1.24 (m, 8H, (CH₂)₄), 0.86 (t, $J = 6.6$ Hz, 3H, CH₃).

For **5.4**: ¹H NMR (700 MHz, D₂O) δ 7.75 (d, $J=9.5$, 1H, H6), 7.21 (m, 1H, H5), 7.19 (s, 1H, H3), 6.31(s, 1H, H8), 4.08 (dd, $J = 10.5, 1.7$ Hz, 1H, H6'), 3.96 (t, $J = 10.0$ Hz, 1H, H5'), 3.89 (m, 1H, H8'), 3.86 (m, 1H, H9'b), 3.80 (m, 1H, H4'), 3.64 (dd, $J = 12.1,$

6.4 Hz, 1H, H9'a), 3.61 (dd, $J = 9.0, 1.5$ Hz, 1H, H7'), 2.88 (dd, $J = 12.7, 4.7$ Hz, 1H, H3'eq), 2.47 (s, 3H, CH₃-Ar), 2.06 (s, 3H, CH₃C=O), 2.01(t, $J=12.1$, 1H, H3'ax).

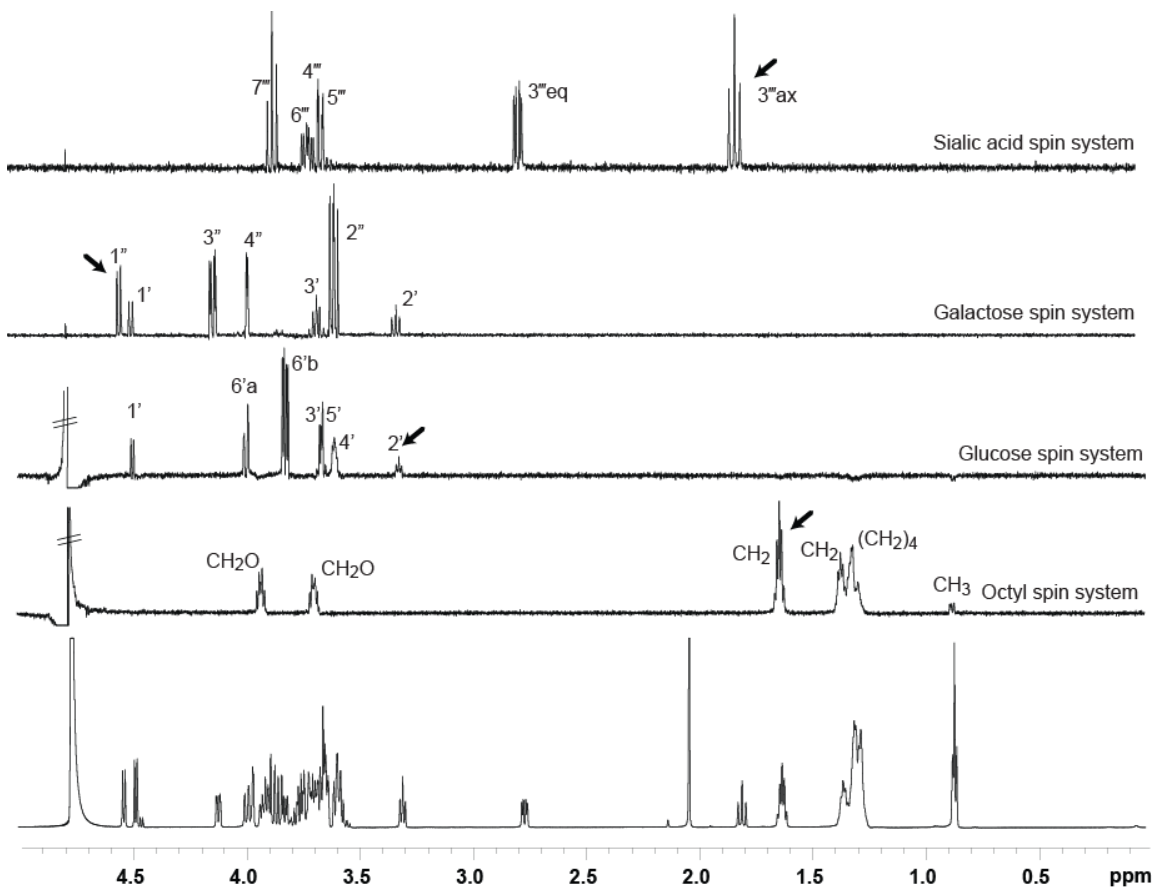


Figure 5.2: NMR assignment of octyl-GM3. *CSSF-TOCSY*^{28, 29} experiments were used to assign protons of 5.2, excitation was at the resonance indicated by an arrow. The mixing time was 120 ms for all experiments. The octyl spin system was excited at the resonance for the aglycone C2 hydrogens with frequency difference of 88 Hz to the closest proton that is not in the octyl spin system. The glucose spin system was excited at H2' and frequency difference of 141 Hz. The galactose spin system was excited at H1'' with the frequency difference of 27 Hz, and sialic acid spin system was excited at the H3''ax and frequency difference of 88 Hz.

Excitation at the octyl-H2 of **5.2** (1.62 ppm) revealed the octyl protons, most of which were well separated. Only the two methylene protons adjacent to the glycosidic linkage (CH₂O, octyl-H1) were difficult to resolve as they occur in the carbohydrate region between 3.5 and 4.0 ppm. Using TOCSY, we found that those protons were centered at 3.92 and 3.69 ppm, respectively. The spin system for the glucose residue was identified by excitation of the H2' proton at 3.30 ppm, allowing full assignment of signals found overlapped in the ring region (Table **5.1**).

Table 5.1: STD and MD results for NEU3–octyl-GM3

Residue	Atom/ Group	Position δ (ppm)	STD signal (%)	Average Distance	STD score**	MD score (average distance)***
Alkyl	CH ₃	0.86	100	10.4 [‡]	++	--
	(CH ₂) ₄	1.273-1.333	200 [†]	8.4 [‡]	+++	--
	CH ₂	1.352	170 [†]	10.2 [‡]	+++	--
	CH ₂	1.622	43	12.0 [‡]	-	--
	O-CH ₂	3.924, 3.690	60	10.4 [‡]	+	--
Glc	1'	4.476	100	6.7	++	--
	2'	3.297	83	6.5	++	-
	3'	3.647	46	7.3	+	--
	4'	3.5695	50	6.0	+	-
	5'	3.57	50	6.4	+	-
	6'	3.815, 3.975	49	7.8	+	--
Gal	1''	4.528	42	7.8	-	--
	2''	3.572	50	6.4	+	-
	3''	4.111	39	9.2	-	--
	4''	3.957	39	7.7	-	++
	5''	3.685	46	7.7	+	--
	6''	3.77, 3.69	41	4.1	-	++
Neu5Ac	3''' ax	1.798	10	3.5	--	++
	3''' eq	2.759	31	2.9	-	+++
	4'''	3.679	37	3.3	-	++
	5'''	3.632	46	7.0	+	-
	6'''	3.701	37	3.3	-	+++
	7'''	3.738	38	3.5	-	++
	8'''	3.884	73	2.9	++	+++
	9'''	3.828, 3.625	43	6.4	-	-
	CH ₃ C=O	2.032	26	3.1	--	+++

[†] Signals were normalized to H1, giving some aglycone signals over 100%

[‡] Average is high due to the flexibility of octyl side chain, see discussion and Figure 5.11

* Average of overlapped signals

** (++) 61 - 100 %, (+) 46 - 60 %, (-) 31 - 45 %, (--) 0 - 30 %

*** total distances: (++++) <3.3, (++) 3.4-5.0, (+) 5.1-6.0, (-) 6.1- 7.0, (--) >7.1

Unfortunately, none of the galactose protons were completely resolved. Excitation at the H1'' anomeric proton (4.52 ppm) resulted in partial excitation of the Glc anomeric proton, H1' (4.48 ppm) and signals for H1''-H4'' of Gal. The remaining signals of the Gal residue were assigned using COSY experiments. The sialic acid spin system was revealed by excitation of the H3''' axial proton (1.79 ppm) which has a strong coupling to H4''' compared to the H3''' equatorial proton. The remaining sialic acid proton signals, up to H7''', were identified in this way. The spectrum of 4MU-NANA was also assigned using a similar strategy (Table 5.2).

Table 5.2: STD and MD results for NEU3–4MU-NANA

Residue	Atom/ Group	Position δ (ppm)	STD signal (%)	Average distance	STD score*	MD score (average distances)**
4MU	H8	6.31	100	4.3	++	++
	H6	7.75	3	6.1	--	-
	H5	7.21	36	5.2	-	+
	H3	7.19	76	5.2	++	+
	CH ₃	2.47	100	4.1	++	++
Neu5Ac	3' ax	2.01	44	3.7	-	++
	3' eq	2.88	49	2.9	-	+++
	4'	3.80	100	3.5	++	++
	5'	3.96	70	7.3	+	--
	6'	4.08	63	3.4	+	++
	7'	3.61	62	4.4	+	+
	8'	3.89	100	3.5	++	++
	9'	3.64,3.86	42	6.8	-	--
	CH ₃ C=O	2.06	51	4.5	+	+

* (++) 76 - 100 % , (+) 51 - 75 % , (-) 26 - 50 % , (--) 0 - 25 %

** total distances: (+++) <3.3, (++) 3.4-4.3, (+) 4.4-5.3, (-) 5.4- 6.3, (--) >6.4

5.2.2 Protein expression

Recombinant NEU3, or the catalytically inactive mutant, NEU3(Y370F) proteins containing an N-terminal maltose-binding protein (MBP) affinity tag, was expressed and purified as previously reported.¹⁶ Aliquots of the protein were stored at -80°C and used immediately after thaw for experiments. To prepare the enzyme sample for STD NMR experiments, the buffer was rapidly exchanged using a spin column (MWCO 30 kDa). The NEU3(Y370F) mutant was found to have only 0.1% neuraminidase activity when

compared to the wild type using **5.4** as a substrate. In addition, MBP alone was expressed and purified the same way and used for control experiments.

5.2.3 STD NMR of NEU3(Y370F)–substrate complexes

To confirm that the substrate and enzyme could be used for STD studies, we conducted control experiments to exclude possible artifacts (Figure 5.3). STD experiments with NEU3 alone, **5.2** alone, or the MBP affinity tag alone showed only minor signals. STD experiments run with **5.1** showed a large signal in the aliphatic region, which we attribute to micelle formation.^{26, 27} GM3 is known to have a very low critical micelle concentration, and our experiments required a high concentration of the substrate (2.5 mM).³⁰ Adding DMSO (up to 8% final concentration) did not disrupt the aliphatic STD NMR signals. Attempts to eliminate the aliphatic signals of GM3 by modification of the on-frequency resonance were unsuccessful. As a result, we concluded that the use of GM3 for STD NMR experiments would mask any protein-lipid interactions due to micelle formation. We then tested **5.2**, an analog of GM3 known to be a good substrate for the enzyme.¹⁴ When used in STD NMR experiments alone, spectra of **5.2** did not contain any signals in the aliphatic region (Figure 5.3b). Based on the known substrate activity for **5.2**, and our STD NMR control experiments, we chose to use this ligand as a proxy for the native substrate.

The mutant enzyme used here also contains a MBP affinity tag at the N-terminus of NEU3. In previous studies we have found that the fusion tag is important for maintaining the stability of recombinant NEU3. Thus, the affinity tag was retained for these studies; however, we needed to confirm that any binding interactions observed by STD NMR were the result of NEU3-substrate interactions alone.¹⁶ To test for

interactions of MBP with **5.2**, we expressed and purified MBP alone, and performed STD NMR experiments with the protein alone and with **5.2**. These experiments showed no significant signals in either the aliphatic or carbohydrate regions of the spectrum, confirming the lack of interactions between **5.2** and MBP. Furthermore, to test the importance of sialic acid for binding of octyl-GM3 to NEU3 we tested a complex of NEU3 and octyl-lactoside (**5.3**). These experiments found a very weak STD signal in the aliphatic (0.9-1.3 ppm) and carbohydrate regions (3.5-4.5 ppm) of the spectrum (Figure 5.3c). The STD NMR spectrum for this interaction was too noisy to make reasonable assignments of interactions, likely due to the low affinity of the ligand.

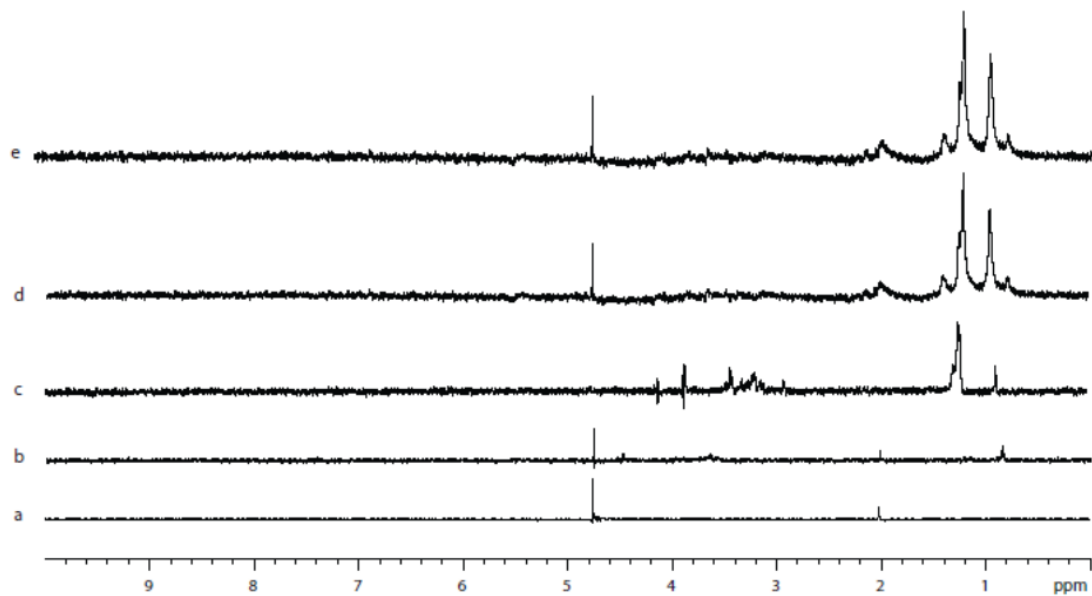


Figure 5.3: STD NMR Controls. Control experiments used to exclude interference with the STD signal for NEU3 complexes. **a.** STD of the enzyme only (no substrate) showing that there is no interference from the enzyme and buffer used. **b.** STD experiment of octyl-GM3 with MBP in buffer. The lack of STD signal indicates that there is no interference from MBP–octyl-GM3 complex formation. **c.** STD experiment of octyl-lactoside with NEU3(Y370F) showing only small STD enhancement, suggesting that the substrate requires sialic acid for recognition by NEU3. **d.** STD of GM3 alone, showing a significant STD effect in the aliphatic region, likely due to the formation of micelles. **e.** STD experiment of GM3 in the presence of 8% DMSO, the additional organic solvent does not significantly disrupt the STD signals observed in the aliphatic region.

In addition to **5.2** and **5.3**, we also tested 4MU-NANA (**5.4**) and 2-deoxy-2,3-didehydro-*N*-acetyl-neuraminic acid (DANA). The STD NMR spectrum of the 4MU-NANA-NEU3(Y370F) complex had good signal-to-noise and could be interpreted (*vide infra*). The NEU3(Y370F)-DANA complex gave poor STD signal under several

conditions and could not be easily interpreted. We also tested DANA with active or inactive NEU3 at different temperatures (25, 32 and 37 °C) and at different times of observation (3, 24 and 48 hours). Unfortunately, none of these conditions resulted in significant improvements to the signal-to-noise ratio of the STD NMR spectra (data not shown).

5.2.4 STD NMR of NEU3(Y370F)–5.2 complex

We next conducted STD NMR experiments of octyl-GM3 (**5.2**) substrate with NEU3(Y370F) (Figure **5.4** and Figure **5.5**). STD NMR spectra were analyzed, and the relative integration of assigned peaks was used to construct an epitope map of the substrate (Figure **5.6** and Table **5.1**). In the case of overlapped signals, peaks were treated together as an average.

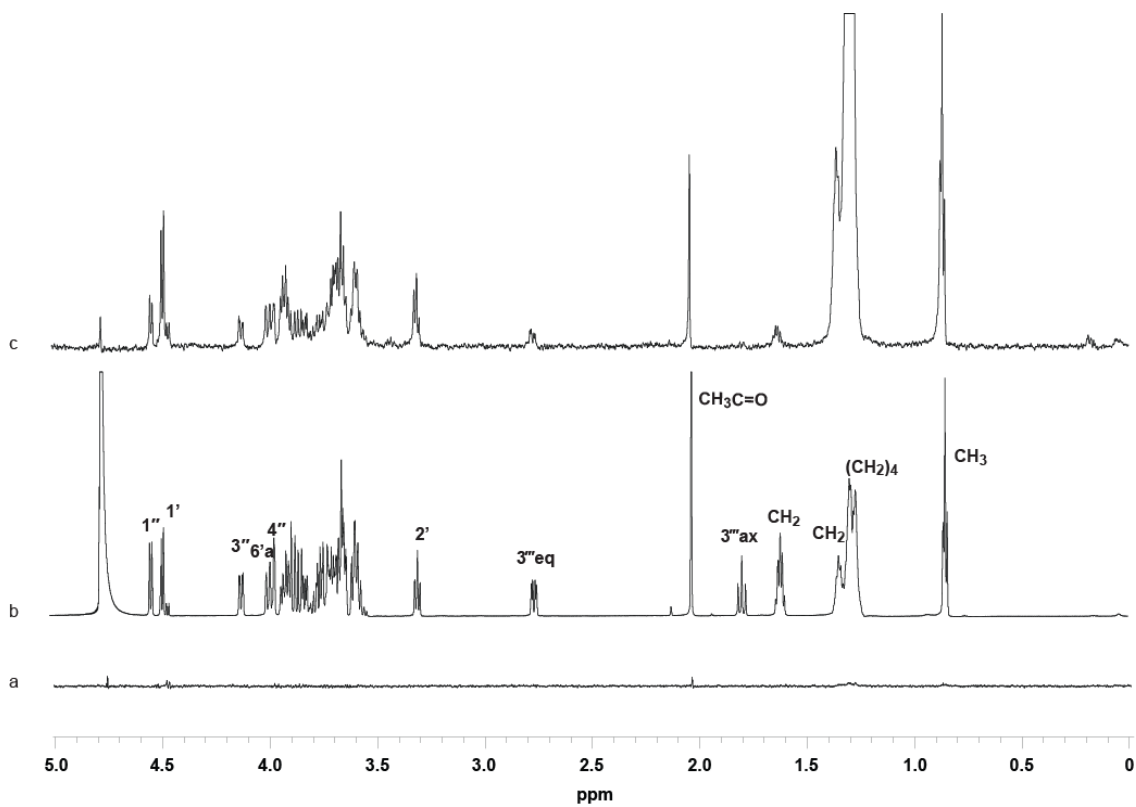


Figure 5.4: NMR studies of **5.2** in complex with NEU3(Y370F). *a.* STD-NMR spectrum of **5.2** alone (2.5 mM). *b.* 1D ^1H NMR of **5.2** (2.5 mM ligand) with NEU3(Y370F) (25 μM protein). *c.* STD-NMR spectrum of **5.2** with NEU3(Y370F).

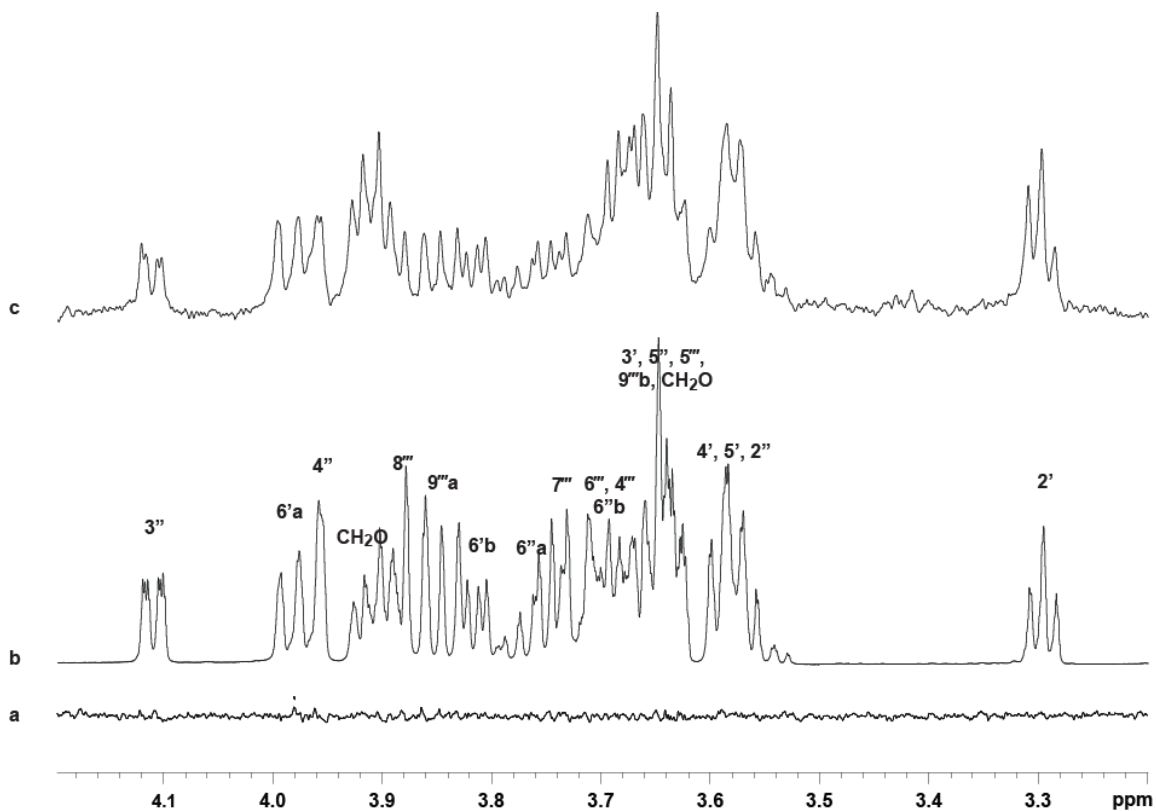
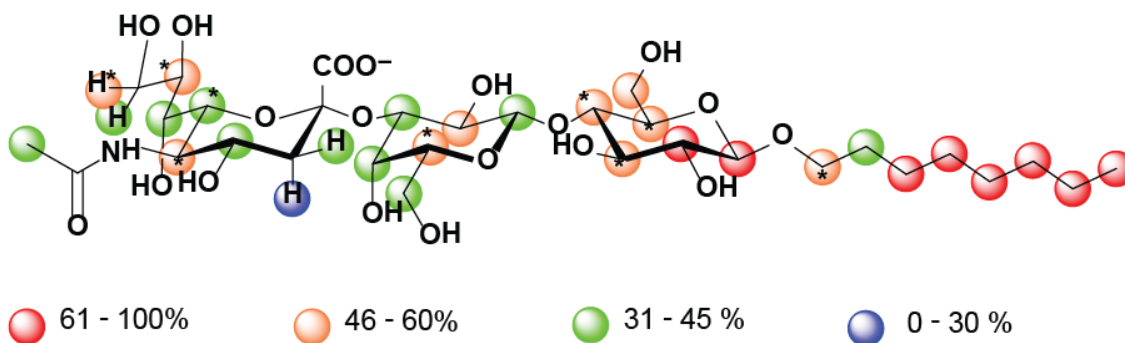


Figure 5.5: NMR studies of 5.2 in complex NEU3(Y370F), expansion of the carbohydrate region (3.2- 4.2 ppm). a. STD-NMR spectrum of 5.2 alone (2.5 mM). b. 1D ^1H NMR of 5.2 (2.5 mM ligand) with NEU3(Y370F) (25 μM protein). c. STD-NMR spectrum of 5.2 with NEU3(Y370F)..



* Average of overlapped signals

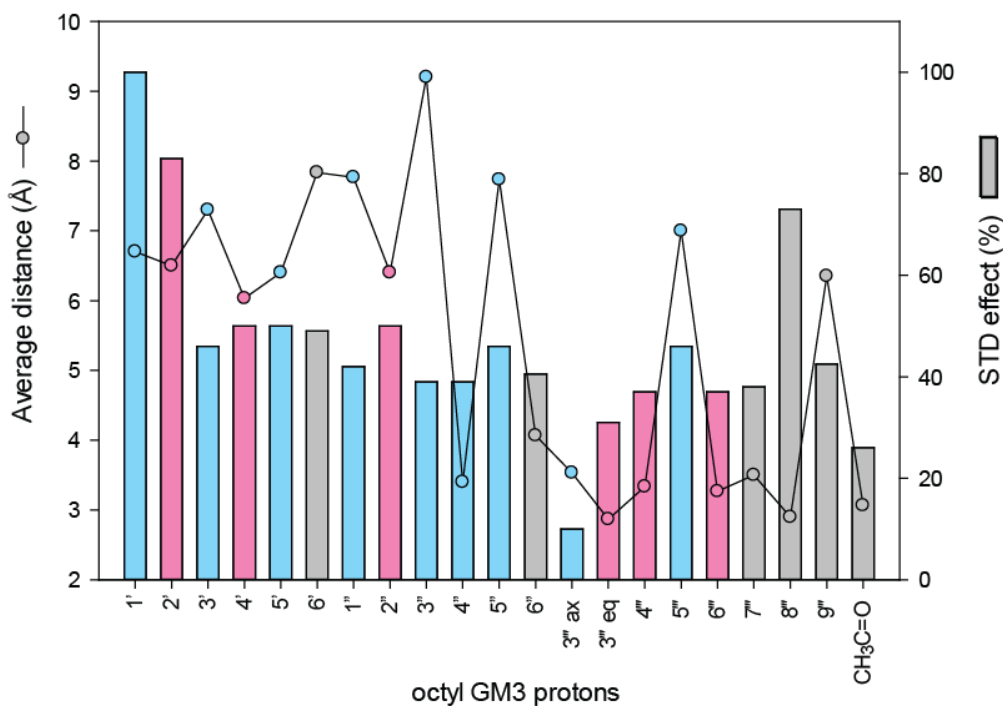


Figure 5.6: STD epitope map of 5.2 (top) and comparison of MD and STD NMR results (bottom). *The MD results are represented by the average distance to closest contacts in the protein, while the STD data are represented as a percentage of the effect. Protons on opposite faces of the carbohydrate residue are indicated by colors, with the A face (pink) and the B face (blue).*

In the epitope map of **5.2**, the strongest STD signal was found for the aliphatic aglycone hydrogens, consistent with the presence of a hydrophobic binding site that recognizes the lipid aglycone, as previously proposed.¹⁴ All signals were normalized to the strongest carbohydrate signal as reference (H1', 100%). Although some of the octyl protons showed stronger signals than H1, we chose to focus on relative differences among the oligosaccharide contacts since these should be more critical for substrate specificity. The strongest STD signals within the glucose residue were seen at H1' (100%) and H2' (83%), suggesting that this residue, distal from the glycosidic linkage cleaved by the enzyme, is important for recognition. The remaining protons of Glc showed only moderate STD signal.

The intervening Gal residue may play a less important role in recognition by NEU3. STD signals for Gal were all moderate, ranging from 37-50%. Among these, the strongest STD signals for Gal were seen for H2'' (50%) and H5'' (46%); which were not completely resolved in the NMR spectrum. It is notable that both A- and B-faces of Gal and Glc residues show significant contact with the protein, suggesting that the glycan is not complexed in a shallow binding site that contacts only one face of each residue.

The Neu5Ac residue of **5.2** showed strong STD signals for several positions. The strongest signal for the Neu5Ac residue was found for the glycerol side chain H8''' (73%) and H9''' (46%). Moderate signals were also observed for portions of the pyranose ring (H3''' (eq), H4''', H6''') and H7''', H9''' while signals for H3''' (ax) and the N5-Ac were relatively weak. In summary, these results are consistent with the aglycone and Glc residues acting as an anchor for the **5.2**. The Gal residue does participate in binding, although the lactoside alone is not sufficient for tight binding (*vide supra*). The presence

of the Neu5Ac residue provides additional contacts, most notably within the glycerol side chain of the residue and likely the C1''' carboxylate (although this second contact cannot be observed in the experiment).

5.2.5 *STD NMR of NEU3(Y370F)–5.4 complex*

We next turned to a fluorogenic NEU3 substrate, **5.4**, which lacks the intervening lactoside and contains an aromatic aglycone. STD NMR of **5.4** with NEU3(Y370F) was performed under the same conditions used for **5.2** (Figure 5.7 and Table 5.2), and an epitope map was constructed (Figure 5.8).

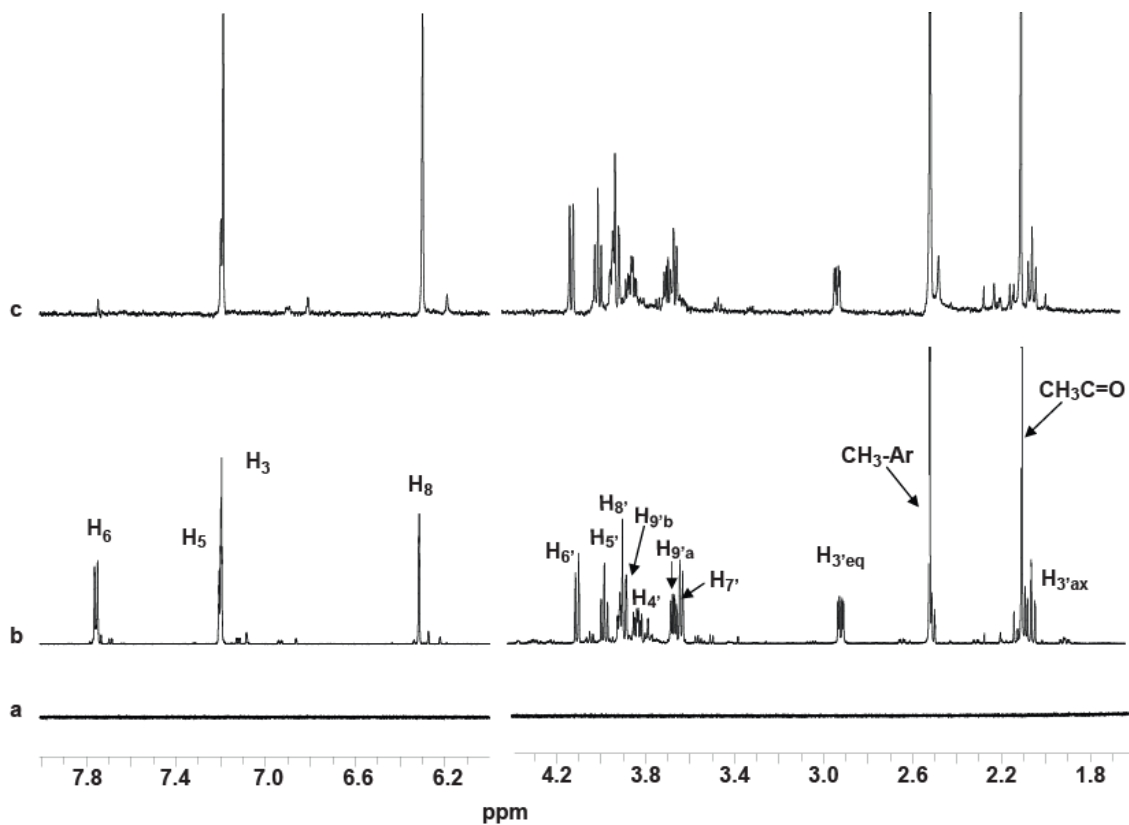


Figure 5.7: STD NMR studies of 4MU-NANA in the presence of NEU3(Y370F). *a.* STD-NMR spectrum of 4MU-NANA alone (2.5 mM). *b.* 1D ^1H NMR of 4MU-NANA (2.5 mM ligand) with NEU3(Y370F) (25 μM protein). *c.* STD-NMR spectrum of 4MU-NANA with NEU3(Y370F). The region of the spectrum between 4.2-6.2 ppm is removed for clarity.

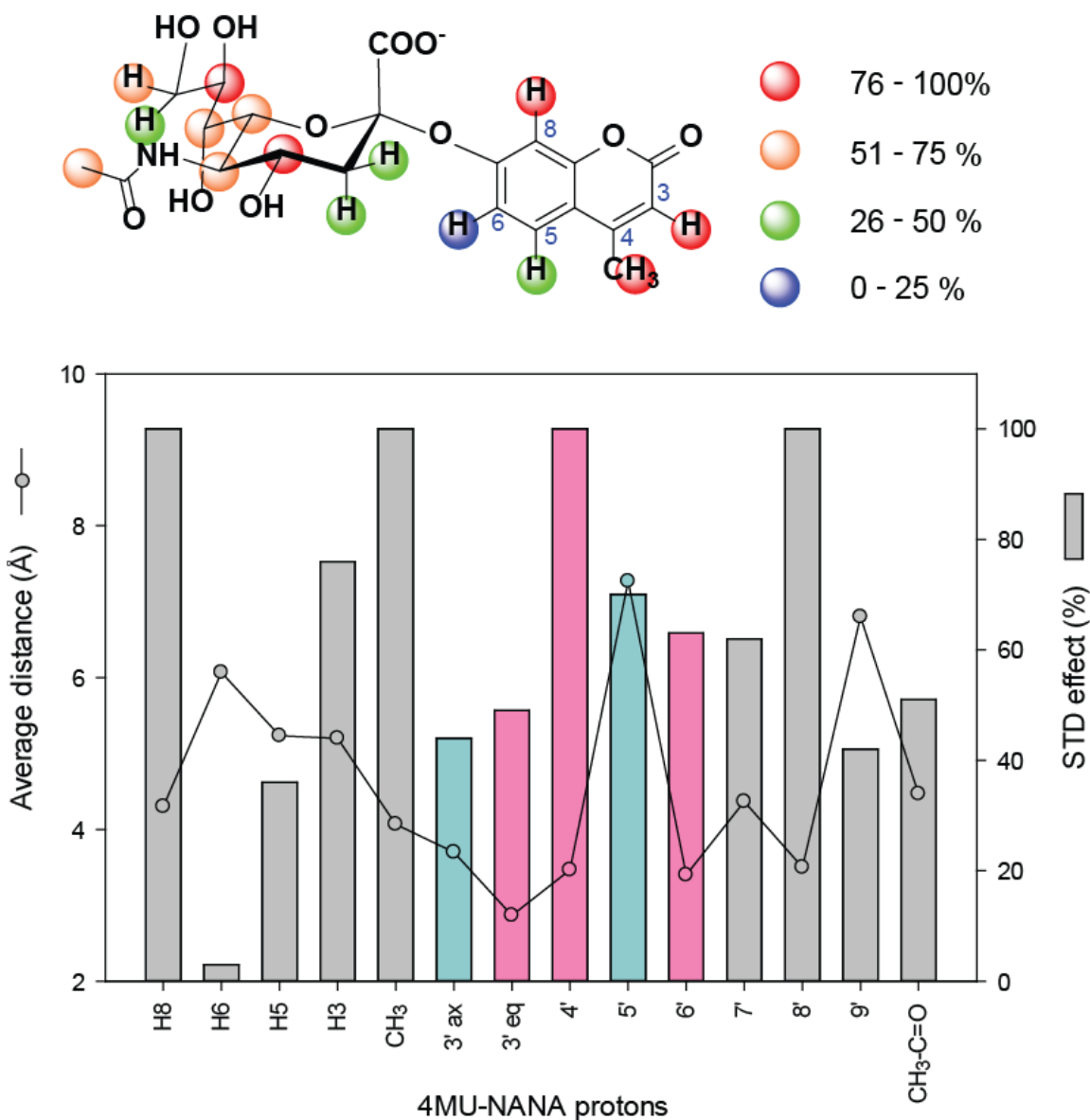


Figure 5.8: STD epitope map of 4MU-NANA (top) and comparison of MD and STD NMR results (bottom). The MD results are represented by the average distance to closest contacts in the protein, while the STD data are represented as a percentage of the effect. Protons on opposite faces of the carbohydrate residue are indicated by colors, with the A face (pink) and the B face (blue).

The strongest signals found were in the sialic acid residue and were then used as reference (H4' and H8'). Signals for H8 and the C4-methyl (100%) and H3 (76%) showed the highest relative intensities within the aglycone. Once again, the glycerol side chain of sialic acid showed strong interactions at H7', H8', and H9'. Within the pyranose ring, H4', H5', and H6' all showed relatively strong contacts with the protein. We observed only a small difference between the H3'(ax) and H3'(eq) signals. Once again, the H3'(eq) signal was the stronger of the two (44% vs. 49%) within Neu5Ac. We have previously proposed that the glycerol side chain of Neu5Ac may be particularly critical for recognition of substrates and inhibitors by NEU3, and these data support that this portion of both substrates is an important enzyme-substrate contact.³¹

5.2.6 MD simulations of NEU3–substrate interactions

To develop molecular models of the NEU3-substrate complexes, we conducted MD simulations of each substrate bound to a homology model of NEU3.¹⁶ For both **5.2** and **5.4**, we first docked the substrate into the active site, and then prepared for a production run by the addition of explicit water (TIP3P)³², minimization of the solvent, followed by minimization of the entire system. Additionally, the system was equilibrated by gradual heating and then cooling followed by a short dynamic cycle (0.1 ns), during which the system was brought to the production temperature (300^oK). For these simulations, we used AMBER 10³³ with the GLYCAM06 forcefield.³⁴ The resulting complexes were then subjected to a 10 ns MD simulations to convergence at constant temperature and pressure (300 K; 1 atm).

We analyzed the MD run of **5.4** by clustering of the 50,000 frames, which showed that sialic acid residue maintained the expected key interactions throughout (Figure 5.9).

Two residues of the arginine triad (R25 and R340) maintain almost constant contact with the C1' carboxylate, while the third (R245) shows some switching between the carboxylate and the glycerol side chain oxygen O9'. We observed that O4' of Neu5Ac maintained a stable hydrogen bond with R45. Additional contacts between the glycerol side chain and the protein included hydrogen bonds with E113, Y181 and R245. The orientation of the 4-methylumbelliferone aglycone was less conserved, and it was able to form non-polar contacts with the methylene groups of the R49 side chain.

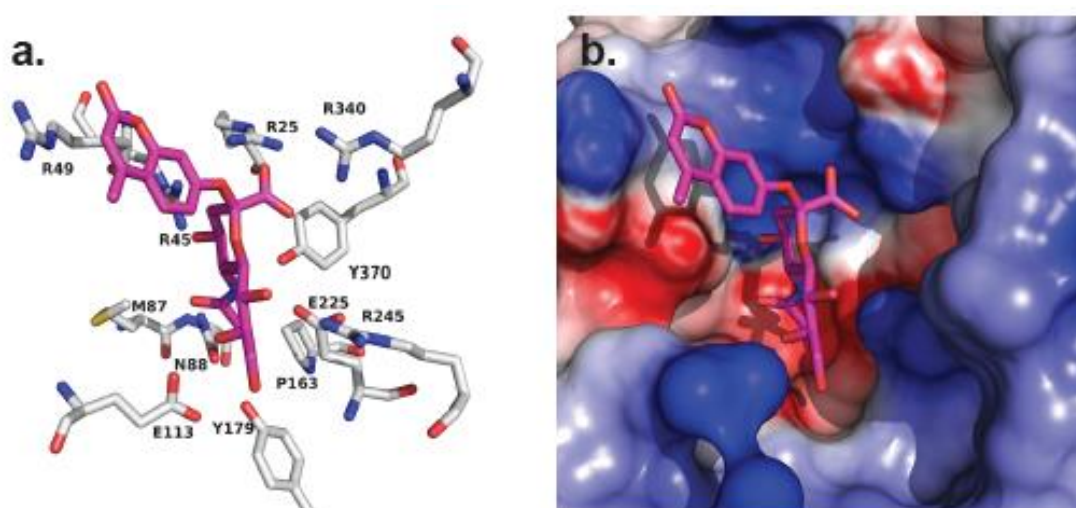


Figure 5.9: Molecular model of 4MU-NANA in the NEU3 active site. a. *Key contacts between the Neu5Ac residue and the protein are maintained. Hydrogen bond contacts are observed between O4 and R45, and between the glycerol side chain O7, O8 and O9 and E113 and Y179. Electrostatic contacts between the arginine triad (R25, R245, R340) and the C1 carboxylate were observed throughout the simulation. Nonpolar contacts between the hydrophobic aglycone and the side chain of R49 are also observed. b.* *An electrostatic potential surface representation of the NEU3 active site with 4MU-NANA in the same pose as shown in a.*

Analysis of MD simulation on the NEU3–**5.2** complex showed similar results to the model with **5.4**, but provided additional information on the interaction of the Glc and Gal residues of the oligosaccharide (Figure 5.10). The Neu5Ac residue exhibited the same contacts in the active site observed for **5.4**. The C1''' carboxylate of **5.2** formed salt bridges with R25 (average distance of 2.97 Å). Additional salt bridges were formed between the C1''' carboxylate and R340 (average distance of 2.90 Å). The third member of the arginine triad, R245, was far from the carboxylate group, with an average distance of 6.54 Å. The average distance between the nucleophile oxygen of Y370 and C2''' of Neu5Ac was 5.33 Å. Meanwhile, the E225 general base maintained a less than 3 Å distance to the nucleophilic tyrosine OH. The position of the octyl side chain exhibited switching between two different positions on the enzyme.

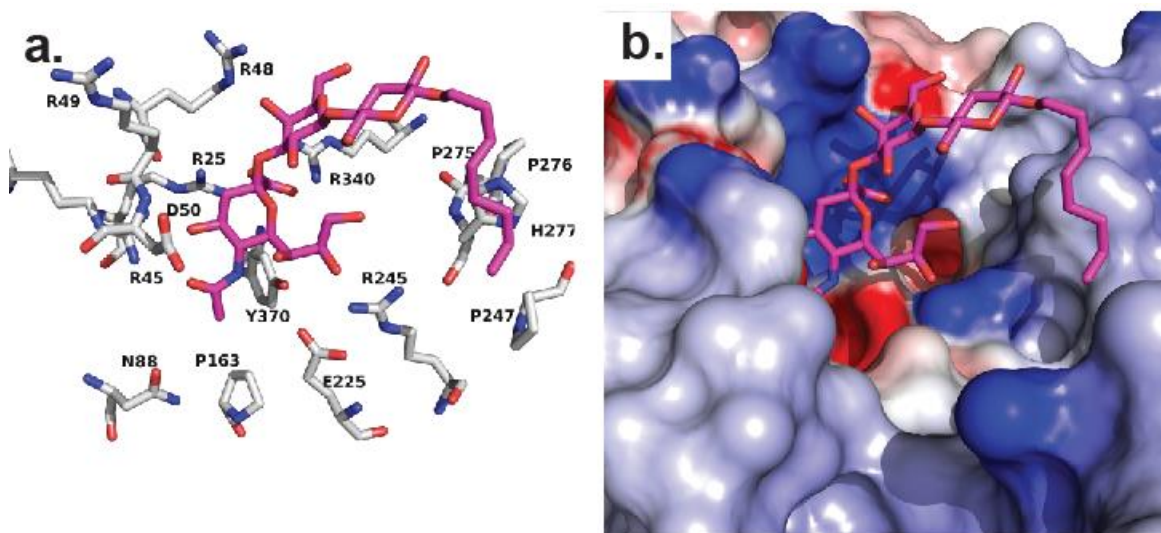


Figure 5.10: Molecular model of octyl-GM3 in the NEU3 active site. *a.* Interaction between octyl-GM3 and NEU3. The more predominant position of the octyl side chain is shown in the hydrophobic pocket composed of V222, V224, P198 and P247 (some residues are omitted for clarity). The O4'' of the Gal residue shows a H-bond contact

with R48 found on the D50 loop. b. An electrostatic potential surface representation of NEU3 with octyl-GM3 bound in the active site in the same pose as shown in a.

The aglycone of the **5.2** spent most of its time in a hydrophobic pocket formed by V222, V224, P198, P247 and the backbone portions of H277 and R197.¹⁶ The octyl group was also found to occupy a second hydrophobic patch composed of I117, V118 and the backbone of R114 (c.a. 20% of the MD run; Figure 5.11). Examination of different clusters showed that the positions of the Neu5Ac and Gal residues were conserved throughout the run; while the Glc residue and the aglycone were more variable.

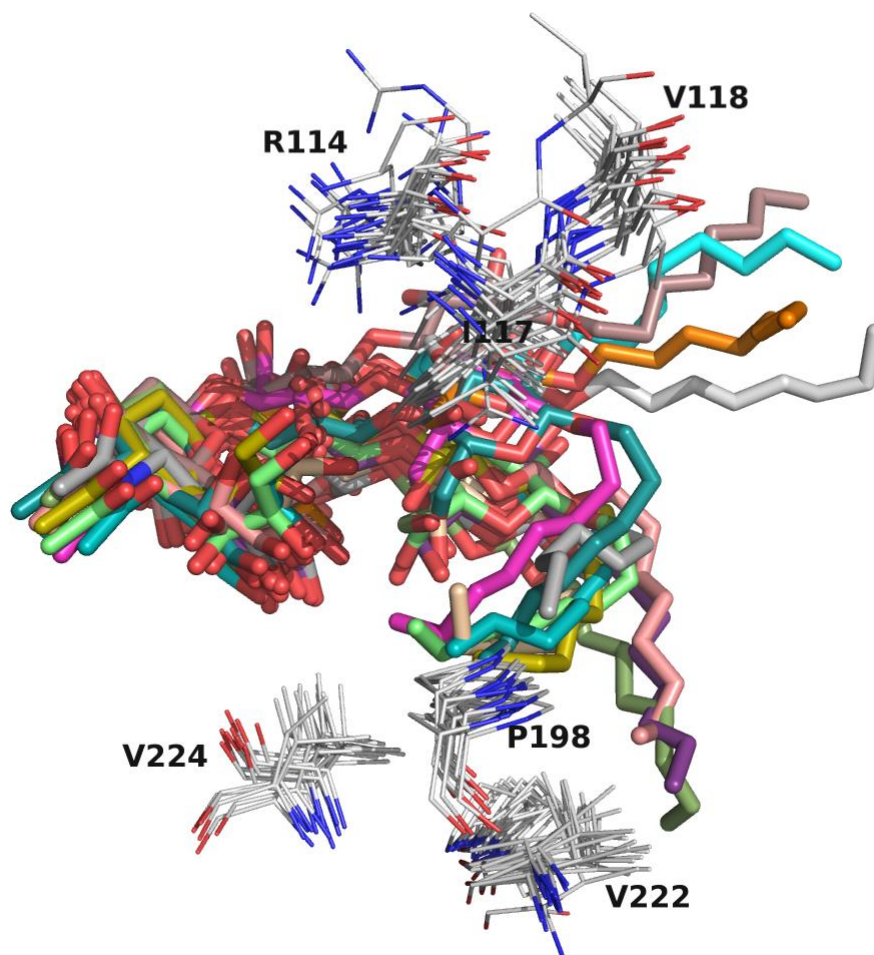


Figure 5.11: Observed conformations of octyl-GM3 aglycone by MD. Trajectories of the MD run were analyzed to find 20 clusters. The sialic acid and galactose residues have significant overlap between clusters, while the glucose residue and aglycone are more dispersed. The hydrophobic aglycone occupies two sites, composed of amino acids V222, V224, P198 and P247 or another containing I117, V118 and the R114.

To compare the results of our STD NMR studies with those of the MD simulations we analyzed the MD trajectories to determine average distances between specific ligand sites and H atoms of the protein. The MD trajectory was analyzed to identify twenty clusters that were then examined to choose potential close interactions between protons of the substrate and enzyme.³⁵ These distances were monitored over all frames of the MD simulation. The three shortest distances between a ligand site and potential close contacts were selected from each frame, and the resulting distances were averaged over the whole run. These average distances are summarized in Table **5.1** for octyl-GM3, and Table **5.2** for 4MU-NANA. Note that these distances are not intended to represent an absolute measure, but they were used as a relative measure of how much contact could be expected for each H atom of the substrate with the enzyme. We then used these average values to compare relative STD signals to the relative MD distances predicted from simulation.

Generally, the results of the STD and MD show partial, but not complete agreement. In the case of the NEU3–**5.4** complex, we find that both methods identify the C4-methyl and H8 of the aglycone to have close contact to the enzyme. From MD simulations, the Neu5Ac residue of **5.4** was predicted to have its closest contacts to the enzyme at H3'(eq), H6', and H8'. However, STD NMR identified H4', H5', and H8' to have the strongest signals. All protons of the Neu5Ac residue show contact to the protein with moderate to strong signals.

For the NEU3–**5.2** complex, we find that the aglycone is found to have close contact to the protein in both methods. From MD simulations, the Glc and Gal residues were predicted to have their closest contacts at H2', H4', H5', and H2''. Although all of

these residues show significant STD NMR signal, the relative signal strength did not track directly with these predicted distances. Additional comparison of the Glc and Gal residues, when treated by A- or B-faces, shows agreement between the methods (see Table SI3). In the case of the Neu5Ac residue of the NEU3–**5.2** complex H3^{'''}, H4^{'''}, H6^{'''}, H7^{'''}, H8^{'''} and the N5Ac group are all expected to be in close contact with the enzyme. Although all these signals show enhancement by STD NMR, the strongest of these is H8^{'''}. Certain relative features of the STD NMR data are predicted well by the MD simulations. For example the order of the Neu5Ac H3^{'''} (ax) versus H3^{'''} (eq) signals is in agreement for both methods.

5.3 Discussion

STD NMR is a valuable technique for the study of carbohydrate-protein interactions.^{23, 24} Here, we have mapped the interactions of NEU3 with two known substrates by STD NMR: 4MU-NANA (**5.4**) and octyl-GM3 (**5.2**). Currently, the only reported crystal structures for the human neuraminidase family are for NEU2.^{36, 37} The hydrophobic nature of the membrane-associated NEU3 likely increases the difficulty in obtaining a crystal structure of the protein. In the absence crystallographic data, homology models of the enzyme, based on the crystal structure of NEU2, have been developed.¹⁶ However, experimental validation of these models has, until now, been restricted to site-directed mutagenesis of the enzyme.¹⁶ In this work, we have used the results of STD NMR to interrogate the NEU3 homology model. We find that, while certain essential features of the model are well supported, some aspects of ligand binding are not clearly predicted by the model. We discuss potential reasons for this disagreement below.

We considered several factors that could interfere with the reliability of the STD NMR results. We employed an inactive mutant of NEU3, NEU3(Y370F), to avoid degradation of the substrate during acquisition of the NMR data. Additionally, we used an analog of GM3 (**5.2**) that significantly reduced the formation of micelle artifacts in the STD NMR data, allowing us to make observations using the aliphatic region of the spectrum. It is interesting to note that STD NMR may be useful for the observation of lipid-lipid interactions within a micellar structure based on our findings with GM3 (Figure 5.3). Indeed, STD NMR has been used previously to study lipid-peptide interactions.^{38, 39} Another potential source of variability in the epitope maps determined here is the lack of stability of the enzyme. The protein does lose activity over time, and as a result the sample may contain some portion of unfolded protein. In previous experiments we have found that the enzyme can maintain activity for approximately three hours at room temperature, and our experiments were conducted within this window. However, we cannot rule out the possibility that a portion of unfolded protein may also interact with the substrate, which could result in a biased epitope map.

Both epitope maps of **5.2** and **5.4** support the involvement of the substrate aglycone in binding to NEU3. We previously proposed a model for recognition of glycolipids by NEU3 based on relative hydrolysis rates of GM3 analogs.¹⁴ The model proposed that at least two sites were required for recognition by the enzyme, including the Neu5Ac residue and the hydrophobic aglycon. Our results here provide the first direct evidence that the aglycone interacts with the protein. Additionally, the epitope maps show significant binding for the Neu5Ac residue of each substrate. The most notable contacts appear to be at H5, H8, and H9 of Neu5Ac. The interaction of the Neu5Ac

glycerol side chain has previously been proposed to be important for human NEU recognition based on inhibitor studies.³¹ The epitope map of octyl-GM3 also suggests that Glc provides an additional point of contact between the ligand and the enzyme. In particular, the reducing end of the sugar (H1' and H2') show some of the strongest STD signals within the entire substrate.

Molecular modeling can be used to interpret STD NMR mapping results. Previous studies have analyzed STD NMR using a range of methods.⁴⁰⁻⁴² Here we compared an averaged set of distances for each H atom obtained from MD simulations of the relevant complex. The close contacts between the aglycone of octyl-GM3 with two hydrophobic patches on the enzyme are consistent with the strong STD effect seen for this portion of the ligand. We identified two hydrophobic patches on NEU3 within the model which may be advantageous for complexation of diacyl sphingolipids in the native substrates. The MD results for both substrates indicate consistent interactions between the protein and the Neu5Ac residue, including the C1-carboxylate interactions with the arginine triad and contacts between the glycerol side chain (H6, H7, and H8 positions of Neu5Ac).

In comparing the STD NMR and MD results for the NEU3–**5.2** complex, we were struck by the apparent disagreement found for the Glc and Gal residues. The STD results give little differentiation between sites on these two residues. With the exception of H1' and H2' of Glc, the STD signal of these residues covers a very small range (39-50%) when compared to Neu5Ac (10-73%). Additionally, we expected to observe evidence of facial selectivity in the Glc and Gal residues based on the predicted binding mode of the ligand (Figure 5.10).¹⁶ Closer examination of the data for the A- versus B-faces of Glc and Gal does show general agreement between MD and STD NMR (Table 5.3; Figure 5.6

and Figure 5.8). However, the degree of difference between individual signals is still small when compared to that of Neu5Ac. We speculate that this finding may indicate a dynamic mode of binding for the lactoside portion of the substrate which tempers the expected differences in this portion of the epitope as observed by STD NMR.

Table 5.3: Facial recognition of lactoside residues by STD NMR and MD.

Site (H atom)	residue face	STD NMR signal*	MD (average distance)*	STD NMR signal**		MD (average distance)**	
				Avg A face	Avg B face	Avg A face	Avg B face
Glc (H1')	B	100	6.7	67	48	6.3	6.8
Glc (H2')	A	83	6.5				
Glc (H3')	B	46	7.3				
Glc (H4')	A	50	6.0				
Glc (H5')	B	50	6.4				
Glc (H6')	na	49	7.8				
Gal (H1'')	B	42	7.8	50	42	6.4	8.2
Gal (H2'')	A	50	6.4				
Gal (H3'')	B	39	9.2				
Gal (H4'')	na	39	7.7				
Gal (H5'')	B	46	7.7				
Gal (H6'')	na	41	4.1				

* Data from Table S11.

** Averages for either the STD NMR or MD data for signals on the indicated face of the residue. Note that STD NMR should be higher for close contacts, and the average distance by MD should be lower.

Although we concluded that our binding model was in general agreement with the STD NMR data, we also considered that potential shortcomings of the homology model may contribute to our observations. Previous structural studies of NEU2 have found that

substrate recognition by the enzyme is dynamic and depends on rearrangement of a flexible loop in the protein (the D46 loop in NEU2).³⁶ The homologous loop in NEU3 contains D50, a site predicted to be in contact with the substrate and mutation of which greatly reduces enzyme activity.¹⁶ The D50 loop of NEU3 shows high homology to the sequence of NEU2 therefore, we expect that the position of the loop in our model is reliable. However, we also note that several loops on the same face of the model have much lower homology to NEU2, and some of these may be close enough to influence substrate binding directly. We identify three candidate loops with low homology to NEU2: Q16-I22; Y182-H199; and C388-C394. Due to the low homology of these regions of the protein with the NEU2 sequence, their conformations may be suspect (see Figure 5.12). Additional contacts to NEU3 through one of these loops could result in a different predicted epitope map for the ligand in MD simulations. Future experimental work is planned to examine the role of these loops through site directed mutagenesis of the protein.

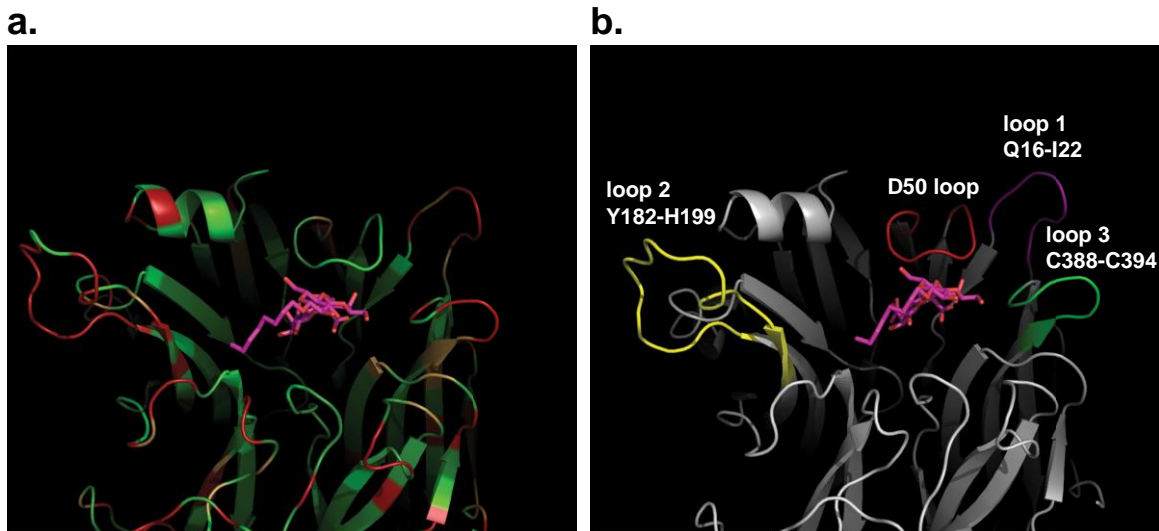


Figure 5.12: Homology map of the NEU3 model. *The homology model of NEU3 is shown (a) with residues homologous to NEU2 shown in green. Residues shown in red indicate a gap in the homology, and residues in orange indicate low homology. (b) Specific regions discussed in the text are highlighted for clarity. Loop 2 is the largest segment of low homology, and may adopt a different conformation in the ordered protein. For an alignment of the NEU2 and NEU3 sequences, see Albohy et al.¹⁶*

Despite the potential shortcomings of the NEU3 homology model, it is worthwhile to mention that the model is still predictive for some aspects of enzyme specificity. For example, the *O*4 of Gal forms a hydrogen bond with R48, which may help to order the D50 loop for catalysis.¹⁶ Additionally, we note that the *O*4'' position of Gal is the site of GlcNAc branching in glycolipid substrates such as GM1 and GM2. These branched glycolipids are known to be poor substrates for the enzyme, and this finding is consistent with blocking of the optimal conformation of the D50 loop of NEU3 and reducing the substrate activity of GM1 and GM2 (Figure 5.10).

5.4 Conclusions

We have used STD NMR to map the epitope of two substrates for NEU3. Additionally, we used molecular dynamics to test the predictions of a homology model of the protein as compared to the epitope maps. Our results confirm the importance of the Neu5Ac residue for recognition by NEU3, as well as provide direct evidence of recognition of the hydrophobic aglycone by the enzyme. Although there is some disagreement between our homology model and the STD NMR data, this is primarily in matter of degree. Our models provide general predictions that agree with the STD NMR data including the facial interactions of both Glc and Gal residues, confirmation of the sites of Neu5Ac and lipid aglycone interactions with the protein, and predictions of substrate specificity. We conclude that the homology model of NEU3 may require some refinement of the conformation of protein loops that lack homology to the known structure of NEU2.

5.5 Methods

5.5.1 Synthetic ligands

GM3 (**5.1**) was purchased from Avanti Polar Lipids Inc. Compounds **5.2**, **5.3** and **5.4** were synthesized as reported earlier.^{14, 43}

5.5.2 Protein expression

Protein was isolated by culturing *E. coli* TB1 cells containing plasmids pMBP-Neu3-Y370F (for expression of the NEU3 inactive mutant) or pMal (for expression of the MBP protein alone) in LB medium containing ampicillin ($100 \mu\text{g mL}^{-1}$) to OD_{600} of 0.5 at

37 °C. Production of the fusion protein was induced by addition of IPTG to a final concentration of 0.3 mM at 20 °C. Cells were harvested by centrifugation after growing overnight from induction. The pellet was resuspended (50 mL L⁻¹ of medium) in resuspension buffer (20 mM morpholinopropane sulfonic acid (MOPS), pH 7.2, 200 mM NaCl, 1 mM EDTA and 0.1% Triton X-100) supplemented with one complete protease inhibitor tablet (Roche). The lysate was passed through a cell disruptor once at 20,000 psi and then immediately pelleted by centrifugation at 105,000 × g for 60 min at 4 °C. The supernatant was loaded onto an amylose column (New England Biolabs) equilibrated with 20 mM MOPS buffer (200 mM NaCl, pH 7.2). MBP-fusion protein was eluted with running buffer containing 10% glycerol (v/v) and 10 mM maltose. The chromatogram showed one single peak for the pure protein and it has one single band on SDS-PAGE at molecular weight of around 93 kDa (Figure 5.13). The final protein concentration was determined by measuring UV absorbance at 280 nm. The NEU3(Y370F) mutant was previously found to show reduced activity as compared to wild type protein.¹⁶

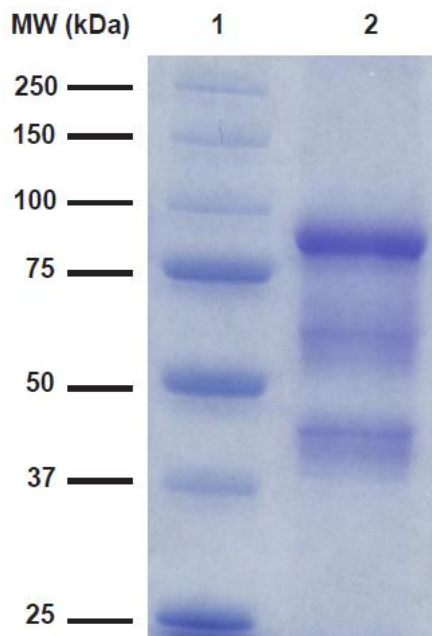


Figure 5.13: SDS-PAGE Analysis of MBP-NEU3(Y370F). *SDS-PAGE of the purified MBP-NEU3(Y370F) dead mutant. The purified protein appears as a major band at 93 kDa in the second lane. Some minor proteolytic fragments are present at ~60 and ~40 kDa. Lane 1 is the marker lane, with standards indicated at left.*

5.5.3 NMR sample preparation

All samples were prepared in the NMR buffer (40 mM sodium phosphate buffer, pH 5.65 in D₂O). The protein sample was dialyzed to the sample buffer and concentrated using an Amicon spin column (MWCO 30 kDa). The final protein concentration was adjusted to 25 μ M and the substrate (**5.2** or **5.4**) was added to a final concentration of 2.5 mM (100 times the protein concentration). The sample was added to either 5 or 3 mm NMR tubes. All the components (buffer, enzyme, and substrate) were subjected to STD experiments separately to check for interference. To confirm that the substrates bind to

NEU3 and not MBP, **5.2** was tested with the MBP protein. No STD signal was observed under these conditions, ruling out MBP-substrate interactions interfering with the measurement. In addition, **5.3** was tested with the NEU3(Y370F) protein and showed STD signal only at the octyl side chain, which we attribute to weak, but specific binding as the protein alone and the substrate alone show no signal (Figure 5.3).

5.5.4 NMR experiments

Spectra were recorded on a Varian 700 MHz spectrometer equipped with cold probe. The STD NMR spectra were collected with 3072 scans. During each scan the protein was saturated with a series of 20 GAUSSIAN-shaped pulses (50 ms, 1 ms delay between pulses), for a total saturation time of 1.02 second.²⁰ Selective saturation of protein resonances was done at -0.5 ppm with **5.2** and **5.4** to excite the protein but not the substrate. Several on-resonance values were tested for **5.1** but none were able to excite the protein without the substrate (on-resonance at -0.25 ppm is shown in Figure 5.3d). The off-resonance frequency used was 27 ppm. A WATERGATE^{44, 45} was used to suppress the water signal in the STD spectrum and the FID was collected for 2.0 seconds afterwards.

5.5.5 Molecular dynamics simulations

The previously reported GM3-NEU3 model was used as the basis for our simulations.¹⁶ Since STD experiments were performed with **5.2**, we replaced GM3 with this substrate in the complex. Previously reported partial charges for the octyl side chain were used,⁴⁶ and the sugar residue names were fixed according to GLYCAM notations.⁴⁷ The LEaP module⁴⁸ in AMBER tools was used to generate AMBER topology and

coordinate files after the solvation and neutralization of the complex. Water (TIP3P) was added in an octahedral box of 7 Å around the complex with 3 Na⁺ ions added.³² MD simulations were done using the AMBER 10 package.³³ The AMBER ff99SB force field⁴⁹ was used for amino acids, and GLYCAM 06 was used to treat the carbohydrates.³⁴ The protocol we used was guided by an earlier report.⁵⁰

Before the production run of the MD simulation, the system was minimized and equilibrated. Water molecules were minimized first while keeping the substrate constrained. This was followed by a minimization of the entire system. In both minimization steps, a steepest descent energy minimization was carried out for 50 cycles followed by 4950 cycles of conjugate gradient minimization. A total of 600 ps of annealing was used during which the temperature was increased every 50 ps from 5 to 300 K and then cooled back from 300 to 5 K. This was then followed by a short equilibration run of 200 ps during which the temperature of the systems was gradually increased from 5 K to 300 K over 150 ps, and then kept constant for 50 ps. The production simulation (10 ns) was performed under constant pressure and temperature (NPT) conditions with periodic boundaries. The temperature was kept at 300 K and the pressure at 1 atm to simulate the experimental conditions. The particle mesh Ewald (PME) method was used to control long range electrostatic interactions and the SHAKE⁵¹ algorithm was used to constrain bond lengths involving hydrogen to their equilibration values. For analysis purposes, 50,000 frames of the MD trajectory were collected during the run and clustered into 20 clusters. Close contacts were chosen from the clusters and the distances were monitored during the whole MD run (10 ns) and the three shortest distances in each frame were selected, and the average of these three was reported.

5.6 References

1. Miyagi, T.; Yamaguchi, K., Mammalian sialidases: Physiological and pathological roles in cellular functions. *Glycobiology* **2012**, *22* (7), 880-896.
2. Zanchetti, G.; Colombi, P.; Manzoni, M.; Anastasia, L.; Caimi, L.; Borsani, G.; Venerando, B.; Tettamanti, G.; Preti, A.; Monti, E.; Bresciani, R., Sialidase NEU3 is a peripheral membrane protein localized on the cell surface and in endosomal structures. *Biochemical Journal* **2007**, *408*, 211-219.
3. Wang, J. F.; Wu, G. S.; Miyagi, T.; Lu, Z. H.; Ledeen, R. W., Sialidase occurs in both membranes of the nuclear envelope and hydrolyzes endogenous GD1a. *Journal of Neurochemistry* **2009**, *111* (2), 547-554.
4. Valaperta, R.; Chigorno, V.; Basso, L.; Prinetti, A.; Bresciani, R.; Preti, A.; Miyagi, T.; Sonnino, S., Plasma membrane production of ceramide from ganglioside GM3 in human fibroblasts. *FASEB Journal* **2006**, *20* (8), 1227-+.
5. Papini, N.; Anastasia, L.; Tringali, C.; Croci, G.; Bresciani, R.; Yamaguchi, K.; Miyagi, T.; Preti, A.; Prinetti, A.; Prioni, S.; Sonnino, S.; Tettamanti, G.; Venerando, B.; Monti, E., The Plasma Membrane-associated Sialidase MmNEU3 Modifies the Ganglioside Pattern of Adjacent Cells Supporting Its Involvement in Cell-to-Cell Interactions. *Journal of Biological Chemistry* **2004**, *279* (17), 16989-16995.
6. Miyagi, T.; Wada, T.; Moriya, S.; Ueno, S.; Kato, K.; Yamaguchi, K., A crucial role of plasma membrane-associated sialidase (NEU3) in the survival of human cancer cells. *Glycobiology* **2004**, *14* (11), 436.
7. Miyagi, T.; Wada, T.; Yamaguchi, K.; Hata, K., Sialidase and malignancy: A minireview. *Glycoconjugate Journal* **2003**, *20* (3), 189-198.

8. Wada, T.; Hata, K.; Yamaguchi, K.; Shiozaki, K.; Koseki, K.; Moriya, S.; Miyagi, T., A crucial role of plasma membrane-associated sialidase in the survival of human cancer cells. *Oncogene* **2007**, *26* (17), 2483-2490.
9. Monti, E.; Preti, A.; Venerando, B.; Borsani, G., Recent development in mammalian sialidase molecular biology. *Neurochemical Research* **2002**, *27* (7-8), 649-663.
10. Kopitz, J.; vonReitzenstein, C.; Sinz, K.; Cantz, M., Selective ganglioside desialylation in the plasma membrane of human neuroblastoma cells (vol 6, pg 367, 1996). *Glycobiology* **1996**, *6* (4), 378-378.
11. Ha, K. T.; Lee, Y. C.; Cho, S. H.; Kim, J. K.; Kim, C. H., Molecular characterization of membrane type and ganglioside-specific sialidase (Neu3) expressed in E-coli. *Molecules and Cells* **2004**, *17* (2), 267-273.
12. Li, S. C.; Li, Y. T.; Moriya, S.; Miyagi, T., Degradation of G(M1) and G(M2) by mammalian sialidases. *Biochemical Journal* **2001**, *360*, 233-237.
13. Oehler, C.; Kopitz, J.; Cantz, M., Substrate specificity and inhibitor studies of a membrane-bound ganglioside sialidase isolated from human brain tissue. *Biological Chemistry* **2002**, *383* (11), 1735-1742.
14. Sandbhor, M. S.; Soya, N.; Albohy, A.; Zheng, R. B.; Cartmell, J.; Bundle, D. R.; Klassen, J. S.; Cairo, C. W., Substrate recognition of the membrane-associated sialidase NEU3 requires a hydrophobic aglycone. *Biochemistry* **2011**, *50* (32), 6753-6762.
15. Magesh, S.; Suzuki, T.; Miyagi, T.; Ishida, H.; Kiso, M., Homology modeling of human sialidase enzymes NEU1, NEU3 and NEU4 based on the crystal structure of

NEU2: Hints for the design of selective NEU3 inhibitors. *Journal of Molecular Graphics & Modelling* **2006**, *25* (2), 196-207.

16. Albohy, A.; Li, M. D.; Zheng, R. B.; Zou, C. X.; Cairo, C. W., Insight into substrate recognition and catalysis by the human neuraminidase 3 (NEU3) through molecular modeling and site-directed mutagenesis. *Glycobiology* **2010**, *20* (9), 1127-1138.

17. Albohy, A.; Zhang, Y.; Smutova, V.; Pshezhetsky, A. V.; Cairo, C. W., Identification of selective nanomolar inhibitors of the human neuraminidase, NEU4. *Acs Medicinal Chemistry Letters* **2013**, *4* (6), 532-537.

18. Zou, Y.; Albohy, A.; Sandbhor, M.; Cairo, C. W., Inhibition of human neuraminidase 3 (NEU3) by C9-triazole derivatives of 2,3-didehydro-N-acetylneuraminic acid. *Bioorganic & Medicinal Chemistry Letters* **2010**, *20* (24), 7529-7533.

19. Mayer, M.; Meyer, B., Characterization of ligand binding by saturation transfer difference NMR spectroscopy. *Angewandte Chemie-International Edition* **1999**, *38* (12), 1784-1788.

20. Mayer, M.; Meyer, B., Group epitope mapping by saturation transfer difference NMR to identify segments of a ligand in direct contact with a protein receptor. *Journal of the American Chemical Society* **2001**, *123* (25), 6108-6117.

21. Mohebbi, S.; Falcon-Perez, J. M.; Gonzalez, E.; Millet, O.; Mato, J. M.; Kobarfard, F., Synthesis, Dihydrofolate Reductase Inhibition, Anti-proliferative Testing, and Saturation Transfer Difference H-1-NMR Study of Some New 2-Substituted-4,6-diaminopyrimidine Derivatives. *Chemical & Pharmaceutical Bulletin* **2012**, *60* (1), 70-78.

22. Viegas, A.; Manso, J.; Corvo, M. C.; Marques, M. M. B.; Cabrita, E. J., Binding of Ibuprofen, Ketorolac, and Diclofenac to COX-1 and COX-2 Studied by Saturation Transfer Difference NMR. *Journal of Medicinal Chemistry* **2011**, *54* (24), 8555-8562.
23. Maggioni, A.; Meier, J.; Routier, F.; Haselhorst, T.; Tiralongo, J., Direct investigation of the Aspergillus GDP-mannose transporter by saturation transfer difference NMR spectroscopy. *Mycoses* **2012**, *55*, 128-128.
24. Plum, M.; Michel, Y.; Wallach, K.; Raiber, T.; Blank, S.; Bantleon, F.; Diethers, A.; Greunke, K.; Braren, I.; Hackl, T.; Meyer, B.; Spillner, E., Close-up of the alpha-Gal epitope as defined by a monoclonal chimeric IgE and human serum using saturation transfer difference nuclear magnetic resonance. *Allergy* **2012**, *67*, 37-37.
25. Haselhorst, T.; Wilson, J. C.; Thomson, R. J.; McAtamney, S.; Menting, J. G.; Coppel, R. L.; von Itzstein, M., Saturation transfer difference (STD) H-1-NMR experiments and in silico docking experiments to probe the binding of N-acetylneuraminic acid and derivatives to Vibrio cholerae sialidase. *Proteins-Structure Function and Bioinformatics* **2004**, *56* (2), 346-353.
26. Sonnino, S.; Cantu, L.; Acquotti, D.; Corti, M.; Tettamanti, G., Aggregation properties of GM3 ganglioside (II3Neu5AcLacCer) in aqueous solutions. *Chemistry and Physics of Lipids* **1990**, *52* (3-4), 231-241.
27. Sonnino, S.; Cantù, L.; Corti, M.; Acquotti, D.; Venerando, B., Aggregative properties of gangliosides in solution. *Chemistry and Physics of Lipids* **1994**, *71* (1), 21-45.
28. Duncan, S. J.; Lewis, R.; Bernstein, M. A.; Sandor, P., Selective excitation of overlapping multiplets; the application of doubly selective and chemical shift filter

experiments to complex NMR spectra. *Magnetic Resonance in Chemistry* **2007**, *45* (4), 283-288.

29. Robinson, P. T.; Pham, T. N.; Uhrin, D., In phase selective excitation of overlapping multiplets by gradient-enhanced chemical shift selective filters. *Journal of Magnetic Resonance* **2004**, *170* (1), 97-103.

30. Palestini, P.; Pitto, M.; Sonnino, S.; Omodeo-Salè, M. F.; Masserini, M., Spontaneous transfer of GM3 ganglioside between vesicles. *Chemistry and Physics of Lipids* **1995**, *77* (2), 253-260.

31. Albohy, A.; Mohan, S.; Zheng, R. X. B.; Pinto, B. M.; Cairo, C. W., Inhibitor selectivity of a new class of oseltamivir analogs against viral neuraminidase over human neuraminidase enzymes. *Bioorganic & Medicinal Chemistry* **2011**, *19* (9), 2817-2822.

32. Jorgensen, W. L.; Chandrasekhar, J.; Madura, J. D.; Impey, R. W.; Klein, M. L., Comparison of simple potential functions for simulating liquid water. *Journal of Chemical Physics* **1983**, *79* (2), 926-935.

33. Case, D. A.; Cheatham, T. E.; Darden, T.; Gohlke, H.; Luo, R.; Merz, K. M.; Onufriev, A.; Simmerling, C.; Wang, B.; Woods, R. J., The Amber biomolecular simulation programs. *Journal of Computational Chemistry* **2005**, *26* (16), 1668-1688.

34. Kirschner, K. N.; Yongye, A. B.; Tschampel, S. M.; Gonzalez-Outeirino, J.; Daniels, C. R.; Foley, B. L.; Woods, R. J., GLYCAM06: A generalizable Biomolecular force field. Carbohydrates. *Journal of Computational Chemistry* **2008**, *29* (4), 622-655.

35. Roe, D. R.; Cheatham, T. E., PTRAJ and CPPTRAJ: Software for Processing and Analysis of Molecular Dynamics Trajectory Data. *Journal of Chemical Theory and Computation* **2013**, *9* (7), 3084-3095.

36. Chavas, L. M. G.; Tringali, C.; Fusi, P.; Venerando, B.; Tettamanti, G.; Kato, R.; Monti, E.; Wakatsuki, S., Crystal structure of the human cytosolic sialidase Neu2 - Evidence for the dynamic nature of substrate recognition. *Journal of Biological Chemistry* **2005**, *280* (1), 469-475.
37. Chavas, L. M. G.; Kato, R.; Suzuki, N.; von Itzstein, M.; Mann, M. C.; Thomson, R. J.; Dyason, J. C.; McKimm-Breschkin, J.; Fusi, P.; Tringali, C.; Venerando, B.; Tettamanti, G.; Monti, E.; Wakatsuki, S., Complexity in Influenza Virus Targeted Drug Design: Interaction with Human Sialidases. *Journal of Medicinal Chemistry* **2010**, *53* (7), 2998-3002.
38. Chatterjee, C.; Majumder, B.; Mukhopadhyay, C., Pulsed-field gradient and saturation transfer difference NMR study of enkephalins in the ganglioside GM1 micelle. *The Journal of Physical Chemistry B* **2004**, *108* (22), 7430-7436.
39. Chatterjee, C.; Mukhopadhyay, C., Interaction and structural study of kinin peptide bradykinin and ganglioside monosialylated 1 micelle. *Biopolymers* **2005**, *78* (4), 197-205.
40. Balazs, Y. S.; Lisitsin, E.; Carmiel, O.; Shoham, G.; Shoham, Y.; Schmidt, A., Identifying critical unrecognized sugar-protein interactions in GH10 xylanases from *Geobacillus stearothermophilus* using STD NMR. *Febs Journal* **2013**, *280* (18), 4652-4665.
41. Guzzi, C.; Munoz-Garcia, J. C.; Enriquez-Navas, P. M.; Rojo, J.; Angulo, J.; Nieto, P. M., NMR studies on carbohydrate interactions with DC-SIGN towards a quantitative STD analysis. *Pure and Applied Chemistry* **2013**, *85* (9), 1771-1787.

42. Krishna, N. R.; Jayalakshmi, V., Quantitative Analysis of STD-NMR Spectra of Reversibly Forming Ligand–Receptor Complexes. In *Bioactive Conformation II*, Peters, T., Ed. Springer Berlin Heidelberg: 2008; Vol. 273, pp 15-54.
43. Zhang, Y.; Albohy, A.; Zou, Y.; Smutova, V.; Pshezhetsky, A. V.; Cairo, C. W., Identification of selective inhibitors for human neuraminidase isoenzymes using C4,C7-modified 2-deoxy-2,3-didehydro-N-acetylneuraminic acid (DANA) analogues. *Journal of Medicinal Chemistry* **2013**, *56* (7), 2948-2958.
44. Piotto, M.; Saudek, V.; Sklenar, V., Gradient-tailored excitation for single-quantum NMR-spectroscopy of aqueous-solutions. *Journal of Biomolecular Nmr* **1992**, *2* (6), 661-665.
45. Sklenar, V.; Piotto, M.; Leppik, R.; Saudek, V., Gradient-tailored water suppression for H-1-N-15 HSQC experiments optimized to retain full sensitivity. *Journal of Magnetic Resonance Series A* **1993**, *102* (2), 241-245.
46. Dupradeau, F.-Y.; Cezard, C.; Lelong, R.; Stanislawiak, E.; Pecher, J.; Delepine, J. C.; Cieplak, P., REDDB: A database for RESP and ESP atomic charges, and force field libraries. *Nucleic Acids Research* **2008**, *36*, D360-D367.
47. Abel, S.; Dupradeau, F. Y.; Raman, E. P.; MacKerell, A. D.; Marchi, M., Molecular simulations of dodecyl-beta-maltoside micelles in water: Influence of the headgroup conformation and force field parameters. *Journal of Physical Chemistry B* **2011**, *115* (3), 487-499.
48. Zhang, W.; Hou, T.; Schafmeister, C.; Ross, W. S.; Case, D. A., LEaP in AmberTools12. *Univeristy of California, San Francisco*. **2012**.

49. Hornak, V.; Abel, R.; Okur, A.; Strockbine, B.; Roitberg, A.; Simmerling, C., Comparison of multiple amber force fields and development of improved protein backbone parameters. *Proteins-Structure Function and Bioinformatics* **2006**, *65* (3), 712-725.
50. Islam, S. M.; Richards, M. R.; Taha, H. A.; Byrns, S. C.; Lowary, T. L.; Roy, P. N., Conformational analysis of oligoarabinofuranosides: Overcoming torsional barriers with umbrella sampling. *Journal of Chemical Theory and Computation* **2011**, *7* (9), 2989-3000.
51. Ryckaert, J. P.; Ciccotti, G.; Berendsen, H. J. C., Numerical-integration of Cartesian equations of motion of a system with constraints - molecular-dynamics of N-alkanes. *Journal of Computational Physics* **1977**, *23* (3), 327-341.

6 Future directions

6.1 Finding potent selective inhibitors for each of the four human sialidases

Selectivity and potency are very important when it comes to a family of enzymes with high homology such as the human sialidases. If we could selectively target one of the four enzymes in the presence of the others, we will have powerful tools to control the physiological and pathological roles played by them. As described in this thesis, only the NEU4 enzyme has a nanomolar selective inhibitor identified.¹ For all the other sialidases the best inhibitors have only micromolar activity. In terms of selectivity, most of the reported inhibitors have not been tested against all the human sialidases.

In order to find new selective and potent inhibitors we need to have a system to test them against the four sialidases and we have to find a source to generate compounds. Regarding the ability to test the inhibitors against the sialidase library, the work described in this thesis has established that a combination of recombinant and purified enzymes can be used to assay new inhibitors. We are hopeful that this strategy will be adopted by other groups in the testing of their compounds to establish selectivity of future compounds.

Most of the reported inhibitors for the human sialidases are related to the inhibitor scaffold of DANA. Although variants of DANA have been exhaustively explored for inhibition of the viral NEU, our studies clearly show that there is additional work to be done to optimize DANA analogs for targeting individual hNEU. We believe that rational design of new inhibitors based on the DANA framework, and structure activity studies like those discussed here will allow for

the design of future inhibitors which target the remaining members of the hNEU family with high potency and selectivity.

It is also possible that new scaffolds could be identified that may allow targeting of hNEU. The only reported non sugar human sialidase inhibitor at this time is the 2-fluorobenzoic acid library reported by Magesh in 2009.² Finding new scaffolds could be done in several ways, among them high throughput screening and molecular modeling.

6.1.1 High throughput screening

High throughput screening (HTS) is a very powerful tool to find new inhibitors against target enzymes. To run HTS for an enzyme, you need to have a library of compounds. These may be a custom library, or a commercially available one. In addition, the target enzyme should be available in sufficient quantity to allow testing against a large library with many replicates. The third requirement for HTS is to have a suitable assay method that can be easily implemented for automation.

The work described in this thesis suggests that HTS of hNEU is both possible and likely to obtain useful data. Our recombinant expression systems for NEU2, NEU3, and NEU4 should be scalable for inhibitor screening. Additionally, we have seen that the 4MU-NANA based assays are reliable and can be used to identify potent compounds.

6.1.2 Modeling as a source of new scaffolds.

Magesh and coworkers tried to approach the problem of finding new scaffolds for human sialidases inhibitors through two different techniques. The first method was through the structural based de novo design using Ludi which is a well-known de novo design program that uses a library of fragments and can be subjected to virtual screening protocols.² Several scaffold were generated but they choose to work on 4-acetamido-5-acylamido-2-fluoro benzoic acids. The other way they used to generate new scaffolds was to use structure-based virtual screening which was used to pick only one compound from 72,766 compounds.³ More careful studies for these enzymes will need to be conducted to find better inhibitor scaffolds. We now have a better model for NEU3 that could be used for virtual screening or structural based de novo design of inhibitors.

6.2 The use of new assays to test the specificity of the four sialidases

The substrate specificity of the human sialidases remains to be clearly defined. The lack of sensitive assay methods and pure enzymes has been a limiting factor for these types of experiments. The specificity of the human sialidases was studied before using TLC which has problems of low sensitivity. In the course of our work, we have reported a new mass spectrometric assay⁴ and a modified fluorescence assay using malononitrile that could follow the release of sialic acid from glycoconjugates.¹ These assays could be used to answer several

important questions about human sialidase enzyme specificity such as relative hydrolysis rates of different sphingolipids.

6.3 Follow up on the NEU4 selective nanomolar inhibitor

In chapter 3 we reported the design and evaluation of a potent selective nanomolar inhibitor against NEU4.¹ These results require follow up studies which includes testing this compound *in vitro* and *in vivo* to find if this compound will affect cancer cell growth and motility, or other proposed functions of NEU4. This could be done on the level of cell line and then on experimental animals. A library of derivatives could also be synthesized and tested as alternatives to our compound with more potency and selectivity or even better pharmacokinetic properties such as absorption, distribution metabolism and elimination.

6.4 Improved homology models for NEU3 and NEU4

Modeling of our compounds against NEU2, NEU3 and NEU4 was reported in this thesis. Among the mentioned enzymes, only NEU2 was crystalized. For the purpose of our modeling we used homology models for NEU3 and NEU4 that were build based on the NEU2 crystal structure as a template. Because the homology between NEU2 from one side and NEU3 and NEU4 from the other side is around 40%, the quality of these models may still require refinement. We believe that our models provide good representations of the active site residues where there is higher homology to NEU2. On the other hand, as we go far from the active site the quality of the model likely decreases. This was clear in the octyl GM3 complex with NEU3 reported in chapter 5 with sialic acid STD

results are more correlated to the modeling results. This agreement decreases as we go far from sialic acid. Focused modelling of some of the important loops such as the D50 loop in NEU3 may be critical for understanding the structural basis of NEU3 substrate selectivity.

6.5 References

1. Albohy, A.; Zhang, Y.; Smutova, V.; Pshezhetsky, A. V.; Cairo, C. W., Identification of selective nanomolar inhibitors of the human neuraminidase, NEU4. *Acs Medicinal Chemistry Letters* **2013**, *4* (6), 532-537.
2. Magesh, S.; Savita, V.; Moriya, S.; Suzuki, T.; Miyagi, T.; Ishida, H.; Kiso, M., Human sialidase inhibitors: Design, synthesis, and biological evaluation of 4-acetamido-5-acylamido-2-fluoro benzoic acids. *Bioorganic & Medicinal Chemistry* **2009**, *17* (13), 4595-4603.
3. Magesh, S.; Moriya, S.; Suzuki, T.; Miyagi, T.; Ishida, H.; Kiso, M., Use of structure-based virtual screening in the investigation of novel human sialidase inhibitors. *Medicinal Chemistry Research* **2010**, *19* (9), 1273-1286.
4. Sandbhor, M. S.; Soya, N.; Albohy, A.; Zheng, R. B.; Cartmell, J.; Bundle, D. R.; Klassen, J. S.; Cairo, C. W., Substrate Recognition of the Membrane-Associated Sialidase NEU3 Requires a Hydrophobic Aglycone. *Biochemistry* **2011**, *50* (32), 6753-6762.

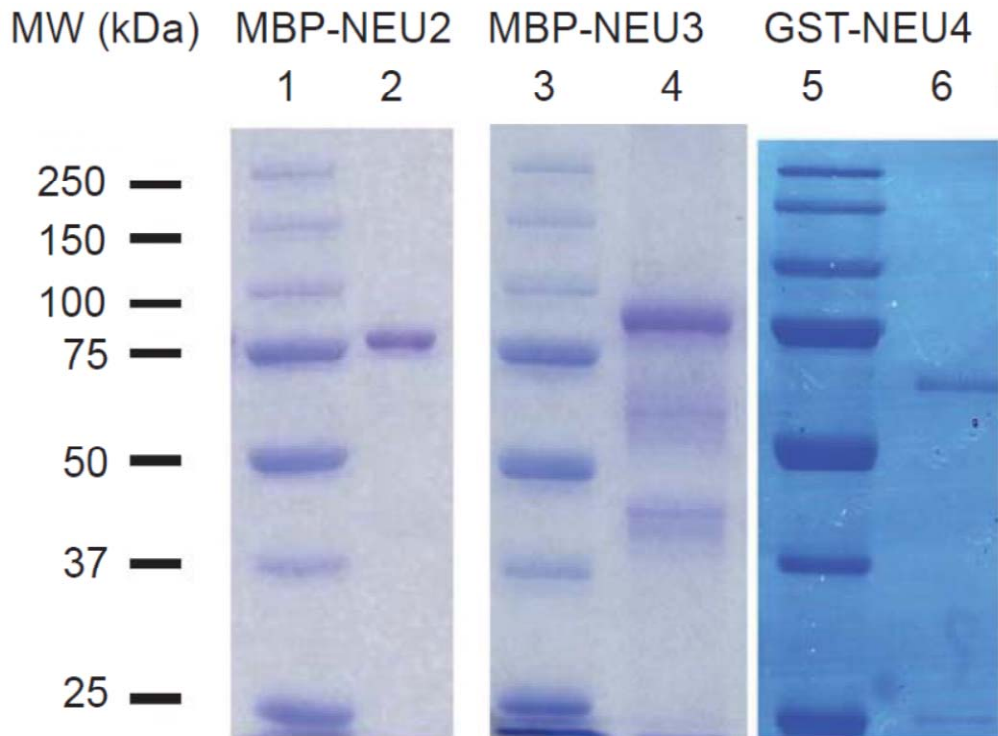
Appendix¹

¹ Portions of the appendix have been published in the following citations: Albohy, A.; Li, M. D.; Zheng, R. B.; Zou, C.; Cairo, C. W., Insight into substrate recognition and catalysis by the human neuraminidase 3 (NEU3) through molecular modeling and site-directed mutagenesis. *Glycobiology* **2010**, *20* (9), 1127-1138, Albohy, A.; Zhang, Y.; Smutova, V.; Pshezhetsky, A. V.; Cairo, C. W., Identification of Selective Nanomolar Inhibitors of the Human Neuraminidase, NEU4. *ACS Med Chem Lett* **2013**, *4* (6), 532-537. and Zou, Y.; Albohy, A.; Sandbhor, M.; Cairo, C. W., Inhibition of human neuraminidase 3 (NEU3) by C9-triazole derivatives of 2,3-didehydro-N-acetyl-neuraminic acid. *Bioorganic & Medicinal Chemistry Letters* **2010**, *20* (24), 7529-7533, Zhang, Y.; Albohy, A.; Zou, Y.; Smutova, V.; Pshezhetsky, A. V.; Cairo, C. W., Identification of Selective Inhibitors for Human Neuraminidase Isoenzymes Using C4,C7-Modified 2-Deoxy-2,3-didehydro-N-acetylneuraminic Acid (DANA) Analogues. *J Med Chem* **2013**, *56* (7), 2948-2958.

A.1 Supporting data for Chapter 1

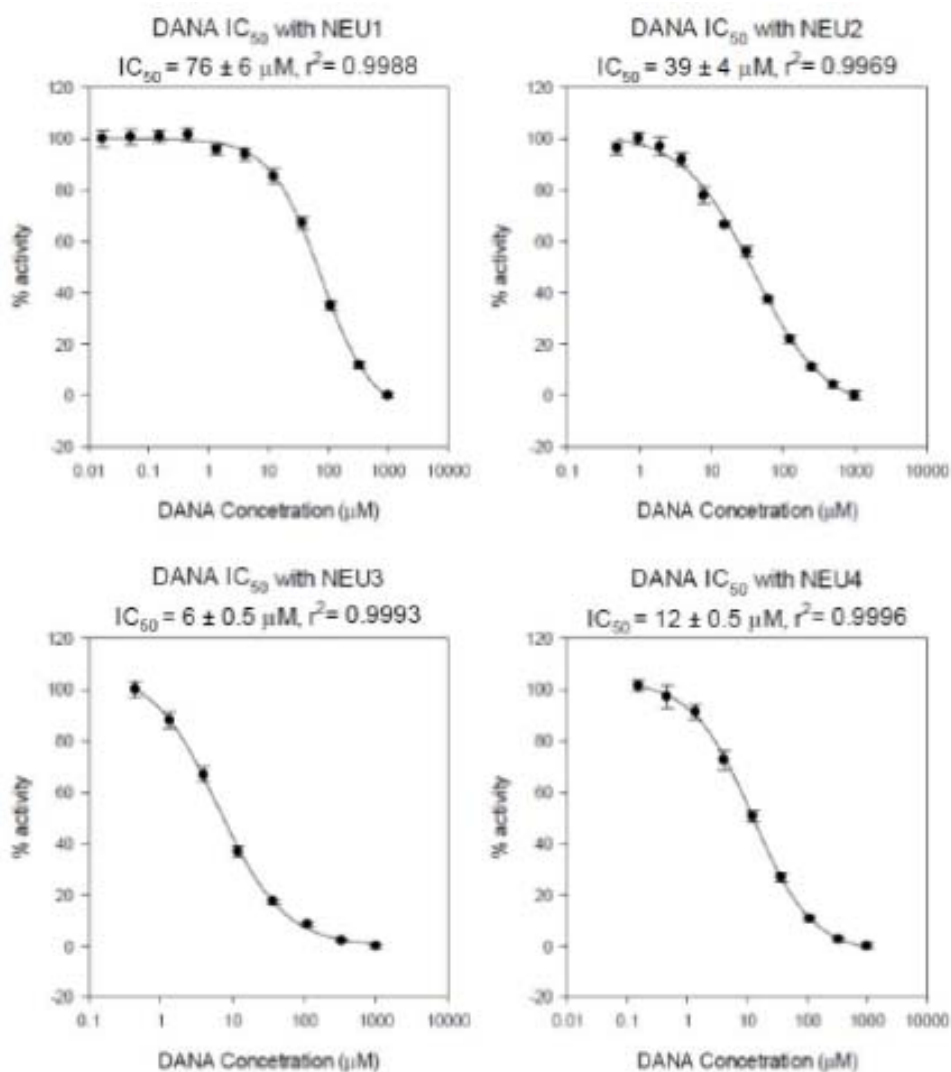
A.1.1 Purification of human sialidase enzymes

Analysis of purified sialidase samples was performed using 10% SDS-PAGE. Each lane was loaded with a 10 μ L sample of protein ($\sim 10 \mu$ g) separated on constant voltage (200 V) for about 40 min. Coomassie stain was used to visualize protein bands. Lanes 1, 3 and 5 contain markers (MW 250, 150, 100, 75, 50, 37, 25 kDa). Lane 2, MBP-NEU2 (MW = 83 kDa). Lane 4, MBP-NEU3 (MW = 92 kDa) Lane 6, GST-NEU4 (MW = 72 kDa).



A.1.2 Inhibition of human neuraminidase isoforms by DANA

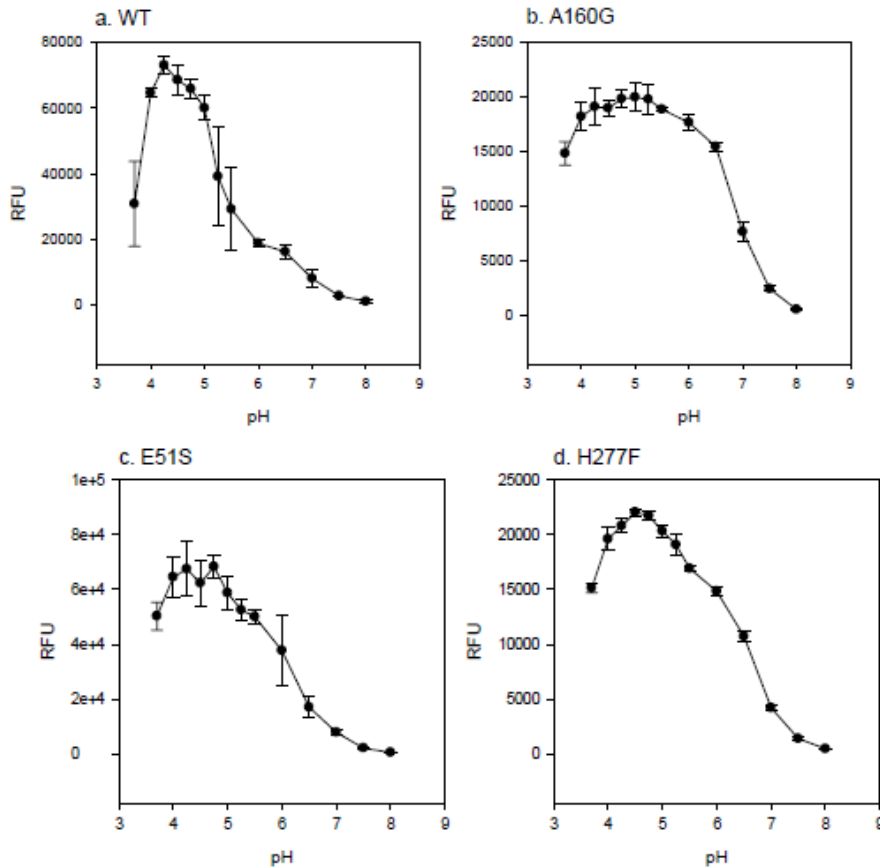
Enzyme assays were performed as described above. Measurements were done at the optimum pH for each enzyme (4.5 for NEU1, NEU3 and NEU4; 5.5 for NEU2) and values were normalized to maximum enzyme activity. DANA is a non-selective micromolar inhibitor of all human sialidase isoforms, with IC₅₀ values ranging from 76 μ M with NEU1 to 6 μ M with NEU3.

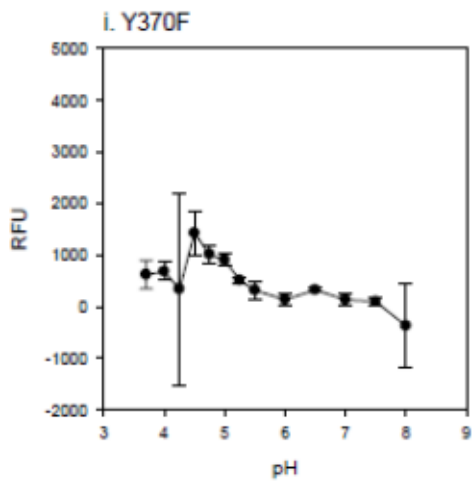
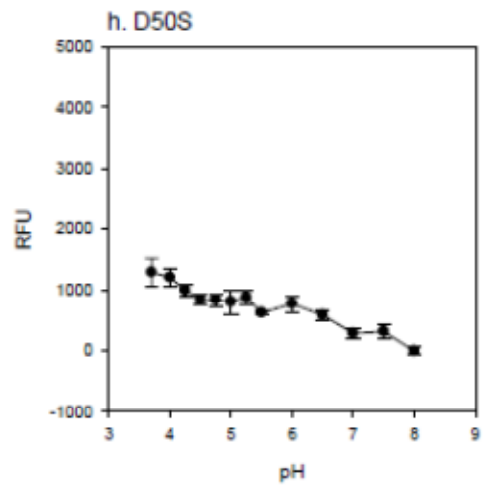
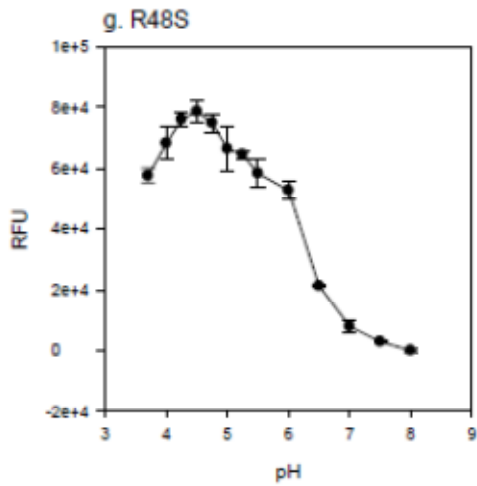
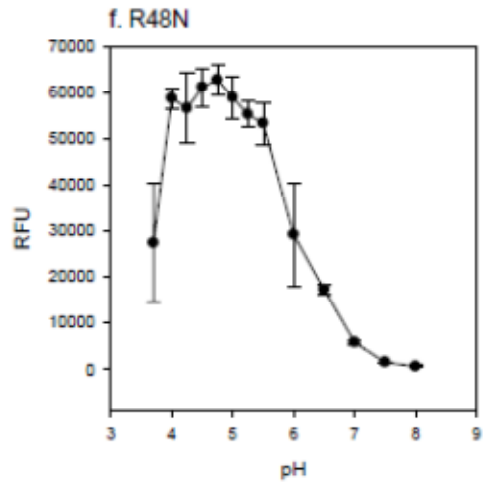
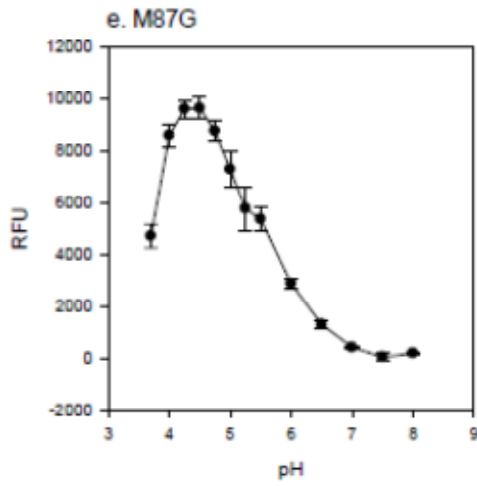


A.2 Supporting data for Chapter 2

A.2.1 pH activity profiles of NEU3 mutants

NEU3 mutants and wild-type protein were expressed in *E. coli* and purified as a MBP-NEU3 fusion protein (pMAL-c2x). NEU3 concentration for experiments was 0.1 mg/mL. The neuraminidase solution was incubated with 500 μ M 4MU-NA for 60 min at 37 °C, and activity was determined by fluorescence (365 nm excitation; 445 nm emission). Enzyme activity was measured at pH 3.7, 4.0, 4.25, 4.50, 4.75, 5.0, 5.5 (0.1 M sodium acetate buffer) and 5.25, 6.0, 6.5, 7.0, 7.5, 8.0 (0.1 M sodium phosphate buffer). Assays were performed in triplicate and error bars indicate the standard deviation of each point.





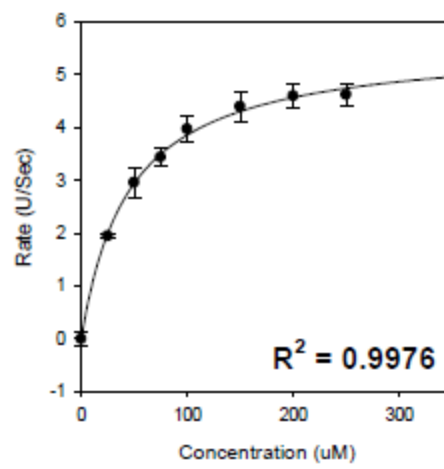
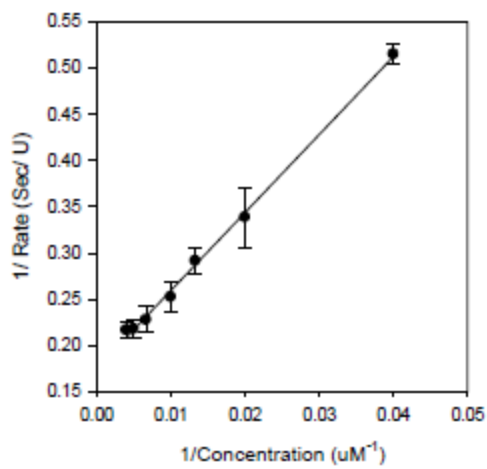
A.2.2 Kinetics of 4MU-NA cleavage by NEU3 mutants

MBP-NEU3 wild-type and mutant fusion proteins were expressed in *E. coli* (pMAL-c2x) and purified. Assays were conducted in 0.1 M sodium acetate buffer pH = 5.0, at a protein concentration of 0.1 mg/mL as determined by A280. The neuraminidase solution was mixed with serial concentrations of 4MU-NA. The reaction was followed by fluorescence (365 nm excitation; 445 nm emission) in real time without quenching of the reaction. Assays were performed with 3 to 5 replicate points and error bars indicate the standard deviation. Initial rates are plotted as both a reciprocal plot (with a linear fit) (*left*) and as raw data (*right*). Values from non-linear regression to the equation

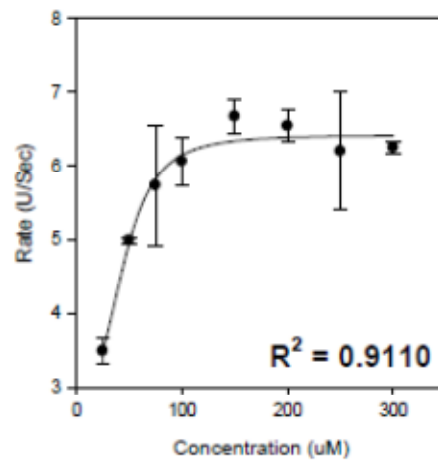
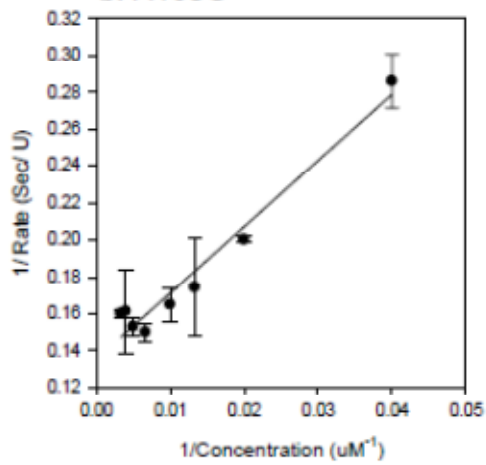
$$v = \frac{V_{max} S}{K_m + S}$$

are given in Table 2.3, r^2 values for the fits are shown at the lower right.

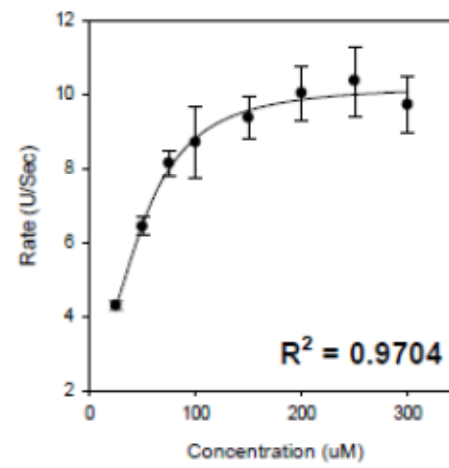
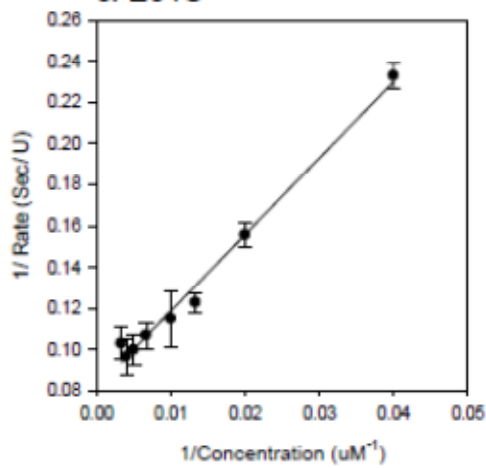
a. WT



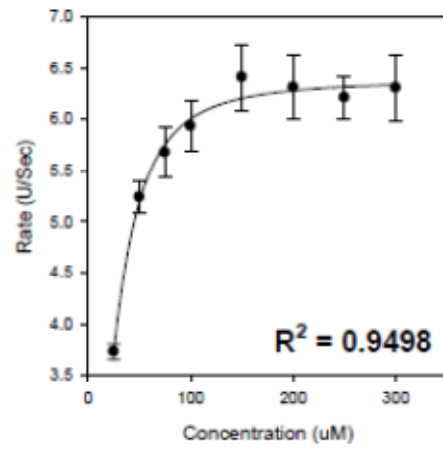
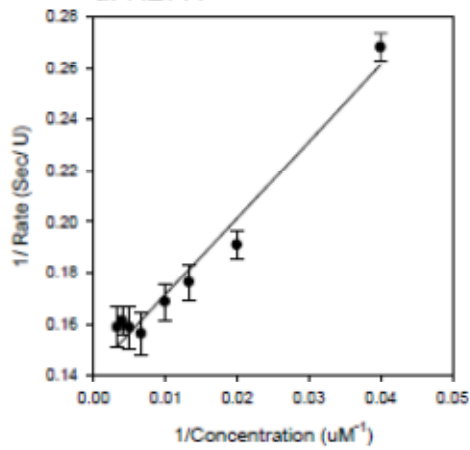
b. A160G



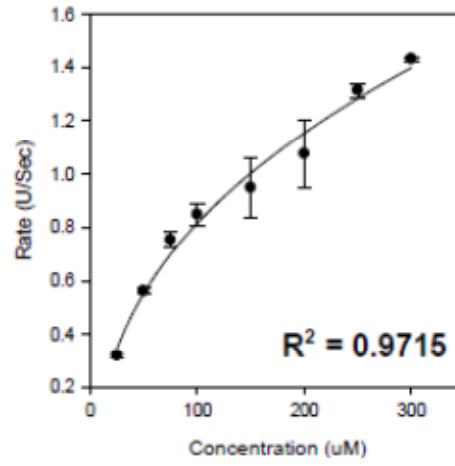
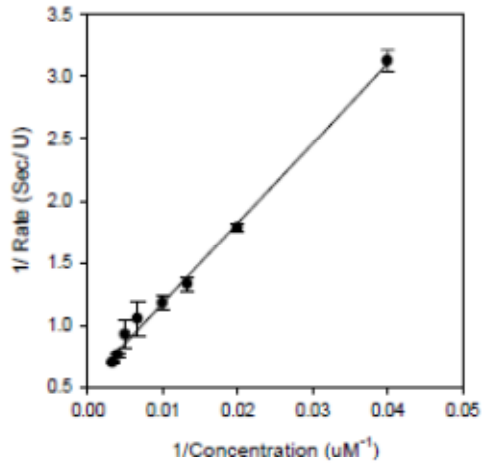
c. E51S



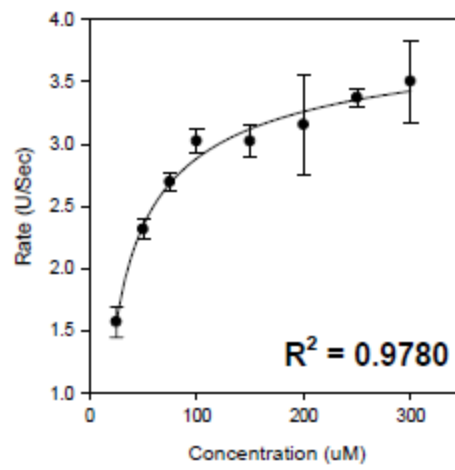
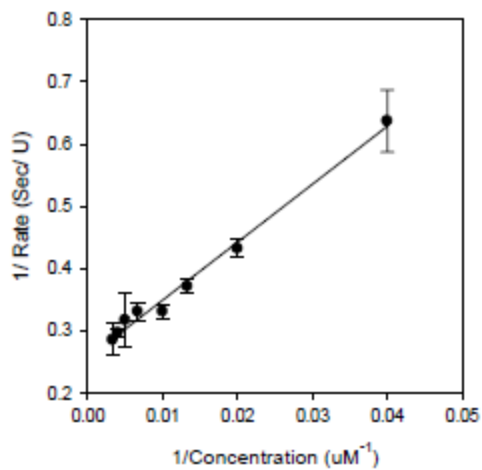
d. H277F



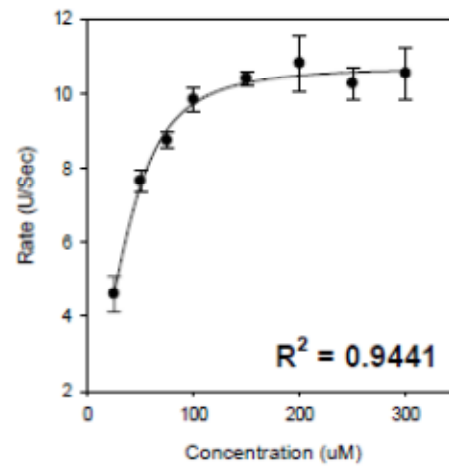
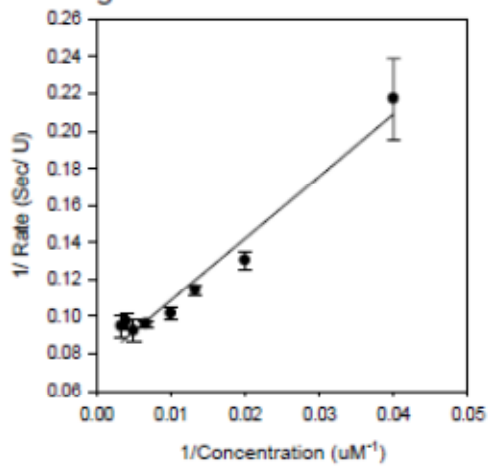
e. M87G



f. R48N

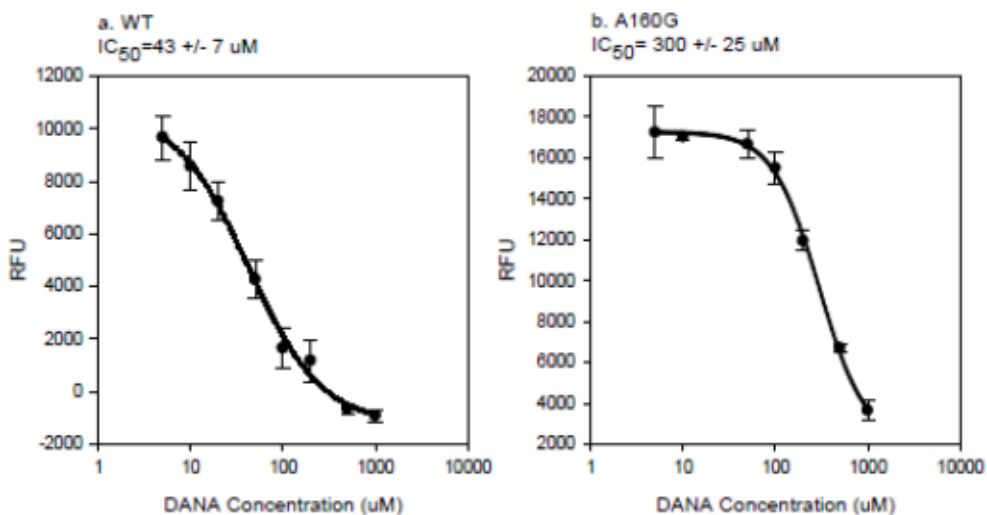


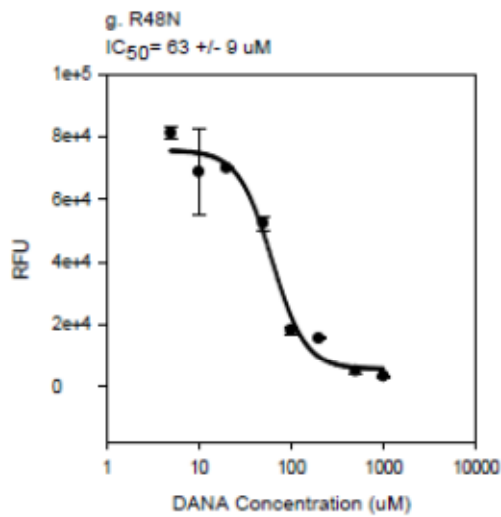
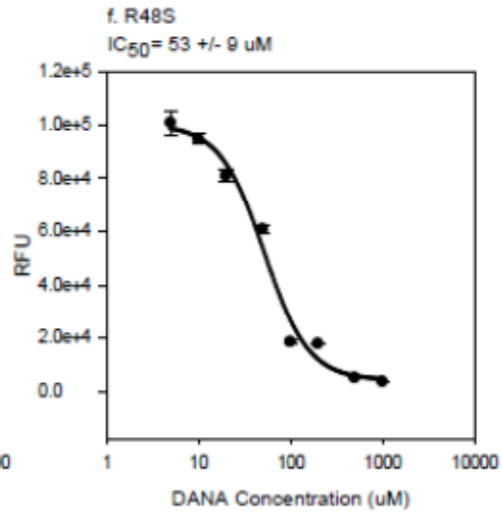
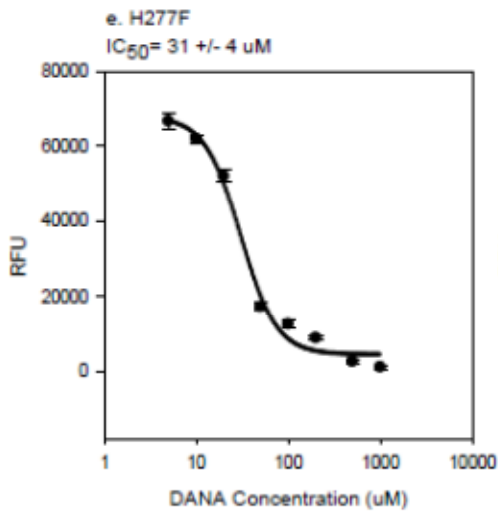
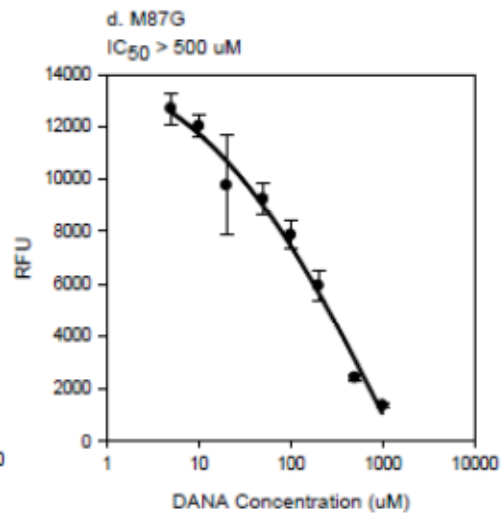
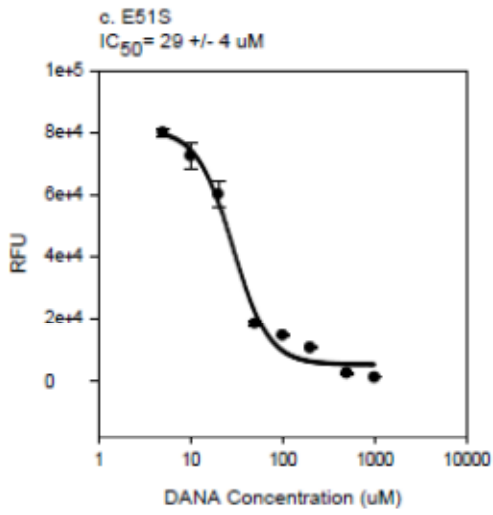
g. R48S



A.2.3 Inhibition of 4MU-NA cleavage by DANA with different NEU3 mutants

NEU3 wild-type and mutants were expressed in *E. coli* as the MBP-NEU3 fusion (pMAL-c2x) and purified. Assays were conducted in 0.1 M sodium acetate buffer pH = 5.0, at a protein concentration of 0.1 mg/mL as determined by A280. The neuraminidase solution was incubated with serial concentrations of 2-deoxy-2,3-didehydro-*N*-acetylneuraminic acid (DANA) (5, 10, 20, 50, 100, 200, 500 and 1000 μ M) for 30 min at 37 °C. Fluorogenic substrate (4MU-NA, 500 μ M final concentration) was added and incubated for 1 h. The reaction was quenched and activity was determined by fluorescence (365 nm excitation; 445 nm emission). Assays were performed in triplicate and error bars indicate the standard deviation of each point. IC₅₀ values were determined by non-linear regression.

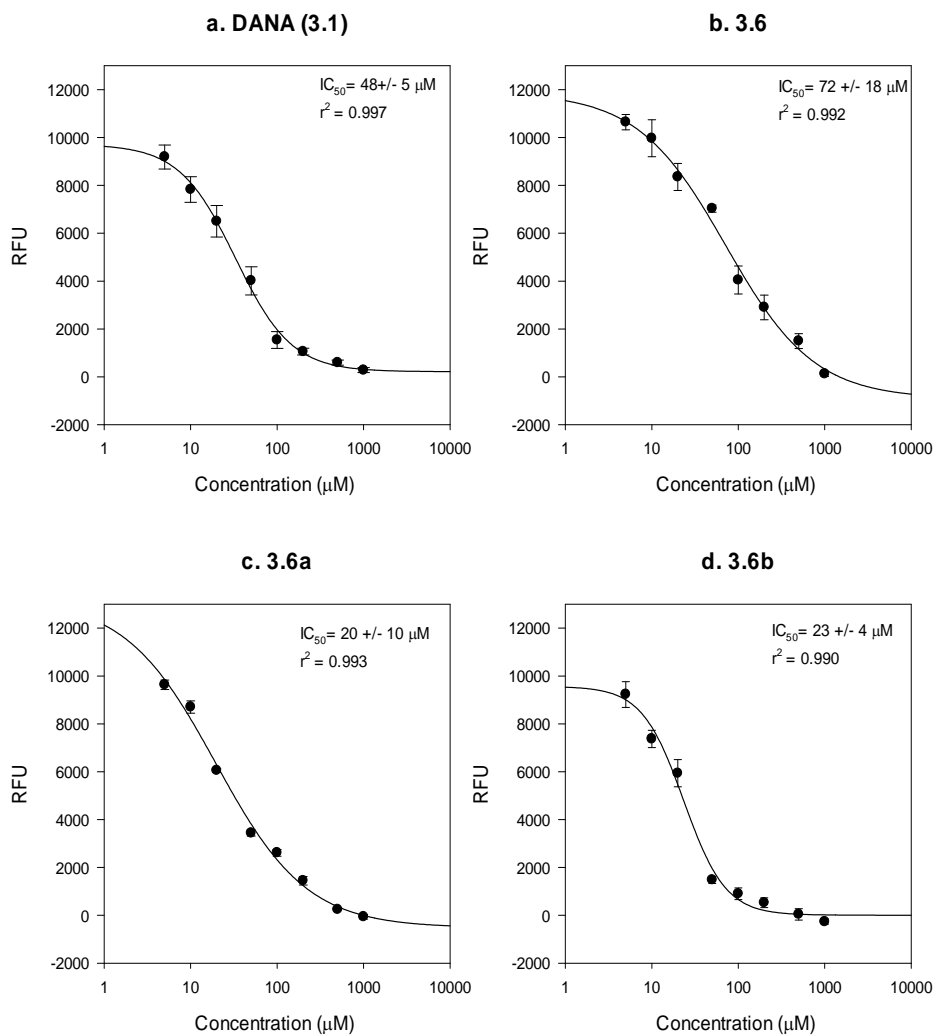




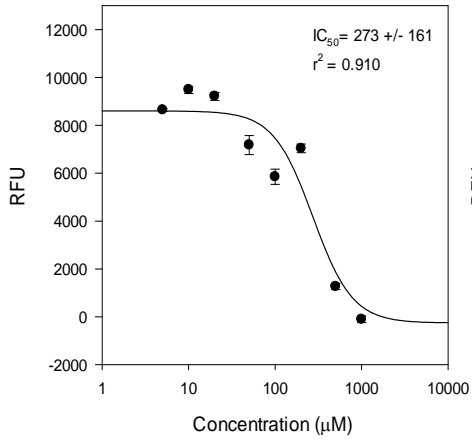
A.3 Supporting data for Chapter 3

A.3.1 General library

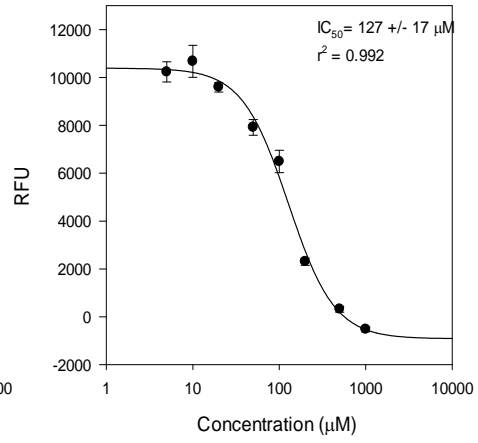
A.3.1.1 IC_{50} curves for C9-derivatives (6, 6a-i) against NEU3



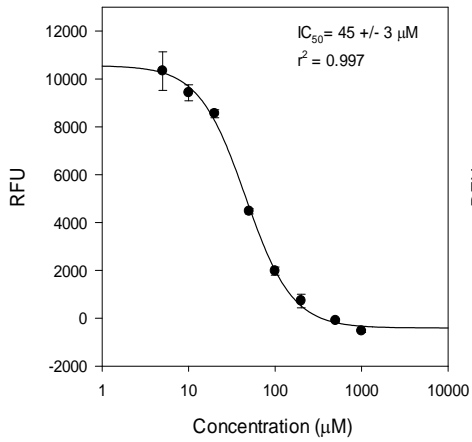
e. 3.6c



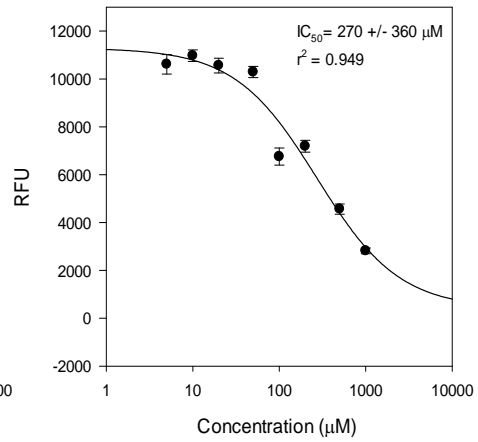
f. 3.6d



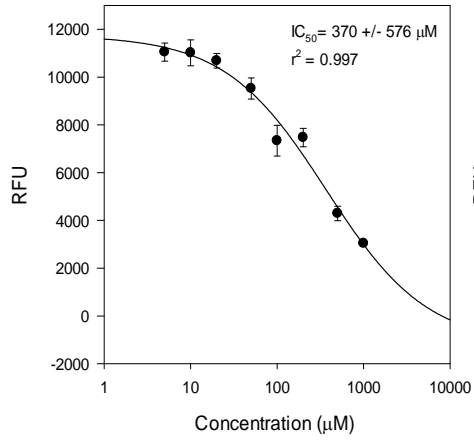
g. 3.6e



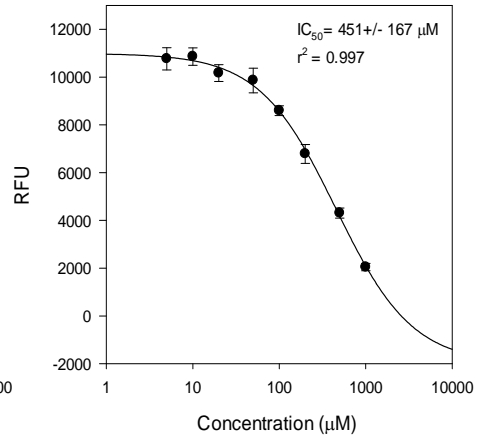
h. 3.6f



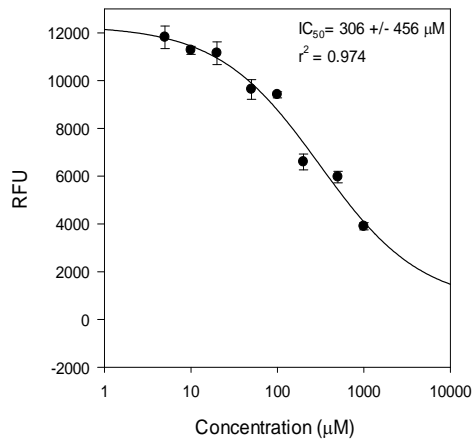
i. 3.6g



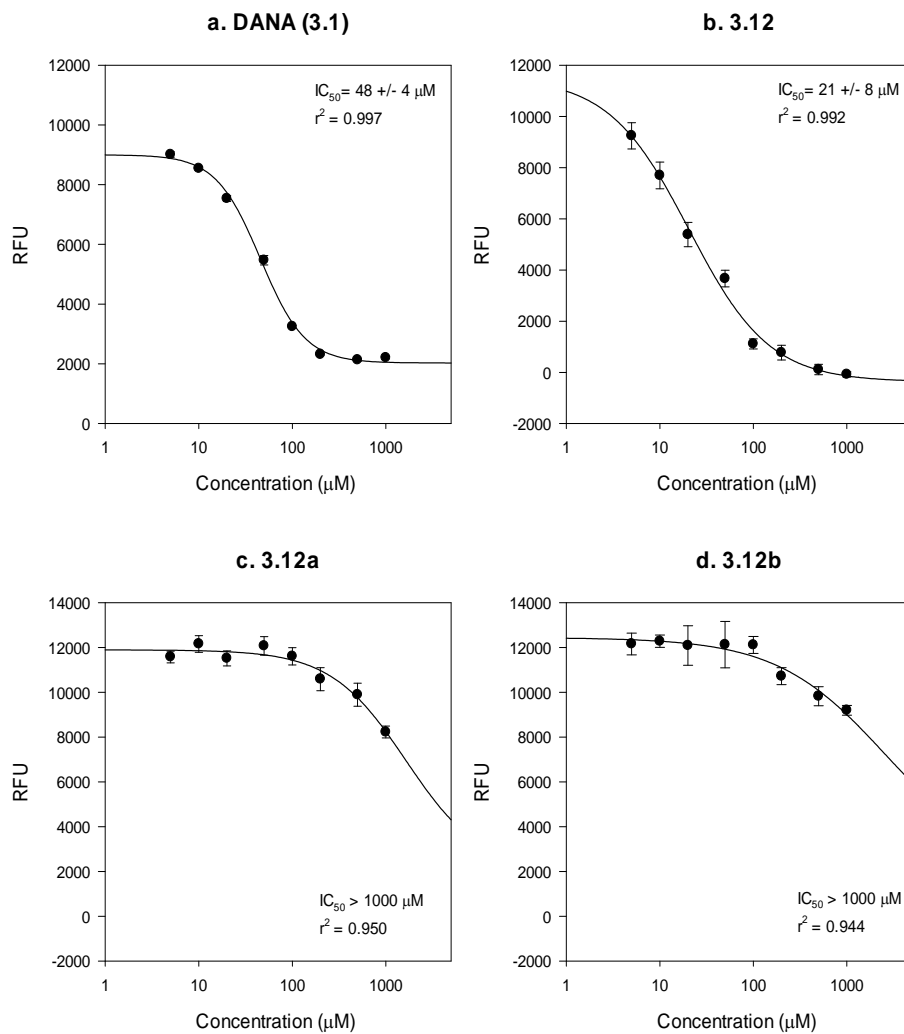
j. 3.6h



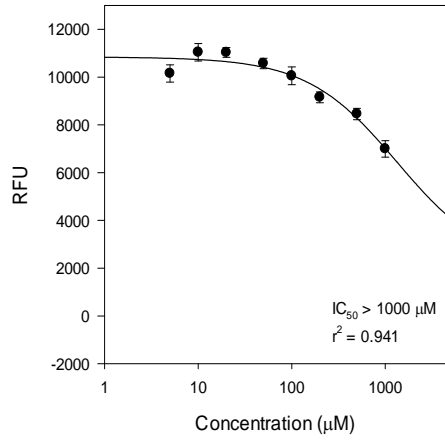
k. 3.6i



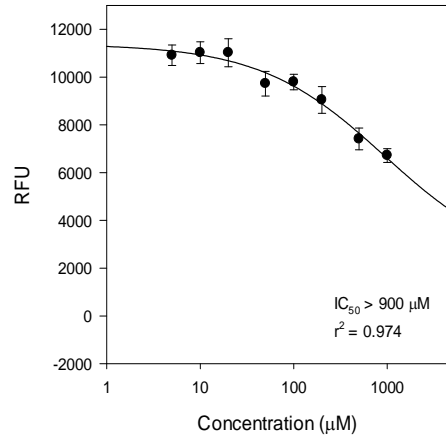
A.3.1.2 IC_{50} curves for N5-derivatives (12, 12a-i) against NEU3



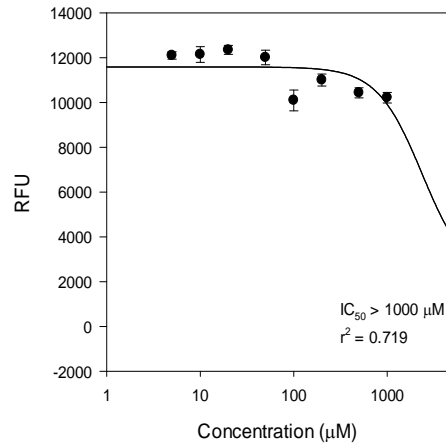
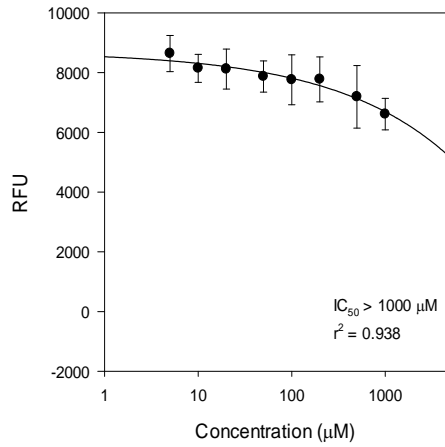
e. 3.12c



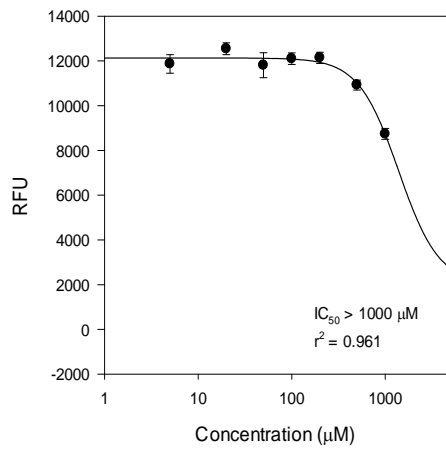
f. 3.12d



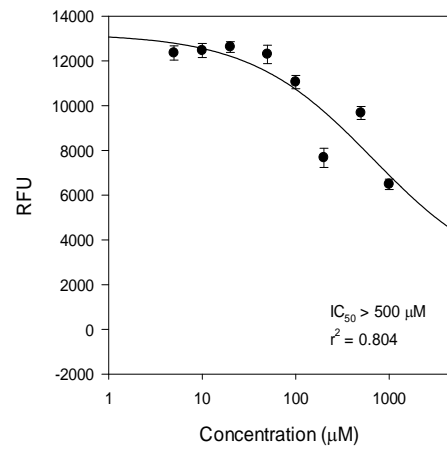
g. 3.12e



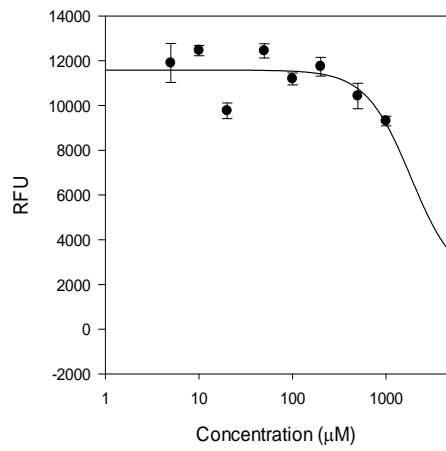
i. 3.12g



j. 3.12h



k. 3.12i



A.3.2 Focused library

A.3.2.1 Purity check of the focused library

To determine the purity of all tested compounds, samples were analyzed using HPLC (Waters® XTerra® RP C18 analytical column), particle size: 3.5µm, column dimensions: 4.8*150 mm. A gradient elution was used following the program given in **Table S11**. Solvent A was 0.05% trifluoroacetic acid in milliQ water, and solvent B was acetonitrile.

Table: HPLC Gradient elution program for testing compound purity.

Step	Time	Flow rate	% A	% B
1	-	0.8	100	0
2	4	0.8	100	0
3	8	0.8	35	65
4	16	0.8	35	65
5	17	0.8	0	100
6	20	0.8	0	100
7	24	0.8	100	0
8	25	0	-	-

The compounds were detected using a Waters 2996 photodiode array detector. The traces below show response at 254 nm.

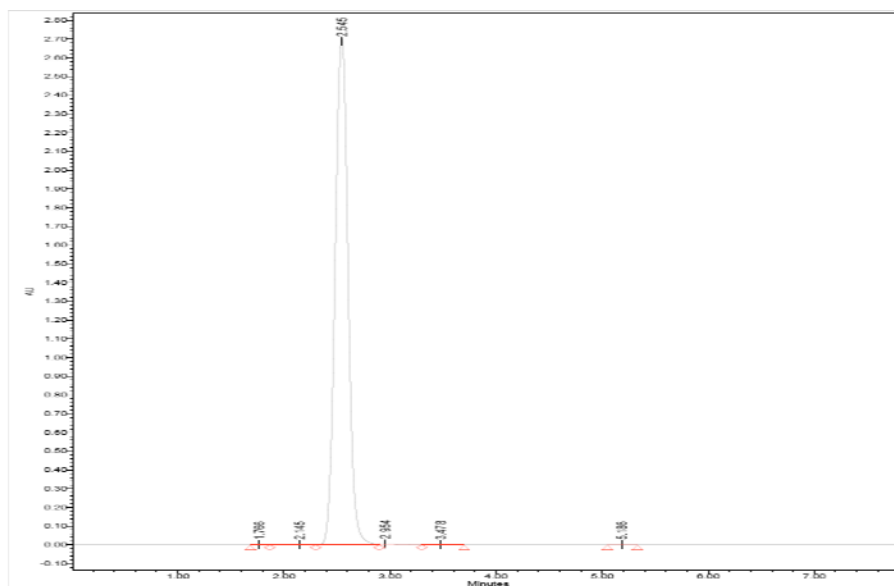
A.3.2.2 HPLC and HRMS results for compounds.

To confirm the identity of the all tested compounds, samples were submitted for high resolution mass spectrometry (HRMS).

Compound Number	HPLC trace		HRMS (M-H) ⁻	
	Retention Time (min)	% Area	Calculated M/z	Found M/z
DANA (1)	2.545	99.53	290.0881	290.0887
6	3.947	99.62	315.0946	315.0954
6a	13.809	95.51	417.1416	417.1421
6c	2.529	95.55	385.1365	385.1363
6e	13.979	97.40	447.1521	447.1527
6f	5.507	99.52	371.1208	371.1208
6g	4.754	96.78	385.1365	385.1362
6h	9.744	95.04	399.1521	399.1518
6i	1.943	100	399.1521	399.1517
12	3.403	98.23	331.0895	331.0893
12a	13.636	100	433.1365	433.1366

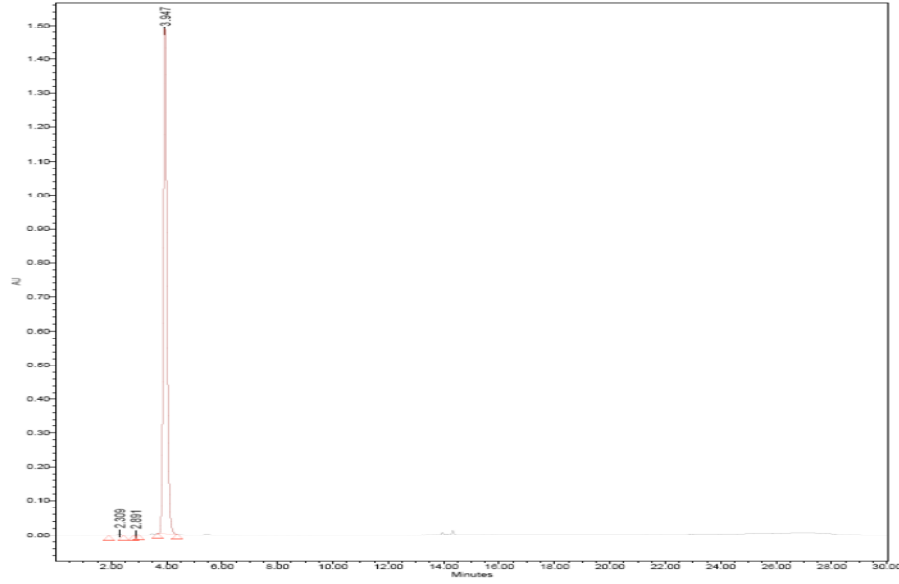
The IC₅₀ curves for all the tested compounds (**1-11**) with the human neuraminidases (NEU1, NEU2, NEU3 and NEU4) are shown in **Figure SI3**. We also measured the inhibition constant (K_i) for **6** and **7** with their target enzyme NEU4 (**Figure SI4**). For each inhibitor, the double reciprocal curve (1/product formation rate versus 1/[S]) for several inhibitor concentrations were plotted and fit by linear regression. The slopes of these lines were plotted versus inhibitor concentration and fit to a standard equation ($y = ax+b$). K_i was given by $-b/a$ and the error was calculated from the linear fit.

A.3.2.3 HPLC traces of the tested compounds (1-11).
a- HPLC trace of DANA (3.1)



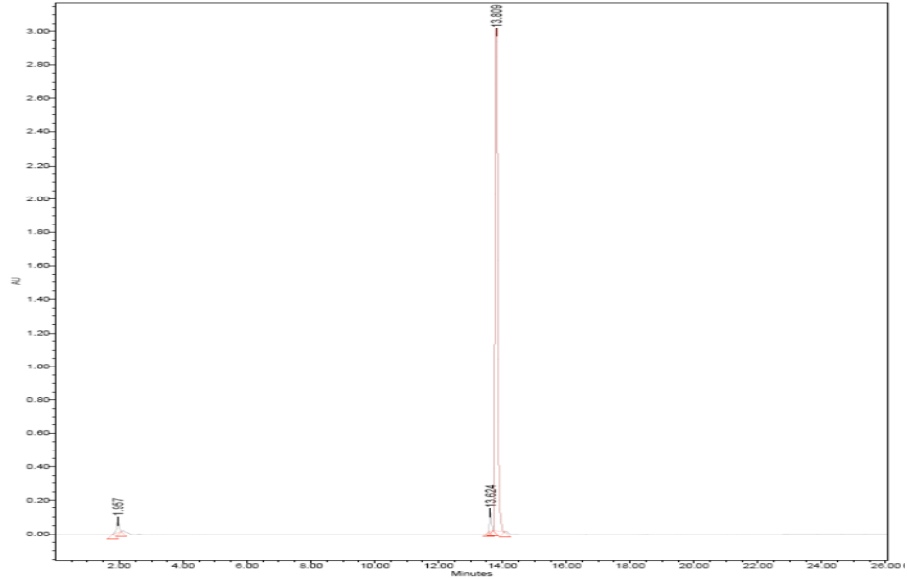
	Retention Time (min)	Area (μV*sec)	%Area	Hight (μV)	Int. Type
1	1.766	1434	0.01	240	BV
2	2.145	15441	0.07	1041	VV
3	2.545	22972011	99.53	2711004	VV
4	2.954	65053	0.28	5414	VV
5	3.478	22964	0.10	1717	VB
6	5.188	3343	0.01	393	BB

b- HPLC trace of 3.6



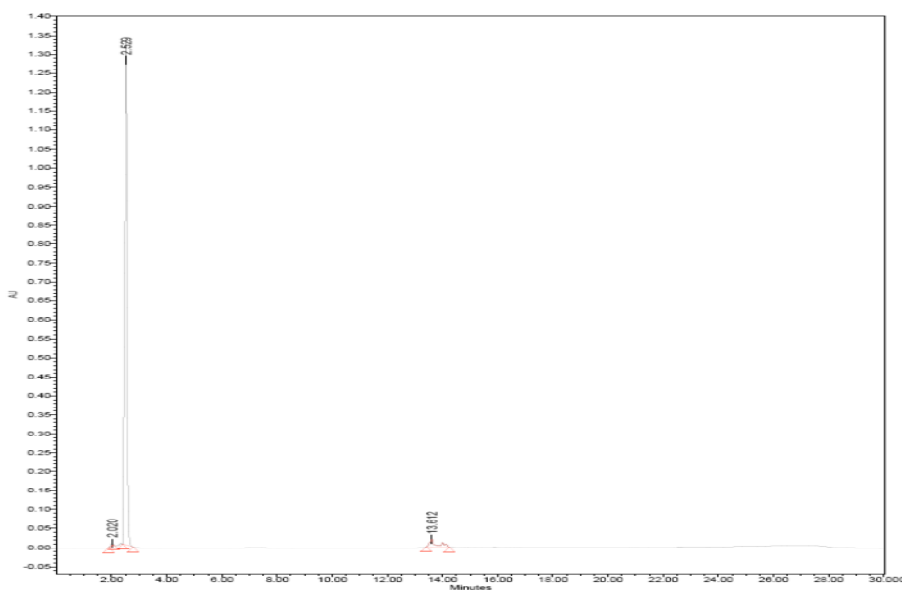
	Retention Time (min)	Area (μV*sec)	%Area	Hight (μV)	Int. Type
1	2.309	39733	0.29	5074	BB
2	2.891	11637	0.09	2223	BB
3	3.947	13551725	99.62	1484883	BB

c- HPLC trace of 3.6a



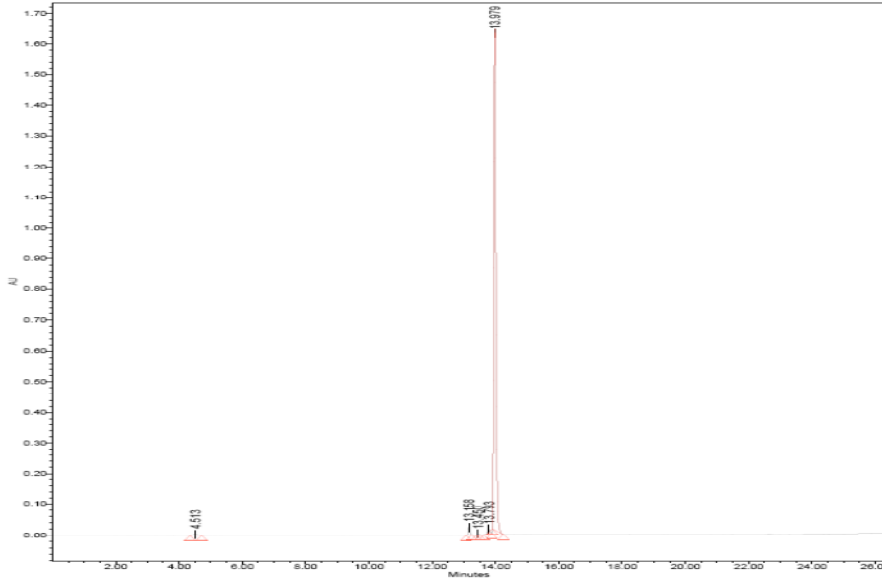
	Retention Time (min)	Area ($\mu\text{V}\cdot\text{sec}$)	%Area	Hight (μV)	Int. Type
1	1.957	393536	2.12	64682	BB
2	13.624	439705	2.37	106983	BB
3	13.809	17722666	95.51	3119332	BB

d- HPLC trace of 3.6c



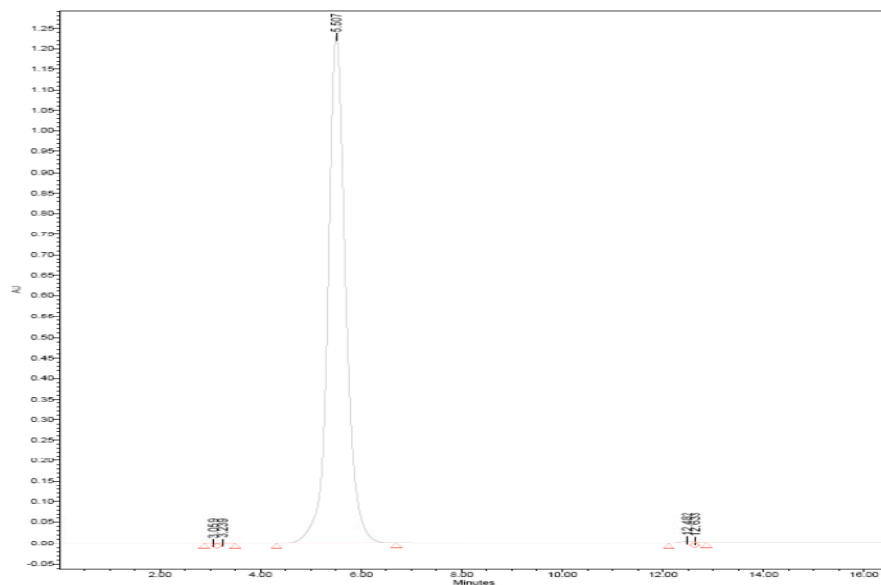
	Retention Time (min)	Area (μV*sec)	%Area	Hight (μV)	Int. Type
1	2.020	27419	0.34	5789	BB
2	2.529	7623335	95.55	1267933	BB
3	13.612	327262	4.10	19026	BB

e- HPLC trace of 3.6e



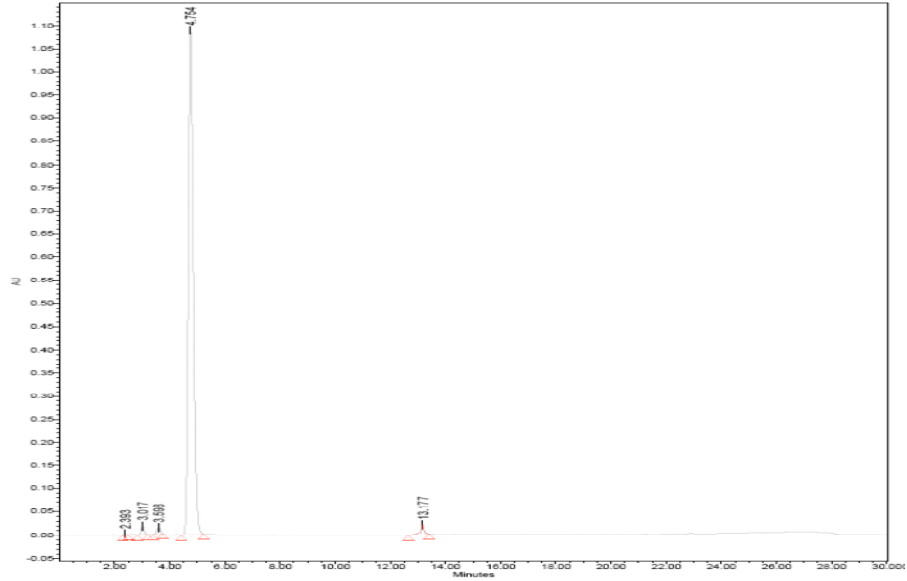
	Retention Time (min)	Area ($\mu\text{V}\cdot\text{sec}$)	%Area	Hight (μV)	Int. Type
1	4.513	33200	0.42	3401	BB
2	13.158	92336	1.16	24174	BB
3	13.450	7984	0.10	2183	BB
4	13.793	73418	0.92	14344	BB
5	13.979	7755670	97.40	1618956	BB

f- HPLC trace of **3.6f**



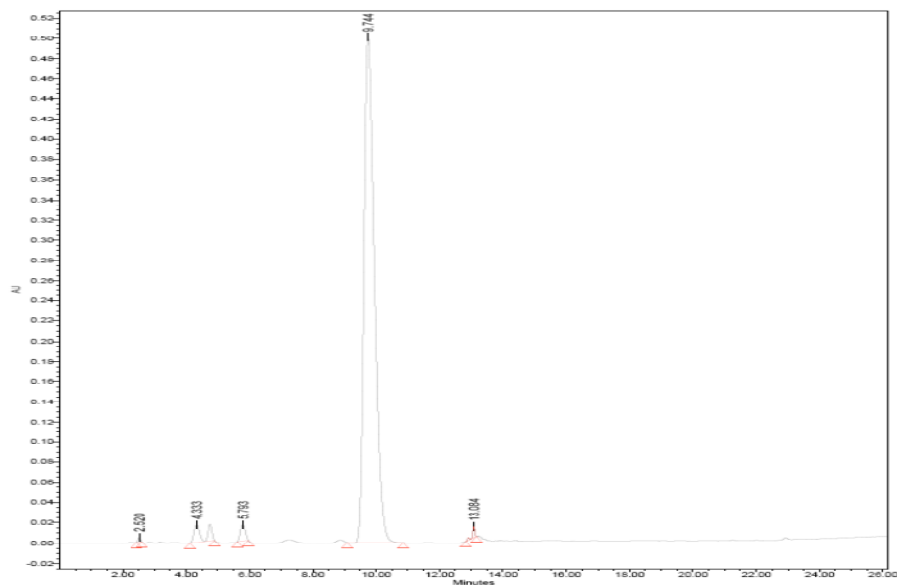
	Retention Time (min)	Area ($\mu\text{V}\cdot\text{sec}$)	%Area	Hight (μV)	Int. Type
1	3.059	6678	0.02	744	BV
2	3.239	17092	0.06	1524	VB
3	5.507	30162534	99.52	1229252	BB
4	12.482	103272	0.34	5997	BV
5	12.633	19365	0.06	4086	VB

g- HPLC trace of 3.6g



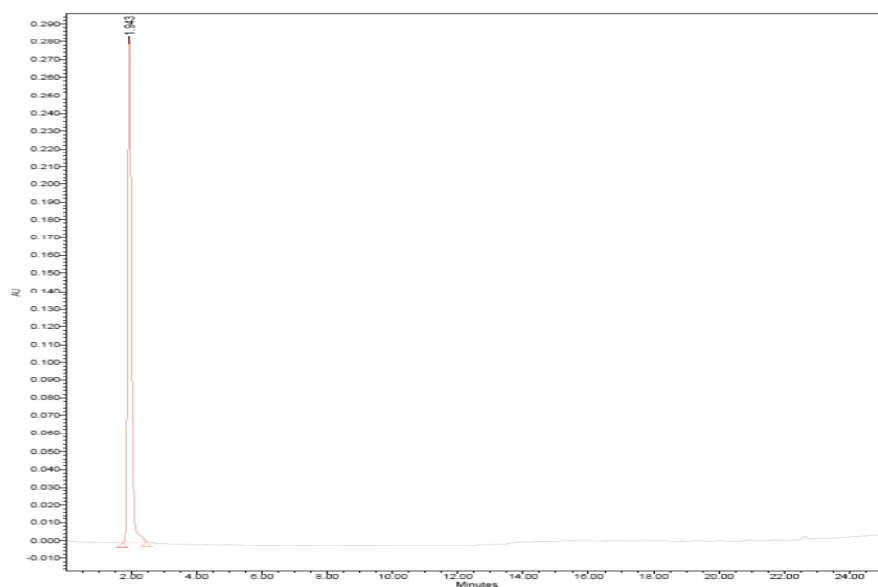
	Retention Time (min)	Area ($\mu\text{V}\cdot\text{sec}$)	%Area	Hight (μV)	Int. Type
1	2.393	13191	0.09	2574	BB
2	3.017	138138	0.99	18289	BB
3	3.598	124768	0.89	13230	BB
4	4.754	13533015	96.78	1093283	BB
5	13.177	173816	1.24	20052	BB

h- HPLC trace of **3.6h**



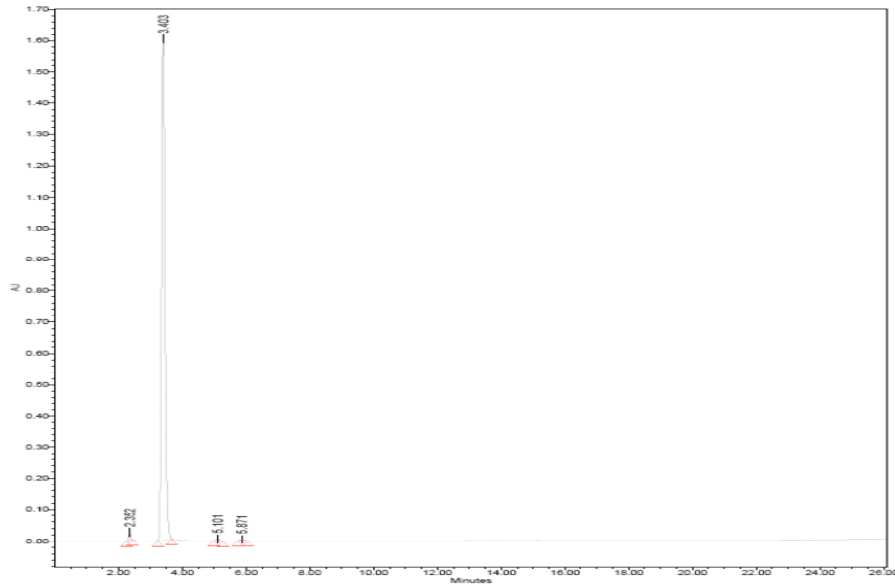
	Retention Time (min)	Area ($\mu\text{V} \cdot \text{sec}$)	%Area	Hight (μV)	Int. Type
1	2.520	24032	0.20	4554	BB
2	4.333	347679	2.90	16945	BB
3	5.793	171629	1.34	15768	BB
4	9.744	11404544	95.04	501348	BB
5	13.084	52279	0.44	10488	BB

i- HPLC trace of 3.6i



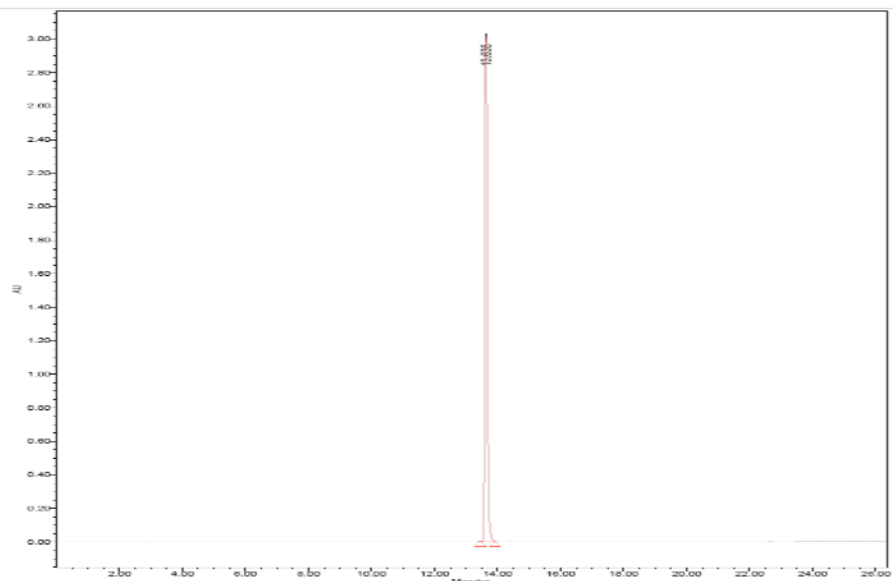
	Retention Time (min)	Area ($\mu\text{V}\cdot\text{sec}$)	%Area	Hight (μV)	Int. Type
1	1.943	2290792	100.00	283664	BB

j- HPLC trace of 3.12



	Retention Time (min)	Area (μV*sec)	%Area	Hight (μV)	Int. Type
1	2.352	111889	0.92	24986	BB
2	3.403	11934962	98.23	1614598	BB
3	5.101	56756	0.47	6185	BB
4	5.871	45875	0.38	4516	BB

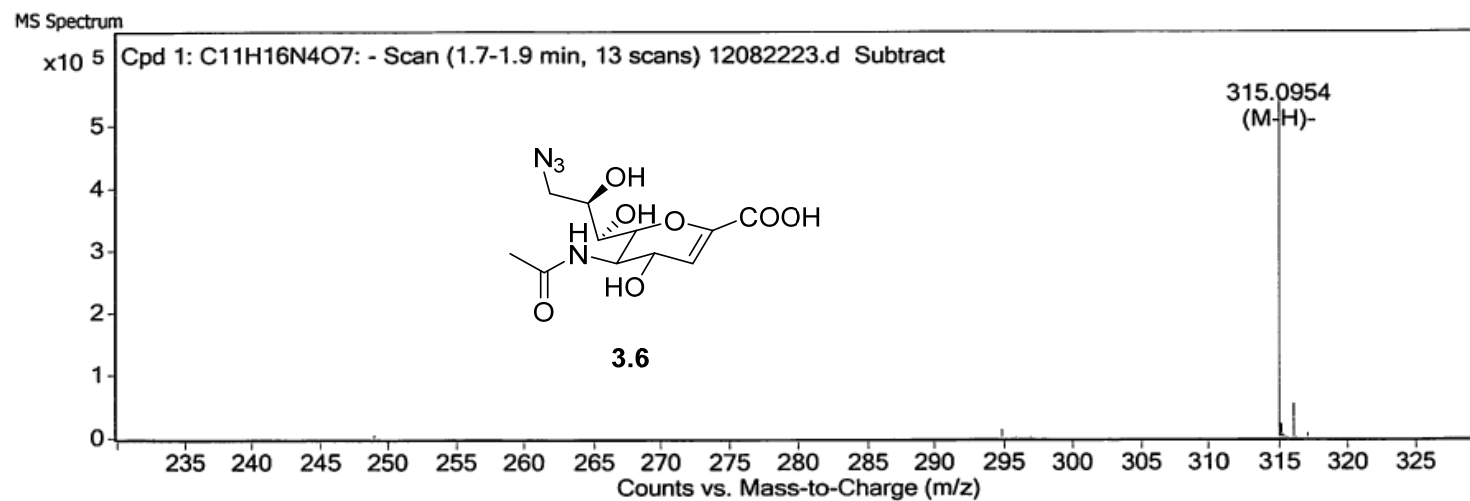
k- HPLC trace of **3.12a**



	Retention Time (min)	Area ($\mu\text{V}\cdot\text{sec}$)	%Area	Hight (μV)	Int. Type
1	13.636	16618000	100.00	3107171	BB

A.3.2.4 HRMS spectra of the focused library compounds.

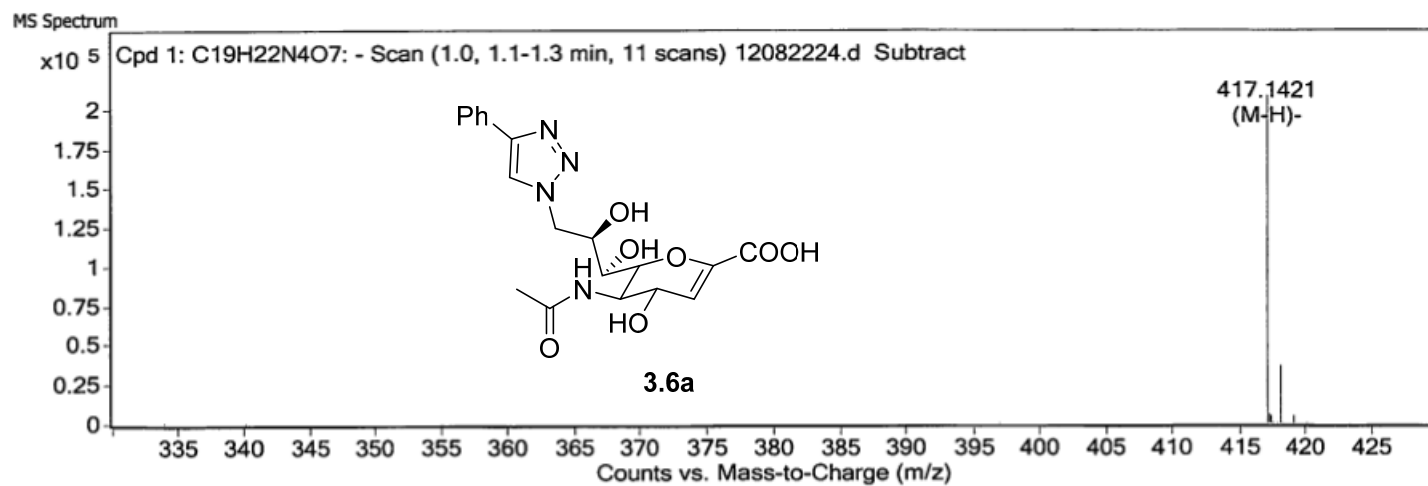
a- HRMS of **3.6**: (M-H)⁻ found 315.0954, calculated 315.0946



MS Spectrum Peak List

m/z	Calc m/z	Diff(ppm)	Abund	Formula	Ion
315.0954	315.0946	2.41	544510	C ₁₁ H ₁₅ N ₄ O ₇	(M-H) ⁻

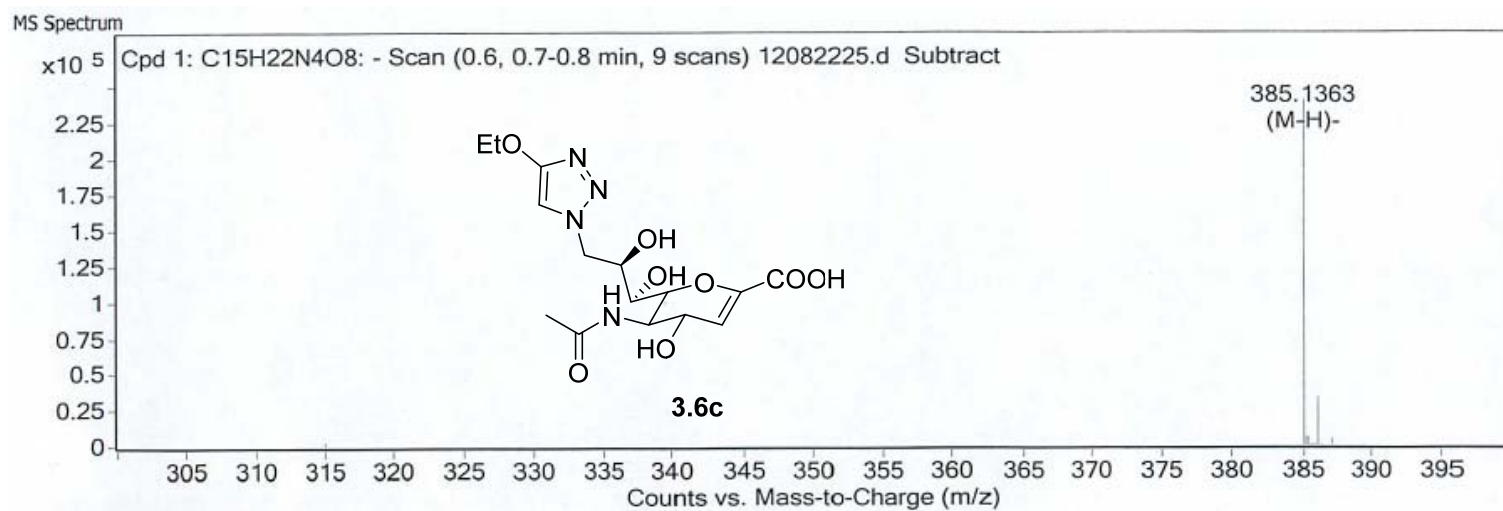
b- HRMS of **3.6a**: (M-H)⁻ found 417.1421, calculated 417.1416



MS Spectrum Peak List

m/z	Calc m/z	Diff(ppm)	z	Abund	Formula	Ion
417.1421	417.1416	1.16	1	209037	C ₁₉ H ₂₁ N ₄ O ₇	(M-H) ⁻

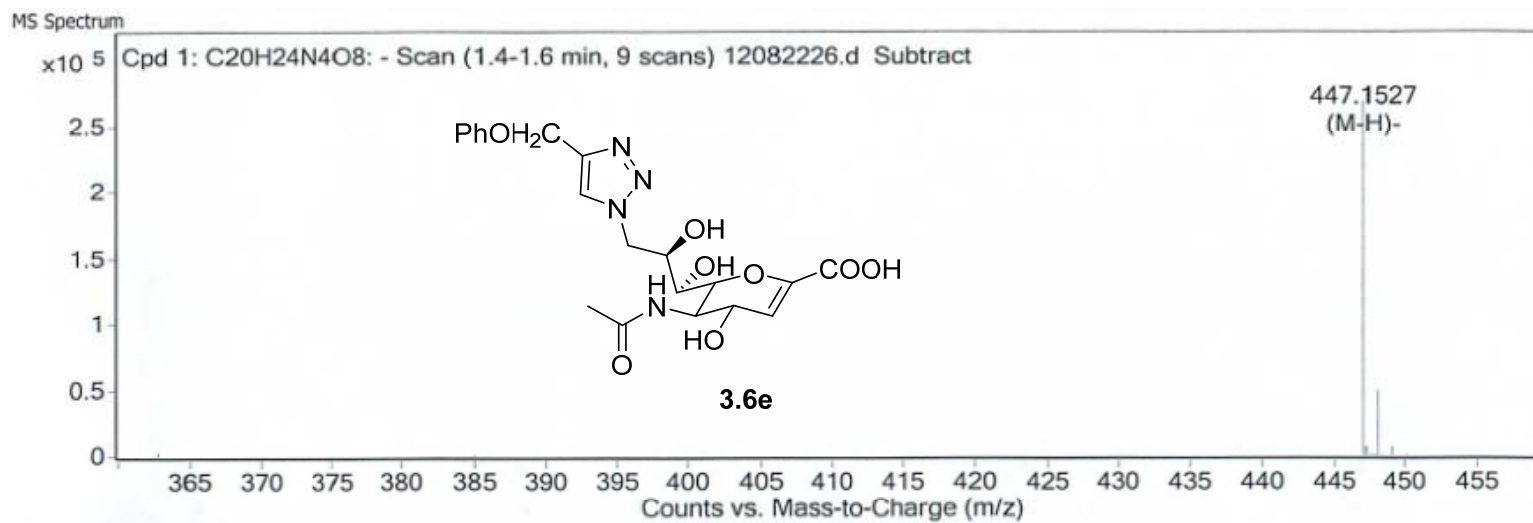
c- HRMS of **3.6c**: (M-H)⁻ found 385.1363, calculated 385.1365



MS Spectrum Peak List

<i>m/z</i>	<i>Calc m/z</i>	Diff(ppm)	Abund	Formula	Ion
385.1363	385.1365	-0.44	240633	C ₁₅ H ₂₁ N ₄ O ₈	(M-H) ⁻

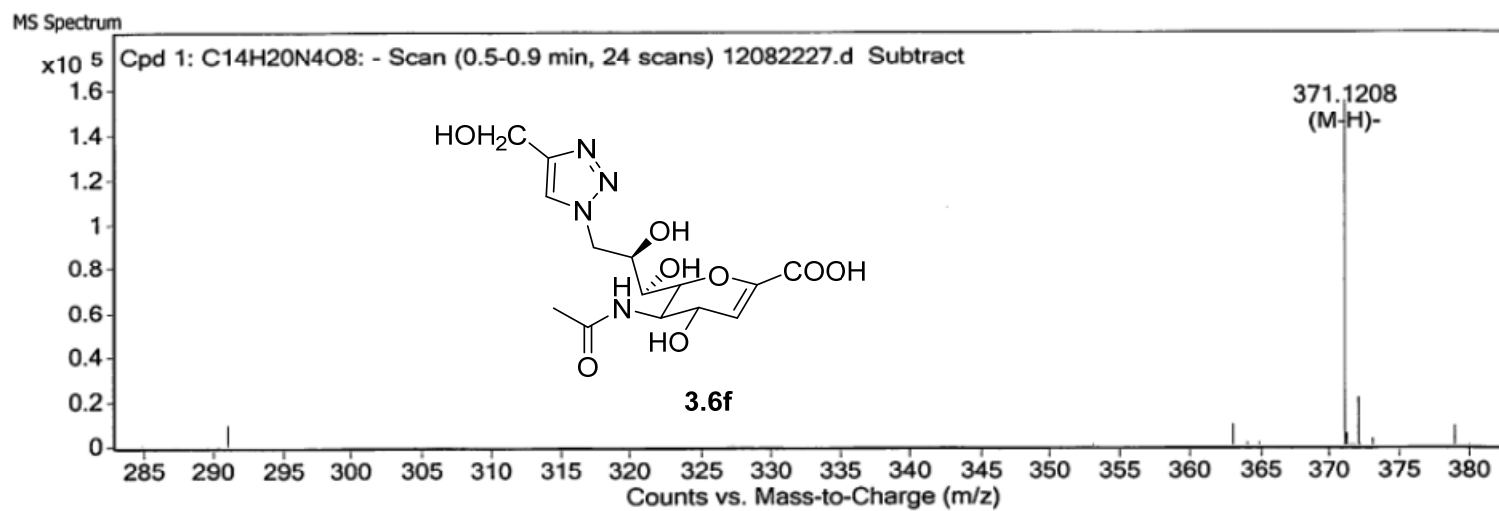
d- HRMS of **3.6e**: (M-H)⁻ found 447.1527, calculated 447.1521



MS Spectrum Peak List

<i>m/z</i>	<i>Calc m/z</i>	Diff(ppm)	Abund	Formula	Ion
447.1527	447.1521	1.18	269017	C ₂₀ H ₂₃ N ₄ O ₈	(M-H) ⁻

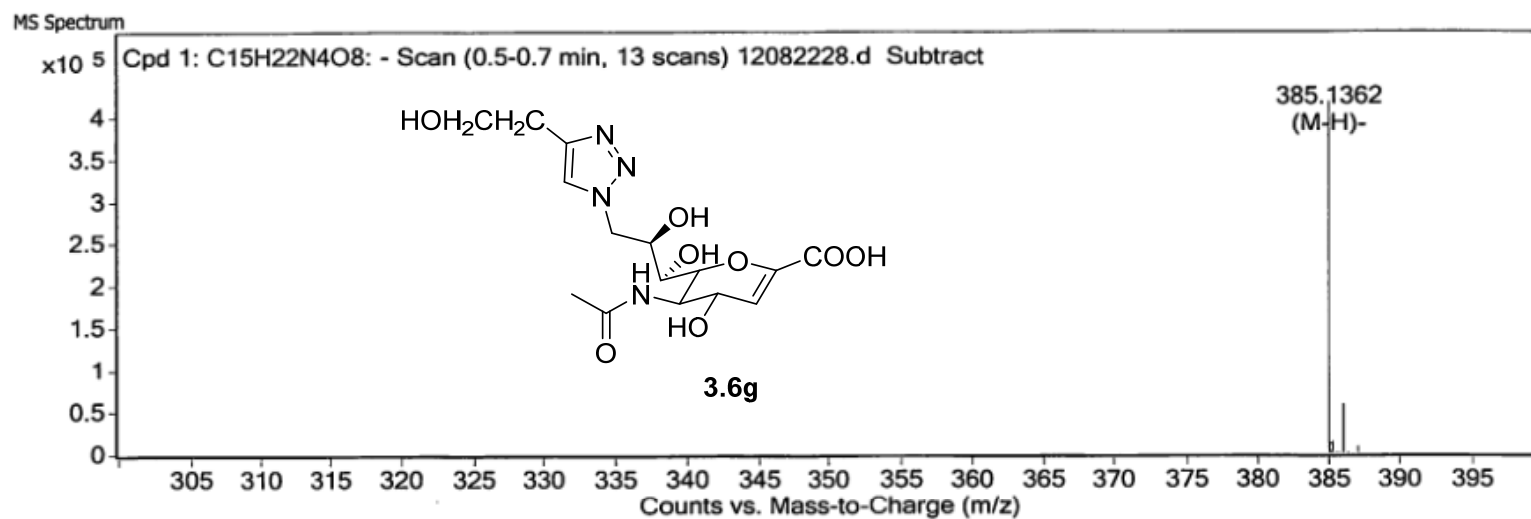
e- HRMS of **3.6f**: (M-H)⁻ found 371.1208, calculated 371.1208



MS Spectrum Peak List

m/z	Calc m/z	Diff(ppm)	z	Abund	Formula	Ion
371.1208	371.1208	-0.17	-1	155741	C ₁₄ H ₁₉ N ₄ O ₈	(M-H) ⁻

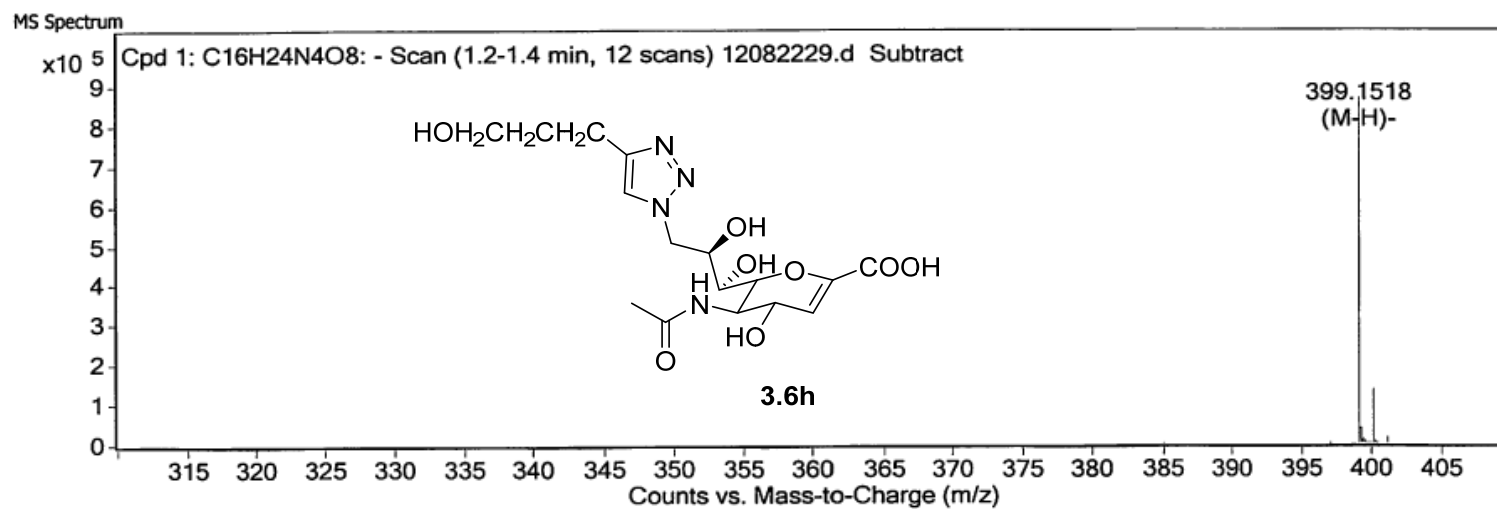
f- HRMS of **3.6g**: (M-H)⁻ found 385.1362, calculated 385.1365



MS Spectrum Peak List

m/z	Calc m/z	Diff(ppm)	Abund	Formula	Ion
385.1362	385.1365	-0.66	419004	C ₁₅ H ₂₁ N ₄ O ₈	(M-H) ⁻

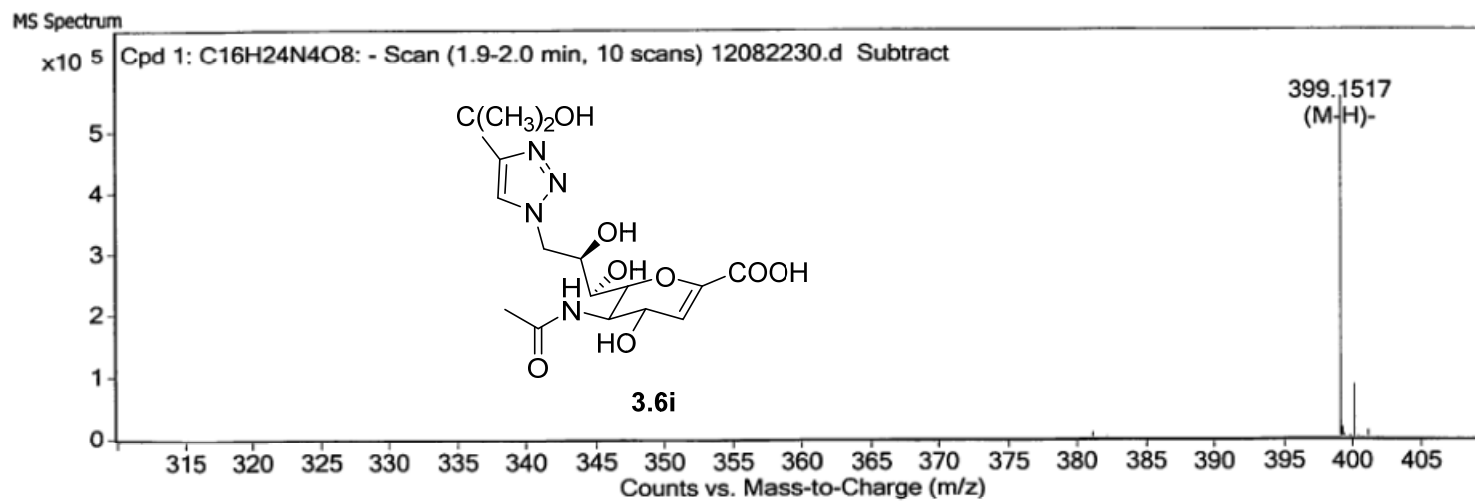
g- HRMS of **3.6h**: (M-H)⁻ found 399.1518, calculated 399.1521



MS Spectrum Peak List

<i>m/z</i>	<i>Calc m/z</i>	<i>Diff(ppm)</i>	<i>Abund</i>	<i>Formula</i>	<i>Ion</i>
399.1518	399.1521	-0.96	870595	C ₁₆ H ₂₃ N ₄ O ₈	(M-H) ⁻

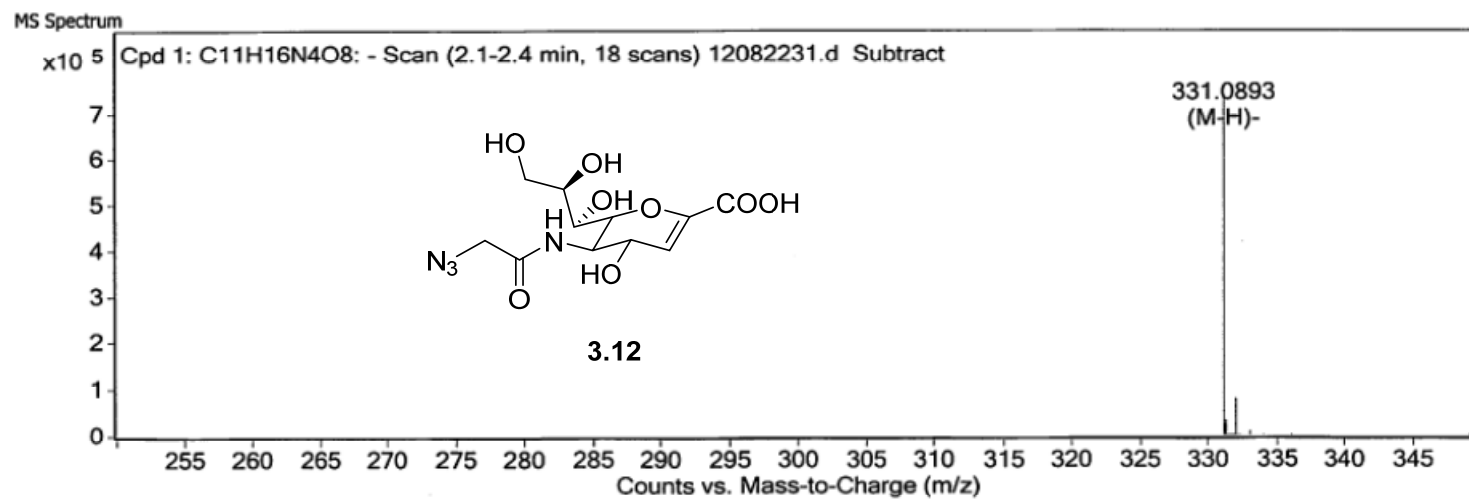
h- HRMS of **3.6i**: (M-H)⁻ found 399.1517, calculated 399.1521



MS Spectrum Peak List

<i>m/z</i>	<i>Calc m/z</i>	Diff(ppm)	Abund	Formula	Ion
399.1517	399.1521	-1.13	555721	C ₁₆ H ₂₃ N ₄ O ₈	(M-H) ⁻

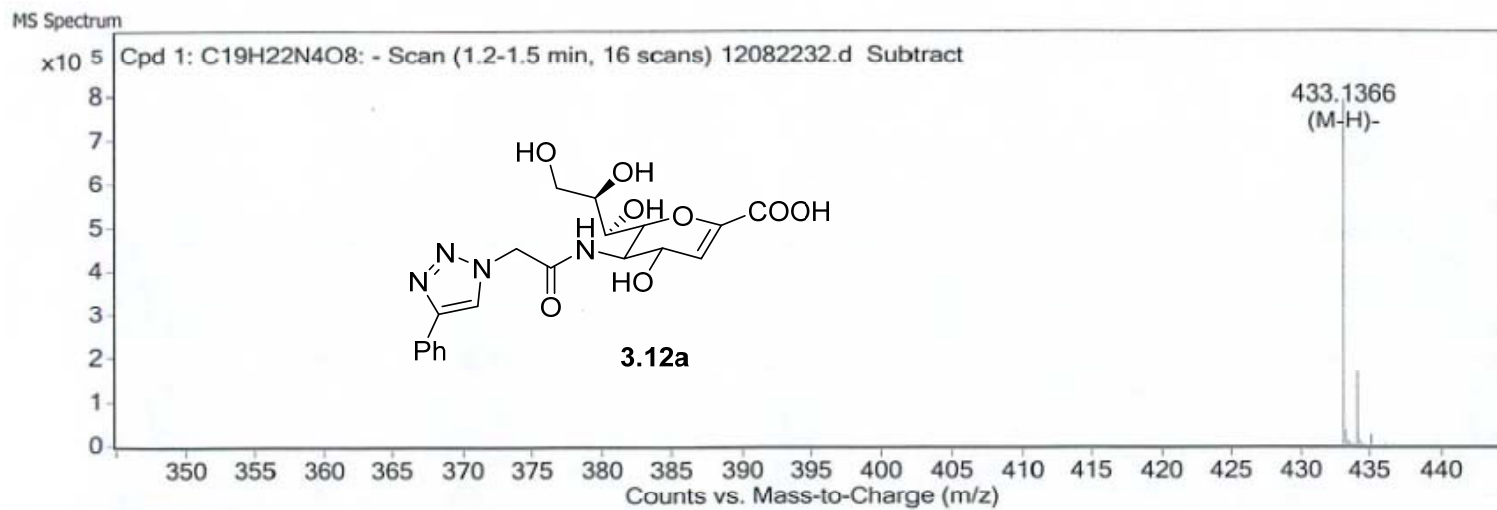
i- HRMS of **3.12**: (M-H)⁻ found 331.0893, calculated 331.0895



MS Spectrum Peak List

<i>m/z</i>	<i>Calc m/z</i>	Diff(ppm)	Abund	Formula	Ion
331.0893	331.0895	-0.64	734783	C ₁₁ H ₁₅ N ₄ O ₈	(M-H) ⁻

j- HRMS of **3.12a**: (M-H)⁻ found 433.1366, calculated 433.1365

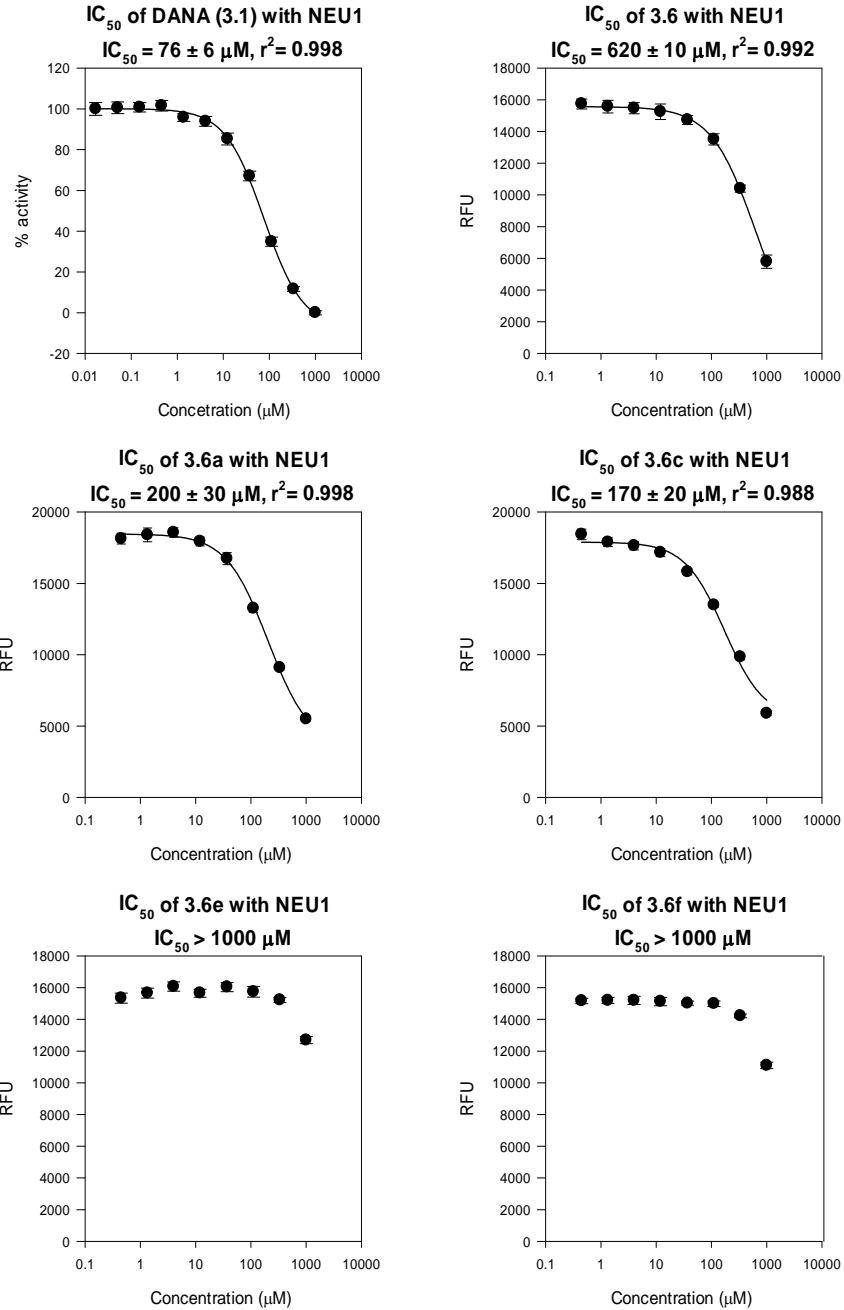


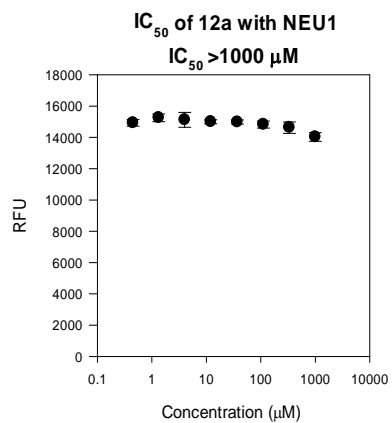
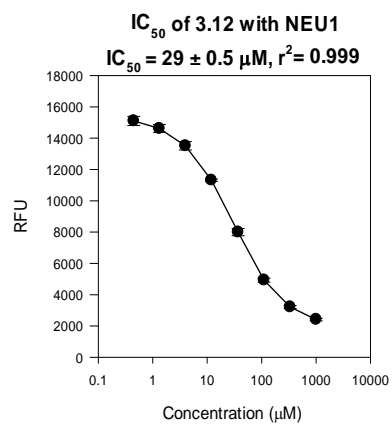
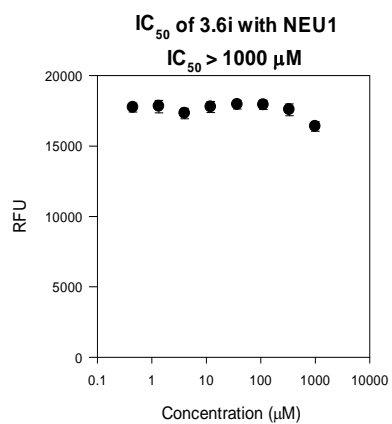
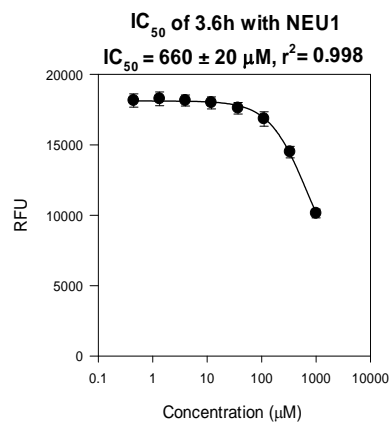
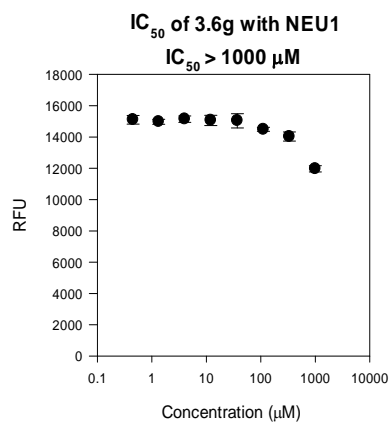
MS Spectrum Peak List

m/z	Calc m/z	Diff(ppm)	Abund	Formula	Ion
433.1366	433.1365	0.36	793553	C ₁₉ H ₂₁ N ₄ O ₈	(M-H) ⁻

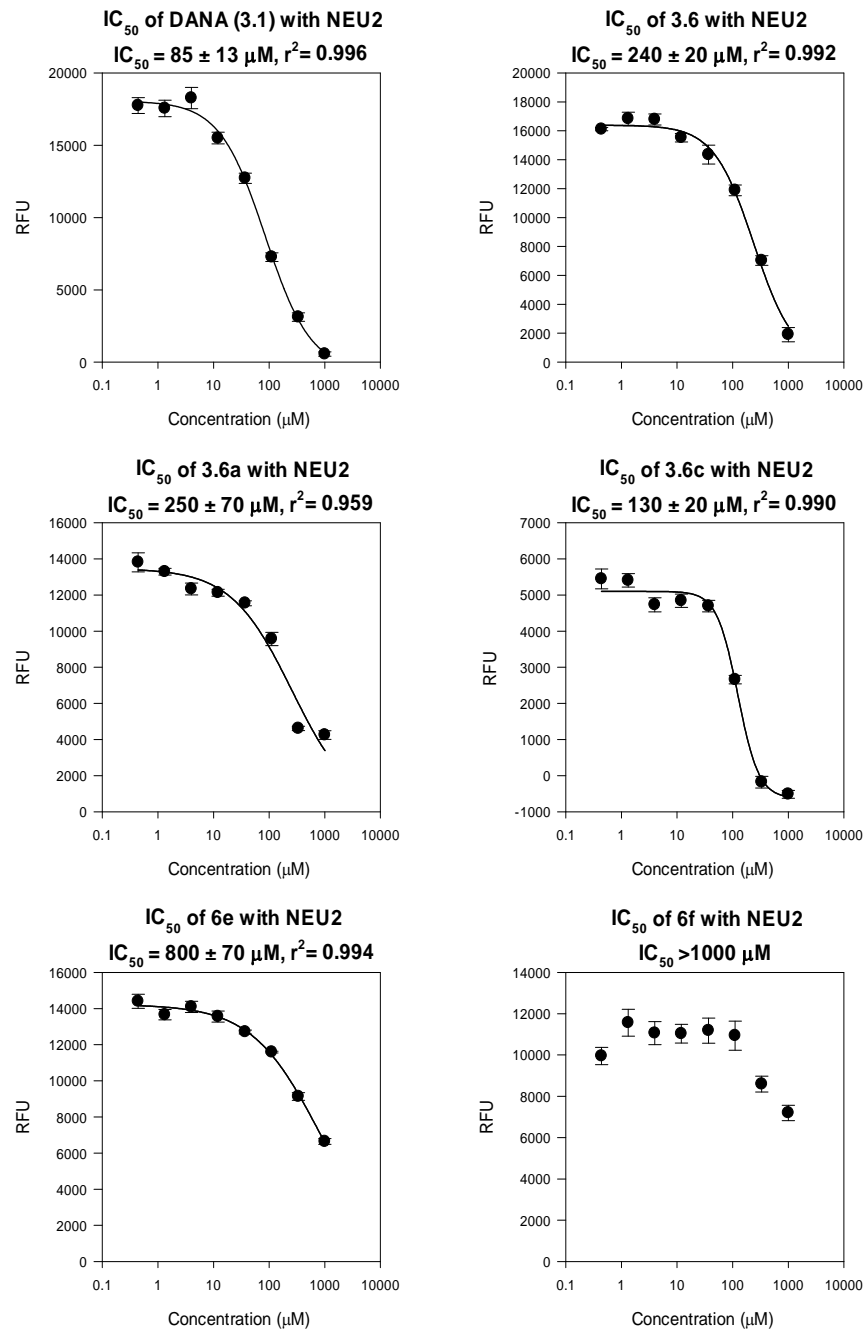
A.3.2.5 *IC₅₀ curves of the focused library compounds with NEU1, NEU2, NEU3 and NEU4.*

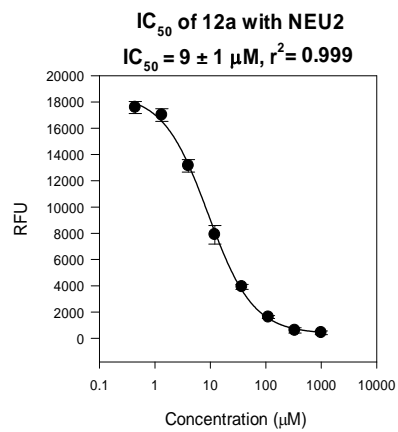
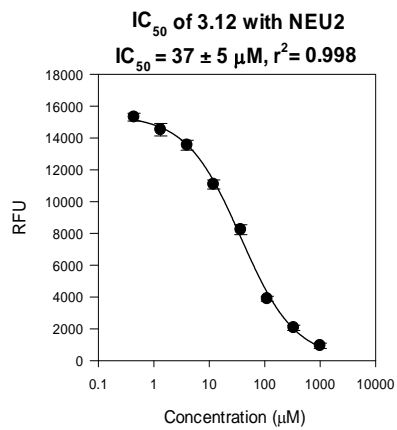
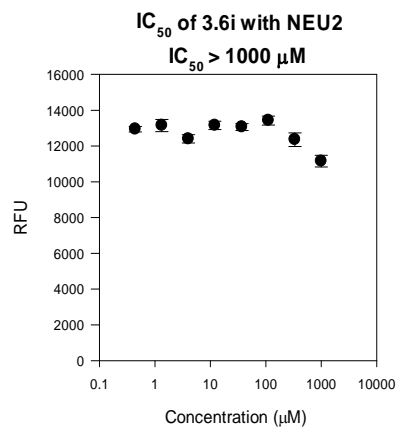
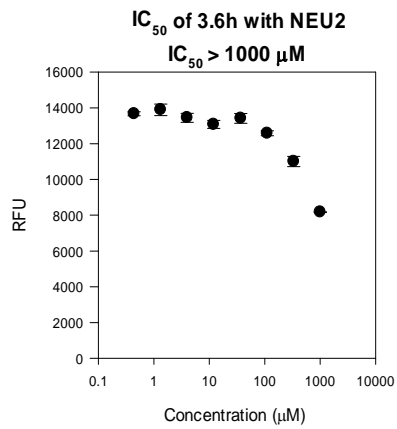
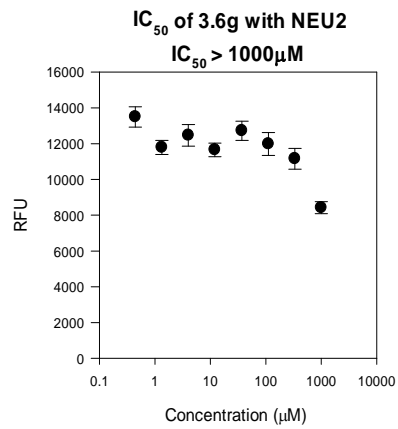
a - *IC₅₀ curves of compounds 1-11 with NEU1*



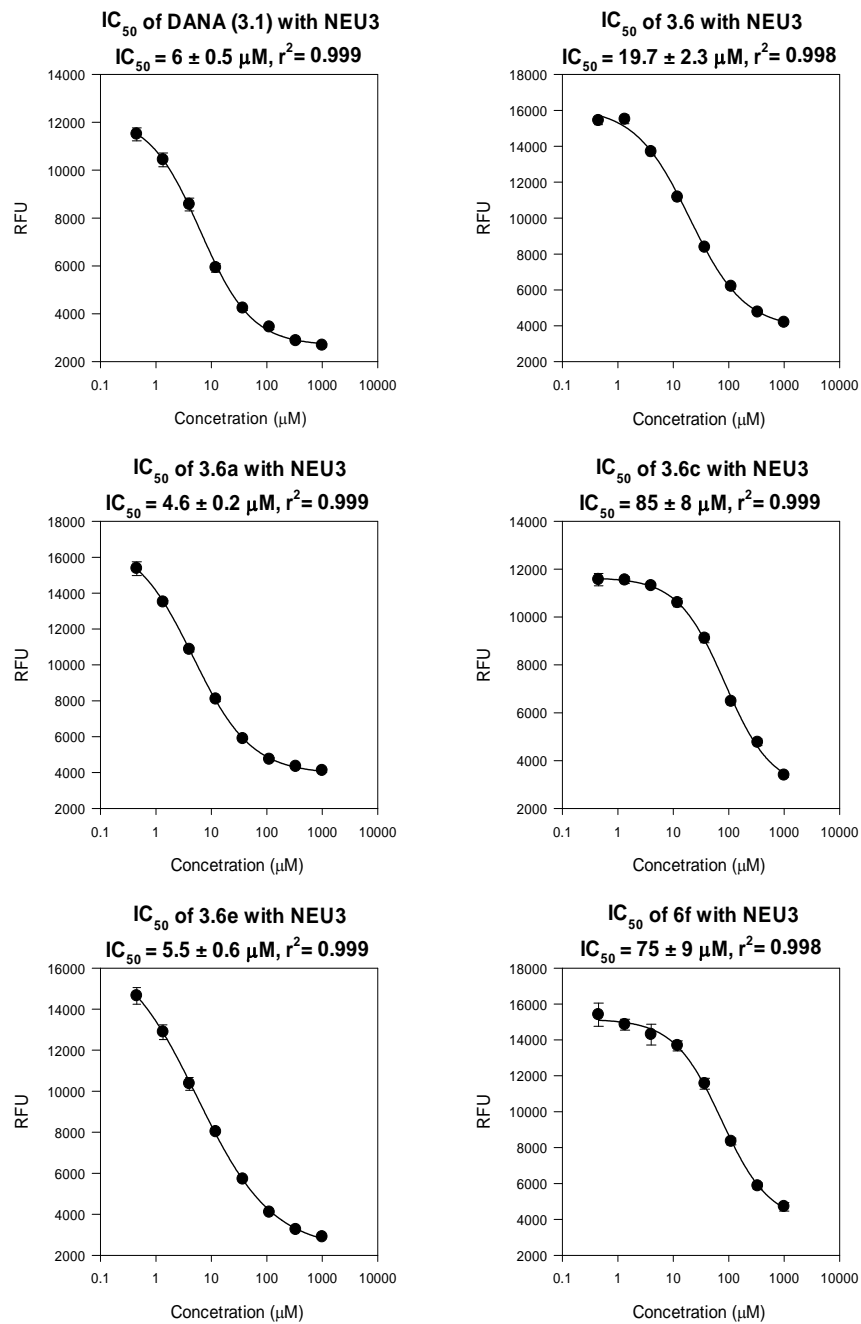


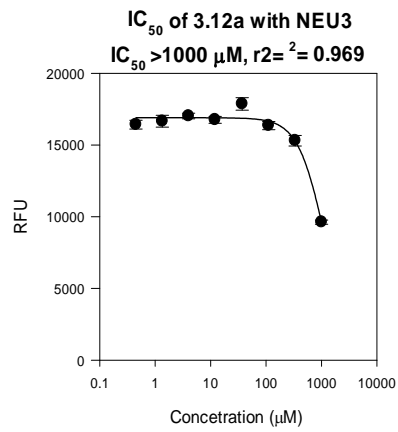
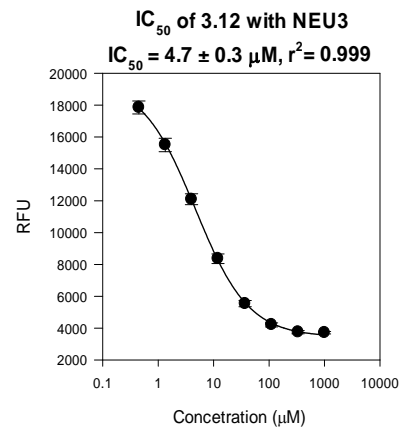
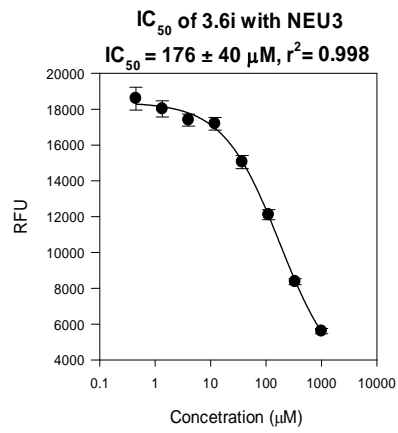
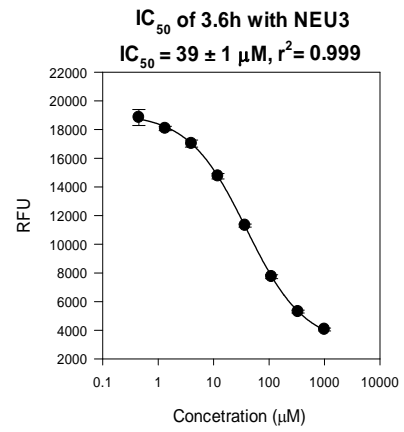
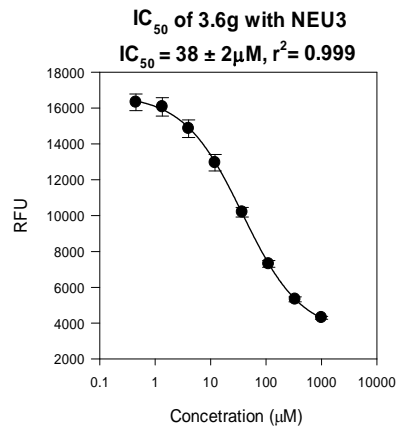
b - IC₅₀ curves of the focused library compounds with NEU2



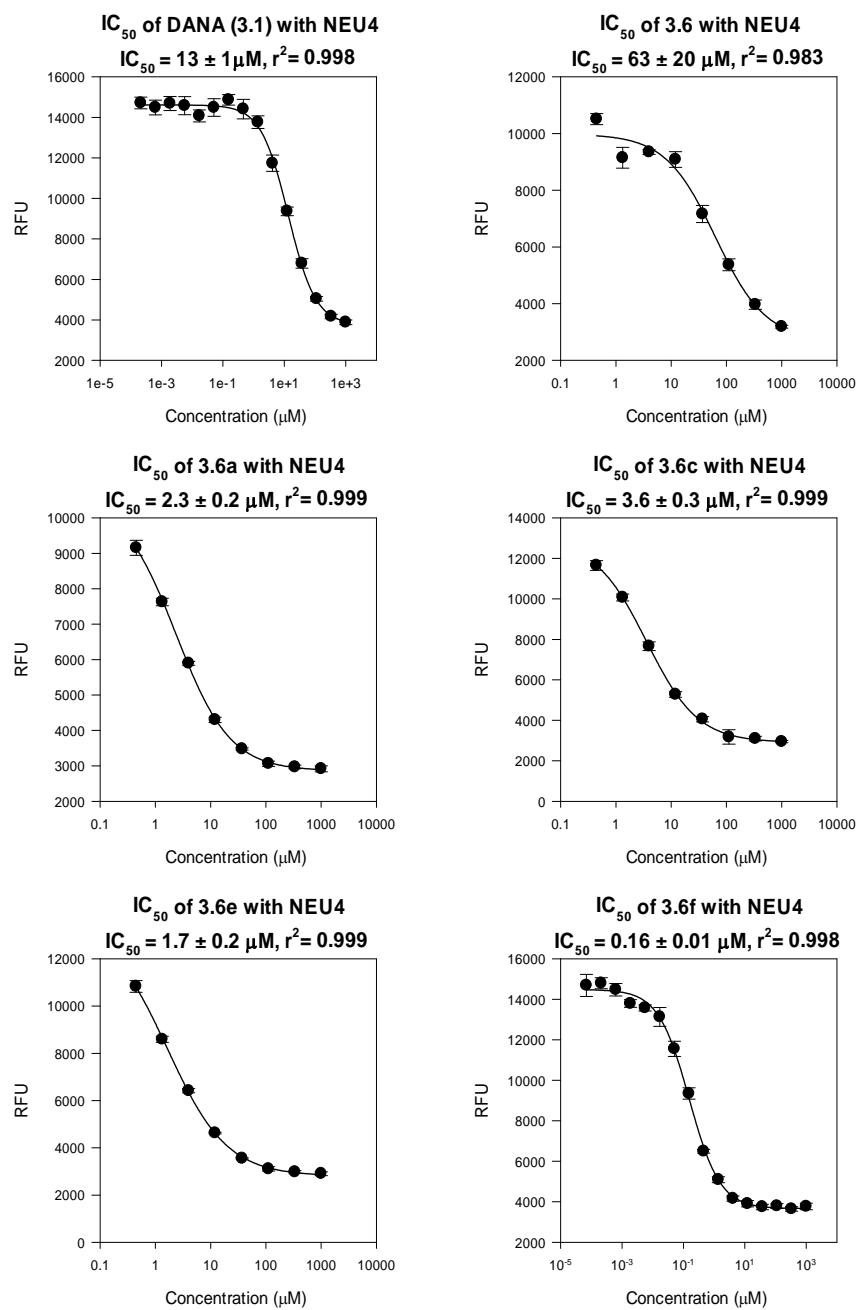


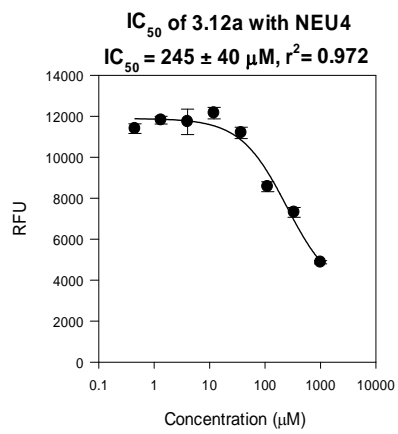
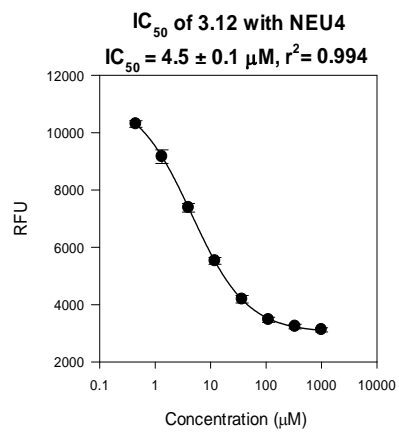
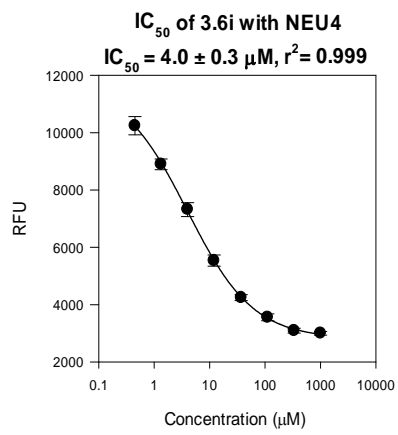
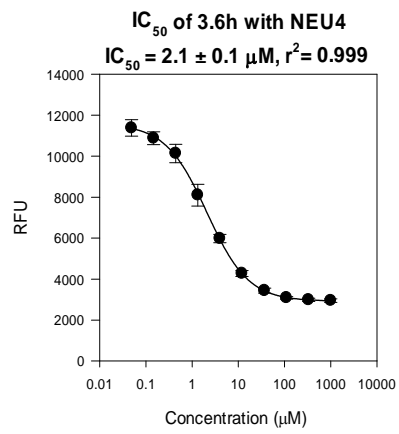
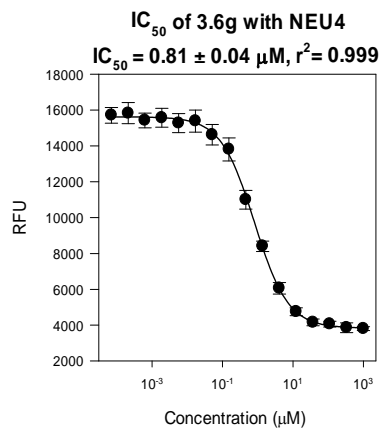
c - IC₅₀ curves of the focused library compounds with NEU3





d - IC₅₀ curves of the focused library compounds with NEU4

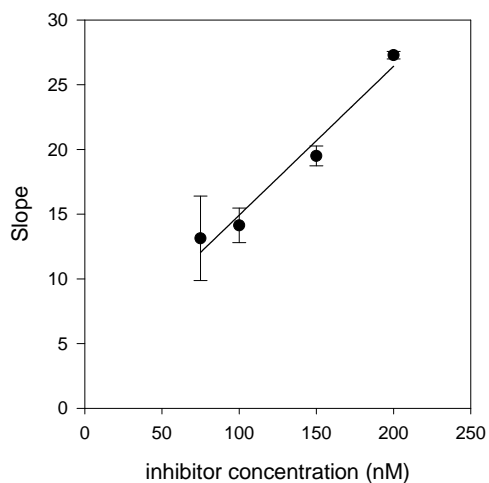
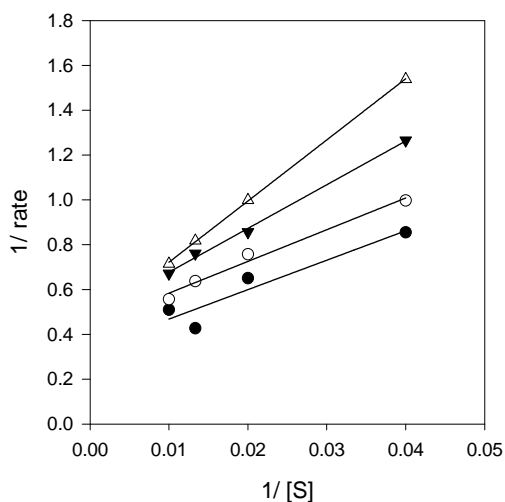




A.3.2.6 K_i curves for compounds 3.6f and 3.6g with NEU4.

Measurements were done according to protocol in Materials and Methods. The top left graph is the double reciprocal curve of rate and the substrate concentration at serial inhibitor concentrations (See table insert for legend and fit results). Plots of the slopes versus inhibitor concentration provide a linear curve ($y= ab + c$) where K_i is found as $-b/a$.

a- K_i of 3.6f with NEU4, $K_i= 30 \pm 19$ nM

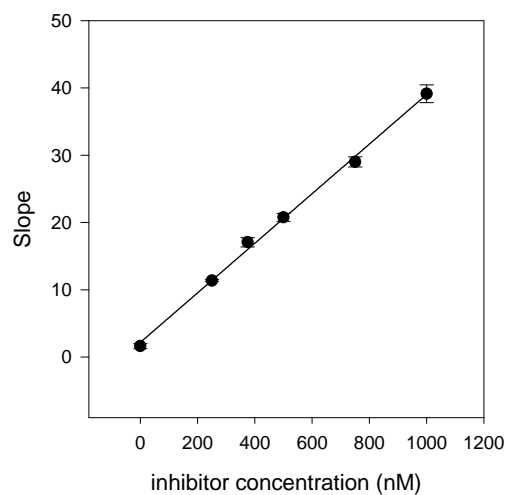
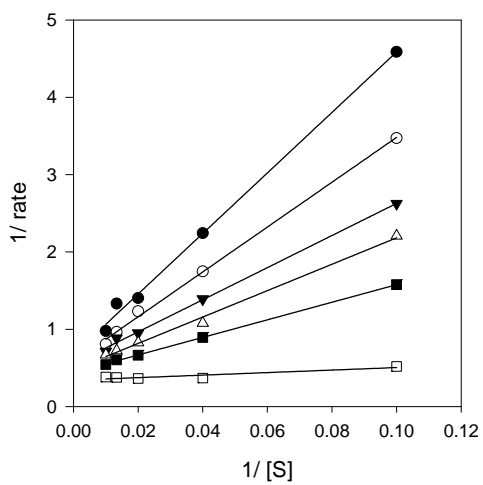


	[I] (nM)	Slope	\pm	r^2
\triangle	200	27.28	0.297	0.999
\blacktriangledown	150	19.5	0.764	0.997
\circ	100	14.15	1.332	0.983
\bullet	75	13.13	3.269	0.890

$$y = 0.115x + 3.4135$$

$$r^2 = 0.9691$$

b- K_i of 3.6g with NEU4, $K_i = 60 \pm 16$ nM



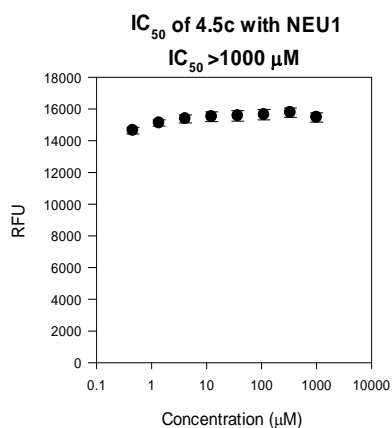
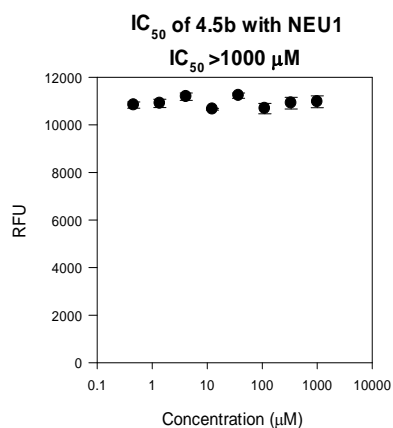
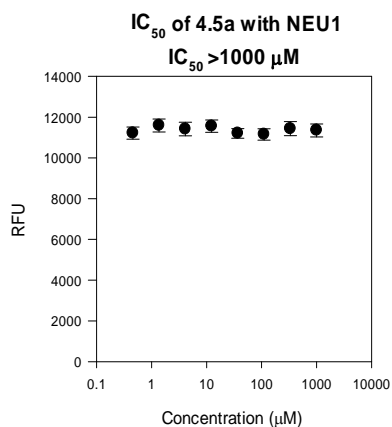
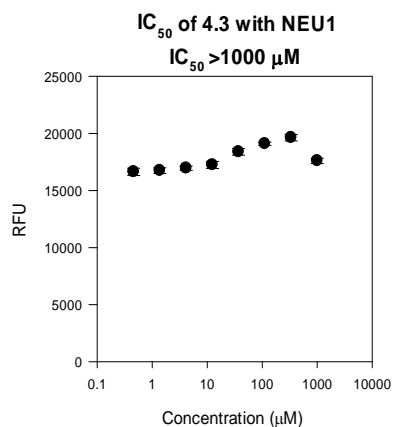
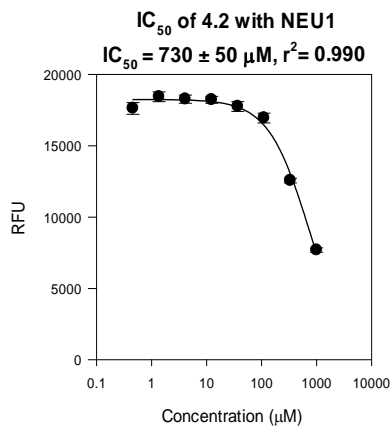
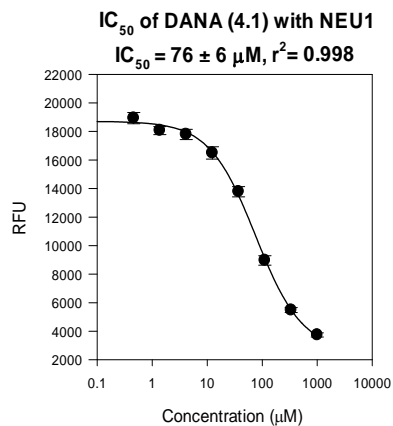
	[I] nM	Slope	\pm	r^2
●	1000	39.147	1.321	0.997
○	750	29.006	0.739	0.998
▼	500	20.771	0.584	0.998
△	375	17.077	0.694	0.995
■	250	11.372	0.129	0.999
□	0	1.632	0.392	0.852

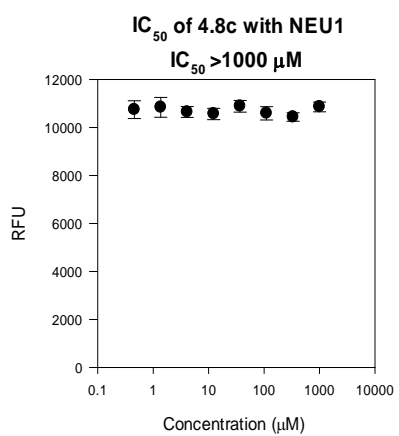
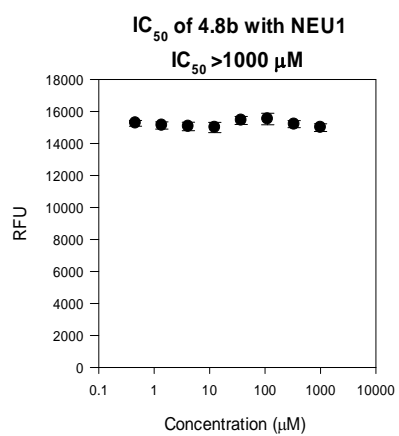
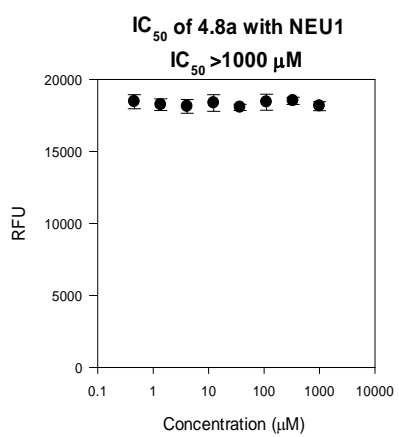
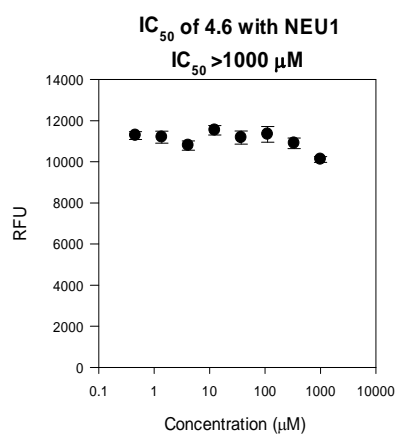
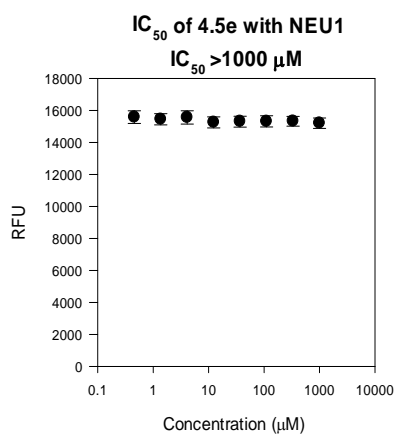
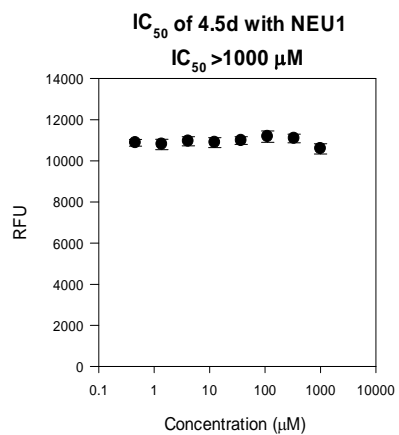
$$y = 0.0368x + 2.1772$$

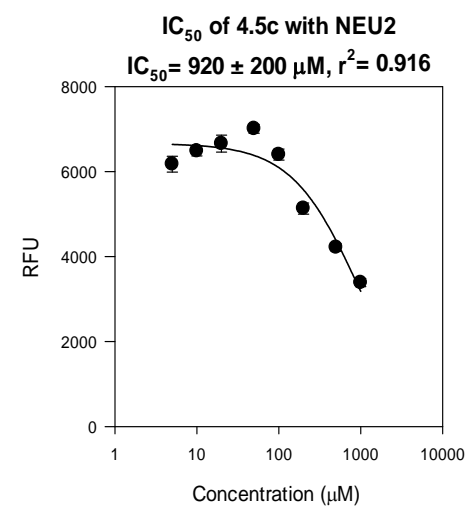
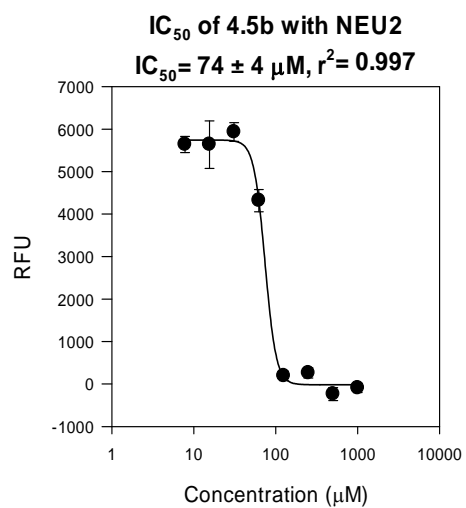
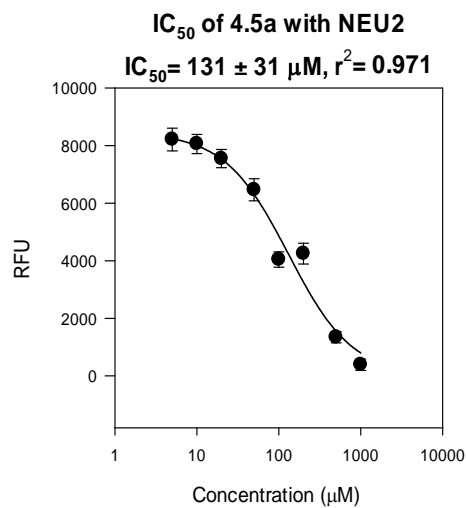
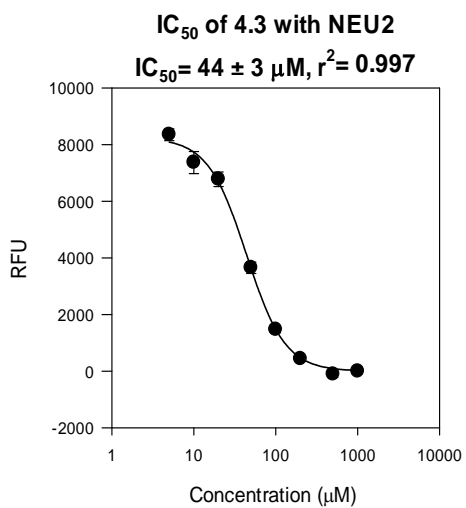
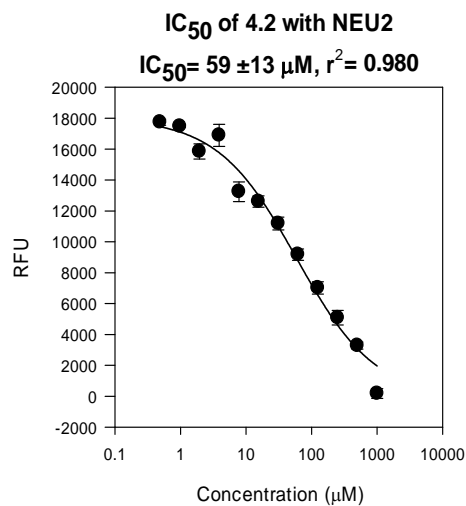
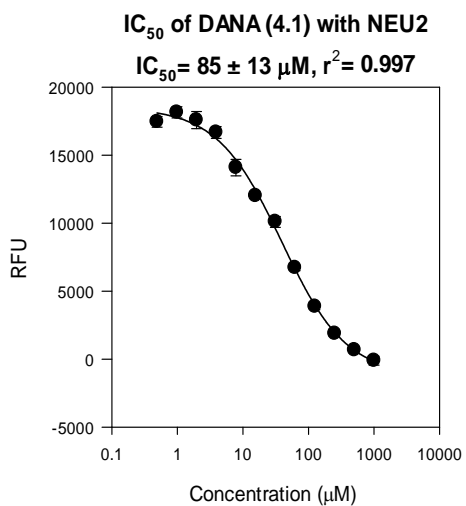
$$r^2 = 0.9975$$

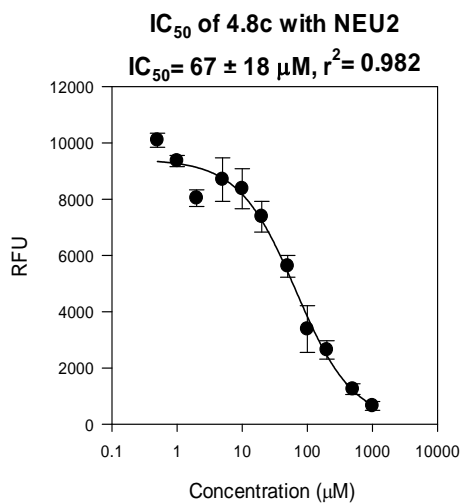
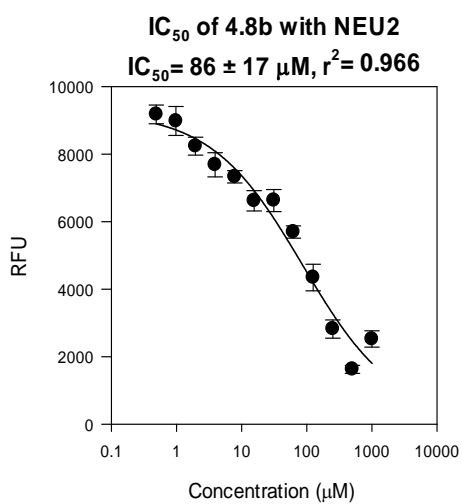
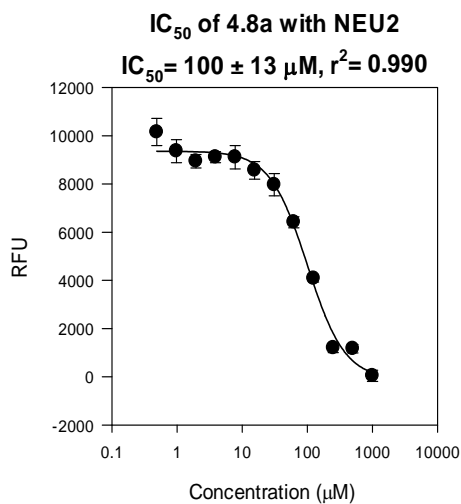
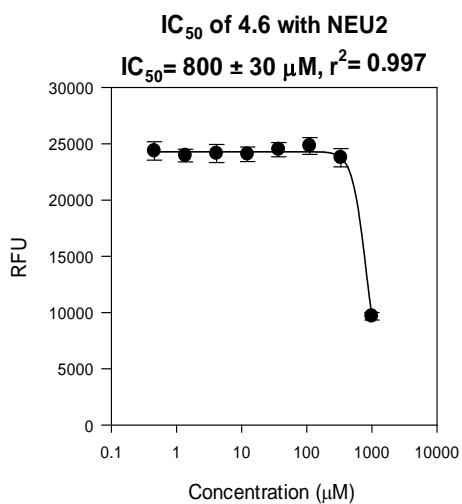
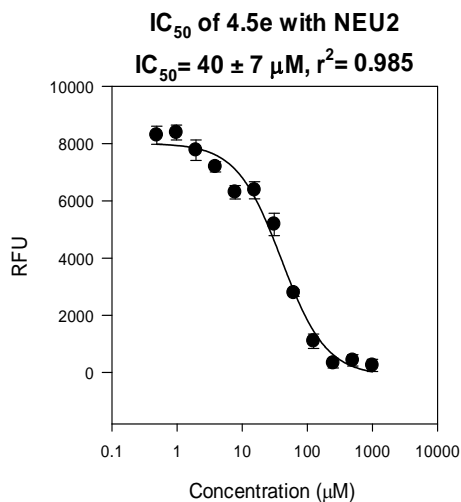
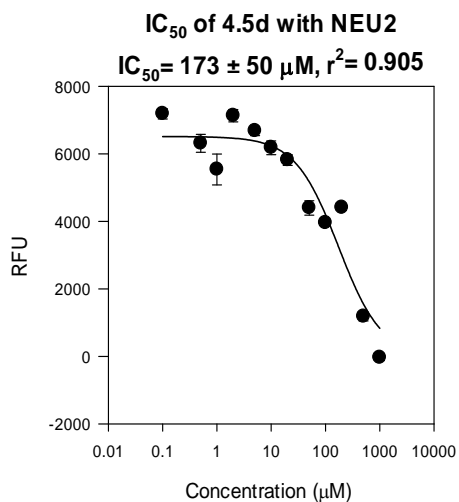
A.4 Supporting data for Chapter 4

A.4.1 Inhibition of human neuraminidase isoforms by tested compounds



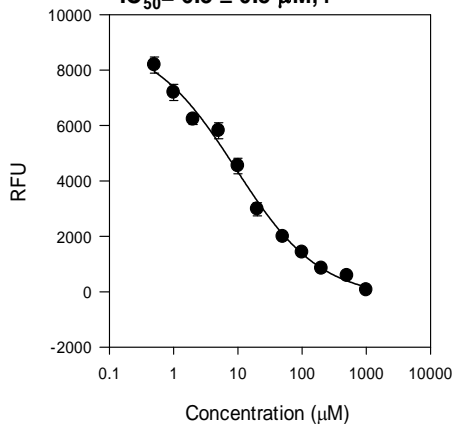






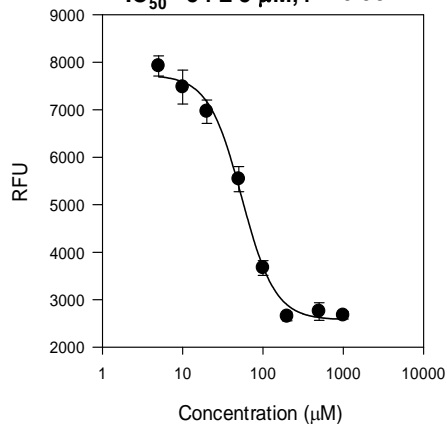
IC₅₀ of DANA (4.1) with NEU3

IC₅₀ = 6.3 ± 0.5 μM, r² = 0.992



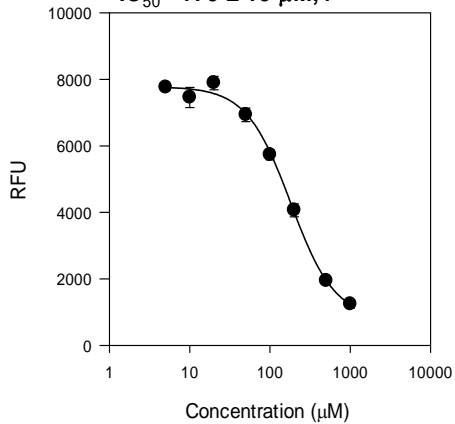
IC₅₀ of 4.2 with NEU3

IC₅₀ = 54 ± 5 μM, r² = 0.994



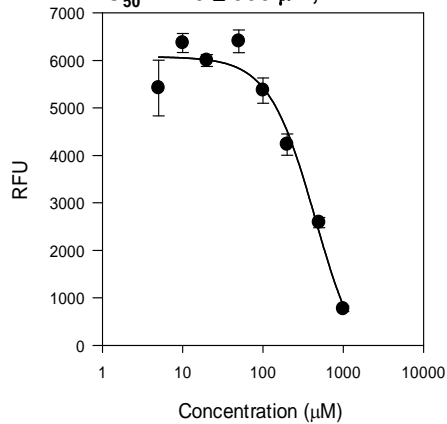
IC₅₀ of 4.3 with NEU3

IC₅₀ = 179 ± 19 μM, r² = 0.996



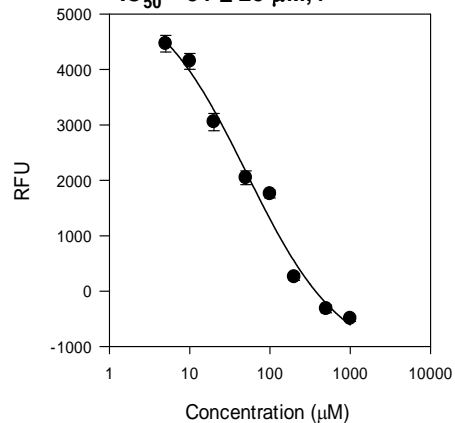
IC₅₀ of 4.5a with NEU3

IC₅₀ = 440 ± 300 μM, r² = 0.989



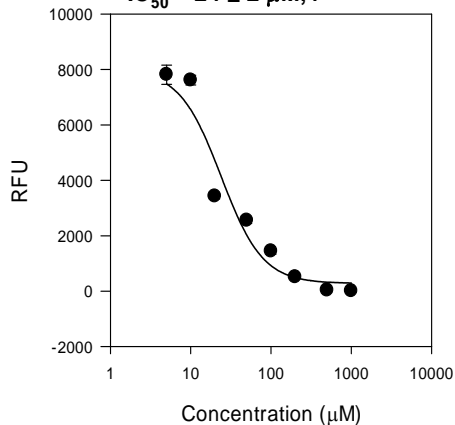
IC₅₀ of 4.5b with NEU3

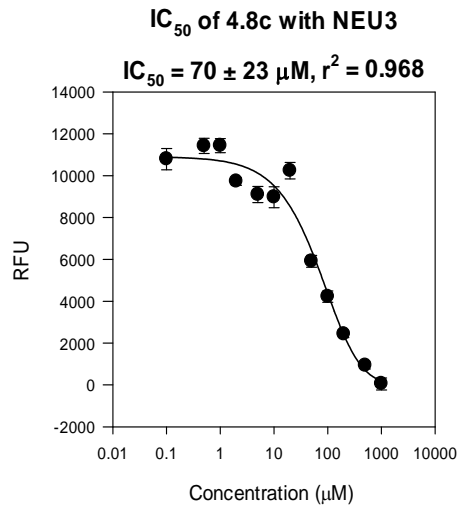
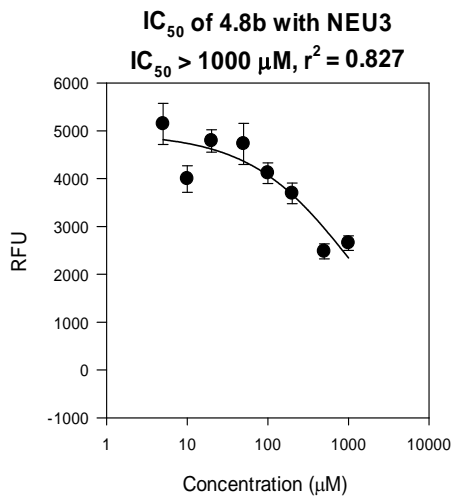
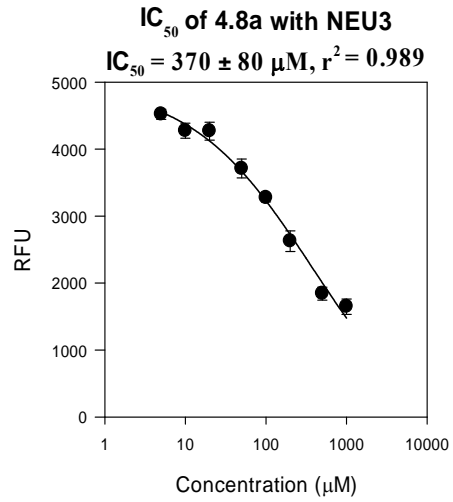
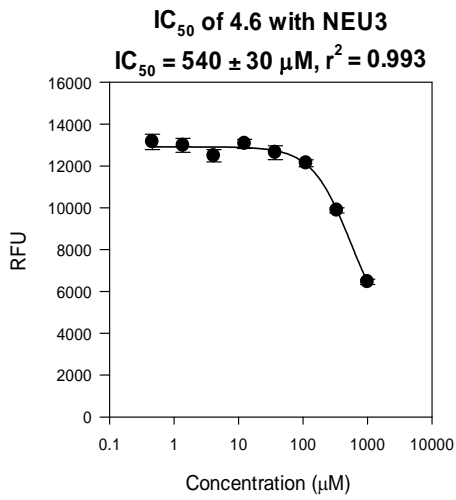
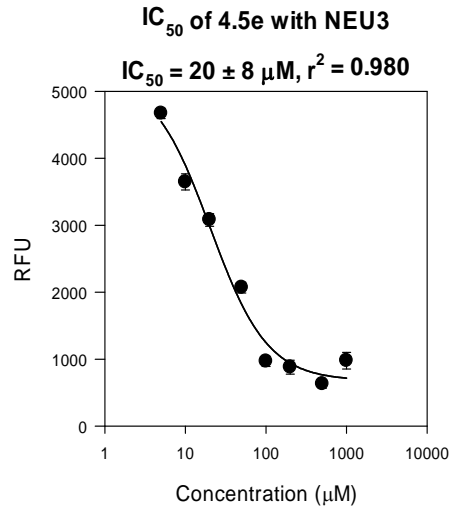
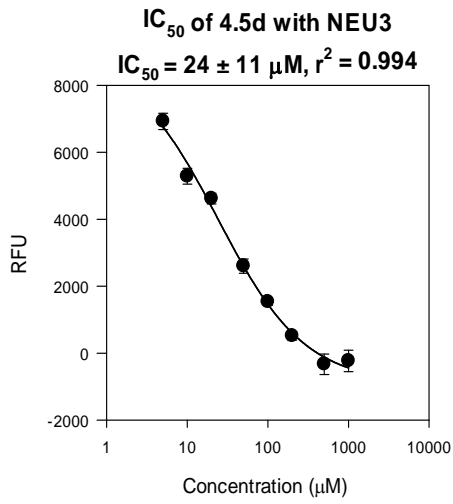
IC₅₀ = 51 ± 25 μM, r² = 0.985



IC₅₀ of 4.5c with NEU3

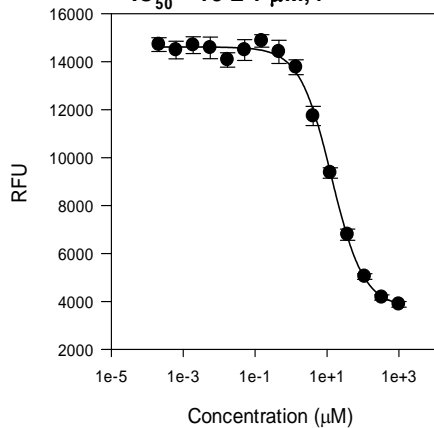
IC₅₀ = 24 ± 2 μM, r² = 0.949





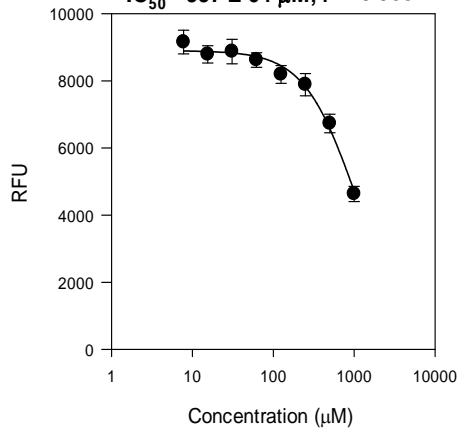
IC₅₀ of DANA (4.1) with NEU4

IC₅₀ = 13 ± 1 μM, r² = 0.998



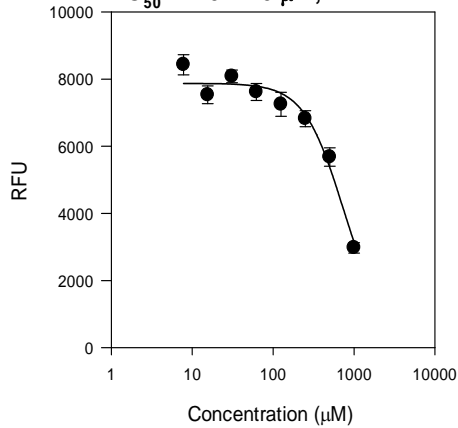
IC₅₀ of 4.2 with NEU4

IC₅₀ = 997 ± 64 μM, r² = 0.988



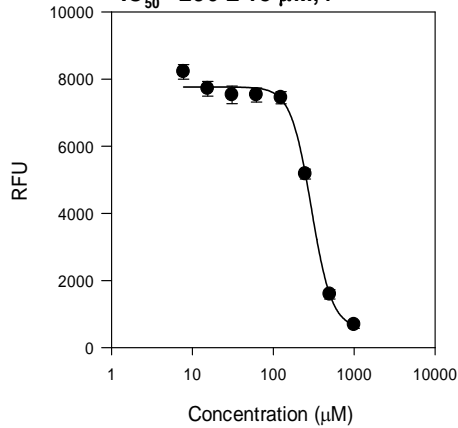
IC₅₀ of 4.3 with NEU4

IC₅₀ = 720 ± 70 μM, r² = 0.965



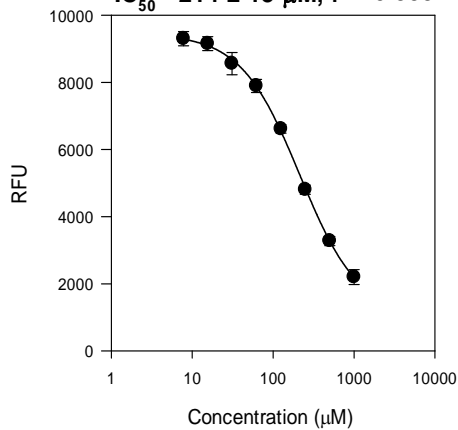
IC₅₀ of 4.5a with NEU4

IC₅₀ = 296 ± 18 μM, r² = 0.995



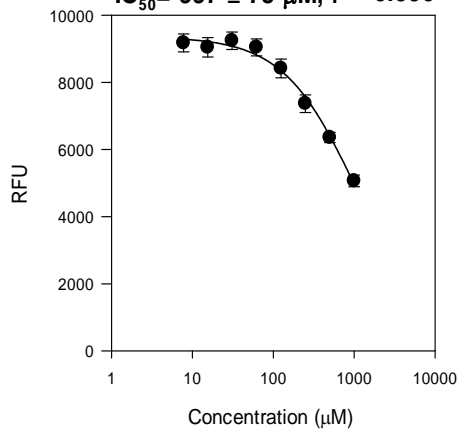
IC₅₀ of 4.5b with NEU4

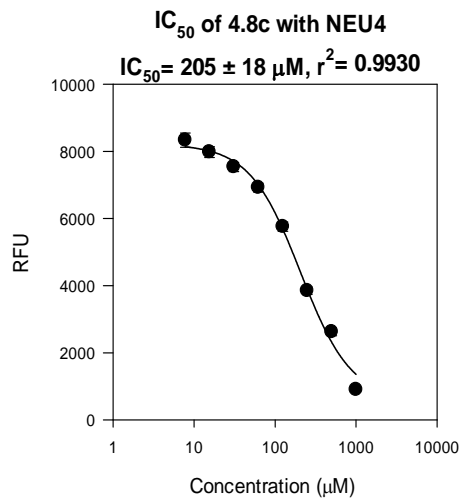
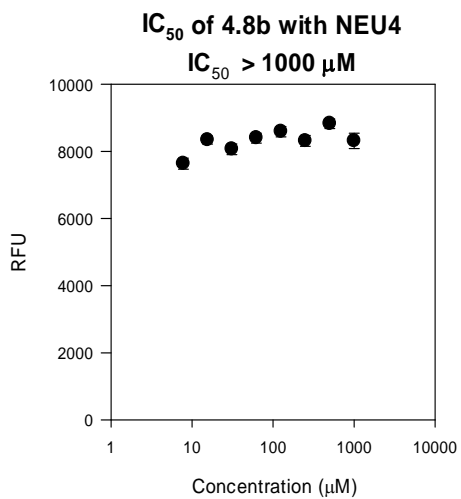
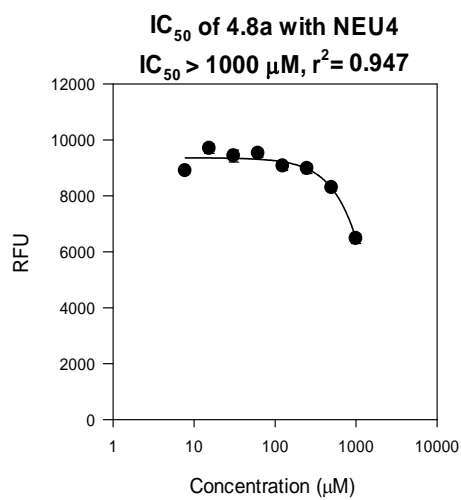
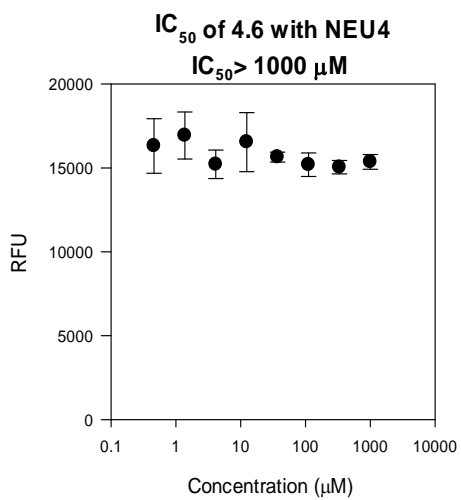
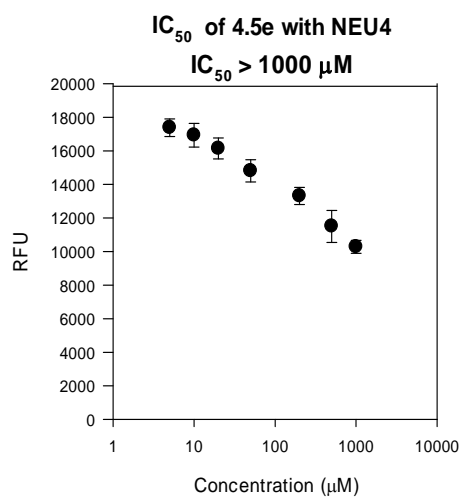
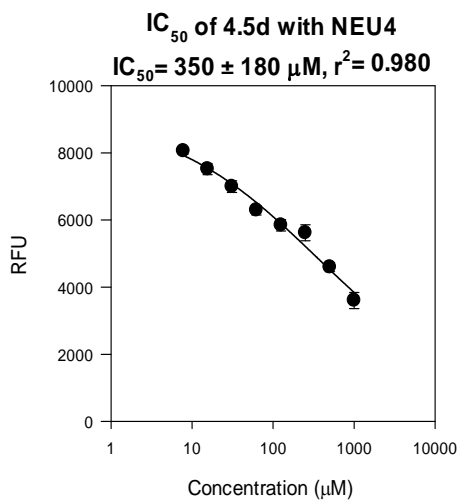
IC₅₀ = 214 ± 13 μM, r² = 0.999



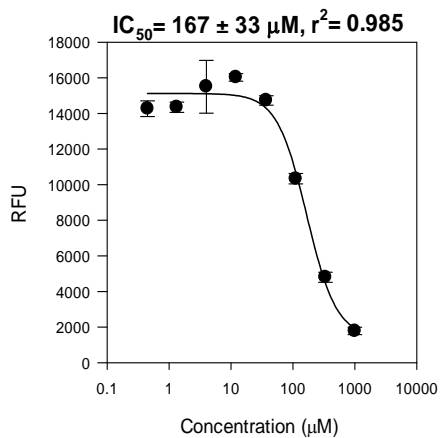
IC₅₀ of 4.5c with NEU4

IC₅₀ = 997 ± 75 μM, r² = 0.990

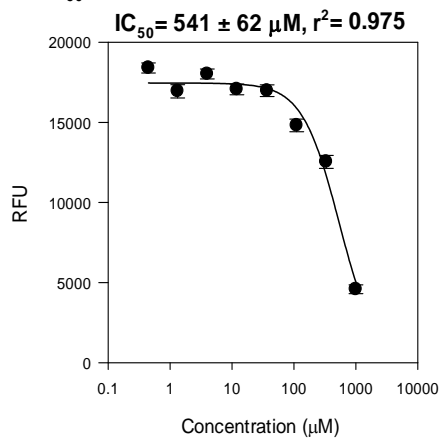




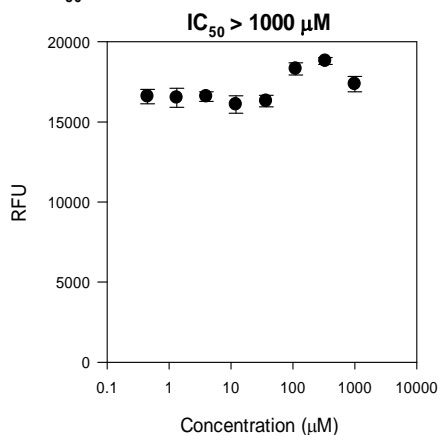
IC₅₀ of DANA (4.1) with *Vibrio Cholerae* sialidase



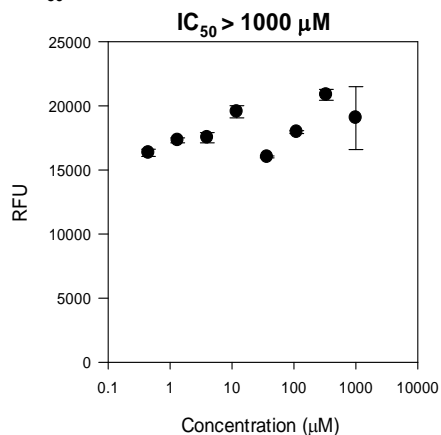
IC₅₀ of 4.2 with *Vibrio Cholerae* sialidase



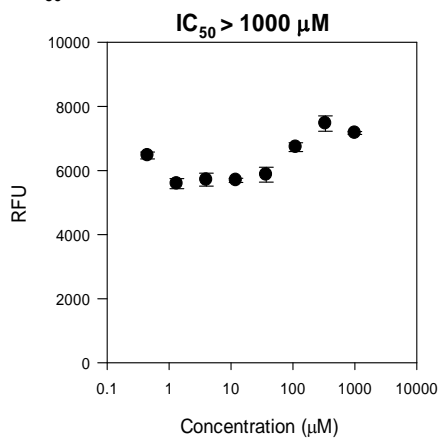
IC₅₀ of 4.3 with *Vibrio Cholerae* sialidase



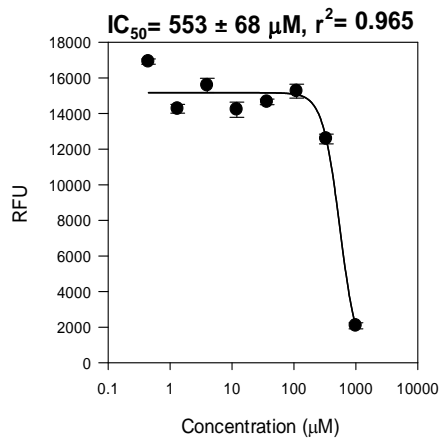
IC₅₀ of 4.5a with *Vibrio Cholerae* sialidase



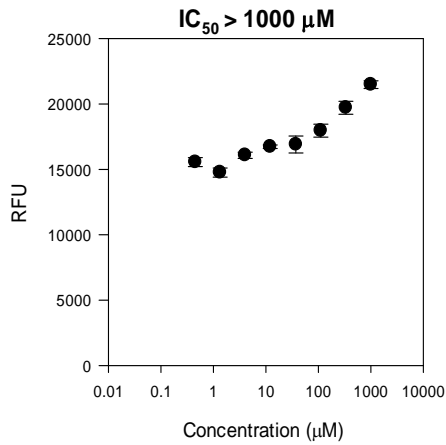
IC₅₀ of 4.5b with *Vibrio Cholerae* sialidase



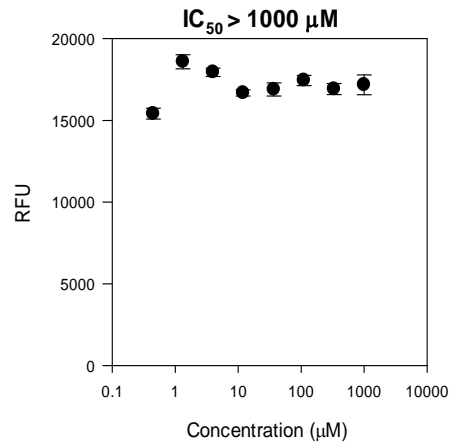
IC₅₀ of 4.5c with *Vibrio Cholerae* sialidase



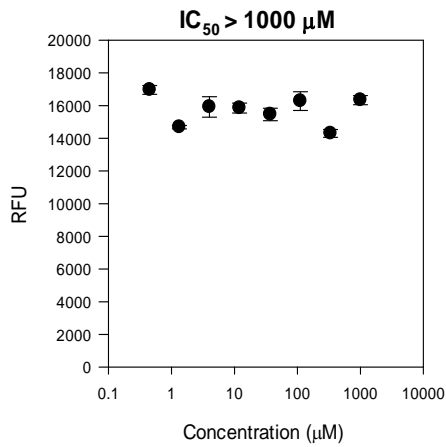
IC₅₀ of 4.5d with *Vibrio Cholerae* sialidase



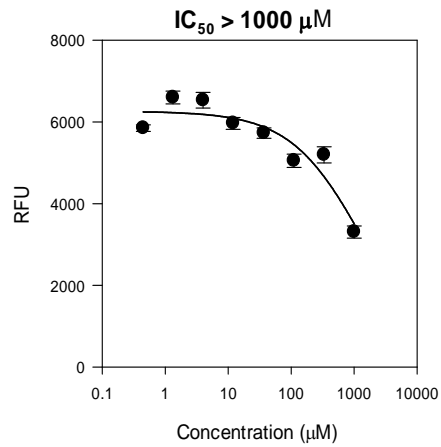
IC₅₀ of 4.5e with *Vibrio Cholerae* sialidase



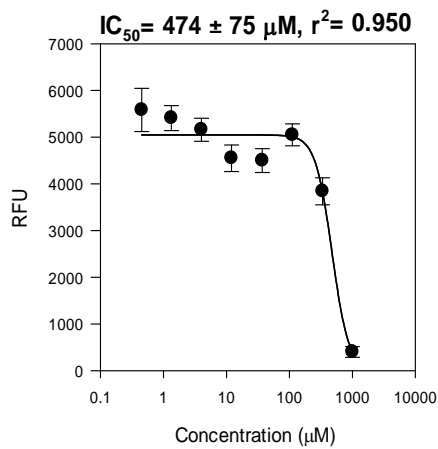
IC₅₀ of 4.6 with *Vibrio Cholerae* sialidase



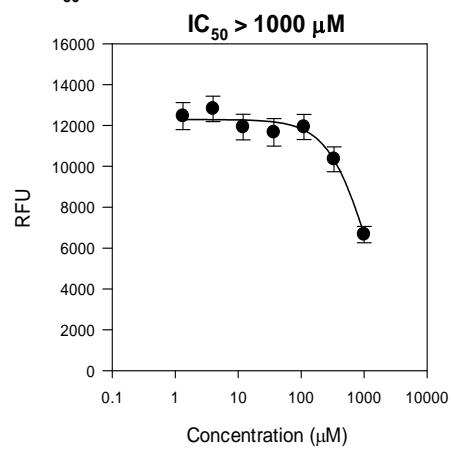
IC₅₀ of 4.8a with *Vibrio Cholerae* sialidase



IC₅₀ of 4.8b with *Vibrio Cholerae* sialidase



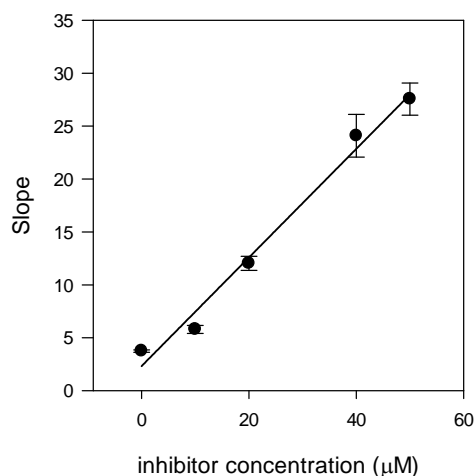
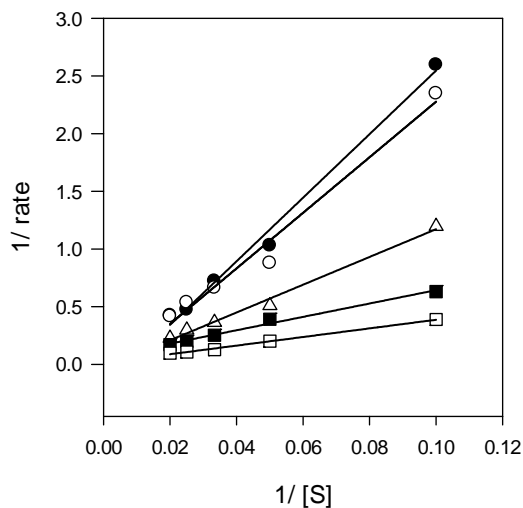
IC₅₀ of 4.8c with *Vibrio Cholerae* sialidase



A.4.2 K_i determinations for DANA, 4.5c, and 4.5e

K_i determinations were performed using a kinetic version of the enzyme assay protocol above. For each compound, a double reciprocal plot of $[1/\text{rate}]$ vs. $[1/\text{substrate concentration}]$ is shown at left along with a table providing the legend and parameters for each inhibitor concentration. A plot of the slope vs. inhibitor concentration was fit to a linear curve ($y = bx + c$). The value of K_i was calculated as $-c/b$ and error was calculated as $[(b \cdot \delta c) - (c \cdot \delta b)]/b^2$ where δb and δc are the error associated with b and c respectively.

(a) DANA (4.1) with NEU2; $K_i = 4.5 \pm 2 \mu\text{M}$

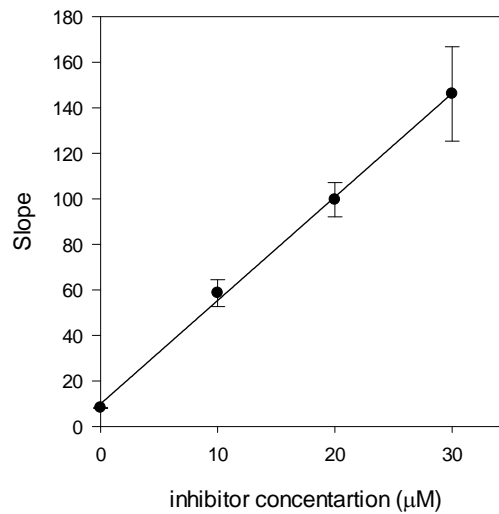
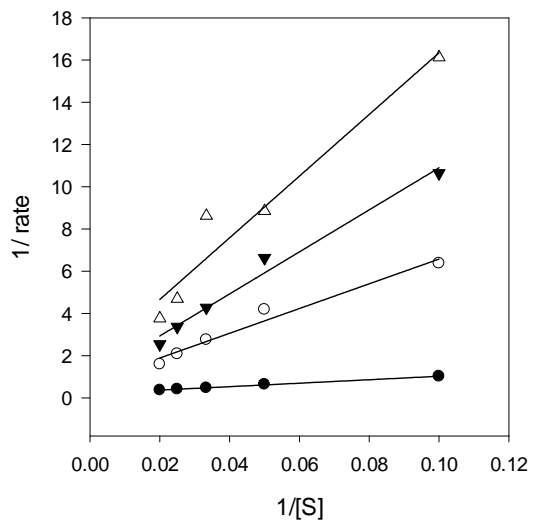


	[I] (μM)	Slope	\pm	r^2
●	50	27.549	1.519	0.991
○	40	24.087	2.019	0.979
△	20	12.032	0.659	0.991
■	10	5.791	0.378	0.987
□	0	3.737	0.121	0.997

$$y = 0.5132x + 2.3214$$

$$r^2 = 0.9852$$

(b) DANA (4.1) with NEU3; $K_i = 2.2 \pm 0.5 \mu\text{M}$

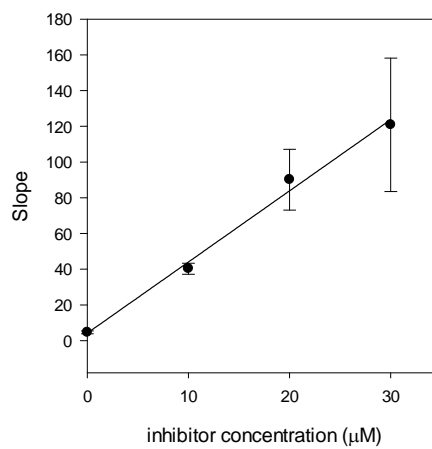
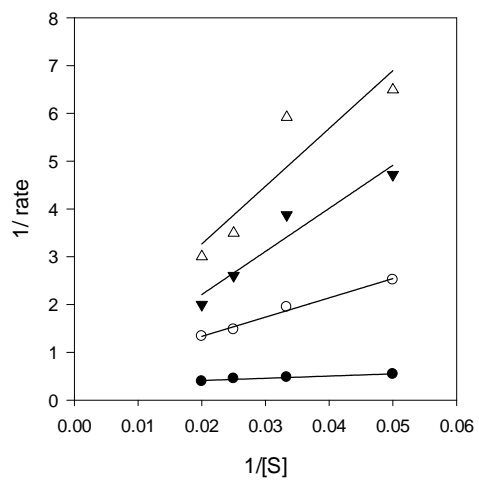


$$y = 4.5433x + 9.948$$

$$r^2 = 0.9986$$

	[I] (μM)	Slope	\pm	r^2
\triangle	30	146.0843	20.74	0.943
\blacktriangledown	20	99.5776	7.5319	0.983
\circ	10	58.5935	5.8972	0.971
\bullet	0	8.218	0.2459	0.997

(c) DANA (4.1) with NEU4; $K_i = 1.0 \pm 0.6 \mu\text{M}$

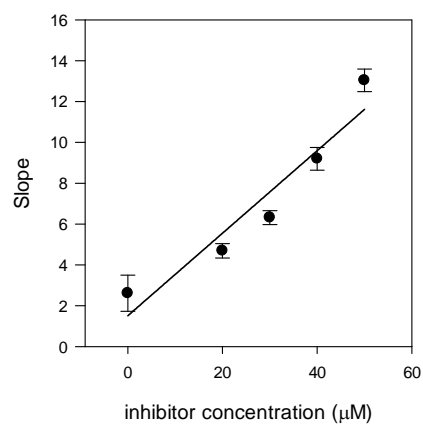
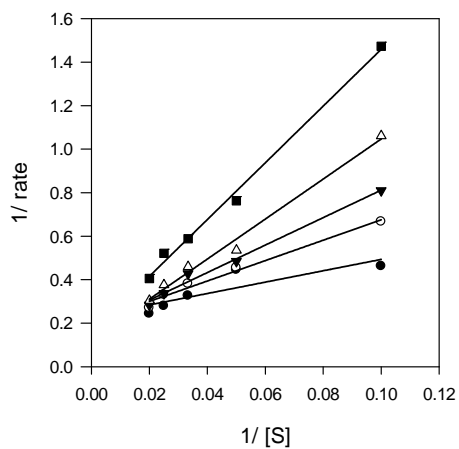


	[I] (μM)	Slope	Error	r^2
△	30	120.8390	37.3648	0.840
▼	20	90.1103	17.0494	0.933
○	10	40.2837	3.0415	0.989
●	0	4.6548	0.7777	0.947

$$y = 3.9838x + 4.2144$$

$$r^2 = 0.9923$$

(d) 4.5c with NEU3; $K_i = 7.5 \pm 1 \mu\text{M}$

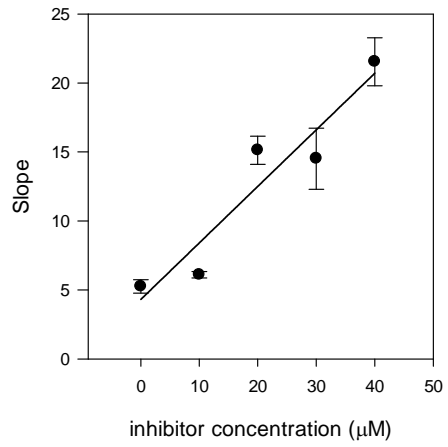
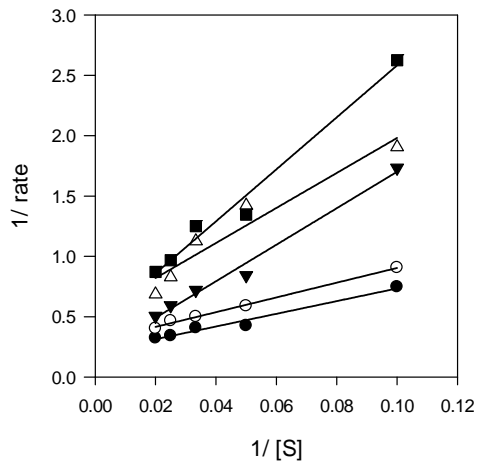


$$y = 0.2021x + 1.5112$$

$$r^2 = 0.9134$$

	[I] (μM)	Slope	\pm	r^2
■	50	13.039	0.551	0.995
△	40	9.197	0.558	0.989
▼	30	6.315	0.340	0.988
○	20	4.689	0.352	0.983
●	0	2.614	0.886	0.744

(e) 4.5e with NEU3; $K_i = 11 \pm 3 \mu\text{M}$



$$y = 0.4098x + 4.3122$$

$$r^2 = 0.9024$$

	[I] (μM)	Slope	\pm	r^2
■	40	21.540	1.737	0.980
△	30	14.514	2.219	0.929
▼	20	15.127	1.024	0.986
○	10	6.100	0.231	0.996
●	0	5.258	0.486	0.975